Masters Theses   Student Theses and Dissertations

Fall 2007

Performance evaluation of existing analytical methods to compute the shear contribution provided by externally bonded FRP sheets in concrete structures

Rocio Patricia Tumialan

Recommended Citation

PERFORMANCE EVALUATION OF EXISTING ANALYTICAL METHODS

TO COMPUTE THE SHEAR CONTRIBUTION PROVIDED BY EXTERNALLY

BONDED FRP SHEETS IN CONCRETE STRUCTURES

by

ROCIO PATRICIA TUMIALAN

A THESIS

Presented to the Faculty of the Graduate School of the

UNIVERSITY OF MISSOURI-ROLLA

In Partial Fulfillment of the Requirements for the Degree

MASTER OF SCIENCE IN CIVIL ENGINEERING

2007

Approved by

_____   _____
Abdeldjelil Belarbi, Advisor   Ashraf Ayoub

_____   _____
Victor Birman   Sang-Wook Bae

ABSTRACT

External application of FRP composites has been adopted for strengthening and/or repair of concrete structures in many applications during the last two decades. However, the research into shear strengthening using FRP composites has not been widely conducted as compared to flexural strengthening and axial load capacity increase, and the results obtained thus far are scarce and sometimes controversial.

This study presents a review of analytical studies and design guidelines on shear strengthening of concrete structures with externally-bonded FRP laminates, and their assessment with experimental data collected from the literature. The strengths and weaknesses of each model and design guidelines/codes/specifications are identified and evaluated in order to understand the behavior of the concrete structures strengthened in shear with FRP systems and to propose additional research required to develop a more accurate analytical model.

In addition, the predictions obtained by the analytical models and design guidelines/codes/specifications were compared to the experimental results to evaluate the accuracy. This comparative evaluation showed that none of the analytical models and design guidelines/codes/specifications was able to provide reliable estimates, which indicates that the mechanisms of FRP strengthening for shear are still poorly understood. As a result, parameters that are not taken into account in these analytical and design methodologies, but that affect the behavior of members strengthened in shear with FRP were identified.

ACKNOWLEDGMENTS

TABLE OF CONTENTS

LIST OF ILLUSTRATIONS

LIST OF TABLES

NOMENCLATURE

Symbol	Description
a_g	Maximum aggregate size
a/d	Shear span-to-depth ratio
A_c	Concrete area
A_f	Cross sectional area of FRP
A_{ps}	Area of prestressing steel on flexural tension side
A_{sv}	Area of steel shear reinforcement
b_w	Minimum width of cross section over the effective depth
d	Distance from extreme compression fiber to centroid of tension reinforcement
d_f	Effective FRP depth
$d_{f,t}$	Distance from beam compression face to upper edge of FRP
d_s	Stirrup height
D_f	FRP stress distribution factor
$D_{f\theta}$	Modified FRP strain distribution factor
E_f	Elastic modulus of FRP
E_s	Elastic modulus of steel reinforcement
f'_c	Concrete compressive strength
f_{fe}	Effective FRP tensile stress in direction of the principal fibers
f_{ct}	Concrete tensile strength
f_{cu}	Cubic concrete compressive strength
f_{fdd}	Debonding FRP strength
f_{fed}	Effective FRP debonding strength
f_{fu}	Ultimate tensile stress of the FRP
f_{yv}	Yield strength of stirrups

h	Height of RC member
h_{fe}	Effective FRP height
h_w	Height of beam web
k_a	Coefficient describing anchorage condition
k_b	Covering/scale factor coefficient
k_e	Integer describing number of debonding ends
K	Shear reinforcing efficiency
L_b	Available bond length
L_e	Effective bond length
L_{max}	Maximum bond length
M_d	Design bending moment
M_o	Decompression moment
M_u	Factored moment
n	Number of plies of FRP reinforcement
N_u	Decompression moment
P_{max}	Ultimate load capacity of the FRP sheet
r_c	Corner rounding radius of beam
r_f	Factor depending on the FRP strengthening scheme
R	Ratio of effective FRP strain to its ultimate strain
$R*$	Additional reduction factor when transverse steel reinforcement is present
R_L	Ratio of the remaining bonded width over the initial width
s	Debonding slip between FRP and concrete
s_f	Spacing of FRP strips
s_v	Spacing between stirrups
t_f	FRP thickness
T_f	Tension force in FRP
T_v	Tension force in stirrups

V_c	Concrete shear contribution
V_{exp}	Experimental shear capacity
V_f	FRP shear contribution
V_n	Nominal shear capacity
V_p	Design bending moment
V_s	Transverse steel reinforcement shear contribution
z_b	Coordinate of lower edge of effective FRP
z_t	Coordinate of upper edge of effective FRP
α	Angle of the inclination of steel stirrups to longitudinal axis of member
β	Angle of the inclination of FRP fibers to longitudinal axis of member
β_L	Effect of bond length
β_w	Effect of FRP to concrete width ratio
ε_{cr}	Critical FRP strain
ε_{fe}	Effective tensile strain of the FRP
ε_{fu}	Ultimate tensile strain of the FRP
ε_{max}	Maximum FRP strain
εv_{cu}	Ultimate tensile strain of concrete
ϕ	Angle between the principal tensile stress and the fiber direction
γ_b	Member factor
γ_c	Concrete partial coefficient
γ_f	Partial safety factor for FRP
Γ_{Fk}	Specific fracture energy of the FRP-concrete bond interface
η	Average FRP fiber utilization
φ_R	Fraction of ultimate FRP strength
λ	Normalized maximum bond length
θ	Shear crack angle

ρ_f	FRP area fraction
ρ_s	Shear steel reinforcement ratio
$\rho_{s,f}$	stiffness ratio between transverse steel and FRP reinforcement
ρ_{tot}	Total shear reinforcement ratio
$\sigma_{f,\max}$	Maximum stress in FRP intersected by the shear
τ_{bu}	Bond strength between the FRP and concrete
$\tau_{\max}$	Ultimate direct shear strength
ψ_f	Additional reduction factor applied to the FRP shear contribution

1. INTRODUCTION

1.1. FIBER REINFORCED POLYMER COMPOSITE MATERIALS

Fiber Reinforced Polymer (FRP) composite materials consist of advanced composites made of small, continuous, non-metallic, and large number of fibers embedded in a resin matrix. FRP fibers are the main load-carrying components and exhibit very high strength and stiffness when pulled in tension. The type of FRP fibers are selected depending on the magnitude of strength, durability, and stiffness required. The type of resin is selected based on the FRP environmental exposure and the FRP manufacturing method (Nanni, 1999).

FRP fibers used for civil engineering applications are classified into carbon fiber reinforced polymers (CFRP), aramid fiber reinforced polymers (AFRP), and glass fiber reinforced polymers (GFRP). CFRP fibers exhibit high durability, resist most environmental conditions, and withstand high fatigue loading conditions. However, they exhibit susceptibility to galvanic corrosion. AFRP fibers are less attractive for strengthening applications due to their high moisture absorption, high cost, and relatively poor compressive properties. However, they exhibit excellent toughness, damage tolerance, and fatigue characteristics. GFRP fibers are classified into E-glass fibers, S-glass fibers, and AR-glass fibers. GFRP fibers are susceptible to moisture, especially in the presence of high alkaline environments, creep fracture and sustained loads (Bank et al., 1995). The main advantages of GFRP fibers are their capacity of being excellent thermal insulators and inexpensive cost.

1.2. APPLICATIONS OF FRP IN CIVIL ENGINEERING

FRP composite materials have become increasingly popular in different sectors of industry, such as the aerospace industry and relatively most recently in concrete and masonry construction (Nanni, 1993). The application of FRP composite materials for internal reinforcement and for repair and strengthening of reinforced concrete (RC) structures is more advantageous than traditional strengthening schemes. This is because FRP systems are more resistant to corrosion, exhibit high strength, and usually provide the most cost effective solution.

FRP composites can be produced in different shapes and forms such as reinforcing bars, prestressing tendons, precured laminates and fiber sheets. FRP bars and prestressing tendons are applied as internal reinforcement, while FRP laminates and sheets are applied as external reinforcement for repair and strengthening purposes.

FRP materials used for maintenance, repair, retrofit, and strengthening of reinforced concrete (RC) structures are among the popular applications of FRP composites in structural engineering. The retrofitting of existing RC infrastructures may be needed in cases where the original strength or ductility of a structure is increased due to additional loading. Repair of existing structures may also be needed when the existing structure has deteriorated due to environmental factors or mechanical actions, such as blast and impact loading. In addition, the need for repair and strengthening may be required for extending the service life of structures or for lacking proper detailing due to design errors.

The application of FRP composites externally applied for strengthening structures has evolved in the late 1980s in Europe, Japan, the United States, and Canada. Research initially focused on flexural strengthening and confinement of RC structures. Both of these FRP applications evolved from the experience gained in retrofitting RC structures using steel plates. The FRP plate bonding technology was first investigated at the Swiss Federal Laboratories for Material Testing and Research (EMPA) (Meier et al., 1995), where tests on RC beams strengthened with CFRP plates started in 1984. In the United States, the first investigation on FRP strengthening developed in the early 1990s by the University of San Diego (Priestley et al., 1992). This research focused on the evaluation of GFRP systems for seismic retrofitting of RC columns. In addition, numerous investigations on flexural strengthening of RC beams using hand lay-up GFRP and CFRP sheets developed in the early 1990s (Saadamanesh, 1994). All of these and other extensive investigations on flexural strengthening have shown that FRP systems improve the bending capacity of RC structures by applying FRP sheets or plates to the tension sides of members. Numerous studies have also shown that FRP systems can improve the strength and ductility of columns by wrapping the entire column member. On the other hand, investigations on shear strengthening of RC structures started to develop quite lately (early 1990s) in comparison to those of flexural strengthening. These

investigations have shown that FRP systems improve the shear capacity of RC structures by bonding FRP sheets or plates to the web of members. FRP systems have also been used to strengthen concrete masonry wall systems to resist lateral loads. However, code-based design guidelines are yet scarce for this type of application.

1.3. ISSUES RELATED TO SHEAR STRENGTHENING

The subject of shear has always been difficult to understand. Since shear failures occur suddenly and catastrophically, it is generally preferred to insure that flexural failure governs. For RC structures deficient in shear, FRP systems have been proven to increase the total shear resistance of existing RC structures by fully-wrapping or partially-wrapping FRP composites around the structures.

Extensive research on the application of FRP systems by bonding FRP systems to the web of members to increase the shear capacity has been developed over the last 20 years. However, the results obtained thus far are scarce and sometimes controversial. This is in essence due to the intrinsic difficulty of shear behavior of RC structures. Adding FRP to the equation, which has its own specific design issues and modes of failures, brings another level of complication in the analysis and design. In addition, since FRP strengthening systems are applied to web of concrete members, FRP shear strengthening systems are only effective over short lengths on the sides of the member, thus the area provided for anchorage of FRP systems is very limited.

Most researches have provided analytical models and design approaches that assume that FRP systems behave in the same way as transverse steel reinforcement in regular RC structures. However, the behavior of FRP materials is linear elastic up to final brittle fracture when subject to tension, while steel reinforcement exhibits yielding and plastic deformation. As a consequence, the brittleness exhibited by FRP materials limits the ductile behavior of RC structures strengthened with FRP systems. Therefore, the design strain in the FRP cannot be used in the same way as the yield strain for steel stirrups because of the non-uniform distributions of the FRP strain along the shear crack.

In addition, several researches have published analytical models where a 45 deg shear crack angle is assumed, which is consistent with the assumption of the shear design provisions in current RC design codes. This simplified truss model is known to be

conservative; however a variable concrete crack angle will give a more realistic and accurate prediction of the behavior and strength of beams failing in shear.

Another issue is that several parameters affect the behavior of RC structures strengthened in shear with FRP systems. To account all of these parameters into an analytical approach to determine the FRP shear contribution has shown to be difficult. Most analytical models have included some of these parameters into their formulations; however, additional research studies are required to account for all these parameters and therefore develop a more accurate analytical approach.

Finally, most design guidelines evaluate the shear capacity of RC structures by individually adding the shear contribution of each material used in a structural member. However, the interaction between the concrete, steel reinforcement and the FRP system used in combination to carry shear loads in RC structures needs to be taken into consideration.

1.4. OBJECTIVES OF THIS STUDY

The objectives of this study are:

1. Review previous experimental work in order to identify and evaluate the parameters that affect the behavior of RC structures shear strengthened with FRP systems.
2. Review and discuss existing analytical models and design guidelines that compute the shear contribution provided by externally-applied FRP sheets.
3. Perform a comparative evaluation of the accuracy in predicting the FRP shear contribution between the examined methodologies and the experimental data collected from the literature.
4. Propose conclusions and recommendations for additional research required to provide a better understanding of the mechanics involved in the behavior of RC structures shear strengthened with FRP systems.

1.5. RESEARCH PLAN AND METHODOLOGY

The first step in this study was to develop an extensive and detailed database based on previous experimental studies. From reviewing previous experimental studies,

the parameters that influence the behavior of RC structures shear-strengthened with FRP were identified. An in-depth analysis of the collected experimental data was performed to evaluate the influence of the major parameters on the behavior of RC beams shear-strengthened with externally-bonded FRP sheets. From the literature, a total of fourteen analytical models and seven design methodologies were collected. These analytical models and design guidelines were discussed and classified according to the approach adopted to predict the FRP effective strain at the time of failure to determine the FRP shear contribution.

When performing the comparative evaluation of the different methods for calculating the FRP shear contribution, only a segment of the total experimental data was used in the comparative evaluation. For this purpose, a critical review of the experimental data collected and the criteria for the selection of a subset of the data was conducted.

The comparative evaluation of the different methods for calculating the FRP shear contribution was performed by comparing the predicted shear strength of FRP with the observed experimental results. In addition, the FRP shear contribution for each method was evaluated in terms of parameters that affect the shear behavior of RC structures strengthened with FRP sheets. For each analytical model, the predicted total shear capacity was also compared with the observed experimental results. The predictions of total shear capacities were computed by applying each analytical model in combination with four RC design codes, i.e., ACI 318-05 (2005), Eurocode 2 Part I (2003), CSA A23.3-94 (1994), and AASHTO LRFD Bridge Design Specifications (1998). Additionally, the predictions of total shear capacities by each design methodology were compared with the collected experimental results. The predictions of the total shear capacities were computed by applying each design guideline with their corresponding RC design code.

Finally, due to the complexity and variety of the different methods for calculating the FRP shear contribution, the comparative evaluation between these methods was also performed through specific examples. These examples represent different types of RC structures, with different FRP strengthening schemes. The comparison of the magnitude

of the FRP shear contribution was performed in terms of the axial rigidity provided by the FRP sheets.

1.6. ORGANIZATION OF THE THESIS

This thesis is organized according to the stages followed for the development of the investigation. Thus, Section One introduces the significance of the strengthening of RC structures with FRP composite materials. In addition, issues related to shear strengthening with FRP systems are also introduced, which led to setting the objectives of the research. Section Two provides a brief description of shear strengthening with FRP composite materials, shear strengthening schemes, potential failure modes, and the effects of different anchorage systems. In addition, this section summarizes and examines previous experimental work, existing analytical models and design guidelines to determine the shear strength of RC structures strengthened with FRP systems.

In Section Three, the identification and evaluation of parameters that influence the behavior of RC beams shear strengthened with FRP systems is presented. The effect of the FRP properties, the shear span-to-depth ratio, and the interaction between transverse steel reinforcement and FRP reinforcement on the behavior of RC shear strengthened with FRP systems are analyzed in terms of the gain in shear due to FRP systems.

Section Four summarizes and examines analytical models and design methodologies, to determine the shear strength of RC structures strengthened with FRP systems. Afterwards, a comparative evaluation between the analytical models and design guidelines are developed in Section Five and Section Six respectively. In addition, due to the complexity and variety of these analytical approaches to evaluate the FRP shear contribution, specific examples are provided in Section Seven for effectively comparing the FRP shear contribution among different analytical approaches.

Finally, Section Eight provides conclusions and recommendations for future work in the area of shear strengthening with externally-bonded FRP sheets.

2. REVIEW OF LITERATURE

2.1. GENERAL

The following literature review provides information on the different types of shear strengthening schemes, and the potential failure modes of RC structures shear-strengthened with FRP composites. In addition, the effects of anchoring FRP strengthening systems are presented and discussed. Finally, existing experimental and analytical studies, conducted to investigate the shear performance and to evaluate the shear capacity of RC structures strengthened with FRP composites, are reviewed.

2.2. SHEAR STRENGTHENING WITH FRP SYSTEMS

2.2.1. FRP Shear Strengthening Schemes. One of the main advantages of strengthening RC structures with externally-bonded FRP sheets is the availability of different strengthening schemes. Different types of strengthening schemes can be selected depending on the required application. Figure 2.1 illustrates three different FRP wrapping schemes than can be used to increase the shear capacity of RC structures.

(a) Side-bonded FRP   (b) U-wrapped FRP   (c) Fully-wrapped FRP
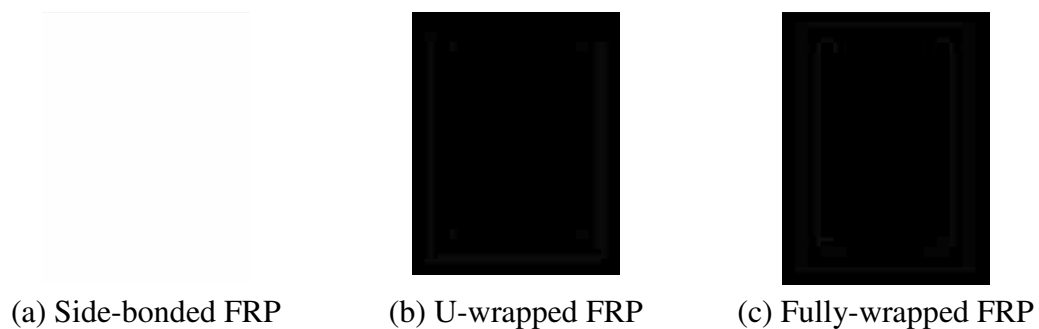
Figure 2.1. FRP Wrapping Schemes

Side-bonded FRP is applied by bonding the FRP sheet on both sides of the RC member as shown in Figure 2.1 (a). This wrapping scheme is not recommended because of its vulnerability to debonding failure of the FRP system at the ends of the members,

unless this type of failure can be avoided by providing adequate anchorage. The second FRP wrapping scheme, known as U-wrapped, is applied by partially-wrapping the FRP sheet on the sides and bottom of the RC member as shown in Figure 2.1 (b). This strengthening scheme is moderately effective in increasing the shear resistance of the RC member; however, it is also vulnerable to debonding failure unless anchorage is provided. The third and final wrapping scheme, known as fully-wrapped scheme, consists on fully-wrapping the FRP sheet around the RC member as shown in Figure 2.1 (c). This strengthening scheme is the most effective especially in column applications, where the member can be fully-wrapped. However, in the presence of slabs, its application can rather be complicated because the RC member cannot be fully wrapped. For both U-wrapped and fully-wrapped schemes, the corners of the RC member need to be rounded to avoid FRP failure due to stress concentration.

FRP sheets can also be applied in the form of continuous wraps as shown in Figure 2.2 (a) or as finite strips along the side of the member as shown in Figure 2.2 (b). Among the main advantages on using FRP strips are the flexibility in controlling the amount of FRP and the potential savings in material; however, its application require more labor hours. On the other hand, the application of continuous sheets protects RC members from further environmental damage; however, it is more difficult to achieve a uniform adhesive layer.

(a) Continuous   (b) Strips

Figure 2.2. FRP Distribution

Since FRP sheets are more effective when placed in the direction of its fibers, FRP sheets have to be applied in such direction to prevent shear cracks from widening.

Typically, the fibers are oriented vertical to the beam axis or perpendicular to the shear crack as shown in Figure 2.3. FRP fibers can also be oriented at 45° to attain additional control for shear crack widening. Finally, as illustrated in Figure 2.4, FRP fibers can also be oriented at two different directions to increase the effectiveness of the shear strengthening system by providing additional control for shear crack widening. The application of bi-axial FRP systems consists on applying two unidirectional FRP sheets in perpendicular directions.

(a) FRP fibers oriented at 90°   (b) FRP fibers oriented at 45°
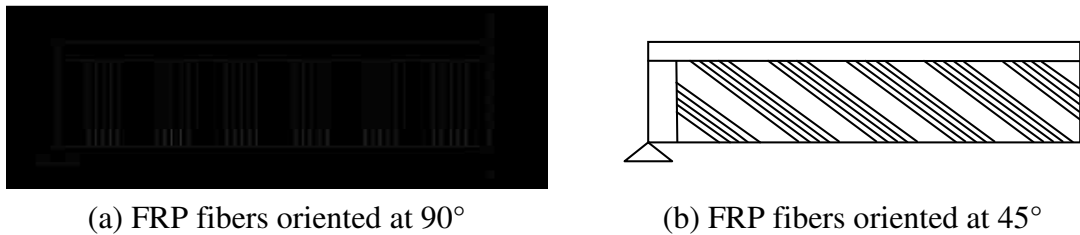
Figure 2.3. FRP Fiber Orientations

(a) FRP fibers oriented at 90°/0°   (b) FRP fibers oriented at 45°/135°
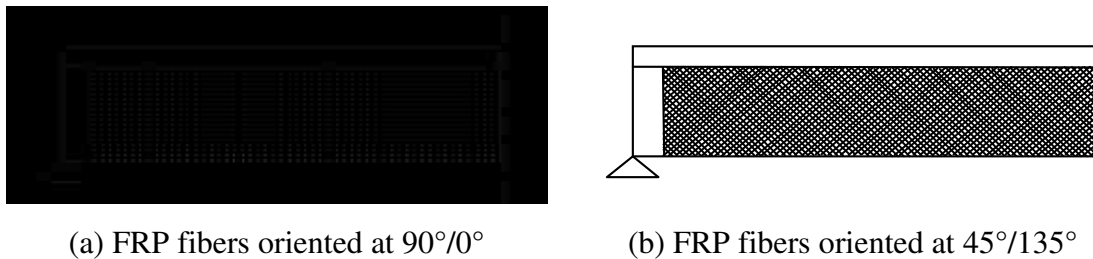
Figure 2.4. Bi-axial FRP Fiber Orientations

2.2.2. Failure Modes. From previous experimental studies, RC structures shear-strengthened with FRP sheets mostly fail by diagonal tension. This failure may be initiated prematurely due to FRP debonding (Figure 2.5) or correspond to fracture of the FRP system (Figure 2.6). In addition due to strain variations in the FRP along the shear

crack, local debonding at both sides of the shear crack may occur before ultimate failure is governed by fracture of the FRP.

Shear failure due to FRP debonding mostly occurs in the concrete at a small distance from the concrete/adhesive interface. Since debonding failure of the FRP occurs in the concrete, the properties related to the concrete are crucial in this mode of failure (Chen and Teng, 2003a). Previous experimental investigations indicate that most RC members strengthened by side-bonded scheme usually fail due to FRP debonding. Additionally, some members strengthened with U-wrapped schemes fail due to FRP debonding.

Shear failure due to FRP fracture occurs with the development of a diagonal shear crack. As the width of the diagonal crack increases, the FRP sheet eventually reaches its ultimate strain, and fractures, which often occurs at the lower end of the shear crack. Fracture of the FRP continues to propagate along the shear crack leading to brittle failure of the RC member. From previous experimental studies, RC members strengthened with fully-wrapped FRP usually fail due to FRP fracture. Some members strengthened with U-wrapped schemes sometimes also fail in fracture.

Figure 2.5. Shear Failure due to FRP Debonding (Khalifa, 1999)

Figure 2.6. Shear Failure due to FRP Fracture (Cao et al., 2005)

2.2.3. Effects of Anchorage Systems. From numerous experimental investigations, it has been proven that anchorage of FRP systems increases the shear contribution provided by FRP composite materials. Anchorage between the FRP sheet and concrete may develop in two forms.

The first form of providing anchorage between the FRP sheet and concrete is by ensuring that the bond at the FRP/concrete interface is maintained. This type of anchorage can provide adequate bond strength on either side of the shear crack. Chajes et al. (1995) determined that extra bond strength cannot be achieved by increasing the available bond length. Therefore, there exists an effective bond length beyond which an extension of the bond length cannot increase the bond strength (Chen and Teng 2003a). For these reasons, the application of other anchorage systems is required, to insure FRP sheets do not detach from the concrete.

The other form of providing adequate anchorage between the FRP composite and concrete is the application of mechanical or other types of anchorage systems. Experimental investigations on the effects of anchorage systems have been developed by many researches. Sato et al. (1997) applied mechanical anchorage by means of a steel plate attached by bolting to the compression zone of the web as shown in Figure 2.7.

From the experimental results, Sato et al (1997) reported that this anchorage system effectively increased the bond strength between the FRP and the concrete, and as a consequence, the FRP shear contribution to shear capacity increased. However, one of the main disadvantages of this anchorage system is that stress concentration may develop where the mechanical anchorage system is placed. In addition, discontinuity of the FRP system due to steel bolts could be another disadvantage in applying this anchorage system.
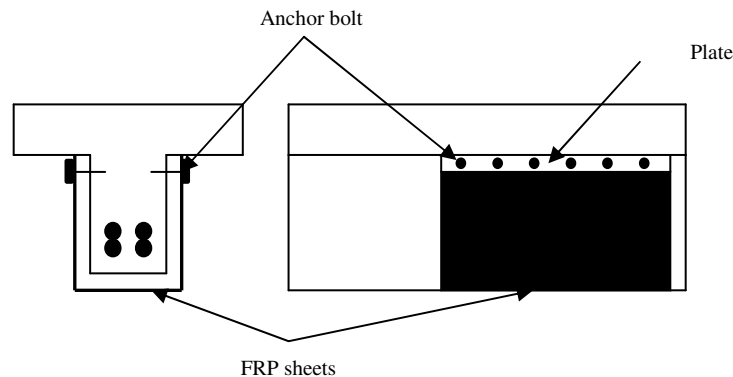
Figure 2.7. Mechanical Anchorage System by Sato et al. (1997)

Khalifa (1999b) introduced the concept of applying a U-anchor system. This anchorage system was obtained by grooving the concrete flanges at the corner along the entire length of the beam, as shown in Figure 2.8. Then, the FRP sheets are attached to the concrete surface and the walls of the groove. The groove was then half filled with a high viscosity epoxy paste. Afterwards, a FRP rod was placed into the groove, and it was then filled with epoxy paste. From this investigation, this anchorage system not only significantly increased the shear capacity, but also modified the failure mode from shear failure due to FRP debonding to flexural failure. In addition, Khalifa (1999b) concluded that this anchorage system avoided high stress concentration and durability issues in

comparison to the traditional mechanical anchorage systems made of steel plates and bolts.

Micelli et al. (2002) also applied the U-anchor system for the strengthening of short shear spans RC T-joists. This anchorage system increased the shear capacity of the FRP system; however, debonding failure due to anchor pullout could not be prevented. Therefore, the effectiveness of this anchoring configuration needs to be further investigated for members with short shear spans because of potential anchor pullout failure around the web-flange corner.
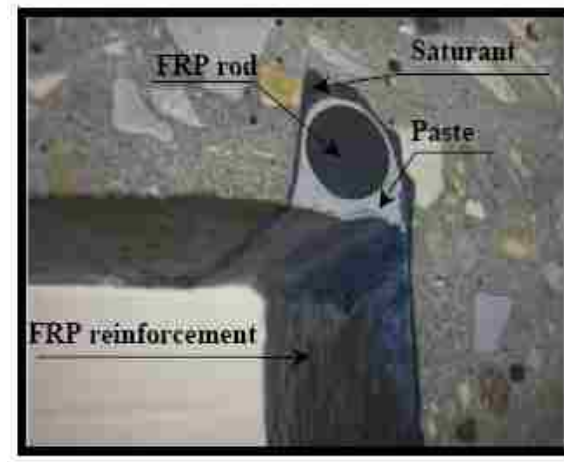
Figure 2.8. U-anchor System by Khalifa (1999b)

Finally, Schuman (2002) applied a mechanical anchorage system to increase the shear contribution of CFRP systems by means of embedding anchor rods into the cross-section with the use of a GFRP bearing plate. Schuman performed an experimental program which covered bonded anchor rods without tying the externally bonded L-shaped CFRP systems to the longitudinal reinforcement, and anchor rods embedded past the longitudinal reinforcement as shown in Figures 2.9 (a) and (b), respectively. From this investigation, Schuman (2002) concluded that the application of shallow anchors lead to an increase in load carrying and displacement capacity. In addition, the shallow

anchors caused the CFRP reinforcement to be activated before the steel reinforcement yielded. The application of deeper anchors showed to be more beneficial in using this anchorage system because the CFRP reinforcement was activated earlier and delayed the yielding in the steel stirrups.

(a) Shallow embedment depth   (b) Deep embedment depth
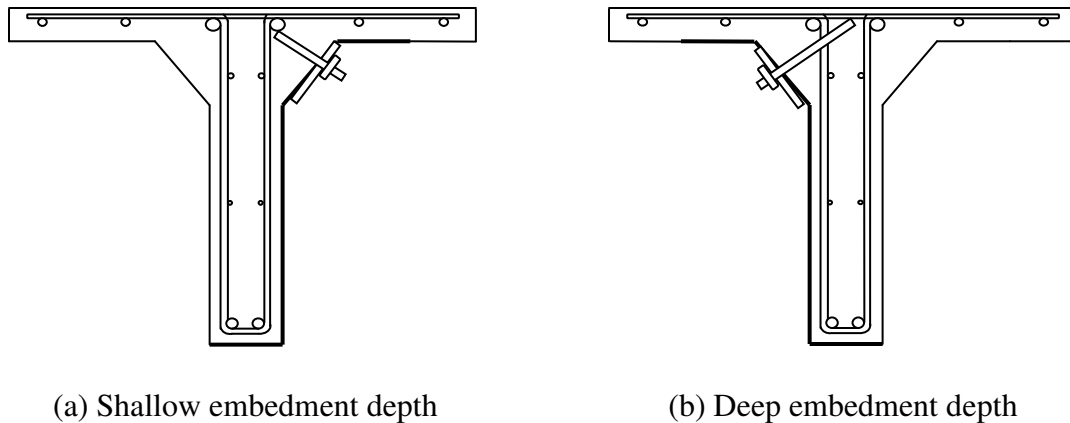
Figure 2.9. Mechanical Anchorage System by Schuman (2002)

2.3. EXISTING EXPERIMENTAL WORK

The following section presents experimental studies on the behavior of RC members shear-strengthened with externally-bonded FRP sheets. Experimental data are collected from these investigations and assembled in a database that will be discussed in Section Three.

Sato et al. (1996) tested RC beams with various wrapping schemes to demonstrate the effectiveness of FRP sheets. From this study, U-wrapped schemes were found to be more effective than side-bonded scheme. In addition, the authors concluded that the FRP strain along the shear crack is high at the middle of the shear crack, and low at the ends of the crack.

Funakawa et al. (1997) tested RC beams strengthened with continuous and fully-wrapped FRP sheets with different thickness. From this study, the authors indicated that

the shear capacity increased with the increase of FRP sheet thickness. They also confirmed that FRP fibers did not reach their ultimate tensile strength at failure.

Kamiharako (1997) tested RC beams with fully-wrapped FRP strips. Two tested-beams did not use epoxy resin to examine the effect of bond strength. From the test results, the shear capacity of beams with bonded FRP strips is higher than that of unbonded FRP strips. The authors proposed a design model assuming that the strain distribution of FRP along the shear crack is not uniform.

Sato et al. (1997) applied mechanical anchorage by means of a steel plate attached by bolting to the compression zone of the web. From the experimental results, Sato et al (1997) determined that this anchorage system effectively increased the bond strength between the FRP and the concrete.

Taerwe et al. (1997) tested RC beams strengthened with U-wrapped FRP strips and continuous sheets. The authors concluded that considerable shear strengthening can be obtained by applying FRP sheets. They also suggested that FRP increases the shear capacity in a similar way to that of steel reinforcement.

Taljsten (1997) presented three different methods for the application of CFRP sheets to RC beams; hand lay-up systems, vacuum injection systems and pre-preg systems. Test results showed that the application of FRP systems increased the shear capacity; however, significant energy was released at failure, which led to brittle failures. This study also concluded that the use of hand lay-up systems were preferable than the other systems.

Umezu et al. (1997) carried out an extensive investigation to determine the effects of fully-wrapped AFRP and CFRP sheets on the shear capacity of RC beams. The authors concluded that the FRP sheets enhanced the shear capacity. In addition, they concluded that the AFRP shear contribution can be evaluated by applying the truss theory, based on an average AFRP stress equal its tensile strength multiplied by a reduction coefficient, which was found to be 0.4 from the analysis.

Khalifa et al. (1999a) carried out an experimental program that consisted of two-span continuous beams with different FRP wrapping schemes. The test results indicated that FRP sheets could be used to enhance the FRP shear capacity in both positive and negative moment regions. In addition, the authors concluded that the FRP shear

contribution increases for beams without stirrups than those with adequate steel shear reinforcement. The authors also proposed a design model, based on truss theory and a reduced ultimate FRP strength

Khalifa and Nanni (2000a) carried out an investigation to determine the effects of different configurations of CFRP sheets on the shear capacity of RC T-beams. The authors concluded that the FRP can increase the shear capacity of RC beams significantly. In addition, the test results indicated that the most effective FRP configuration was the U-wrapped with end anchorage. The authors also proposed a design algorithm to predict the shear capacity of RC members. Results indicated that this design model is conservative and acceptable.

Khalifa et al. (2000b) investigated the performance of RC T-beams shear strengthened with FRP sheets. For this purpose, externally applied FRP sheets and near-surface mounted (NSM) FRP rods were used. Tests results confirmed that externally bonded CFRP sheets and NSM CFRP rods can be used to increase the shear capacity. The test results were also used to validate a previously proposed design approach.

Deniaud and Cheng (2001) investigated the interaction between the concrete, steel stirrups, and external FRP sheets in carrying shear loads in RC beams. Three types of FRP sheets were applied: uniaxial GFRP, uniaxial CFRP, and triaxial GFRP. Test results showed that FRP systems enhance the shear capacity of RC beams. This increase is shear capacity was found to be not only dependent on the FRP type, but also on the amount of steel stirrups. In addition, the FRP strains were found to be uniformly distributed along the shear crack. The authors also proposed a design approach based on the failure mechanisms of the tested specimens.

Li et al. (2002) carried out an extensive investigation on the performance of RC beams shear strengthened with CFRP sheets. Test results indicated that the shear capacity increases as the area of FRP composite increases. In addition, test results indicated that the FRP shear contribution increases as the spacing between stirrups increases. This study also concluded that the FRP shear contribution depends on the presence of longitudinal and vertical steel reinforcement. The authors proposed an analytical approach to predict the FRP shear contribution. The results obtained from this approach were found to be in close agreement to the observed test results.

Khalifa and Nanni (2002) examined the performance of RC beams shear strengthened with CFRP sheets. The parameters investigated in this experimental study were the presence of internal steel reinforcement, shear span-to-depth ratio, and the amount and distribution of FRP reinforcement. Test results indicated that the FRP shear contribution is affected by the shear span-to-depth ratio. In addition, it was concluded that additional FRP reinforcement does not reflect in an increase of FRP shear contribution. The FRP shear contribution was also to be dependent on the presence of internal steel reinforcement.

Pellegrino and Modena (2002) investigated the behavior of RC beams shear strengthened with side-bonded FRP sheets. This study is based on an experimental program carried out on beams with and without transverse steel reinforcement. The test results provided insight in the interaction between FRP sheets and internal steel reinforcement. From the experimental study, the authors reported that the efficiency of the FRP strengthening decreases not only when the rigidity of the FRP sheets increases, but also when the ratio between the amount of transverse steel reinforcement and that of FRP shear reinforcement increases. To account for this effect, Pellegrino and Modena introduced an additional reduction factor, which acts as a further reduction when transverse steel reinforcement is present.

Deniaud and Cheng (2003) conducted an experimental investigation on the behavior of RC T-beams shear strengthened with FRP sheets. Three types of FRP sheets were applied: uniaxial GFRP, uniaxial CFRP, and triaxial GFRP. Test results indicated that the FRP shear contribution is not only dependent on the FRP type, but also on the amount of transverse steel reinforcement. In addition, the authors concluded that the shear forces carried by arching action are delayed when FRP sheets are used. In addition, it was concluded that the triaxial GFRP sheet provided the beam with more ductile failure. The authors also presented a rational analytical model that predicted the experimental results accurately.

Taljsten (2003) presented examples of shear strengthening methods, among them shear strengthening with CFRP sheets. In addition, a field application of a parking slab shear strengthened with unidirectional CFRP sheets is presented. The experimental

results demonstrated the importance of considering the principal directions of the shear crack in relation to the unidirectional fiber.

Adhikary et al. (2004) carried out an experimental investigation that focused on the behavior of RC beams shear strengthened with FRP sheets. This study focused on the effect of extending the length of the FRP sheet on the top surface of the beam to delay or prevent debonding failure. From test results, it was confirmed that FRP sheets with bonded anchorage is more effective than U-wrapped schemes without anchorage. The author also presented two equations for determining the FRP shear contribution, one was developed based on FRP debonding and the other one based on bonded anchorage.

Monti and Liotta (2005) performed tests involving 24 RC beams with rectangular cross-sections and with transverse steel reinforcement. They used totally-wrapped, U-wrapped and side-bonded CFRP strips and sheets at 90°, 45°, and 60° fiber orientations. The authors proposed an analytical model to predict the shear contribution of FRP based on fracture mechanics. The authors first defined the generalized constitutive law of an FRP layer bonded to concrete. Then, the compatibility imposed by the shear crack opening and the appropriate boundary conditions were included on the formulations to predict the shear contribution of FRP. Finally, analytical expressions that depict the behavior of the stress field in the FRP crossing a shear crack were obtained.

Carolin and Taljsten (2005a) used a database consisting of 23 RC beams with rectangular cross-sections, with and without transverse steel reinforcement. The database consisted of CFRP sheets with fibers oriented at 45 and 90 degree fiber orientation. The wrapping configurations consisted on fully-wrapping and two-side bonded FRP systems. Some of the RC beams were precracked before the strengthening was applied, while other beams were subjected to fatigue loading after strengthening. From the experimental study, Carolin and Taljsten (2005b) derived a modified truss model that takes into account the non-uniformity of the strain distribution and the anisotropy of the composite.

Bousselham and Chaallal (2006a) presented an extensive experimental investigation on RC T-beams shear strengthened with CFRP sheets. Test results indicated that the FRP shear contribution is not proportional to the FRP stiffness. In addition, it was confirmed that the FRP shear contribution depends on the presence of

internal steel reinforcement. The influence of the shear span-to-depth ratio on the FRP shear contribution was also confirmed. Finally, a comparison between the experimental results and the predictions from four design guidelines was performed. From this analysis, it was concluded that these guidelines fail to take into account important parameters that affect the FRP shear contribution, and overestimate the shear resistance for high FRP stiffness.

2.4. EXISTING ANALYTICAL MODELS

This section introduces analytical models developed from 1995 to 2005 that determine the shear capacity of RC members shear strengthened with FRP sheets. A total of fourteen analytical models were found from the literature. The analytical models that will be discussed in detail in Section Four are: (1) Chajes et al. (1995), (2) Triantafillou (1998), (3) Khalifa et al. (1998), (4) Khalifa et al. (1999), (5) Triantafillou and Antonopoulos (2000), (6) Pellegrino and Modena (2002), (7) Chaallal et al. (2002), (8) Hsu et al. (2003), (9) Chen and Teng (2003a-b), (10) Deniaud and Cheng (2004), (11) Monti and Liotta (2005), (12) Cao et al. (2005), (13) Zhang and Hsu (2005), and (14) Carolin and Taljsten (2005b).

2.5. EXISTING DESIGN GUIDELINES

This section introduces the design methodologies in the application of FRP composite systems for strengthening of RC structures. From the literature, seven design guidelines were collected. The following are the design guidelines that will be discussed in detail in Section Four:

1. Japan Building Disaster Prevention Association (JBDPA) Guidelines (1999)
2. Great Britain Technical Report No. 55 (2004)
3. Féderation Internationale Du Béton (fib) Bulletin 14 Task Group 9.3 (2001)
4. Japan Society of Civil Engineers (JSCE) Recommendations (2001)
5. The Canadian Network of Centers of Excellence on Intelligent Sensing for Innovative Structures (ISIS) Design Manual 4 (2001)
6. American Concrete Institute (ACI) 440.2R (2002), and
7. Canadian Standards Association (CSA) S806-02 (2002).

3. PARAMETRIC STUDY OF EXISTING EXPERIMENTAL DATA

3.1. GENERAL

This section identifies criteria that influence the behavior of RC structures shear-strengthened with FRP sheets. For this purpose, an extensive and detailed database has been developed for data analysis (refer to Table A.1 in Appendix A). From the database, the parameters that are influential to the behavior of RC structures shear-strengthened with FRP sheets are identified and discussed. The following parameters and criteria are successively subjected to an in-depth analysis: mechanical and geometric properties of FRP, shear span-to-depth ratio, and transverse steel reinforcement. Prior to perform the parametric study of the collected experimental data, a critical discussion of the database is performed. Additionally, other parameters that have not been sufficiently evaluated and documented, but that are influential in the behavior of RC structures strengthened in shear with FRP systems, are also identified and discussed. These parameters include the scale factor effect, longitudinal steel reinforcement and concrete strength.

3.2. EXPERIMENTAL DATABASE

Before performing the parametric study of the collected experimental data, a critical discussion of the database is performed. An extensive and detailed database is developed for data analysis (refer to Table A.1 in Appendix A). The database conveniently allows the identification of certain parameters and criteria that greatly influence the behavior of RC structures strengthened in shear with FRP systems. The shear database covers 283 experimental tests collected from papers and reports dating from 1992 to 2006. A sample of this database is shown in Tables 3.1 through 3.3. This database includes all relevant data from the experimental results, such as the geometry of test specimens, concrete mechanical properties, transverse steel reinforcement properties, longitudinal steel reinforcement properties, FRP properties, observed total shear resistance, shear contribution due to the FRP system, and mode of failure. The consistency of all numerical data presented in this database has been thoroughly verified; however, some specimens have been rejected due to inaccuracy in results or incomplete information.

Table 3.1. Sample of Database - Cross-Section Properties (Uji et al.)

Test No.	Beam Shape	a/d	f'_c (MPa)	Section Dimensions			Longitudinal Reinforcement	Transverse Reinforcement		
				b_w (mm)	d (mm)	d_f (mm)	A_s (mm^2)	f_{yv} (MPa)	A_v (mm^2)	s (mm)
3	Rectangular	2.5	24.1	100	170	170	401.2	-	0	-

Table 3.2. Sample of Database - FRP Properties (Uji et al.)

Test No.	FRP type	w_f (mm)	t_f (mm)	n_f	s_f (mm)	E_f (GPa)	f_{fu} (MPa)	Wrapping Scheme	$\beta°$	ρ_f (x10^{-3})
3	CFRP	1	0.097	1	1	230	2648	Total Wrap	90	1.94

Table 3.3. Sample of Database - Failure Conditions (Uji et al.)

Test Specimen	V_{exp} (kN)	V_f (kN)	Failure Mode
3	58.3	33.8	Fracture

In order to critically discuss the experimental data presented in the database, all experimental data have been distributed with respect to certain parameters. As shown in Table 3.4, nearly 70% of the beam specimens are rectangular beams. However, in practice, T-sections are more widely used than rectangular beams; therefore, additional experimental results on T-beam sections should be included. Additionally, nearly two-thirds of the total beam specimens are slender beams ($a/d \leq 2.5$), and about 70% of beam specimens correspond to beams with a total height larger than or equal to 300 mm. Most beam specimens were tested in the presence of none or less than the minimum amount of internal transverse steel reinforcement since all beam specimens needed to fail

in shear. Nearly 60% of all beam specimens were tested without the presence of transverse steel reinforcement. In addition, as shown in Table 3.5, most experimental specimens correspond to CFRP strengthening systems, which are most widely used in practice because of their excellent mechanical properties. Moreover, U-Wraps are used as wrapping configuration for nearly 42% of the beam specimens. From Table 3.6, FRP fabrics, and FRP fiber orientation at 90 degrees are most used as wrapping schemes for most data specimens. Finally, of the 283 tests, 118 failed due to FRP debonding, 57 failed due to FRP fracture, and 108 failed due to other reasons.

Table 3.4. Number of Specimens in Terms of Cross-Section Properties

Beam Geometry		Beam Cross-Section				Transverse steel reinforcement	
Rectangular Beams	T-Beams	a/d ≥ 2.5	a/d < 2.5	h ≥ 300 mm	h < 300 mm	With stirrups	Without stirrups
198	85	192	86	198	82	114	158

Table 3.5. Number of Specimens in Terms of FRP Properties

FRP Material			FRP Wrapping Configuration				
CFRP	GFRP	AFRP	Sides	U-Wrap	U-Wrap w/ anchor	Total Wrap	Other
233	23	27	56	119	17	81	10

Table 3.6. Continuation of Number of Specimens in Terms of FRP Properties

FRP Distribution		FRP fiber orientation		Failure Modes		
Strips	Continuous	90°	Other than 90°	Fracture	Debonding	Other
98	173	220	63	57	118	108

3.3. PARAMETERS THAT AFFECT THE SHEAR BEHAVIOR OF RC MEMBERS STRENGTHENED IN SHEAR WITH FRP

The parameters that could affect the behavior of RC members strengthened in shear with FRP are discussed and evaluated by performing a comparative analysis of the database. The experimental data from the database is analyzed in terms of $E_f \rho_f / f'_c{}^{2/3}$, which simultaneously includes the effects of the amount of FRP reinforcement (expressed in terms of the FRP ratio, ρ_f), the fiber type (expressed in terms of the modulus of elasticity of FRP, E_f), and the concrete strength, defined as f'_c. Moreover, the database is evaluated in terms of the shear span-to-depth ratio, defined as a/d; and the ratio between the transverse steel and FRP reinforcement, defined as $\rho_s E_s / \rho_f E_f$, where ρ_s represents the transverse steel reinforcement ratio. Each parameter is further evaluated and discussed in terms of the increase in shear due to FRP, defined as $V_f / (V_c + V_s)$; FRP wrapping schemes; and failure modes. The modes of failure included in this analysis are shear failure due to FRP debonding, and shear failure with or without FRP fracture. The latter means that the FRP can carry additional load after the concrete fails. Finally, in this analysis, experimental data that presented flexural failure modes are disregarded.

3.3.1. Effect of Mechanical and Geometric Properties of FRP. If the dominant failure mode of RC members is due to FRP fracture, the type of FRP material is relevant to the shear resistance of the FRP system because of the different fracture capacities among different FRP materials (Triantafillou and Antonopoulos, 2000).

In addition, FRP systems have been proven to increase the total shear resistance of existing RC members by fully-wrapping or partially-wrapping FRP composites around the members. These different wrapping configurations have an effect on the dominant mode of failure. The potential failure modes observed on RC beams shear-strengthened with FRP systems include FRP fracture, shear failure without FRP fracture, and FRP debonding.

The distribution of FRP fibers also influences the performance of the shear strengthening system. The application of FRP strips allows flexibility in controlling the amount of FRP; however the use of continuous FRP sheets allows the interception of all

diagonal cracks. Additionally, FRP fibers can be oriented in different directions in order to effectively control shear cracks. FRP fibers oriented at 45° are more effective in controlling shear cracks; thus the shear resistance is higher than when applying fibers oriented at 90°.

Previous studies have shown that the FRP properties, such as its axial rigidity, play an important role in the shear resistance attributed to FRP systems. These studies have also reported that the strain distribution along a shear crack is not uniform, and because of possible bond failure, it appears that the FRP contribution is limited to an effective tensile strain, ε_{fe}, which is usually lower than the ultimate tensile strain in the FRP. Triantafillou (1998) showed that the FRP effective strain decreases as its axial rigidity increases. On a later study, Triantafillou and Antonopoulos (2000) reported that the FRP effective strain not only depends on its axial rigidity, but also on the concrete compressive strength. This is attributed to the fact that the effective FRP strain depends on the development length, which is the length necessary to reach FRP fracture before debonding occurs. The development length is proportional to the FRP axial rigidity and inversely proportional to the tensile concrete strength, which is a function of its compressive strength and is defined as $f'^{2/3}_c$ (Triantafillou and Antonopoulos 2000). Therefore, the parameter $E_f\rho_f / f'^{2/3}_c$ is taken into consideration for data analysis.

From analyzing the shear gain versus $E_f\rho_f / f'^{2/3}_c$ for all test specimens that failed due to FRP debonding and other shear failure modes, no clear trendline could be observed. Therefore, to refine the analysis further, the influences of the presence of transverse steel reinforcement and the type of beam (slender vs. deep) are eliminated. Figure 3.1 illustrates the increase in shear resistance due to the FRP in terms of $E_f\rho_f / f'^{2/3}_c$ only for slender beams without transverse steel reinforcement. For specimens that failed due to FRP debonding, no clear trendline could be observed for specimens strengthened with U-wrapped FRP systems. However, for other type of strengthening schemes, an increasing trend is observed as $E_f\rho_f / f'^{2/3}_c$ increases. It seems though that beyond $E_f\rho_f / f'^{2/3}_c$ equal to 0.08, additional amount of FRP does not reflect an increase in the shear gain as shown in Figure 3.1(a). The same trend is observed for specimens failing due to other shear failure modes. It can be observed that

beyond $E_f \rho_f / f'^{2/3}_c$ equal to 0.05, additional amount of FRP does not reflect an increase in the shear gain as shown in Figure 3.1(b).
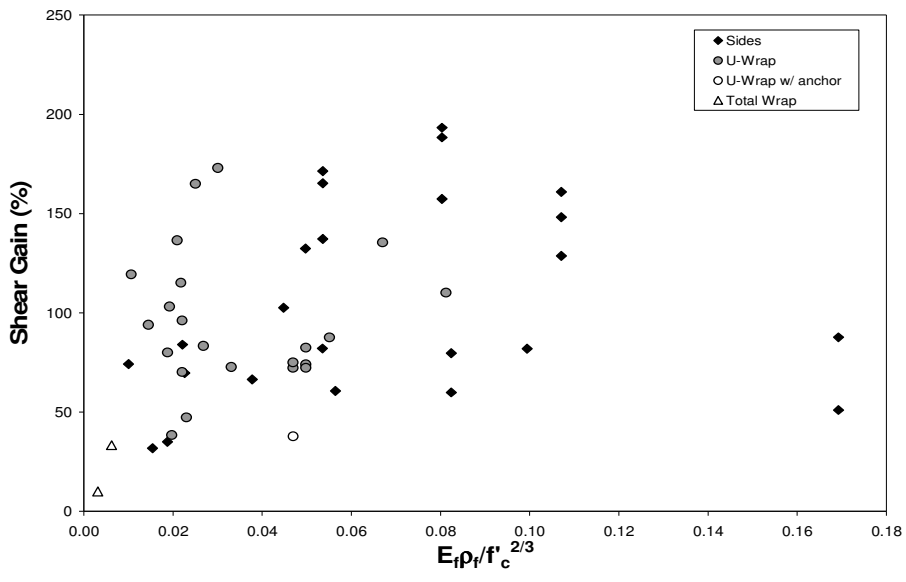
(a) FRP Debonding
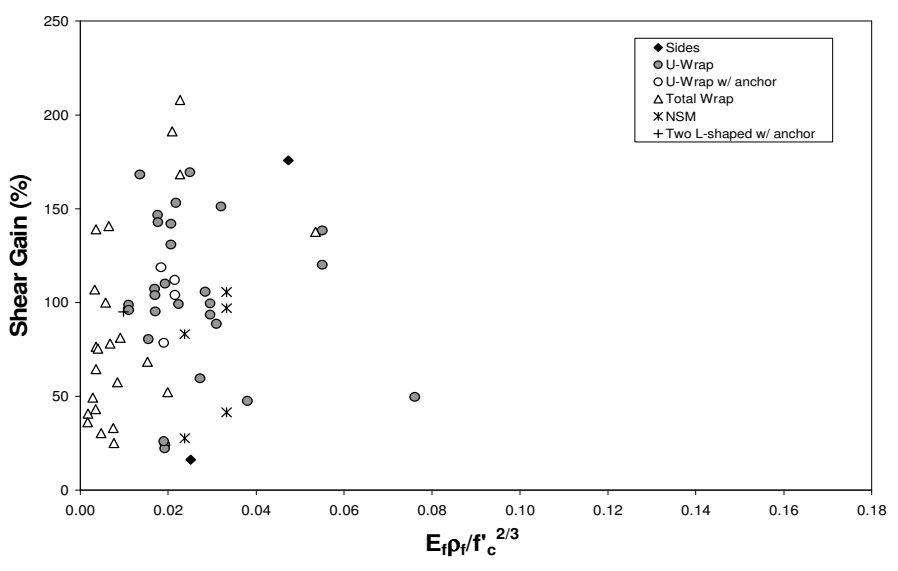
(b) Other Shear Failure Modes

Figure 3.1. Shear Force Gain vs. $E_f \rho_f / f'^{2/3}_c$ – Slender Beams without Transverse Steel Reinforcement

**3.3.2. Effect of Shear Span-to-Depth Ratio.** The shear span-to-depth ratio plays an important role in the behavior of RC members shear-strengthened with FRP systems. The behavior of slender members ($a/d \geq 2.5$) is different from that of deep members ($a/d < 2.5$). Most experimental and analytical studies have focused on the performance of slender beams strengthened in shear with FRP systems. However, the studies from Chaallal et al. (2002) and Zhang et al. (2004) reported test results on the performance of deep beams strengthened in shear with FRP sheets. However, these studies did not provide a comparison in the behavior between slender and deep beams. Most recently, Bousselham and Chaallal (2006b) reported the influence and difference in behavior in both slender and deep beams strengthened with FRP systems. They indicated that deep beams provide higher shear resistance; however, the gain in shear capacity due to additional FRP is minimal. This could be attributed to arch action, which is the characteristic behavior of deep beams. For all these reasons, the influence of the shear span-to-depth ratio to the shear resistance has been clearly indicated in previous studies; however, most design guidelines have not yet included the influence of this parameter when developing formulations to compute the FRP shear contribution.

Figure 3.2 illustrates the increase in the shear contribution attributed to the FRP systems in terms of the shear span-to-depth ratio for specimens without transverse steel reinforcement failing due to FRP debonding or other shear failure modes. In addition, Figure 3.3 illustrates the shear gain due to the FRP systems in terms of the shear span-to-depth ratio for specimens with transverse steel reinforcement. From these figures, it can be observed that the increase in shear gain attributed to the FRP seems to be greater for slender beams ($a/d \geq 2.5$). This could be due to arch action in a way that, in comparison to slender beams, the externally applied FRP reinforcement does not significantly contribute to the shear resistance. In addition, it can be observed that test specimens that failed due to FRP debonding are more frequent in members with higher a/d ratios. Furthermore, by comparing the beams with and without transverse steel reinforcement, it can be confirmed the effect of transverse steel reinforcement on additional shear gain due to FRP systems. This additional gain in shear due to the FRP is smaller in beam specimens with transverse steel reinforcement than in beam specimens without transverse steel reinforcement.
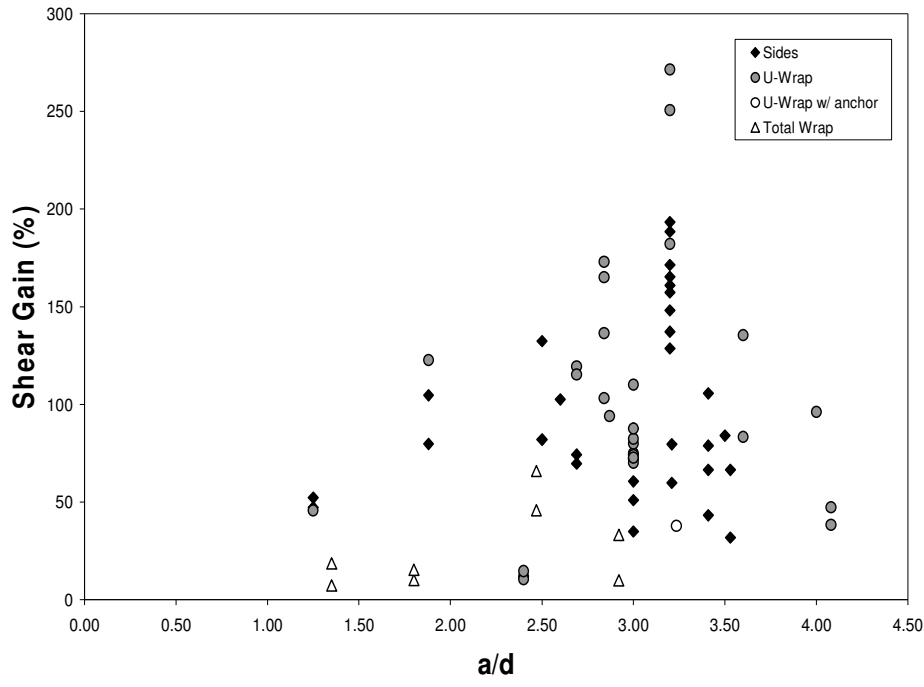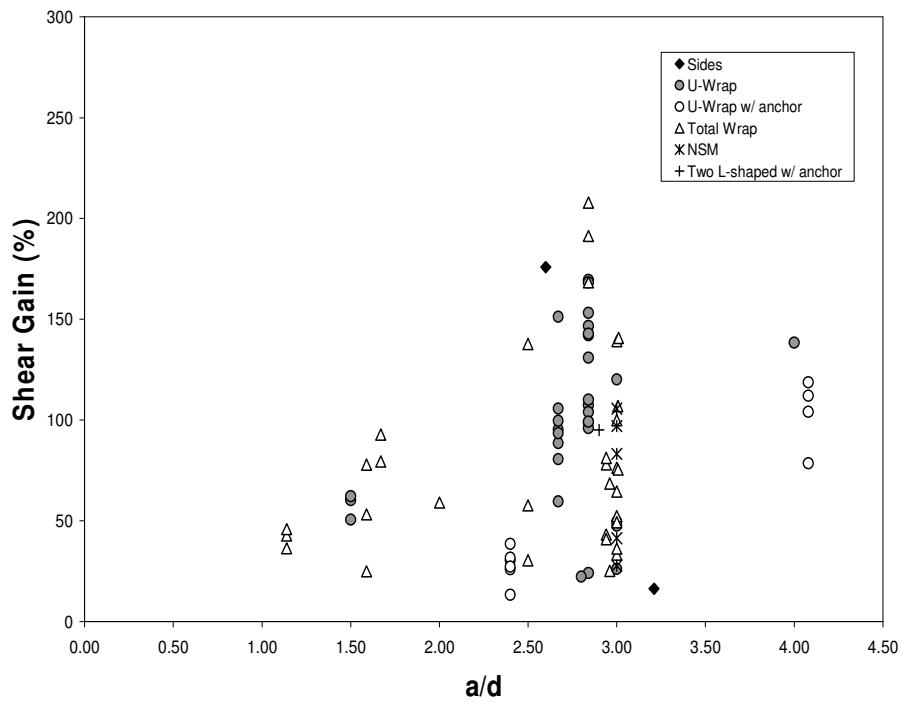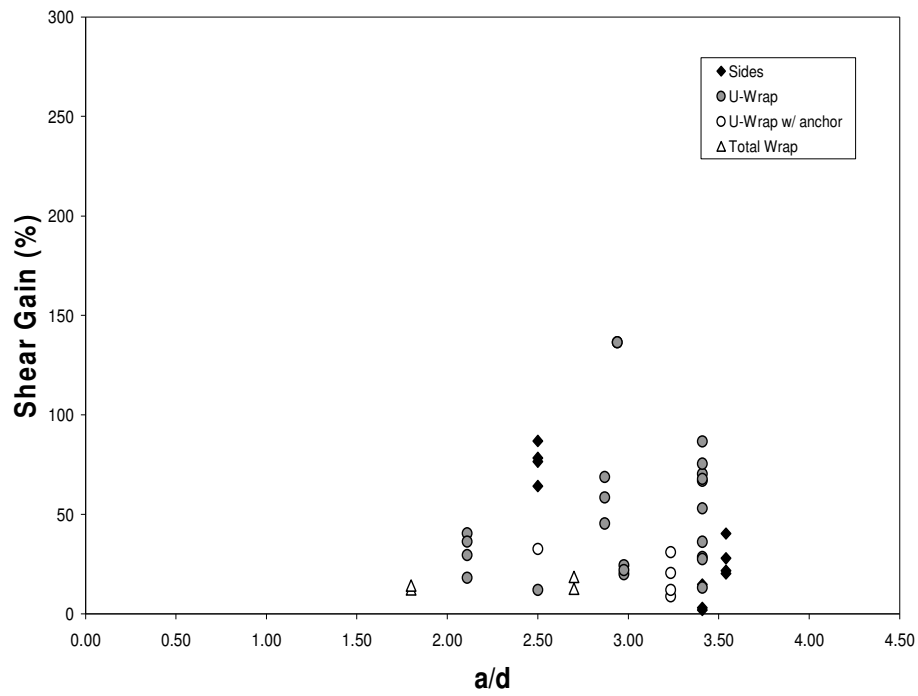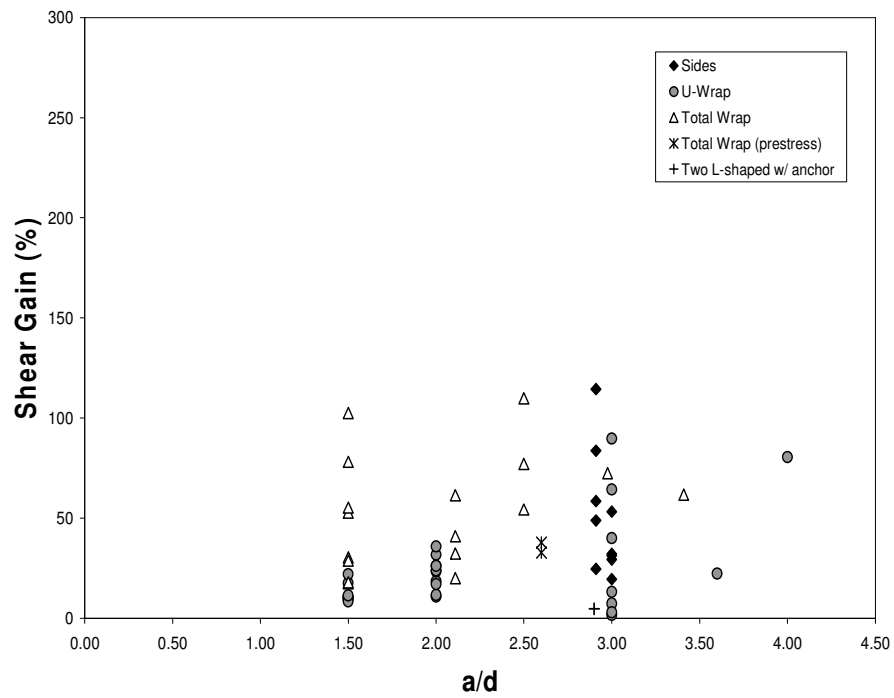
(a) FRP Debonding

(b) Other Shear Failure Modes

Figure 3.2. Shear Force Gain vs. a/d - Beams without Transverse Steel Reinforcement

(a) FRP Debonding

(b) Other Shear Failure Modes

Figure 3.3. Shear Force Gain vs. a/d - Beams with Transverse Steel Reinforcement

3.3.3. Effect of Transverse Steel Reinforcement. The presence of transverse steel reinforcement greatly influences the behavior of RC members strengthened with FRP systems. Numerous studies have shown that the contribution to shear resistance of externally bonded FRP is less in beams strengthened with FRP and containing internal transverse steel than in the same retrofitted beams without internal transverse steel (Pellegrino et al. 2002, Chaallal et al. 2002, Bousselham and Chaallal 2004). Most recently, Bousselham and Chaallal (2006 a-b) reported that additional internal steel reinforcement results in a significant decrease of shear gain provided by FRP systems in slender beams. However, this influence is minimal in the case of deep beams. This study also showed that the internal transverse steel is less stressed in the presence of FRP reinforcement. However, the mechanisms that play a role in the interaction between the transverse steel reinforcement and the externally-bonded FRP reinforcement are not completely understood; therefore, additional experimental and analytical investigations are recommended.

Figure 3.4 illustrates the increase in the shear contribution attributed to the FRP systems in terms of the amount of transverse steel reinforcement for slender beams failing due to FRP debonding or other shear failure modes. In addition, Figure 3.5 illustrates the shear gain due to the FRP systems in terms of the amount of transverse steel reinforcement for deep beams. These figures clearly indicate that the gain in shear resistance due to FRP decreases as the ratio of $\rho_s E_s / \rho_f E_f$ increases. Some data points in these figures present very low values of shear gain due to the FRP because the failure load did not reach the maximum load attained by the corresponding control specimen. Furthermore, Figures 3.4 and 3.5 show that the gains in shear due to the FRP systems for beams with transverse steel reinforcement are greater in slender beams than those corresponding to deep beams.

Finally, from the data analysis, it can be concluded that the influence of the transverse steel reinforcement on the FRP contribution to the total shear resistance of RC members can be now confirmed by this experimental analysis. However, additional experimental and analytical investigations may be needed to provide a better understanding of the mechanisms involved in the interaction between transverse steel and FRP reinforcement.
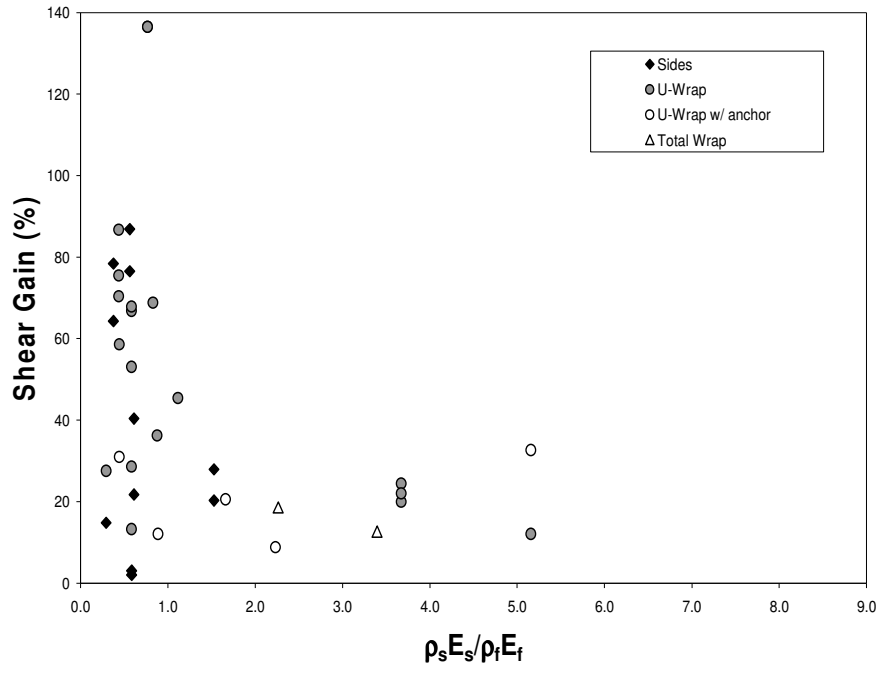
(a) FRP Debonding
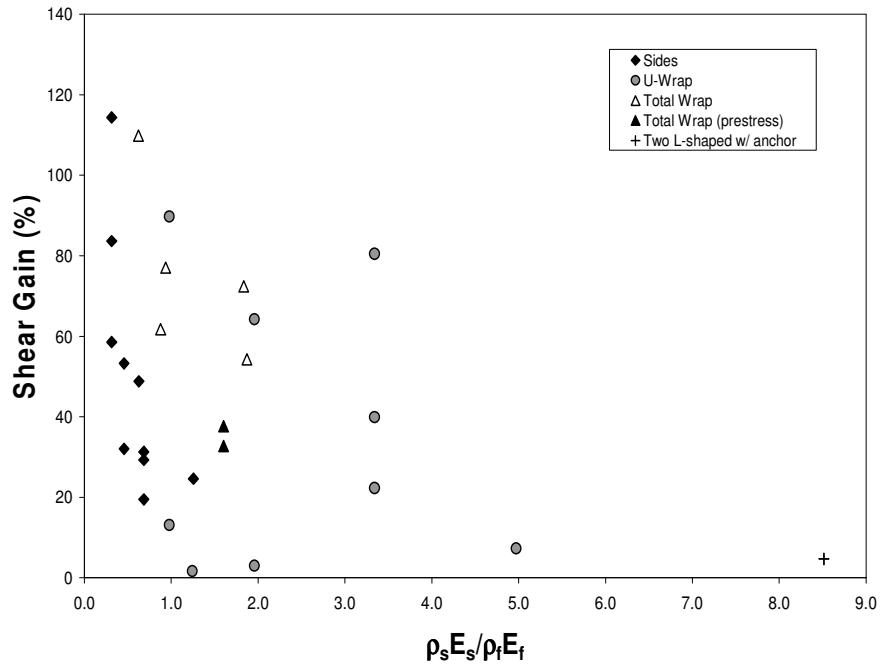
(b) Other Shear Failure Modes

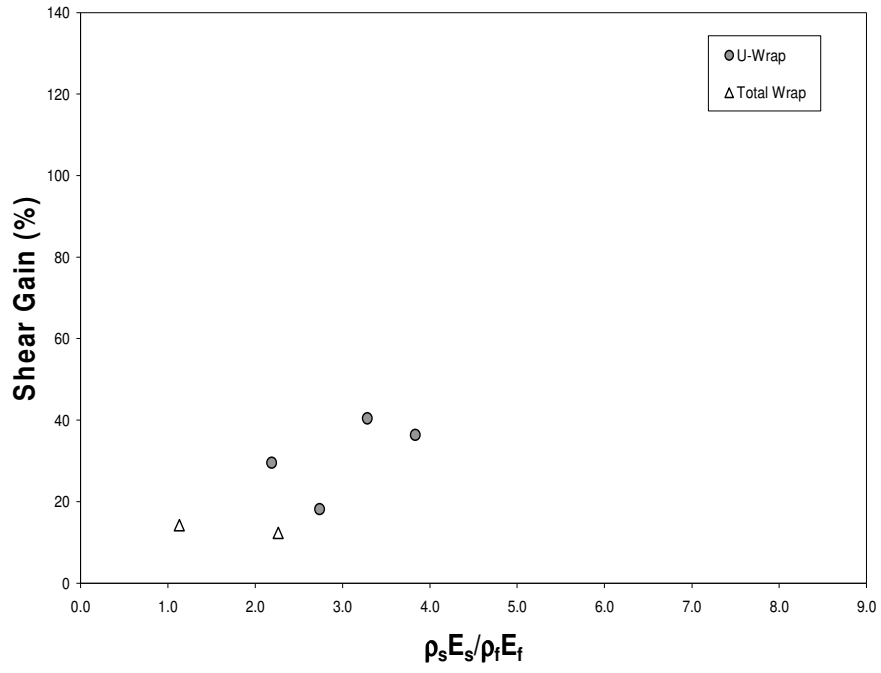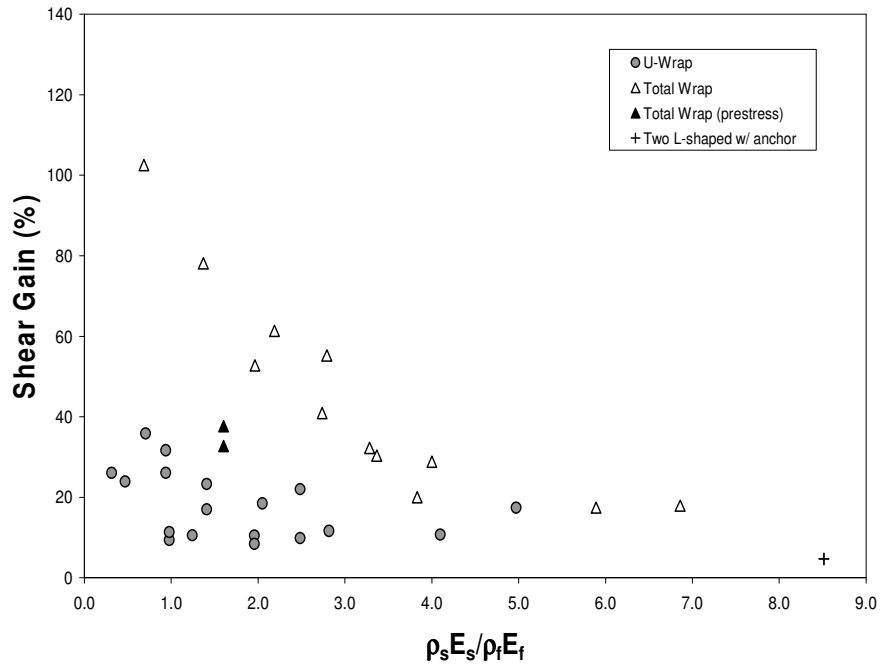Figure 3.4. Shear Force Gain vs. $\rho_s E_s / \rho_f E_f$ - Slender Beams

(a) FRP Debonding

(b) Other Shear Failure Modes

Figure 3.5. Shear Force Gain vs. $\rho_s E_s / \rho_f E_f$ - Deep Beams

3.3.4. Effect of Other Parameters. Other parameters relevant to the behavior of RC members strengthened in shear with FRP, which have not been thoroughly analyzed and documented in previous studies, are discussed in this section.

3.3.4.1 Effect of scale factor. The majority of the experimental tests in the database correspond to small specimens. However, numerous studies have determined the influence of the size of RC beams without transverse steel reinforcement to the shear resistance. These studies reported that as the depth of beams increases, the crack widths tend to increase, which results on a reduction of the shear stress (Mac Gregor and Wight, 2005). The assessment of the scale factor performed by Bousselham and Chaallal (2004) indicated that the gain in shear resistance due to FRP decreases as the effective depth of the RC beams increases. Most analytical models and design guidelines that compute the FRP shear contribution have been derived based on the experimental results of small test specimens. However, since it appears the scale effect plays an important role in the behavior of RC members strengthened in shear with FRP, the reliability of these analytical models and design approaches need to be confirmed. As a consequence, additional in-depth investigations are required to provide a better understanding of the effect of this parameter.

3.3.4.2 Effect of longitudinal steel reinforcement. Numerous studies have determined the influence of longitudinal steel reinforcement to the shear resistance. It has been established that the lower the longitudinal reinforcement ratio, the larger the cracks, thus the contribution from the aggregate interlocking decreases. The assessment of this parameter performed by Bousselham and Chaallal (2004) indicated that the gain in shear resistance due to the FRP decreases as the amount of longitudinal steel reinforcement increases. Therefore, it appears that the longitudinal steel reinforcement affects the shear strength of beams strengthened with FRP systems.

3.3.4.3 Effect of concrete strength. The bond strength between the FRP and concrete surface depends on the compressive strength of concrete. As the concrete compressive strength becomes stronger, the bond strength between FRP systems and concrete also increases (Zhang and Hsu, 2005); therefore, failure due to FRP debonding is avoided. Previous analytical and experimental study from Horiguchi and Saeki (1997)

have shown that the bond strength between FRP sheets and the concrete surface is proportional to the 2/3 power of the concrete compressive strength.

Despite its importance with regards to the performance of shear strengthening with FRP, the effect of concrete strength has not been thoroughly evaluated and analyzed. However, it is important to note that most design guidelines for RC structures strengthened with externally applied FRP take into account the concrete strength when estimating the FRP shear contribution, such as ACI-440.2R (2002), *fib* TG 9.3 (2001), JSCE Recommendation (2001), and the Great Britain Technical Report No. 55 (2000). Therefore, the influence of this parameter needs to be further evaluated and analyzed.

3.4. SUMMARY AND CONCLUDING REMARKS

In order to attain a better understanding of the parameters that influence the behavior of RC members shear strengthened with FRP systems, an extensive and detailed database was developed for data analysis (refer to Table A.1 in Appendix A). The shear database covered 283 experimental tests collected from papers and reports dating from 1992 to 2006. This database included all relevant data from the experimental results, such as the geometry of test specimens, concrete mechanical properties, transverse and longitudinal steel reinforcement properties, FRP properties, shear span-to-depth ratio, ultimate load, shear contribution due to FRP, and failure mode.

After a critical review of the shear database, an in-depth analysis of the experimental data was performed to identify the major parameters and criteria that influence the behavior of RC beams shear-strengthened with externally applied FRP systems. For this purpose, the tests specimens from the subset data were analyzed in terms of the FRP axial rigidity and the concrete compressive strength, defined as $E_f \rho_f / f'^{2/3}_c$; the shear span-to-depth ratio (a/d); and the interaction between transverse steel reinforcement and FRP reinforcement, defined as $\rho_s E_s / \rho_f E_f$. Each parameter was further evaluated and discussed in terms of the increase in shear due to FRP, defined as $V_f / V_c + V_s$; FRP wrapping scheme; and failure modes. The modes of failure included in this analysis were shear failure due to FRP debonding, FRP fracture and other shear failure modes. From the data analysis and evaluation, the following observations can be drawn:

1. As extensively confirmed in previous studies, the parameters related to the FRP properties have a significant influence on the shear behavior of RC members shear-strengthened with FRP systems. From the evaluation for specimens that failed in debonding, no clear trendline could be observed for specimens strengthened with U-wrapped FRP systems. However, for other type of strengthening schemes, an increasing trend is observed as $E_f \rho_f / f'_c{}^{2/3}$ increases. However, beyond $E_f \rho_f / f'_c{}^{2/3}$ equal to 0.08, additional amount of FRP does not reflect an increase in the shear gain. The same trend is observed for specimens failing in other shear failure modes. For $E_f \rho_f / f'_c{}^{2/3}$ values beyond 0.05, additional amount of FRP does not reflect an increase in the shear gain..

2. The influence of the shear span-to-depth ratio on the shear behavior of the test specimens was investigated. From this study, it was observed that test specimens that failed due to FRP debonding are more frequent in members with higher a/d ratios. In addition, the increase in shear gain attributed to the FRP seems to be greater for slender beams ($a/d \geq 2.5$). This could be due to arch action in a way that, in comparison to slender beams, the externally applied FRP reinforcement does not significantly contribute to the shear resistance. Furthermore the effect of transverse steel reinforcement on additional shear gain due to FRP systems was observed. This additional shear gain is smaller in beam specimens with transverse steel reinforcement than in beam specimens without transverse steel.

3. The influence of transverse steel reinforcement has been confirmed in the present study. The gain in shear resistance due to FRP decreases as the ratio of $\rho_s E_s / \rho_f E_f$ increases. However, the resistance mechanisms associated with this phenomenon are still not fully understood; therefore, additional experimental investigations, targeted to clarify the influence of transverse steel reinforcement are needed.

4. Additional analytical and experimental studies are required to investigate the effect of the size factor, the longitudinal steel reinforcement and concrete strength on the behavior of RC members strengthened in shear with FRP systems.

4. EXISTING ANALYTICAL MODELS AND DESIGN GUIDELINES ON SHEAR STRENGTHENING OF RC MEMBERS USING FRP SYSTEMS

4.1. INTRODUCTION

This section summarizes existing analytical models and design guidelines, developed since 1995 up to 2005 to determine the shear strength of RC members strengthened with FRP systems. A total of fourteen analytical models and seven design guidelines are discussed as shown in Figure 4.1. This figure also shows how some design guidelines relate to certain analytical models in terms of their similar approach to determine the FRP shear contribution, defined as V_f.
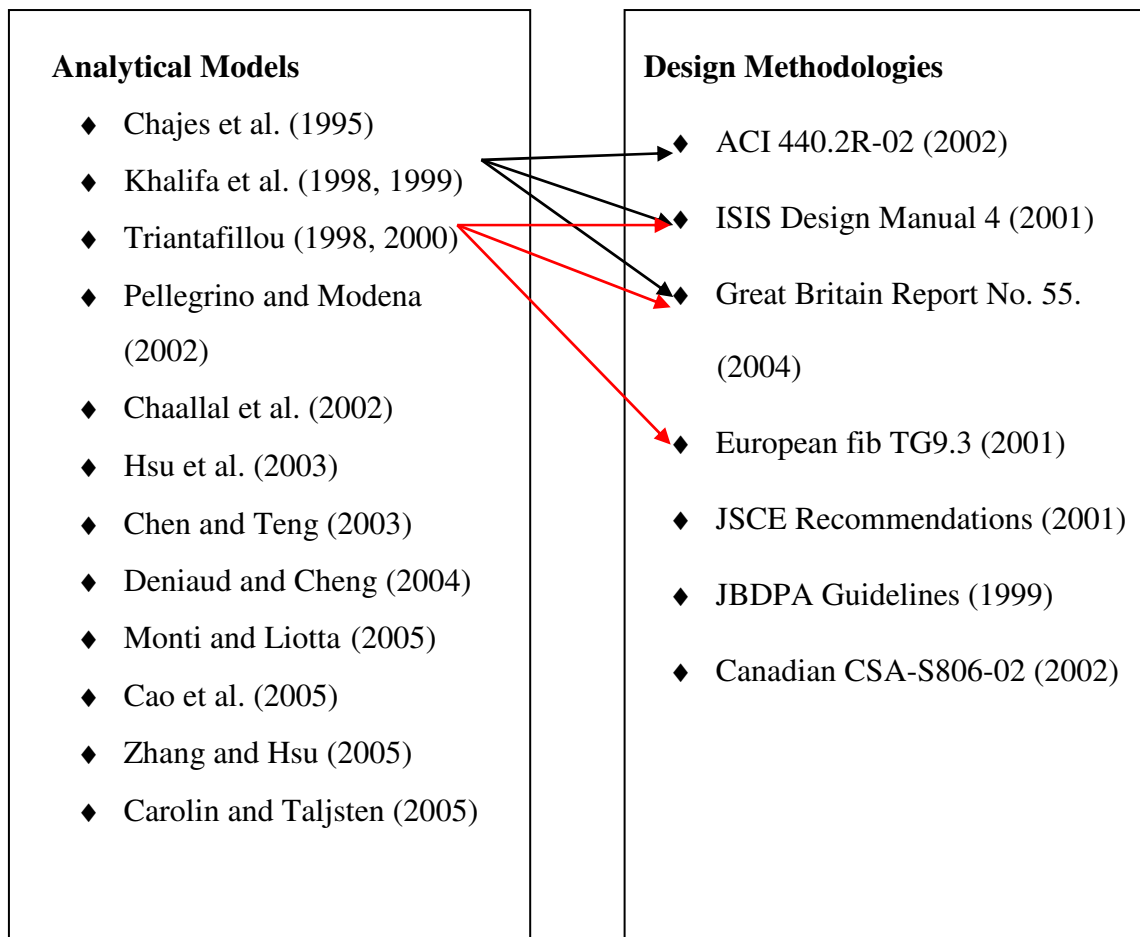

Figure 4.1. Correlations between Analytical Models and Design Guidelines

Previous studies have shown that the shear strength contribution of FRP is influenced by many factors, such as the type of FRP, the FRP strengthening scheme, the concrete strength, the beam geometry, transverse steel reinforcement, loading conditions, and the shear span to depth ratio. Design guidelines and codes establish that the nominal shear capacity of an FRP-strengthened RC member, V_n, is determined by adding the contribution of the FRP strengthening systems to the existing shear capacity and is given as

$$V_n = V_c + V_s + V_f \tag{1}$$

where: V_c = shear contribution of concrete, V_s = shear contribution of transverse steel reinforcement, and V_f = shear contribution of FRP.

Both the shear contribution of concrete and steel can be calculated according to different shear design provisions provided by RC design codes. Almost all analytical models and design guidelines discussed in this section determine the FRP shear contribution by applying the same truss analogy used to determine the shear contribution of transverse steel reinforcement. Thus, most analytical models and guidelines assume that the FRP fibers carry tensile stresses at a strain that is equal either to its ultimate tensile strain, ε_{fu}, or to a reduced fraction. Because the strain distribution along a shear crack is not uniform and because of possible bond failure, it appears that the FRP contribution is limited to an effective tensile strain, ε_{fe}, which is usually lower than the ultimate tensile strain in the FRP. In order to estimate the effective strain in the FRP, analytical models and design guidelines have rigorously analyzed experimental data for the purpose of developing approaches to determine the effective strain. In addition, to determine the effective FRP strain the type of failure at ultimate needs to be identified. This failure could either have occurred prematurely due to bond failure of the FRP or due to FRP fracture. Therefore, the main difference between the analytical models and design guidelines lies in the approach to predict the shear contribution of FRP by predicting the FRP strain at ultimate. Furthermore, because the effective FRP strain highly depends on the FRP bonded length and its bond strength (Triantafillou and Antonopoulos, 2000), analytical models have developed several bond strength models,

which adopt different type of approaches. Therefore, all analytical models and design guidelines investigated have been classified, as shown in Table 4.1, according to the approach adopted to predict the FRP effective strain at the time of failure to determine the FRP shear contribution.

Table 4.1. Classification of Analytical Models and Design Guidelines

Category	Analytical Model	Design Guideline
Fixed effective strain	• Chajes et al. (1995)	• JBDPA (1999) • CSA S806-02 (2002)
Effective strain as a function of FRP stiffness or based on bond mechanism	• Triantafillou (1998) • Triantafillou and Antonopoulos (2000) • Khalifa et al. (1998) • Khalifa et al. (1999) • Pellegrino and Modena (2002) • Chaallal et al. (2002) • Hsu et al. (2003) • Zhang and Hsu (2005) • Deniaud and Cheng (2004)	• ACI 440.2R-02 (2002) • *fib* TG 9.3 (2001) • JSCE Recommendations (2001) • ISIS Design Manual 4 (2001) • Great Britain Technical Report No. 55 (2004)
Effective strain based on non-uniform strain distribution	• Chen and Teng (2003) • Monti and Liotta (2005) • Cao et al. (2005) • Carolin and Taljsten (2005)	

4.2. ANALYTICAL MODELS

4.2.1. Models Based on Fixed Effective FRP Strain. These analytical models applied a fixed effective FRP strain to determine the FRP shear contribution. From all fourteen analytical models, only the model from Chajes et al. (1995) corresponds to this category.

Chajes et al. (1995) conducted an experimental investigation of eight reinforced concrete T-beams to evaluate the effectiveness of using externally applied FRP

composite fabrics to increase the shear capacity of RC beams. For this purpose, different types of FRP materials and different fiber orientations were used to evaluate the influence of diverse FRP stiffness and strengths. In addition, all test specimens were strengthened with U-wrapped FRP systems. In addition, the specimens were not pre-cracked and were tested without the presence of transverse steel reinforcement.

Based on the experimental results from this investigation, Chajes et al. proposed a simple analytical model based on the following assumptions:

(1) Linear stress-strain behavior of the FRP composite

(2) Failure of the beam is initiated by failure of the concrete

(3) Perfect bond between the fabric and concrete prior to failure

(4) FRP contributes to the shear resistance in a similar way as the transverse steel reinforcement.

From the experimental study, an average value of 0.005 for the vertical strain of the concrete at failure was determined. This average strain was used to obtain theoretical predictions for the FRP shear contribution. The equations to predict the FRP shear contribution, V_f, proposed by Chajes et al. are expressed as

$$V_f = A_f E_f \varepsilon v_{cu} d \quad \text{for fiber orientation of 90°} \qquad (2)$$

$$V_f = A_f E_f \varepsilon v_{cu} d \sqrt{2} \quad \text{for fiber orientation of 45°} \qquad (3)$$

where: A_f = cross sectional area of FRP per inch of beam length, E_f = elastic modulus of FRP, εv_{cu} = ultimate tensile strain of concrete (0.005), and d = distance from extreme compression fiber to centroid of tension reinforcement.

From the analysis developed by Chajes et al., the theoretical predictions for the FRP shear contribution were in good agreement with the experimental results. However, the formulations to predict the FRP shear contribution were developed based on test results of continuous FRP sheets. In addition, this analytical model only predicts the FRP shear contribution for fibers oriented at 45° and 90°. Therefore, this analytical model needed to be validated through an extensive experimental data that includes different strengthening schemes. Finally, this analytical model fixes a value for the strain in the FRP; however, as proven later by Triantafillou (1998), the FRP contribution is limited to

an effective tensile strain, ε_{fe}, which is usually lower than the ultimate tensile strain in the FRP. Therefore, using a fixed value of 0.005 for the FRP strain is conservative.

4.2.2. Models Based on Effective FRP Strain as a Function of FRP Stiffness or Based on Bond Mechanism. These analytical models are based directly on the calibration of experimental data and regression analysis to estimate the effective strain in the FRP. These models basically estimated experimental values for the effective FRP strain by back calculating from the experimental values of the FRP shear contribution. Then, a relationship for the effective FRP strain in terms of the FRP stiffness was obtained by regression analysis. In addition, analytical models based on empirical bond mechanism approaches are included.

4.2.2.1 Triantafillou (1998). Triantafillou tested nine RC beams with rectangular cross sections reinforced in shear with side-bonded CFRP reinforcement at different fiber orientations. There was no pre-cracking or transverse steel reinforcement. To supplement these test results, additional 33 tests specimens on RC beams from previous experimental studies were used. These tests consisted of beams FRP-strengthened in shear with different FRP materials, fiber orientations and wrapping configurations. From, the experimental study, Triantafillou proposed an analytical model to predict the contribution of FRP to shear capacity based on ultimate limit states. This analytical model has been developed by adopting the classical truss analogy as in the case of transverse steel reinforcement. Therefore, the contribution of the FRP to the shear resistance, V_f, proposed by Triantafillou is given by

$$V_f = \frac{0.9}{\gamma_f} \rho_f E_f \varepsilon_{fe} b_w d (1 + \cot \beta) \sin \beta \tag{4}$$

where: γ_f = partial safety factor for FRP, ρ_f = FRP area fraction = $2t_f / b_w$, t_f = FRP thickness, E_f = FRP elastic modulus, ε_{fe} = effective FRP strain, b_w = minimum width of cross section over the effective depth, d = effective depth of cross section, and β = angle of strong FRP material direction to longitudinal axis of member.

Triantafillou realized that the FRP contribution is limited to an effective tensile strain, ε_{fe}, which is usually lower than the ultimate tensile strain in the FRP. By

realizing that the FRP strain depends on the FRP development length, which in turn is proportional to the FRP axial rigidity, Triantafillou suggested that as the amount of FRP increases, the effective FRP strain decreases. The relationship between the FRP effective strain and the amount of FRP was estimated based on all experimental results and is shown in Figure 4.2.
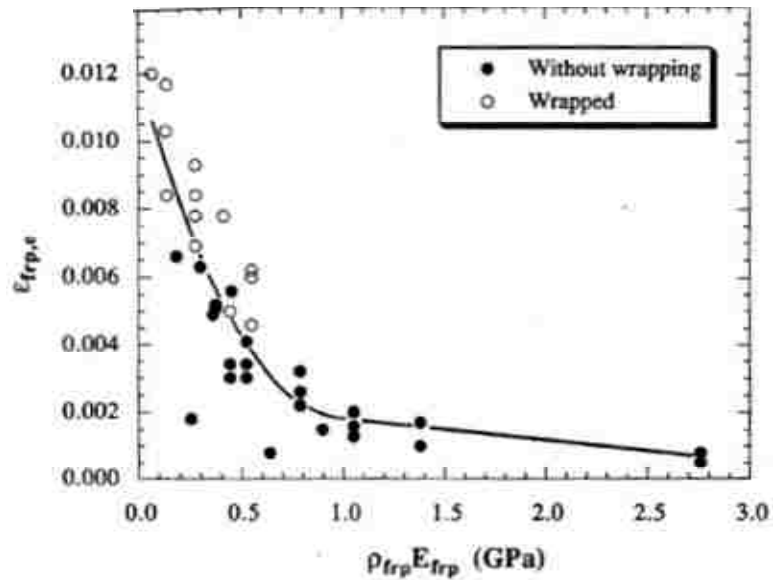

Figure 4.2. Effective Strain in FRP vs. $\rho_f E_f$ (Triantafillou, 1998).

From Figure 4.2, it can be observed that a single curve was used for all modes of failure because the same trend was observed for all data points. Therefore, when determining a best-fit equation for the effective FRP strain, different equations for different failure modes were not considered necessary. From Figure 4.2, the relationship between the FRP effective strain and its axial rigidity, $\rho_f E_f$, was obtained from the best - fit second order equation up to $\rho_f E_f$ equal to 1 GPa, and by the equation of a straight line for values of $\rho_f E_f$ larger than 1 GPa. These two expressions are given by the following two equations,

$$\varepsilon_{fe} = 0.0119 - 0.0205\left(\rho_f E_f\right) + 0.0104\left(\rho_f E_f\right)^2, \text{ when } 0 \leq \rho_f E_f \leq 1\,\text{GPa} \quad (5)$$

$$\varepsilon_{fe} = -0.00065\left(\rho_f E_f\right) + 0.00245, \text{ when } \rho_f E_f > 1\,\text{GPa} \quad (6)$$

From the analytical study, Triantafillou determined that the effective strain in the FRP is not constant. On the contrary, it varies and is dependent on the FRP stiffness. However, since this analytical model was based on limited experimental data, one single expression for determining the FRP effective strain was used without considering different failure modes. Therefore, this analytical model needed to be validated through a more extensive database in order to develop formulations to determine the effective FRP strain for different failure modes. In addition, because different FRP materials have different fracture capacities; the types of FRP materials needed to be included as a variable in this model. Different wrapping configurations are crucial in determining the failure mode; therefore, they should also be included in the model. Moreover, this analytical model also needed to set a limit on the maximum FRP strain to preclude web crashing failure. Finally, the concrete strength also needed to be taken into consideration since it greatly affects the bond failure of FRP.

4.2.2.2 Triantafillou and Antonopoulos (2000). The authors presented a revised and improved version of the original model proposed earlier by Triantafillou in 1998. The FRP shear contribution can be determined by applying Equation (4) from the earlier version. From, the experimental study, the effective strain in the FRP was calibrated from 75 experimental results. In order to determine the effective FRP strain, the type of failure at ultimate state needs to be identified. This failure could either have occurred prematurely due to FRP debonding or due to FRP fracture. From the experimental data, Triantafillou and Antonopoulos determined that the effective FRP strain depends on the FRP development length, which in turn is proportional to the FRP axial rigidity and inversely proportional to the tensile strength of concrete. Therefore, the FRP effective strain depends on the parameter, expressed as $E_f \rho_f / f'^{2/3}_c$. This relationship was calibrated with the experimental data and is shown in Figures 4.3 (a) and (b) for shear failure due to FRP debonding and for shear failure combined with or followed by FRP fracture.
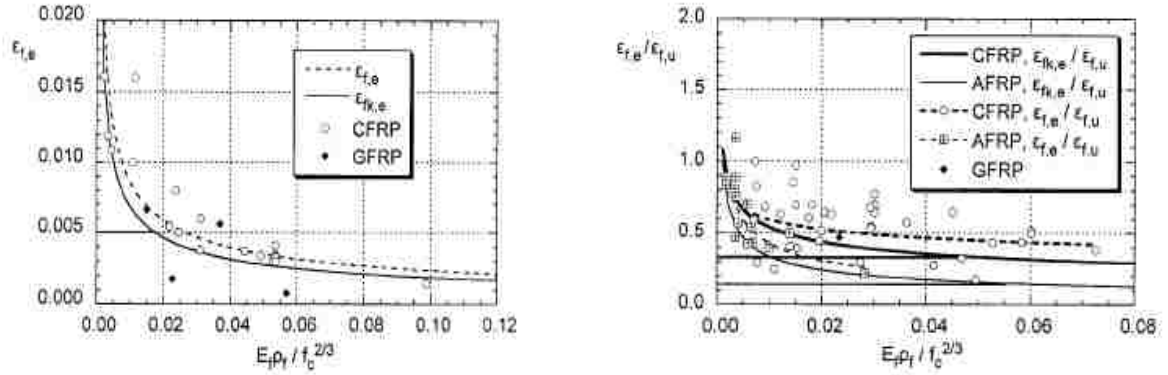
(a) Shear Failure due to FRP Debonding   (a) Shear Failure due to FRP Fracture

Figure 4.3. FRP Effective Strain and Normalized FRP Strain vs. $E_f \rho_f / f'^{2/3}_c$

(Triantafillou and Antonopoulos, 2000)

From Figure 4.3, the effective FRP strain decreases as $E_f \rho_f / f'^{2/3}_c$ increases. For debonding failure, the type of FRP material is not a crucial parameter. However, for fracture failure, the type of FRP material is important because of the different fracture strains exhibited by different FRP materials. Considering the different types of FRP materials, the strengthening schemes of FRP, and the effect of the concrete compressive strength; the effective FRP strain, ε_{fe}, can be determined from the following expressions

For fully-wrapped CFRP:

$$\varepsilon_{fe} = 0.17 \left(\frac{f'^{2/3}_c}{E_f \rho_f} \right)^{0.30} \varepsilon_{fu} \tag{7}$$

For side or U-wrapped CFRP

$$\varepsilon_{fe} = \min \left[0.65 \left(\frac{f'^{2/3}_c}{E_f \rho_f} \right)^{0.65} \times 10^{-3}, \ 0.17 \left(\frac{f'^{2/3}_c}{E_f \rho_f} \right)^{0.30} \varepsilon_{fu} \right] \tag{8}$$

For fully-wrapped AFRP:

$$\varepsilon_{fe} = 0.048 \left(\frac{f'^{2/3}_c}{E_f \rho_f} \right)^{0.47} \varepsilon_{fu} \tag{9}$$

where f'_c is the concrete compressive strength, and ε_{fu} is the ultimate FRP tensile strain.

The analytical model proposed by Triantafillou and Antonopoulos takes into consideration different FRP materials, strengthening schemes and failure modes when calculating the effective strain in the FRP as opposed to its earlier version. However, this analytical model does not make a distinction between specimens wrapped with side-bonded and U-wrapped FRP. In addition, the FRP bonded length should be taken into consideration since it controls FRP debonding.

4.2.2.3 Khalifa et al. (1998). Khalifa et al. assumed that the FRP contributes to the shear resistance in the same way as the transverse steel reinforcement, and is expressed as

$$V_f = \frac{A_f f_{fe}(\sin \beta + \cos \beta)d_f}{s_f} \tag{10}$$

where: A_f = area of FRP = $2t_f w_f$, w_f = width of FRP strip, f_{fe} = effective FRP tensile stress in direction of the principal fibers, d_f = effective FRP depth, and s_f = spacing of FRP strips. The geometric dimensions of a typical cross-section applied in this model are shown in Figure 4.4.
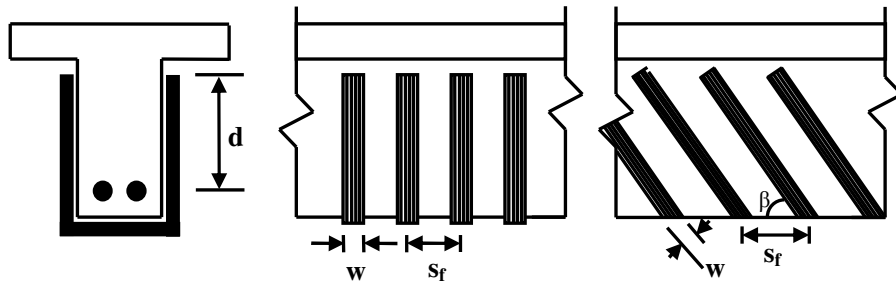

Figure 4.4. Definition of Geometric Parameters (Khalifa, 1999)

Khalifa et al. proposed two different approaches for computing the effective FRP tensile stress. These two approaches represent two possible failure modes: FRP

debonding and FRP fracture. The first design approach based on the effective FRP stress was modified from its original version, which was developed by Triantafillou (1998). The modification consisted in using the ratio of effective FRP strain to its ultimate strain, expressed as $R = \varepsilon_{fe} / \varepsilon_{fu}$. The relationship between this ratio and the axial rigidity of FRP, defined as $\rho_f E_f$, is shown in Figure 4.5.
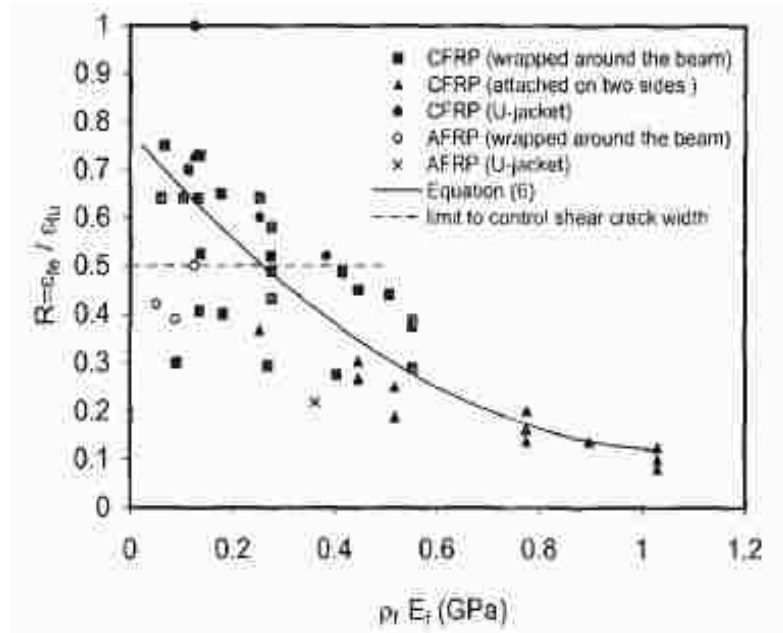

Figure 4.5. Ratio of $\varepsilon_{fe} / \varepsilon_{fu}$ in Terms of $\rho_f E_f$ (Khalifa et al. 1998).

From Figure 4.5, a polynomial regression of the experimental data, which consisted of 48 experimental test specimens, was performed to determine the relationship between $R = \varepsilon_{fe} / \varepsilon_{fu}$ and $\rho_f E_f$ for the cases where $\rho_f E_f$ is smaller than 1.1 GPa. This polynomial regression led to the following expression for estimating the ratio of effective stress of the FRP, R:

$$R = 0.5622 \left(\rho_f E_f\right)^2 - 1.2188\left(\rho_f E_f\right) + 0.778 \le 0.5, \text{ when } \rho_f E_f < 1.1 \text{GPa} \qquad (11)$$

The upper limit of the reduction coefficient, R, limits the effective FRP strain in order to maintain the aggregate interlock. Because the behavior of FRP strengthening systems is linearly elastic up to ultimate failure, the effective tensile stress of the FRP is expressed as:

$$R = f_{fe} / f_{fu} \qquad (12)$$

where f_{fu} is the ultimate tensile stress.

By recognizing that the effective stress method can only be applicable when failure is governed by FRP fracture, Khalifa et al. (1998) proposed a bond mechanism analytical approach, which is based on the bond strength model developed by Maeda et al. in 1997. This approach takes into consideration the effect of the different bonded surface configurations.

When a shear crack develops, only the portion of the FRP system extending past the shear crack by the effective bond length is able to resist the total shear capacity. Maeda et al. (1997) defined the effective bond length, L_e, to be the length beyond which any increase in the available bond length does not reflect an increase in the bond strength. Therefore, Khalifa et al. (1998) proposes the use of an effective FRP width, w_{fe}, which depends on the shear crack angle and the bonded surface configuration as shown in Figures 4.6 and 4.7
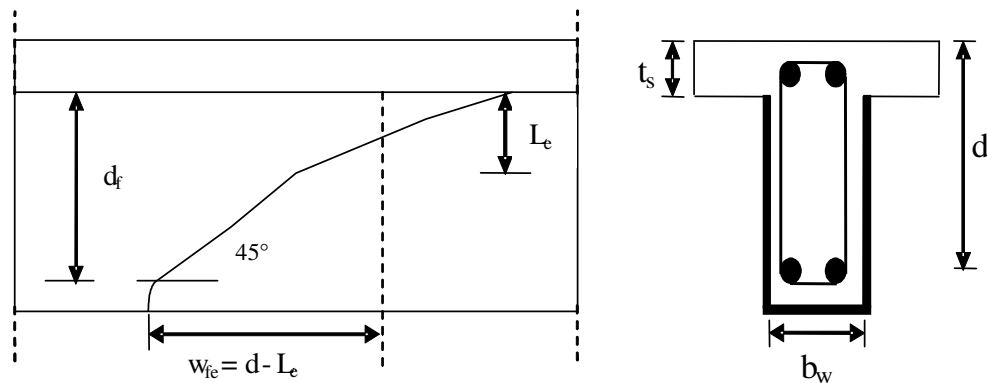

Figure 4.6. Effective FRP Width U-Wrapped (Khalifa et al. 1998)
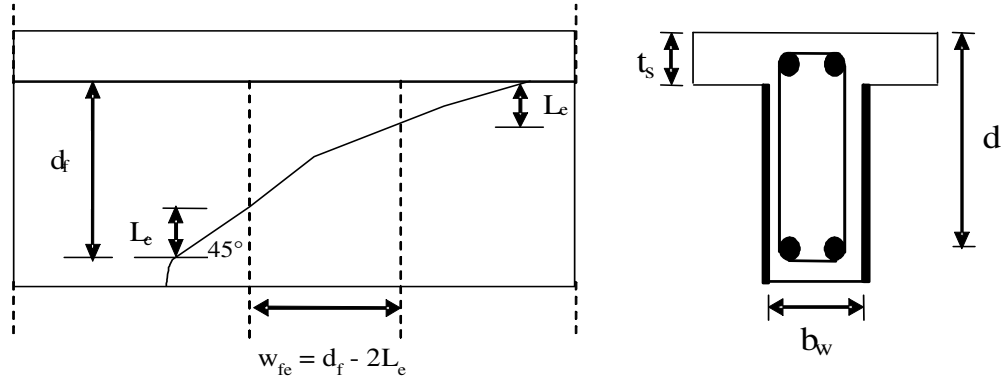
Figure 4.7. Effective FRP Width Side-Bonded (Khalifa et al. 1998)

The effective width proposed can be calculated by the following expressions:

$$w_{fe} = d_f - L_e \text{ for U-wrapped} \tag{13}$$

$$w_{fe} = d_f - 2L_e \text{ for Side-bonded} \tag{14}$$

Maeda et al. (1997) reported that the effective bond length decreases and the FRP stiffness increases. Therefore, the effective bond length is given as follows

$$L_e = e^{6.134 - 0.58\ln(t_f E_f)} \tag{15}$$

In addition, from the experimental study of Maeda et al. (1997), the average bond strength at the FRP and concrete interface, τ_{bu} is determined as

$$\tau_{bu} = kE_f t_f \tag{16}$$

where k = experimental constant equal to 110.2×10^{-6}. By considering the active FRP bond area equal to the effective bond length times the width of the bonded FRP sheet, the ultimate load capacity of the FRP sheet, P_{max}, is expressed as:

$$P_{max} = L_e w_f \tau_{bu} \tag{17}$$

Khalifa et al. also considered the effect of the concrete compressive strength on the bond strength between the FRP and concrete. Maeda et al. used a constant compressive strength of 42 MPa when developing the bond strength model. However, the effect of concrete strength was included by introducing a term proposed by Horiguchi and Saeki (1997). Therefore, Equation (16) was modified by introducing this term and is expressed as

$$\tau_{bu} = k \left(f'_{c}/42 \right)^{2/3} E_f t_f \tag{18}$$

The ultimate load capacity of the FRP sheet, $P_{\max}$, is developed on both sides of the member; therefore, the effective stress is determined from:

$$2P_{\max} = A_f f_{fe} \tag{19}$$

From Equations (17) and (18)

$$2L_e w_f \tau_{bu} = A_f f_{fe} \tag{20}$$

$$R = L_e k \left(\frac{f'_c}{42} \right)^{2/3} \frac{E_f}{f_{fu}} \tag{21}$$

By using Equation (15) and $k = 110.2 \times 10^{-6}$,

$$R = \frac{0.0042 \left(f'_c \right)^{2/3}}{\left(E_f t_f \right)^{0.58} \varepsilon_{fu}} \tag{22}$$

This expression determines that only those strips in the width, w_{fe}, are effective; therefore, Equation (22) can be modified by multiplying w_{fe}/d_f. The final expression for R is given as:

$$R = \frac{0.0042 \left(f'_c \right)^{2/3} w_{fe}}{\left(E_f t_f \right)^{0.58} \varepsilon_{fu} d_f} \leq 0.50 \tag{23}$$

The FRP shear contribution was computed from Equation (10) and the effective stress was limited to the lower of the two R values from Equations (11) and (23).

Although Khalifa et al. analytical model includes the effect of bonded surface configuration and concrete compressive strength, this model exhibits some shortcomings. First, from Equations (10) and (23), this model suggests that no more than half the ultimate tensile stress of the FRP can be used. Khalifa et al. does not provide a theoretical explanation for this small value for the reduction coefficient rather than it was obtained from the regression data. In addition, the approach based on bond mechanism adopts the formulation for the effective bond length from Maeda et al. However, Equation (15) can only be applied when the FRP bonded length is larger than the effective bond length.

4.2.2.4 Khalifa et al. (1999). This analytical model is a revised version of the original developed by Khalifa et al. in 1998. The experimental study consisted of six RC beams with rectangular cross sections strengthened only with CFRP. Different fiber orientations, wrapping schemes and amounts of FRP were applied.

As on the previous version, the authors proposed two approaches representing the two possible failure modes. The first approach, based on effective stress, did not change from the previous version; however, the upper limit of the reduction coefficient was reduced to 0.7 GPa. Therefore, the reduction coefficient is expressed as:

$$R = 0.5622\left(\rho_f E_f\right)^2 - 1.2188\left(\rho_f E_f\right) + 0.778 \text{, when } \rho_f E_f < 0.7 \text{ GPa} \qquad (24)$$

The design approach based on the bond mechanism from the earlier version slightly changed. Based on analytical and experimental data from bond tests developed by Miller in 1999, a conservative value of 75 mm for the effective bond length has been adopted in this model. This analytical model also has adopted the equation from Miller (1999) to calculate the average bond stress, which is expressed in terms of the axial rigidity of the FRP and is expressed as

$$\tau_{bu} = \left[119.06\left(t_f E_f\right) - 0.654\left(t_f E_f\right)^2\right] \times 10^{-6} \qquad (25)$$

By taking into consideration the concrete compressive strength and from Horiguchi and Saeki (1997), Equation (25) can be modified as

$$\tau_{bu} = \left[119.06\left(t_f E_f\right) - 0.654\left(t_f E_f\right)^2\right]\left(f'_c/42\right)^{2/3} \times 10^{-6} \qquad (26)$$

From Equation (20) and (26), and by adopting a value of 75 mm for the effective bond length, the new reduction coefficient can be expressed as:

$$R = \frac{\left(f'_c\right)^{2/3} w_{fe}}{\varepsilon_{fu} d_f}\left[738.93 - 4.06(t_f E_f)\right] \times 10^{-6} \qquad (27)$$

Finally, Khalifa et al. also proposed an upper limit of the effective stress ratio in order to control the shear crack width and loss of aggregate interlock. This upper limit is expressed as

$$R = \frac{0.006}{\varepsilon_{fu}} \qquad (28)$$

The strain reduction factor should be taken as the least of Equations (24), (27) and (28). The shear contribution of FRP can then be determined from Equation (10).

Khalifa et al. analytical model slightly improved its earlier version from 1998; however, this model is only valid for low values FRP of axial rigidity (i.e. $\rho_f E_f < 0.7$ GPa). In addition, this model adopts a constant value of 75 mm for the effective bond length (Miller, 1999), which may result on conservative predictions for the FRP shear capacity.

Later studies have developed bond strength models that results on more accurate predictions. The suggested value for the upper limit of the reduction coefficient is based on the limited experimental data, thus giving conservative results. Finally, Khalifa et al. suggested applying this model only for CFRP systems.

4.2.2.5 Pellegrino and Modena (2002). The authors modified the formulations proposed by Khalifa et al. (1999) by investigating the correlation between the transverse steel reinforcement and the FRP reinforcement. Pellegrino and Modena (2002) tested

eleven RC rectangular sectioned beams with and without transverse steel reinforcement. The FRP was side-bonded, multi-layered and oriented at a 90 degree fiber orientation. From the experimental study, Pellegrino and Modena reported that the efficiency of the FRP strengthening decreases not only when the rigidity of the FRP sheets increases, but also when the ratio between the amount of transverse steel reinforcement and that of FRP shear reinforcement increases. To account for this effect, Pellegrino and Modena modified the strain reduction factor, R, originally proposed by Khalifa et al. (1999), by introducing an additional reduction factor, $R*$, which acts as an additional reduction factor when transverse steel reinforcement is present and is expressed as:

$$R* = -0.53 \ln \rho_{s,f} + 0.29 \text{ with } 0 \leq R* \leq 1 \tag{29}$$

where $\rho_{s,f}$ is the stiffness ratio between transverse steel reinforcement and FRP shear reinforcement, and is expressed as:

$$\rho_{s,f} = E_s A_{sv} / E_f A_f \tag{30}$$

where E_s is the elastic modulus of steel reinforcement, and A_{sv} is the area of transverse steel reinforcement.

The contribution of FRP to the total shear capacity of an RC beam with transverse steel reinforcement can be determined from Equation (31), where the reduction factor, R, may be taken as the lowest of:

$$V_f = \rho_f b_w 0.9 d R f_{fu} (\sin \beta + \cot \beta) \tag{31}$$

$$R = 0.5622 \left(\rho_f E_f \right)^2 - 1.2188 \left(\rho_f E_f \right) + 0.778, \text{ when } \rho_f E_f < 0.7 \, \text{GPa} \tag{32}$$

$$R = R* \left[\frac{0.0042 (f'_c)^{2/3} w_{fe}}{(E_f t_f)^{0.58} \varepsilon_{fu} d} \right] \tag{33}$$

$$R = \frac{0.006}{\varepsilon_{fu}} \tag{34}$$

Pellegrino and Modena slightly improved the analytical model developed by Khalifa et al. (1999). This improvement consisted of taking into consideration the effect of the transverse steel reinforcement in the behavior of RC beams shear strengthened

with FRP systems. However, since the derivation of $R*$ was validated only with the experimental data corresponding to this study, an extensive database, which includes different types of FRP strengthening schemes, different amounts of FRP and transverse steel reinforcement, is required to validate and improve this analytical model.

4.2.2.6 Chaallal et al. (2002). Chaallal et al. (2002) investigated the effects of FRP strengthening systems on the behavior of deep beam specimens shear-strengthened with FRP. The experimental study consisted of twelve RC half-scale T-section girders. Chaallal et al. included transverse steel reinforcement in the specimens. In addition, multi-layer U-wrapped CFRP systems with a 90 degree fiber orientation were used in the tests.

From the experimental study, the optimum number of FRP layers to achieve the maximum gain in shear resistance due to the FRP was found to be dependent on the transverse steel reinforcement. In addition, the effective strain in the FRP depends on the amount of transverse steel reinforcement. A regression of the measured experimental FRP strains from this study was compared to the strains calculated by using Triantafillou (1998) analytical relationships to determine the effective FRP strain. This comparison resulted in a higher correlation coefficient as illustrated in Figure 4.8. The difference is attributed to the fact that the analytical model from Triantafillou (1998) did not take into consideration the transverse steel reinforcement. Therefore, Chaallal et al. (2002) proposed Equation (35) to determine the effective strain of the FRP, ε_{fe}, which is correlated to the total shear reinforcement consisting of the transverse steel reinforcement and externally applied FRP reinforcement.

$$\varepsilon_{fe} = 3(10)^{-5}(\rho_{tot})^{-0.6522} \tag{35}$$

where ρ_{tot} is the total shear reinforcement ratio and is expressed as

$$\rho_{tot} = n\rho_f + \rho_s \tag{36}$$

where: $n = E_f / E_s$, ρ_s = transverse steel reinforcement ratio = $A_{sv} / s_v bd$, and s_v = spacing between stirrups.
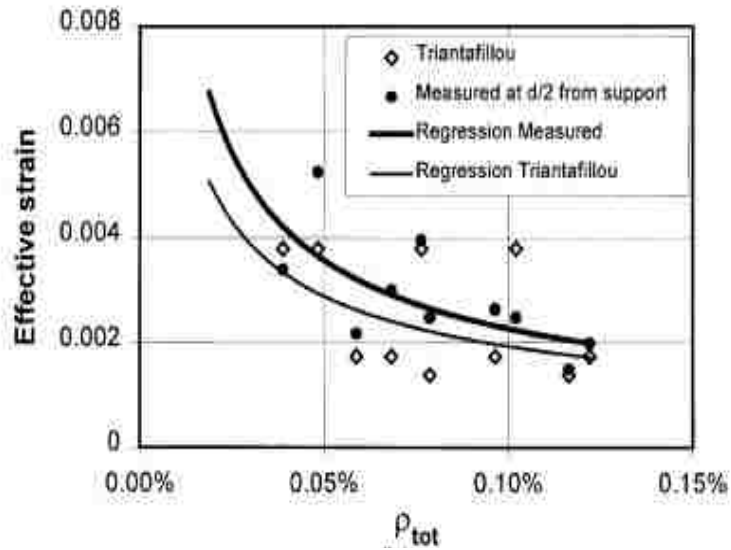
Figure 4.8. Effective Strain in Terms of ρ_{tot} (Chaallal et al., 2002)

Furthermore, the experimental study shows that the addition of CFRP layers tends to modify the behavior of the beam from deep to slender type. As a consequence, Chaallal et al. proposed that the deep beam coefficient, $f(a/d)$, defined in Equation (37) should be included in the expression to determine the shear capacity of the FRP. In addition, this analytical model suggests that the deep beam coefficient should be related to the total shear reinforcement as given in Equation (38). The shear contribution of the FRP to the total shear capacity can then be determined from Equation (39).

$$f(a/d) = (1 + 2a/d)/12 \tag{37}$$

$$f\left(\frac{a}{d}, \rho_{tot}\right) = \left(\frac{1 + 2\dfrac{a}{d}}{12}\right) + (1000\rho_{tot} - 0.6) \leq 1 \tag{38}$$

$$V_f = f\left(\frac{a}{d}, \rho_{tot}\right)\left(\frac{A_f}{s_f}\right)E_f \varepsilon_{fe} d_f \tag{39}$$

where: a = shear span, and $f\left(\dfrac{a}{d}, \rho_{tot}\right)$ = new deep beam coefficient.

This analytical model was developed based on the results of an experimental investigation on the shear performance of large scale RC T-Girders. Therefore, the formulations for predicting the FRP contribution were derived by analyzing the influence of a deep beam coefficient. When calibrating the formulations to compute both the effective FRP strain and the deep beam coefficient, only data points from this experimental study were used, thus more research work is needed to validate these formulations.

4.2.2.7 Hsu et al. (2003). The analytical model from Hsu et al. (2003) is a modification of the model proposed by Khalifa et al. in 1998. The experimental investigations from Hsu et al (2003) consisted of five RC beams with rectangular cross-sections and without transverse steel reinforcement or pre-cracking. The RC beams were strengthened with CFRP strips systems. The FRP fibers were oriented at 0, 45, and 90 degrees.

Hsu et al. proposed two different approaches to determine the strain reduction factor, R, which is needed to predict the effective strain and the shear contribution of FRP. The first analytical approach, based on test data calibration, determined that the effective FRP strain is not only a function of the FRP axial rigidity, but also a function of the concrete compressive strength. Therefore, a relationship between the effective strain and the FRP axial rigidity was obtained by the power regression of the experimental data. However, as the concrete compressive strength increases, the bond strength between the FRP and concrete increases; therefore by curve fitting, a relationship between the effective FRP ratio and $\rho_f E_f / f'_c$ was developed and is expressed as

$$R = 1.48712(\rho_f E_f / f'_c)^{-0.7488} \tag{40}$$

The design approach based on bonding mechanism also considers the effect of the concrete compressive strength on the direct shear behavior. This analytical model proposes an empirical design equation for calculating the ultimate direct shear strength, which is expressed as

$$\tau_{max} = (7.64 \times 10^{-4} f'^2_c) - (2.73 \times 10^{-2} f'_c) + 6.38 \text{ (MPa)} \tag{41}$$

where $\tau_{\max}$ is the ultimate direct shear strength. For design purposes, Hsu et al. simplifies the concrete shear stress distribution as a triangular shape along the effective length. Therefore, the strain reduction factor is expressed as

$$R = \frac{\tau_{\max} L_e}{2 f_{fu} t_f} \leq 1 \qquad (42)$$

where L_e is taken to be equal to 75 mm from the bond strength model of Miller (1999).

The strain reduction factor should be taken as the smaller from Equations (40) and (42). The shear contribution of FRP can then be determined from Equation (10).

The analytical model proposed by Hsu et al. (2003) improved the formulations from Khalifa et al. (1999) by introducing the concrete compressive strength in Equation (40). This equation was derived by the calibration of a more extensive experimental database and by developing a power regression for fitting the data. However, Equation (40) was calibrated only with data specimens that failed in debonding.

4.2.2.8. Zhang and Hsu (2005). The authors presented a revised version of the original model proposed by Hsu et al (2003). The experimental investigation from Zhang and Hsu (2005) consisted of eleven RC beams with rectangular cross-sections and without transverse steel reinforcement or pre-cracking. The RC beams were strengthened with CFRP strips systems. The FRP fibers were oriented at 0, 45, and 90 degree fiber orientations.

This analytical model consists of two different approaches to determine the reduction factor, R, which is needed to predict the effective FRP strain and the shear contribution of FRP. The first analytical approach was based on test data calibration. Zhang and Hsu (2005) determined that the effective FRP strain is not only a function of the FRP axial rigidity, but also a function of the concrete compressive strength. A relationship between the effective FRP strain ratio, R, and its axial rigidity was obtained by a power regression instead of using a polynomial as a best fit of the experimental data. For a more accurate analysis, the experimental results were divided into two categories; one was based on tests failing due to FRP fracture and the other one on tests failing due to FRP debonding as shown in Figure 4.9.
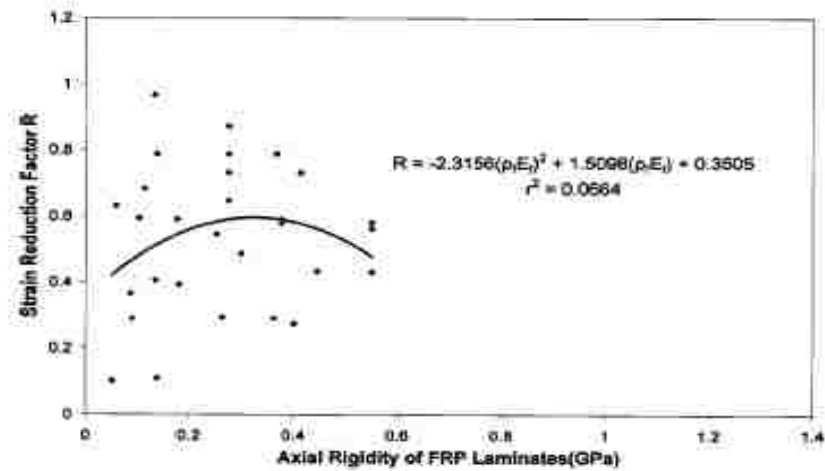
(a) FRP Fracture
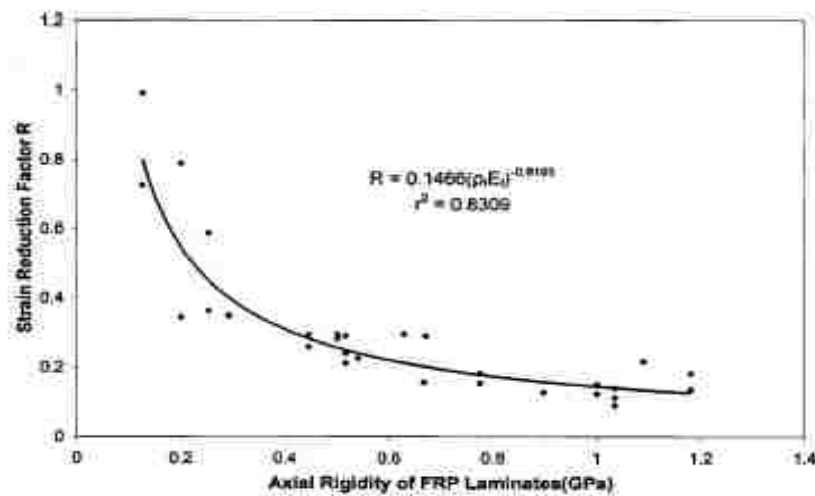
(b) FRP Debonding

Figure 4.9. Strain Reduction Factor in Terms of $\rho_f E_f$ (Zhang and Hsu, 2005)

Zhang and Hsu determined that as the concrete compressive strength increases, the bond strength between the FRP and concrete increases; therefore by curve fitting, a relationship between the effective FRP ratio and $\rho_f E_f / f'_c$ was developed and is shown in Figure 4.10 and expressed as
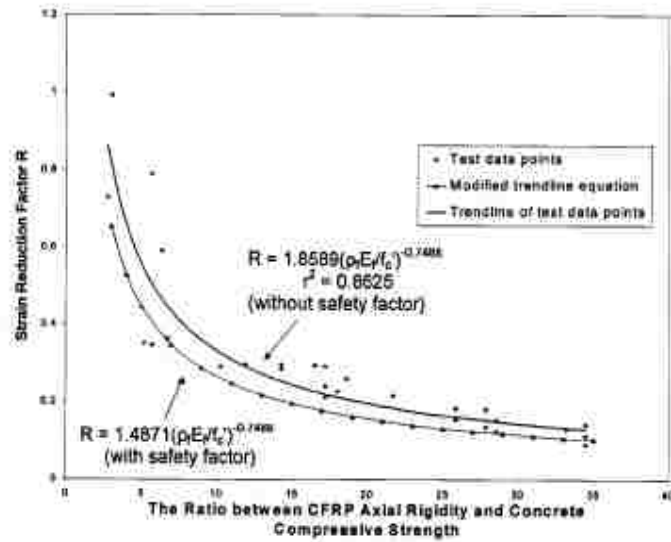
$$R = 1.8589(\rho_f E_f / f'_c)^{-0.7488} \tag{43}$$

Figure 4.10. Strain Reduction Factor in Terms of $\rho_f E_f / f'_c$ (Zhang and Hsu, 2005)

A safety factor was applied to Equation (43) to account for the data points that are not distributed on the curve. The modified strain reduction factor was applied to Equation (43), thus resulting on Equation (40).

The design approach based on bonding mechanism also considers the effect of the concrete compressive strength on the direct shear behavior. This analytical model proposes an empirical design equation for calculating the ultimate direct shear strength, which is given in Equation (41). For design purposes, Hsu et al. simplifies the concrete shear stress distribution as a triangular shape along the effective length. Therefore, the strain reduction factor based on this approach is given by Equation (42).

The only modification to the previous version was the equation to predict the shear contribution of FRP, which is expressed as

For FRP continuous fiber sheet:

$$V_f = w_{fe} t_f f_{fe} \sin^2 \beta \tag{44}$$

For FRP strips:

$$V_f = \frac{A_f f_{fe}(\sin \beta + \cos \beta) d_f}{s_f} \tag{45}$$

As in the previous version, the analytical model proposed by Zhang and Hsu (2005) improved the formulations from Khalifa et al. (1999) by introducing the concrete compressive strength in Equation (40). This equation was derived by the calibration of a more extensive experimental database and by developing a power regression for fitting the data. However, Equation (40) was calibrated only with data specimens that failed in debonding. Because when a shear crack develops, only that portion of the FRP extending past the shear crack by the effective bond length is able to resist the shear capacity. Therefore, for continuous FRP sheets, the width is suggested to be changed by w_{fe}, as expressed in Equation (44).

4.2.2.9 Deniaud and Cheng (2004). Deniaud and Cheng (2004) proposed model was developed based on an experimental investigation, which consisted of 35 experimental test results. The test specimens consisted of small and full-scale specimens. The FRP wrapping schemes applied were side-bonded and U-wrapped FRP sheets. From the experimental results, Deniaud and Cheng proposed a simplified analytical model, which is based on the strip model developed by Alexander and Cheng (1997) and the shear friction approach developed by Loov (1998).

The strip method is based on evaluating each individual FRP strip crossing the shear crack in order to find the maximum allowable FRP strain. To evaluate the bond strength between the concrete and the FRP, and the maximum allowable FRP strain of each strip, Deniaud and Cheng developed an interface mean shear stress curve. Deniaud and Cheng then developed a parametric study to determine the maximum FRP strain, ε_{max}, which is expressed by

$$\varepsilon_{max} = \frac{3\sqrt{f'_c}\,d_f^{0.16}}{\left(tE_f\right)^{1.5}\left(k_a \sin\beta\right)^{0.1}}\left(\%\right) \tag{46}$$

where k_a is the coefficient describing anchorage condition It is necessary to note that both the width and the spacing of the FRP bands are taken perpendicular to the direction of the principal fibers, but not along the longitudinal direction of the beam as was done in other analytical models. From calibration of the expression above, the coefficient for anchorage conditions, k_a, was found to be equal to 0.79 when the FRP sheets were

extended underneath the flange. For FRP bonded on the sides, k_a was found to be equal to 2, while for FRP bonded as a U-wrapped, k_a was found to be equal to 1. For fully-wrapped FRP sheets, Equation (46) reaches infinity; therefore, the maximum strain is not governed by debonding. From the parametric study, the ratio of the remaining bonded width over the initial width, denominated as R_L, can also be determined and is expressed as

$$R_L = 1 - 1.2 \exp\left[-\left(\frac{d_f}{k_e L_e \sin \beta}\right)^{0.4}\right] \tag{47}$$

where k_e is the integer describing number of debonding ends. For FRP bonded on the sides, $k_e = 2$; for FRP bonded as U-wrapped, $k_e = 1$; and for FRP extended underneath flange, $k_e = 1$. The effective length is given by Equation (15) from Maeda et al. (1997) bond strength model.

Deniaud and Cheng developed an equation to determine the effect of the FRP sheets and is expressed as

For 90 degree fiber orientation:

$$T_f = \frac{s_v}{d_s} d_f t E_f \varepsilon_{\max} R_L \quad \text{with } \varepsilon_{\max} \le \varepsilon_{fu} \tag{48}$$

For inclined fiber orientations and FRP strips:

$$T_f = d_f t_f E_f \varepsilon_{\max} R_L \left(\frac{w_f}{s_f}\right)^2 \left(\frac{s_v}{d_s} \sin \beta + \cos \beta\right) \sin \beta \tag{49}$$

where: T_f = tension force in FRP and d_s = stirrup height

Deniaud and Cheng proposed a continuous equation to determine the total shear resistance of a beam, V_n, which is expressed as

$$V_n = k \sqrt{f'_c A_c \left(T_v + T_f\right) \frac{s}{d_s}} - T_v \tag{50}$$

where: k = experimentally determined factor = $2.1\left(f'_c\right)^{-0.4}$, A_c = concrete area, T_v = tension force in stirrups = $A_{sv}f_{yv}$, A_v = area of stirrups, and f_{yv} = yield strength of stirrups.

Deniaud and Cheng used a significantly different approach in predicting the capacity of RC beams shear strengthened with FRP systems. This model is based on the shear friction theory with the lowest shear strength among all potential failure planes governing the shear strength of the beam. In addition, this model treats and describes the interaction between the concrete, steel stirrups, and FRP.

According to Deniaud and Cheng (2004), this analytical model accurately evaluates the cracking pattern as well as the resisting shear force. The main advantage of this model is that the strain compatibility is satisfactory. However, one drawback of this model is that it does not address FRP fracture for fully-wrapped specimens.

4.2.3. Models Based on Non-uniform Strain Distribution. These analytical models are based on bond strength models that have been developed based on fracture mechanics at the FRP/concrete interface. These analytical models determine the specific fracture energy of the FRP/concrete interface to determine the bond strength. Before the FRP shear contribution can be determined, the maximum shear force transferred from the concrete to the FRP as well as the normal and shear stressed need to be determined. The maximum shear force between concrete and FRP prior to debonding depends on the available bond length. If the effective bond length is higher than the available bond length, debonding occurs and the force transferred between concrete and FRP ceases.

4.2.3.1 Chen and Teng (2003). Chen and Teng proposed two separate analytical models for predicting the FRP shear contribution: the FRP debonding approach and the FRP fracture approach. Both approaches were developed separately because of the difference between the two possible failure modes. Both approaches proposed an equation to determine the FRP shear contribution, V_f, and is expressed as

$$V_f = 2f_{fe}t_f w_f \frac{h_{fe}(\cot\theta + \cot\beta)}{s_f}\sin\beta \tag{51}$$

where: h_{fe} = effective FRP height and θ = shear crack angle

The analytical model from Chen and Teng (2003) is based on the assumption that the shear crack ends at a distance of $0.1d$ below the compression face of the beam as shown in Figure 4.11.
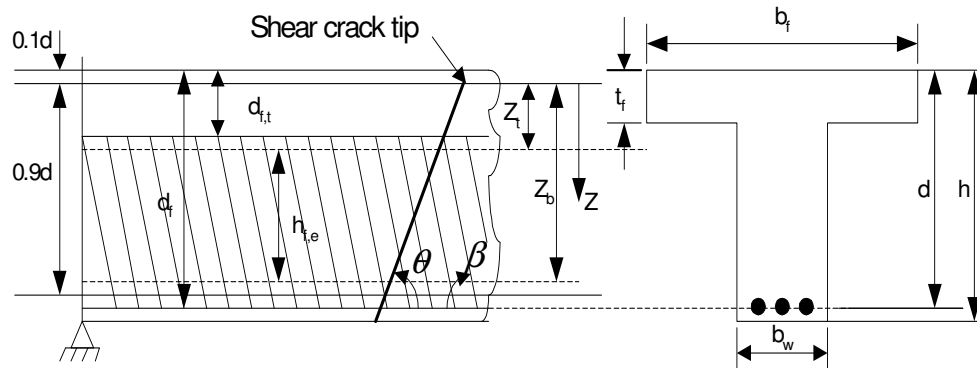
Figure 4.11. General Shear Strengthening Scheme Notations (Chen and Teng, 2003)

From Figure 4.11, the following expressions were determined by Chen and Teng:

$$h_{fe} = z_b - z_t \tag{52}$$

$$z_t = d_{f,t} \tag{53}$$

$$z_b = d_f - h + 0.9d \tag{54}$$

where: z_t = coordinate of upper edge of effective FRP, z_b = coordinate of lower edge of effective FRP, $d_{f,t}$ = distance from beam compression face to upper edge of FRP, and d_f = distance from beam compression face to lower edge of FRP.

Furthermore, the analytical model from Chen and Teng takes into consideration the orientation of the FRP fibers in the case of continuous FRP sheets shown in Figure 4.12 and given Equation (55).

$$s_f = w_f / \sin \beta \tag{55}$$
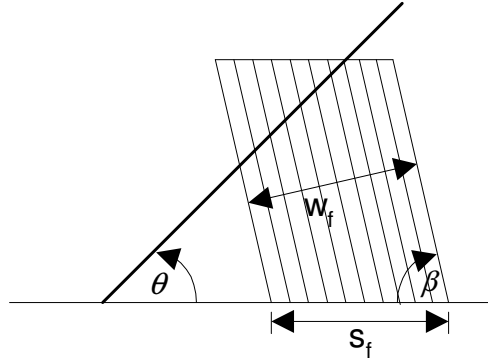
Figure 4.12. Relationship between w_f and s_f for Continuous FRP Sheets

Chen and Teng also revealed that the FRP stress distribution along the shear crack is not uniform for both FRP fracture and FRP debonding; therefore, the effective or average FRP stress, f_{fe}, proposed by Chen and Teng is expressed as

$$f_{fe} = D_f \sigma_{f,\max} \tag{56}$$

where: D_f = FRP stress distribution factor and $\sigma_{f,\max}$ = maximum stress in FRP intersected by the shear

4.2.3.1.1 FRP debonding approach. This approach can only be applied for RC beams shear strengthened with FRP bonded on the sides and U-wrapped because debonding is the governing failure mode. However, in the case of U-wrapped, the fracture approach also needs to be evaluated because RC beams shear strengthened with U-wrapped can also fail in fracture. In this case, the smaller value for the prediction of the FRP shear contribution between the two approaches needs to be taken as the controlling FRP shear capacity.

Chen and Teng developed a bond strength model in 2001, which predicts the bond strength and the effective bond length between the FRP and concrete. This proposed bond strength model was used by Chen and Teng to determine the maximum stress in the FRP along a shear crack, which is limited by the ultimate bond strength or the FRP ultimate tensile stress. The maximum stress in the FRP, $\sigma_{frp,\max}$, can be determined by

$$\sigma_{f,\max} = \min\left[f_{fu}, 0.427\beta_w\beta_L\sqrt{\frac{E_f\sqrt{f'_c}}{t_f}} \right] \tag{57}$$

$$\beta_L = \begin{cases} 1 & if \ \lambda \geq 1 \\ \sin(\pi\lambda/2) & if \ \lambda < 1 \end{cases} \tag{58}$$

$$\beta_w = \sqrt{\frac{2 - w_f / s_f \sin\beta}{1 + w_f / s_f \sin\beta}} \tag{59}$$

where: β_w = effect of FRP to concrete width ratio, β_L = effect of bond length, λ = normalized maximum bond length = $L_{\max} / L_e$. The maximum bond length, $L_{\max}$, is given by:

For U-wrapped:

$$L_{\max} = h_{fe} / \sin\beta \tag{60}$$

For Side-bonded:

$$L_{\max} = h_{fe} / 2\sin\beta \tag{61}$$

The effective bond length determined from the bond strength model developed by Chen and Teng (2001) is given by:

$$L_e = \sqrt{E_f t_f / \sqrt{f'_c}} \tag{62}$$

Chen and Teng proposed an expression to determine the FRP stress distribution factor for debonding failure by assuming that the FRP intersected by the shear crack fully develops its bond strength at the ultimate state. The FRP stress distribution factor, D_{frp}, can be obtained from Equation (63) and is shown in Figure 4.13.

$$D_f = \begin{cases} \dfrac{2}{\pi\lambda}\dfrac{1-\cos(\pi\lambda/2)}{\sin(\pi\lambda/2)} & if \ \lambda \leq 1 \\ 1 - \dfrac{\pi-2}{\pi\lambda} & if \ \lambda > 1 \end{cases} \tag{63}$$
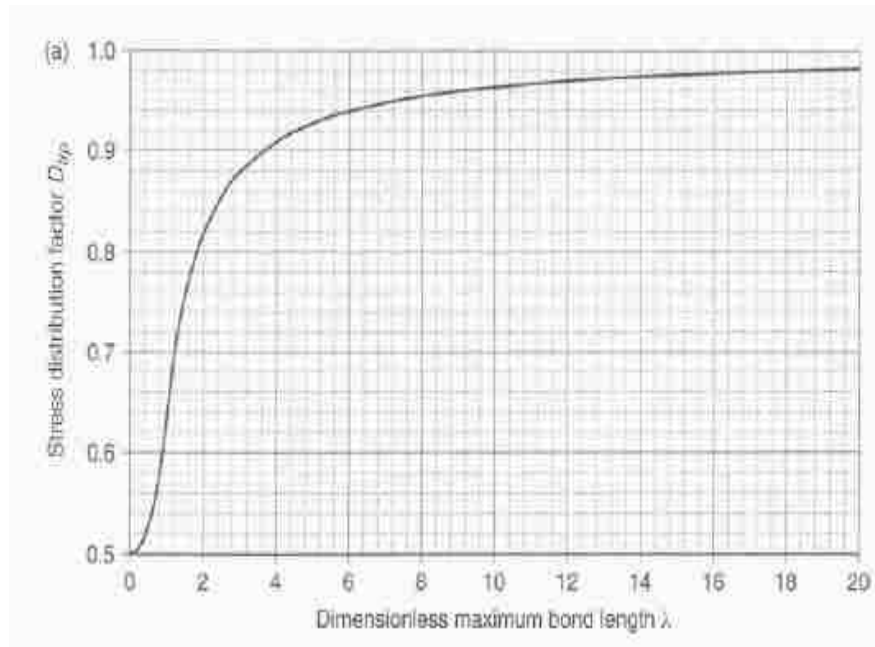
Figure 4.13. Stress Distribution Factor for U-Wrapped and Side-Bonded

The FRP debonding approach developed by Chen and Teng (2003) is based on the bond strength model developed by the authors in 2001. This model was developed by combining fracture mechanics analysis with experimental results. Chen and Teng assumed that the shear-slip behavior of FRP bonded to concrete can be represented as a triangular shape. In addition, this model determined that the ratio of the FRP width to the width of the concrete member greatly affects the bond strength at failure. The effective bond length of FRP was found to be proportional to the FRP stiffness and inversely proportional to the concrete tensile strength.

4.2.3.1.2 FRP fracture approach. This approach can only be applied for RC beams shear strengthened with fully-wrapped and U-wrapped FRP because fracture is the governing failure mode. As mentioned in the previous section, in the case of U-wrapped, the debonding approach also needs to be evaluated because RC beams shear strengthened with U-wrapped can also fail in debonding

Chen and Teng pointed out the non uniformity of the FRP stress along a shear crack; therefore, Chen and Teng proposed a parabolic stress distribution for the FRP

intersected by the critical shear crack. However, Chen and Teng recommended the use of a linear stress distribution as approximation because the stress in the FRP can be taken to be proportional to the width of the shear crack. Thus, the stress distribution factor is expressed as

$$D_f = \frac{1+\xi}{2} \qquad (64)$$

where ξ is a coefficient and is equal to z_t / z_b

When the ultimate shear strength is reached at or after FRP fracture, the maximum stress in the FRP along a shear crack reaches its ultimate strength; therefore, the maximum stress in the FRP, $\sigma_{f,\max}$, is expressed as

$$\sigma_{f,\max} = f_{fu} \qquad (65)$$

If the ultimate shear strength is reached before FRP fracture, the maximum allowable strain should be limited. This analytical model proposes a value of 1.5% for the maximum usable FRP strain.

4.2.3.2 Monti and Liotta (2005). Monti and Liotta (2005) tested 24 RC concrete beams with rectangular cross-sections and with transverse steel reinforcement. They used fully-wrapped, U-wrapped and side-bonded CFRP strips and sheets at 90°, 45°, and 60° fiber orientations.

Monti and Liotta (2005) proposed an analytical model to predict the shear contribution of FRP based on fracture mechanics. First, Monti and Liotta defined the generalized failure criteria at the FRP and concrete interface. For the case of FRP strips and sheets, the effective bond length and the debonding strength are introduced and expressed as:

$$L_e = \sqrt{\frac{E_f t_f}{2 f_{ct}}} \qquad (66)$$

$$f_{fdd} = \frac{0.80}{\gamma_f} \sqrt{\frac{2 E_f \Gamma_{Fk}}{t_f}} \qquad (67)$$

where f_{ct} = concrete tensile strength = $0.27 f_{cu}^{2/3}$, R_c = concrete characteristic cubic strength, and Γ_{Fk} = specific fracture energy of the FRP-concrete bond interface and is expressed as

$$\Gamma_{Fk} = 0.03 k_b \sqrt{f'_c f_{ct}} \tag{68}$$

The covering/scale factor coefficient is given by:

$$k_b = \sqrt{\frac{2 - w_f / s_f}{1 + w_f / 400}} \geq 1 \tag{69}$$

When the available bond length, L_b, is lower than the effective bond length, L_e, the debonding strength is reduced as:

$$f_{fdd}(L_b) = f_{fdd} \frac{L_b}{L_e} \left(2 - \frac{L_b}{L_e} \right) \tag{70}$$

For the cases of FRP strips and sheets wrapped around a corner, the FRP exhibits a fraction of its ultimate strength, φ_R, which is expressed as:

$$\varphi_R = 0.2 + 1.6 \frac{r_c}{b_w}, \quad 0 \leq \frac{r_c}{b_w} \leq 0.5 \tag{71}$$

When the available bond length, L_b, is higher than the effective bond length, L_e, the debonding strength is expressed as:

$$f_{fu}(r_c) = f_{fdd} + \left(\varphi_R f_{fu} - f_{fdd} \right) \tag{72}$$

When the available bond length, L_b, is lower than the effective bond length, L_e, the debonding strength is expressed as:

$$f_{fu}(L_b, r_c) = f_{fdd}(L_b) + \left(\varphi_R f_{fu} - f_{fdd}(L_b) \right) \tag{73}$$

Monti and Liotta first defined the generalized constitutive law of an FRP layer bonded to the concrete surface. Then, the compatibility imposed by the shear crack opening and the appropriate boundary conditions were included on the formulations to predict the shear contribution provided by the FRP systems. Finally, analytical expressions that depict the behavior of the stress field in the FRP crossing a shear crack are derived. From these analytical expressions, equations were formulated to compute the effective debonding strength of FRP. The expressions to predict the effective debonding strength, f_{fed}, were a function of the FRP strengthening scheme, and some basic geometric and mechanical parameters. These expressions are given by,

For Side-bonded:

$$f_{fed} = f_{fdd} \frac{z_{rid,eq}}{\min(0.9d, h_w)} \left(1 - 0.6\sqrt{\frac{L_{eq}}{z_{rid,eq}}}\right)^2 \tag{74}$$

$$z_{rid,eq} = z_{rid} + L_{eq} \tag{75}$$

$$z_{rid} = \min(0.9d, h_w) - L_e \sin\beta \tag{76}$$

$$L_{eq} = \frac{s}{f_{fdd}/E_f} \tag{77}$$

For U-wrapped:

$$f_{fed} = f_{fdd} \left(1 - \frac{1}{3}\frac{L_e \sin\beta}{\min(0.9d, h_w)}\right) \tag{78}$$

For Fully-wrapped

$$f_{fed} = f_{fdd} \left(1 - \frac{1}{6}\frac{L_e \sin\beta}{\min(0.9d, h_w)}\right) + \frac{1}{2}\left(\phi_R f_{fd} - f_{fdd}\right)\left(1 - \frac{L_e \sin\beta}{\min(0.9d, h_w)}\right) \tag{79}$$

where s is the debonding slip.

In the case of an RC beam shear strengthened with U-wrapped or fully-wrapped, the FRP shear contribution can be determined by

$$V_f = \frac{1}{\gamma_{Rd}}(0.9d) f_{fed} 2t_f (\cot\theta + \cot\beta)\frac{w_f}{s_f} \tag{80}$$

where θ is the orientation of the shear crack. For RC beams shear strengthened with FRP bonded to the sides, the FRP shear contribution can be determined by

$$V_f = \frac{1}{\gamma_{Rd}} \min(0.9d, h_w) f_{fed} 2t_f \frac{\sin \beta}{\sin \theta} \frac{w_f}{s_f}$$ (81)

The analytical model presented by Monti and Liotta (2005) also considered the non-uniformity of the FRP effective stress along the shear crack. Therefore, this model applies fracture mechanics approach as opposed to regression analysis performed by previous analytical models. In addition, Monti and Liotta apply the truss analogy mechanism for determining the FRP shear contribution of fully-wrapped and U-wrapped configuration. In contrast, a crack-bridging mechanism was used for side-bonded FRP

4.2.3.3. Cao et al. (2005). The authors performed tests involving twelve pre-cracked RC beams with rectangular cross-sections. This was the first study to investigate the effects of pre-cracking for developing an analytical model. The RC beams were strengthened with fully-wrapped CFRP and GFRP strips at a 90 fiber orientation. The purpose of this study was to investigate the debonding of FRP prior to failure because debonding can be considered a serviceability limit state, which can be assumed to be the ultimate limit state for design purposes. Furthermore, this analytical model modified the analytical model from Chen and Teng (2003) by considering the effects of the shear span to effective depth ratio on the critical shear angle and the strain distribution factor. Since the shear span-to-depth ratio also has a significant effect on the strain distribution factor, D_f, a modified distribution factor, $D_{f\theta} = D_f/tan\theta$, was developed to represent the effects of both the strain distribution factor as well as the shear crack angle. This relationship was calibrated with the experimental results from this study as shown in Figure 4.14. Cao et al. proposed a modified strain distribution factor, $D_{f\theta}$, which is expressed as

$$D_{f\theta} = \left(1 - \frac{\pi - 2}{\lambda \pi}\right) \begin{cases} 1 & \text{for } a/d \leq 1.4 \\ \dfrac{1}{1 - 0.2(\lambda - 1.4)^2} & \text{for } 1.4 < a/d < 3 \\ 2.05 & \text{for } a/d \geq 3 \end{cases}$$ (82)
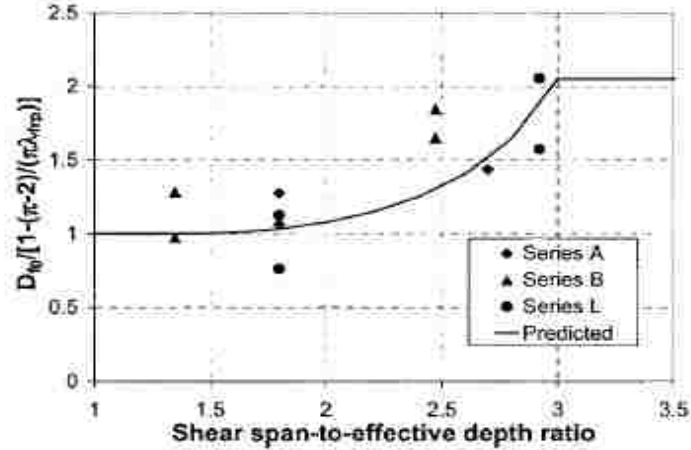
Figure 4.14. Strain Distribution Factor in Terms of Shear Span-to-Depth Ratio
(Cao et al., 2005)

For FRP strips oriented vertically to the longitudinal axis of the beam, the shear
contribution of FRP, V_f , can be calculated as

$$V_f = 2D_{f\theta}t_f w_f E_f \varepsilon_{f,\max} \frac{0.9d}{s_f}$$ (83)

$$\beta_w = \sqrt{\frac{2 - w_f / s_f}{1 + w_f / s_f}}$$ (84)

where: $\varepsilon_{f,\max}$ = maximum FRP strain at debonding and is expressed as:

$$\varepsilon_{f,\max} = 0.427\beta_w \frac{(f'_c)^{1/4}}{\sqrt{E_f t_f}}$$ (85)

The analytical model proposed by Cao et al. (2005) modified the FRP debonding
approach proposed by Chen and Teng (2003) by introducing a modified strain
distribution factor that depends on the shear-span-to depth ratio and the shear crack angle.
This modified strain distribution factor, $D_{f\theta}$, was derived based on experimental results
for shear span-to-depth ratio between 1.4 and 3; therefore, the relationship given in

Equation (82) provides a conservative approximation; therefore additional experimental investigations are needed to validate this relationship.

  4.2.3.4 Carolin and Taljsten (2005). Carolin and Taljsten (2005) developed a database that consisted of 23 RC beams with rectangular cross-sections, with and without transverse steel reinforcement. The database consisted of CFRP strengthening systems with fibers oriented at 45 and 90 degrees. The RC beams were strengthened with fully-wrapped and side-bonded FRP strengthening schemes.

  From the experimental study, Carolin and Taljsten (2005) derived a modified truss model that takes into account the non-uniformity of the strain distribution and the anisotropy of the FRP composite. Carolin and Taljsten (2005) reported that the direction of the possible shear crack is difficult to predict; therefore, three geometric angles are applied in this analysis as shown in Figure 4.15.
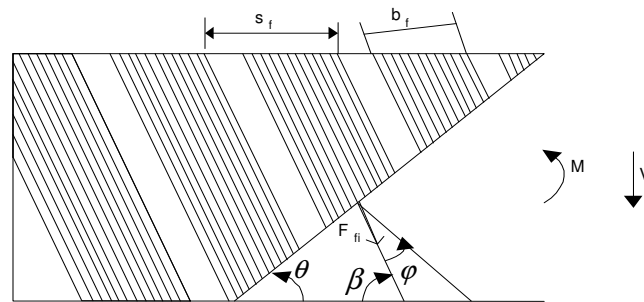
Figure 4.15. Fiber Alignment and Shear Crack Angle (Carolin and Taljsten, 2005)

  From Figure 4.15, θ is the shear crack inclination, β is the fiber direction along the longitudinal axis of the member, and ϕ is the angle between the principal tensile stress and the fiber direction; therefore, $\phi = \theta + \beta - 90$.

  The FRP shear contribution, , according to Carolin and Taljsten (2005)is given as

$$V_f = \eta \varepsilon_{cr} E_f t_f r_f (0.9d) \frac{\cos \phi}{\sin \theta} \tag{86}$$

where η is the average fiber utilization, which is defined as the average FRP strain along the beam height compared to the strain in the most stressed FRP fiber. Carolin and Taljsten suggest a value of average fiber utilization equal to 0.60. The factor r_f becomes $r_f = \sin \beta$ for continuous FRP sheets and $r_f = w_f / s_f$ for FRP strips. The critical FRP strain, ε_{cr}, can be determined by

$$\varepsilon_{cr} = \min \begin{cases} \varepsilon_{fu} \\ \varepsilon_{bond} \cos^2 \varphi \\ \varepsilon_{c\max} \cos^2 \varphi \end{cases} \tag{87}$$

where ε_{fu} is the ultimate tensile strain of the FRP, ε_{bond} is the maximum allowable strain without achieving anchor failure, and ε_{cmax} is the maximum strain to achieve the concrete contribution. The values corresponding to the later two strains were not given in the paper and the authors did not provide a way of estimating them.

4.3. DESIGN GUIDELINES

The design guidelines have also been categorized according to the different approaches to determine the effective FRP strain. Seven design guidelines are classified into the following categories: (1) Design Guidelines based on fixed effective FRP strain and (2) Design Guidelines based on effective FRP strain as a function of FRP stiffness or based on bond mechanism.

4.3.1. Design Guidelines Based on Fixed Effective FRP Strain. These design guidelines applies a fixed effective FRP strain to determine the FRP shear contribution.

4.3.1.1 JBDPA guidelines (1999). The Japan Building Disaster Prevention Association (JBDPA) published the "Seismic Retrofitting Design and Construction Guidelines for Existing Reinforced Concrete (RC) Buildings with FRP Materials" (JBDPA, 1999). These guidelines condense research on seismic retrofitting of RC structures using FRP systems conducted in Japan. The JBDPA guideline provides guidance on the proper handling, design, and installation of the FRP systems used in Japan.

From the "Structural Regulations of Building" (Building Center of Japan, 1997), the ultimate shear capacity of RC members strengthened with FRP composite systems, is evaluated by adding the contribution of the FRP and is expressed as

$$V_n = \left[\frac{0.053 \rho_s^{0.23} \left(17.6 + f'_c\right)}{a/d + 0.12} + 0.845 \sqrt{\sum \rho_{ts} f_y} \right] b(0.9d) \qquad (88)$$

$$\sum p_{ts} f_y = \rho_s f_{yv} + \rho_f f_{fe} \leq 10\, MPa \qquad (89)$$

where ρ_{ts} is the total ratio of existing shear reinforcement and a/d is the shear span-to-depth ratio, which must not be less than one nor larger than three. The tensile strength of FRP, f_{fe} is estimated as

$$f_{fe} = \min \left\{ E_f \varepsilon_{fe}, 2/3 f_{fu} \right\} \qquad (90)$$

where ε_{fe} based on previous investigations is taken to be equal to 0.007. In addition, to avoid FRP fracture, a value of two-thirds of the ultimate tensile strength of the FRP was adopted as a margin of safety.

4.3.1.2 CAN/CSA S806-02 (2002). The Canadian "CAN/CSA S806-02 Design and Construction of Building Components with Fibre-Reinforced Polymers" (CSA 2002) represents the only formalized design code addressing the application of externally bonded FRP reinforcement for RC members. The CSA S806-02 was last updated on May 2004; however, no changes on the design requirements for shear strengthening were found.

From CSA A23.3-94 (CSA, 1994), the nominal shear capacity of beams strengthened with FRP is evaluated by adding the shear contribution of the FRP, V_f, to the shear contribution of concrete and transverse steel reinforcement, which according to CSA A23.3-94 can be computed as

$$V_c = 0.2 \sqrt{f'_c} b_w d \qquad (91)$$

$$V_s = \frac{A_{sv} f_{yv} (\sin \alpha + \cos \alpha) d}{s_v} \qquad (92)$$

The Canadian Standards Association S806-02 (CSA, 2002) estimates the shear capacity provided by FRP sheets as

$$V_f = \frac{A_f E_f \varepsilon_{fe}(\sin\beta + \cos\beta)d_f}{s_f}$$

(93)

For simplicity this design code provides fixed values for the effective strain in the FRP. The value of effective strain, ε_{fe}, may be conservatively assumed to be equal to 0.004 for U-wrapped members, and equal to 0.002 for FRP systems side-bonded to the web.

4.3.2. Design Guidelines Based on Effective FRP Strain as a Function of FRP Stiffness or Based on Bond Mechanism. The design guidelines corresponding to this category are based directly on the calibration of experimental data and regression analysis to estimate the effective strain in the FRP. From the regression analysis, relationships to determine the effective FRP strain were derived. In addition, design guidelines based on empirical bond mechanism approaches are included.

4.3.2.1 fib TG 9.3 bulletin 14 (2001). The "International Federation for Structural Concrete (fib) Bulletin 14 Externally Bonded FRP Reinforcement for RC Structures" (fib, 2001) produced by fib Task Group 9.3, presents a combination of design guideline and state-of-the-art report. This guideline recognizes the difference in expected performance, not only between FRP material types, but between preformed and wet lay-up FRP systems. This difference is expressed in the form of different material safety factors. A new version to fib Bulletin 14 is currently being developed and will be published very soon.

From Eurocode 2 Part I (2003), the nominal shear capacity of RC members strengthened with FRP systems is evaluated by adding the shear contribution of the FRP, V_f, to the shear contribution of concrete and transverse steel reinforcement, which can be calculated as

$$V_c = \left\{ \frac{0.18}{\gamma_c} \min\left(1 + \sqrt{\frac{200}{d}}, 2\right) \sqrt[3]{100 \min\left(0.02, \rho_s\right) f'_c} \right\} b_w d$$

(94)

$$V_s = \frac{A_{sv} f_{yv} 0.9d(1+\cot\alpha)\sin\alpha}{s_v} \qquad (95)$$

The analytical model from Triantafillou and Antonopoulos developed in 2000 was the basis for developing the analytical relationships in fib TG 9.3 bulletin 14. This design guideline calculates the shear contribution provided by the FRP system, V_f, as

$$V_f = 0.9\varepsilon_{fe} E_f \rho_f b_w d(\cot\theta + \cot\beta)\sin\beta \qquad (96)$$

$$\rho_f = \frac{2t_f w_f}{b_w s_f} \text{ for strips of FRP} \qquad (97)$$

The effective strain of the FRP is governed by the failure mode of the FRP, the strengthening scheme and the type of FRP. The best-fit power type expressions for the effective FRP strain were calibrated from the experimental data reported by the analytical study developed by Triantafillou and Antonopoulos in 2000. For RC members fully-wrapped with CFRP systems, when FRP fracture controls, the effective strain can be computed as

$$\varepsilon_{fe} = 0.17\left(\frac{f'^{2/3}_c}{E_f \rho_f}\right)^{0.30} \varepsilon_{fu} \qquad (98)$$

When the strengthening scheme consists of U-wrapped or side-bonded CFRP systems, the effective FRP strain is expressed as

$$\varepsilon_{fe} = \min\left[0.65\left(\frac{f'^{2/3}_c}{E_f \rho_f}\right)^{0.56} \times 10^{-3}, 0.17\left(\frac{f'^{2/3}_c}{E_f \rho_f}\right)^{0.30} \varepsilon_{fu}\right] \qquad (99)$$

For fully-wrapped AFRP, when FRP fracture controls, the effective FRP strain is expressed as

$$\varepsilon_{fe} = 0.048\left(\frac{f'^{2/3}_c}{E_f \rho_f}\right)^{0.47} \varepsilon_{fu} \qquad (100)$$

This design guideline provides shear design provisions that takes into consideration different FRP materials, strengthening schemes and failure modes when calculating the effective strain in the FRP. However, it does not make a distinction between specimens wrapped with side bonded FRP and U-wraps.

4.3.2.2 JSCE recommendations (2001). The "Japanese JSCE Recommendations for the Upgrading of Concrete Structures with use of Continuous Fiber Sheets" (JSCE, 2001) adopts a performance-based approach to the design of externally bonded FRP materials. The shear contribution of concrete according to JSCE Recommendations can be computed as

$$V_c = \beta_d \beta_p \beta_n f_{vc} b_w d / \gamma_b \tag{101}$$

$$\beta_d = (1000/d)^{1/4} \leq 1.5 \tag{102}$$

$$\beta_p = (100\rho_s)^{1/3} \leq 1.5 \tag{103}$$

$$\beta_n = 1 + M_o / M_d \leq 2 \ for \ N_u \geq 0$$
$$\beta_n = 1 + 2M_o / M_d \geq 0 \ for \ N_u < 0 \tag{104}$$

$$f_{vc} = 0.2(f'_c)^{1/3} \leq 0.72 \ N / mm^2 \tag{105}$$

where M_o = decompression moment, M_d = design bending moment, and γ_b = member factor. The transverse steel reinforcement shear contribution provided by the JSCE Recommendations is expressed as

$$V_s = \frac{A_{sv} f_{yv} 0.9d(\sin\alpha + \cos\alpha)}{s_v} \tag{106}$$

The Japanese JSCE Recommendations calculates the FRP contribution to shear capacity, V_f, as

$$V_f = K \frac{A_f f_{fu} 0.9d(\sin\beta + \cos\beta)}{s_f} \tag{107}$$

where *K* is shear reinforcing efficiency.

The shear reinforcing efficiency, K, is expressed in terms of elastic modulus E_f and the amount of FRP ρ_f as

$$0.4 \le K = 1.68 - 0.67R \le 0.8 \tag{108}$$

$$R = \left(\rho_f E_f\right)^{1/4} \left(\frac{f_{fu}}{E_f}\right)^{2/3} \left(\frac{1}{f'_c}\right)^{1/3}, \quad 0.5 \le R \le 2 \tag{109}$$

The JSCE recommendations suggests that Equation (107) is applicable for members strengthened with CFRP sheets, CFRP strands, and AFRP fiber sheets since the shear reinforcing efficiency was calibrated from experimental specimens strengthened with CFRP and AFRP systems.

4.3.2.3. ISIS design manual 4 (2001). The ISIS Design Manual 4 for "Strengthening Reinforced Concrete Structures with Externally-Bonded Fibre Reinforced Polymers" (ISIS Canada, 2001) was written as a state-of-the-art report, referring to design recommendations of other design guidelines, such as ACI 440.2R (2002) and fib-TG 9.3 Bulletin 14 (fib, 2001). A new version to this design manual will be published by ISIS in the fall of 2007.

From CSA Standard A23.3-94, (CSA 1994), the nominal shear capacity of a member strengthened with FRP is evaluated by adding the shear contribution of the FRP, V_f, to the shear contribution of concrete and steel. The values of shear resistance provided by the concrete, V_c, and transverse steel reinforcement, V_s are expressed as

$$V_c = 0.2\sqrt{f'_c} b_w d \tag{110}$$

$$V_s = \frac{A_{sv} f_{yv} (\sin \alpha + \cos \alpha) d}{s_v} \tag{111}$$

The ISIS Design Manual 4 (ISIS, 2001) calculates the FRP contribution to the total shear capacity, V_f, as

$$V_f = \frac{A_f E_f \varepsilon_{fe} (\sin \beta + \cos \beta) d_f}{s_f} \tag{112}$$

The effective FRP strain, ε_{fe} must be limited to a value of 0.004 to assure that aggregate interlock forces can still be transmitted through the shear plane. For fully-wrapped cases, the effective strain should simply be taken to be equal to 0.004. For other strengthening schemes, the effective strain is computed as follows

$$\varepsilon_{fe} = R\varepsilon_{fu} \tag{113}$$

where R is the ratio of effective to ultimate strain in the FRP reinforcement, and is given by

$$R = \lambda_1 \left[\frac{{f'_c}^{2/3}}{\rho_f E_f} \right]^{\lambda_2} \tag{114}$$

where for CFRP fracture: $\lambda_1 = 1.35$ and $\lambda_2 = 0.30$; for AFRP and GFRP fracture: $\lambda_1 = 1.23$ and $\lambda_2 = 0.47$.

To account for possible debonding, the effective FRP strain is computed as follows,

$$\varepsilon_{fe} = \frac{k_1 k_2 L_e}{9525} \tag{115}$$

$$k_1 = \left[\frac{f'_c}{27.65} \right]^{2/3} \tag{116}$$

$$k_2 = \frac{d_f - n_e L_e}{d_f} \tag{117}$$

$$L_e = \frac{25350}{\left(t_f E_f \right)^{0.58}} \tag{118}$$

where n_e is the number of free ends of the FRP reinforcement on one side of the beam. If k_2 is negative, the FRP systems is ineffective unless anchorage is provided. The effective FRP strain, ε_{fe}, shall be taken as the smallest of the limiting effective strain (i.e.

0.004), the value obtained from Equation (113), and the value obtained from Equation (115).

4.3.2.4 ACI 440.2R-02 (2002). The "ACI 440.2R-02 Guide for the Design and Construction of Externally Bonded FRP Systems for Strengthening Concrete Structures" (ACI 440, 2002) provides strength reduction factors based on ductility of the expected failure mode consistent with ACI 318-99 (1999).

The nominal shear capacity of an RC member strengthened with FRP is evaluated by adding the shear contribution of the FRP, V_f, to the shear contribution of concrete and transverse steel reinforcement as shown in Equation (119). An additional reduction factor, ψ_f, is applied to the shear contribution of the FRP system. For fully-wrapped members, ψ_f is equal to 0.95; while for U-wrapped and side-bonded FRP, ψ_f is equal to 0.85.

$$V_n = V_c + V_s + \psi_f V_f \qquad (119)$$

The shear contribution of the concrete and transverse steel reinforcement according to ACI 318-05 can be calculated as

$$V_c = \frac{1}{6}\sqrt{f'_c}\, b_w d \ \ \text{(SI)} \qquad (120)$$

$$V_s = \frac{A_{sv} f_{yv} (\sin \alpha + \cos \alpha) d}{s_v} \qquad (121)$$

where f'_c = compressive cylinder strength of concrete, b_w = minimum width of cross section over the effective depth, d = effective depth of cross section, A_v = area of shear reinforcement, f_{yv} = yield strength of shear reinforcement, α = angle of the shear reinforcement to the longitudinal axis of the member, and s = spacing of shear reinforcement measured along the longitudinal axis.

The model from Khalifa et al. (1999) was the basis for developing ACI 440.2R-02. This design guideline estimates the shear contribution of FRP systems by calculating

the force resulting from the tensile stress in the FRP across an assumed 45 degree crack (Khalifa et al, 1998). The FRP shear capacity provided is given by

$$V_f = \frac{A_{fv} f_{fe} (\sin \beta + \cos \beta) d_f}{s_f} \qquad (122)$$

The area of FRP shear reinforcement can be computed by

$$A_{fv} = 2n t_f w_f \qquad (123)$$

where n = number of plies of FRP reinforcement. The effective tensile stress in the FRP at ultimate is proportional to the level of strain that can be developed at ultimate and is expressed as

$$f_{fe} = \varepsilon_{fe} E_f \qquad (124)$$

The effective strain of the FRP, ε_{fe}, is governed by the failure mode of the FRP strengthening system and by the different configurations of FRP laminates. For fully-wrapped members, the following relationship must be satisfied.

$$\varepsilon_{fe} = 0.004 \leq 0.75 \varepsilon_{fu} \qquad (125)$$

For members bonded with FRP systems as U-wrapped or side-bonded, debonding failure will likely govern; therefore the effective strain, ε_{fe}, is calculated by using a bond reduction factor, k_v.

$$\varepsilon_{fe} = k_v \varepsilon_{fu} \leq 0.004 \qquad (126)$$

The bond reduction factor is a function of the concrete strength, the strengthening scheme and the stiffness of the FRP. The bond reduction factor can be obtained from the following expressions,

$$k_v = \frac{k_1 k_2 L_e}{11,900 \varepsilon_{fu}} \leq 0.75 \ \text{(SI)} \tag{127}$$

$$L_e = \frac{23,300}{(n t_f E_f)^{0.58}} \ \text{(SI)} \tag{128}$$

$$k_1 = \left(\frac{f_c'}{27}\right)^{2/3} \ \text{(SI)} \tag{129}$$

$$k_2 = \begin{cases} \dfrac{d_f - L_e}{d_f} & \text{for } U\text{ - wraps} \\ \dfrac{d_f - 2L_e}{d_f} & \text{for two sides bonded} \end{cases} \tag{130}$$

A revision to ACI 440.2R will be published in 2007. The revision will provide strength reduction factors consistent with ACI 318-05 (2005). In addition, the nominal shear capacity of an RC member strengthened with FRP is evaluated by applying Equation (119); however, the additional reduction factor, ψ_f, for U-wrapped and side-bonded FRP will be equal to 0.75. This reduction factor is recommended based on analysis using data from Bousselham and Chaallal (2006a), Deniaud and Cheng (2001, 2003), Funakawa et al. (1997), Matthys (2000), and Pellegrino and Modena (2002).

4.3.2.5 Great Britain technical report No. 55 (2004). This report is similar to ISIS Design Manual 4 and fib Bulletin 14 in its approach and scope. From the British Standards Institution BS 8110 (1997), the nominal shear capacity of RC members strengthened with FRP systems is evaluated by adding the shear contribution of the FRP, V_f, to the shear contribution of concrete and transverse steel reinforcement, which can be calculated as

$$V_c = \left\{ \frac{0.18}{\gamma_c} \min\left(1 + \sqrt{\frac{200}{d}}, 2\right) \sqrt[3]{100 \min(0.02, \rho_s) f_c'} \right\} b_w d \tag{131}$$

$$V_s = \frac{A_{sv}(0.95 f_{yv})d}{s_v} \tag{132}$$

where γ_c is the concrete partial coefficient.

In addition, by assuming a 45 degree shear crack inclinations, Technical Report No. 55 (2004) expresses the FRP shear contribution to the shear capacity as

$$V_f = E_f \varepsilon_{fe} A_f \frac{\left(d_f - \frac{n}{3} l_{t,\max}\right)}{s_f}(\cos\beta + \sin\beta) \tag{133}$$

$$l_{t,\max} = 0.7\sqrt{E_f t_f / f_{ct}} \tag{134}$$

$$f_{ctm} = 0.18\left(f_{cu}\right)^{2/3} \tag{135}$$

where $n = 0$ for fully-wrapped beam, 1.0 for U-wrapped configuration, and 2.0 for side-bonded configuration; and $l_{t,\max}$ = anchorage length. This technical report determines the FRP effective strain to be the minimum of

$$\varepsilon_{fe} = \min \begin{cases} \varepsilon_{fu}/2 \\ 0.64\sqrt{\dfrac{f_{ct}}{E_f t_f}} \\ 0.004 \end{cases} \tag{136}$$

The firs strain limit corresponds to the average FRP strain due to FRP fracture. The second limit corresponds to FRP debonding and is based on Neubauer and Rostasy (1997) bonding mechanism approach. This strain limit should also be applied for fully-wrapped configurations in order to maintain the integrity of the concrete. The final strain limit was proposed to also ensure the integrity of concrete.

4.3.3. AASHTO LRFD Bridge Design Specifications. Although AASHTO design specifications do not provide shear design guidelines for RC structures strengthened with FRP systems, in this thesis, these design specifications will be used in combination with the formulations from the analytical models for comparison purposes.

From the Sectional Design Model, the nominal shear capacity of RC members is expressed as

$$V_n = V_c + V_s \tag{137}$$

The shear contribution of concrete and transverse steel reinforcement can be computed as

$$V_c = 0.0316\beta\sqrt{f'_c}b_v d_v \tag{138}$$

$$V_s = \frac{A_{sv}f_{yv}d_v(\cot\theta + \cot\alpha)\sin\alpha}{s_v} \tag{139}$$

where β = factor indicating the ability of diagonally cracked concrete to transmit tension, b_v = effective web width, d_v = distance between tensile and compressive force resultants. The values of β and θ can be determined by using the simplified procedure and the general procedure. The simplified procedure states that for non-prestressed members not subjected to axial tension and containing at least the minimum amount of transverse steel reinforcement as specified in Equation (140), or having an overall depth of less than 16.0 in., β shall be taken as 2.0 and θ as 45°.

$$A_{sv} \geq 0.0316\sqrt{f'_c}\frac{b_v s_v}{f_{yv}} \tag{140}$$

For other cases, the general procedure provides two tables to compute the values for β and θ for members that contain at least the minimum required amount of transverse steel reinforcement (Table 4.2) and for members that contain less than that amount (Table 4.3). To obtain values for β and θ from Table 4.2, it is necessary to compute the shear design stress ratio (v/f'_c) and the longitudinal strain ε_x at mid-depth. The longitudinal strain ε_x may be taken as one-half of the strain in the longitudinal steel reinforcement, ε_t, as computed in Equation (141).

$$\varepsilon_x = \frac{\varepsilon_t}{2} = \frac{M_u/d_v + 0.5N_u + 0.5(V_u - V_p)cot(\theta) - A_{ps}f_{po}}{2(E_s A_s + E_p A_{ps})} \leq 0.002 \tag{141}$$

where M_u =factored moment not less than $V_u d_v$, N_u = factored axial force, V_p = component in the direction of applied shear of the effective prestressing force, A_{ps} = area of prestressing steel on flexural tension side, and f_{po}, $= 0.7 f_{pu}$ for usual prestressing levels,

To obtain values for β and θ if the section contains less than the minimum amount of transverse reinforcement, Table 4.3 is used. The value of the longitudinal strain at

mid-depth, ε_x, is computed as given in Equation (142). The crack spacing parameter, s_{xe}, is determined from Equation (143).

$$\varepsilon_x = \frac{\varepsilon_t}{2} = \frac{M_u/d_v + 0.5N_u + 0.5(V_u - V_p)\cot(\theta) - A_{ps}f_{po}}{E_s A_s + E_p A_{ps}} \leq 0.002 \qquad (142)$$

$$s_{xe} = s_x \frac{1.38}{a_g + 0.63} \leq 80in \quad (in.) \qquad (143)$$

where a_g is the maximum aggregate size in inches and s_x is the lesser of either d_v or the maximum distance between layers of longitudinal crack control reinforcement. If ε_x is negative, then the member is uncracked and the axial stiffness of the uncracked concrete needs to be considered with using Equation (144).

$$\varepsilon_x = \frac{M_u/d_v + 0.5N_u + 0.5(V_u - V_p)\cot(\theta) - A_{ps}f_{po}}{2(E_s A_s + E_p A_{ps} + A_{ct}E_c)} \qquad (144)$$

where A_{ct} is the area of the concrete beneath mid-depth

Table 4.2. Values of θ and β for Sections with Transverse Steel Reinforcement

$\dfrac{v_u}{f_c'}$	$\varepsilon_x \times 1{,}000$								
	≤−0.20	≤−0.10	≤−0.05	≤0	≤0.125	≤0.25	≤0.50	≤0.75	≤1.00
≤0.075	22.3	20.4	21.0	21.8	24.3	26.6	30.5	33.7	36.4
	6.32	4.75	4.10	3.75	3.24	2.94	2.59	2.38	2.23
≤0.100	18.1	20.4	21.4	22.5	24.9	27.1	30.8	34.0	36.7
	3.79	3.38	3.24	3.14	2.91	2.75	2.50	2.32	2.18
≤0.125	19.9	21.9	22.8	23.7	25.9	27.9	31.4	34.4	37.0
	3.18	2.99	2.94	2.87	2.74	2.62	2.42	2.26	2.13
≤0.150	21.6	23.3	24.2	25.0	26.9	28.8	32.1	34.9	37.3
	2.88	2.79	2.78	2.72	2.60	2.52	2.36	2.21	2.08
≤0.175	23.2	24.7	25.5	26.2	28.0	29.7	32.7	35.2	36.8
	2.73	2.66	2.65	2.60	2.52	2.44	2.28	2.14	1.96
≤0.200	24.7	26.1	26.7	27.4	29.0	30.6	32.8	34.5	36.1
	2.63	2.59	2.52	2.51	2.43	2.37	2.14	1.94	1.79
≤0.225	26.1	27.3	27.9	28.5	30.0	30.8	32.3	34.0	35.7
	2.53	2.45	2.42	2.40	2.34	2.14	1.86	1.73	1.64
≤0.250	27.5	28.6	29.1	29.7	30.6	31.3	32.8	34.3	35.8
	2.39	2.39	2.33	2.33	2.12	1.93	1.70	1.58	1.50

Table 4.3 Values of θ and β for Sections with Less than Minimum Transverse Steel Reinforcement

s_{xe} (in.)	$\varepsilon_x \times 1000$										
	≤–0.20	≤–0.10	≤–0.05	≤0	≤0.125	≤0.25	≤0.50	≤0.75	≤1.00	≤1.50	≤2.00
≤5	25.4 6.36	25.5 6.06	25.9 5.56	26.4 5.15	27.7 4.41	28.9 3.91	30.9 3.26	32.4 2.86	33.7 2.58	35.6 2.21	37.2 1.96
≤10	27.6 5.78	27.6 5.78	28.3 5.38	29.3 4.89	31.6 4.05	33.5 3.52	36.3 2.88	38.4 2.50	40.1 2.23	42.7 1.88	44.7 1.65
≤15	29.5 5.34	29.5 5.34	29.7 5.27	31.1 4.73	34.1 3.82	36.5 3.28	39.9 2.64	42.4 2.26	44.4 2.01	47.4 1.68	49.7 1.46
≤20	31.2 4.99	31.2 4.99	31.2 4.99	32.3 4.61	36.0 3.65	38.8 3.09	42.7 2.46	45.5 2.09	47.6 1.85	50.9 1.52	53.4 1.31
≤30	34.1 4.46	34.1 4.46	34.1 4.46	34.2 4.43	38.9 3.39	42.3 2.82	46.9 2.19	50.1 1.84	52.6 1.60	56.3 1.30	59.0 1.10
≤40	36.6 4.06	36.6 4.06	36.6 4.06	36.6 4.06	41.2 3.20	45.0 2.62	50.2 2.00	53.7 1.66	56.3 1.43	60.2 1.14	63.0 0.95
≤60	40.8 3.50	40.8 3.50	40.8 3.50	40.8 3.50	44.5 2.92	49.2 2.32	55.1 1.72	58.9 1.40	61.8 1.18	65.8 0.92	68.6 0.75
≤80	44.3 3.10	44.3 3.10	44.3 3.10	44.3 3.10	47.1 2.71	52.3 2.11	58.7 1.52	62.8 1.21	65.7 1.01	69.7 0.76	72.4 0.62

4.4. SUMMARY AND CONCLUDING REMARKS

The purpose of this section was to identify and discuss the analytical models and design guidelines that will be used for a comparative evaluation. From the review of the fourteen analytical models and seven design guidelines to predict the shear contribution of FRP, it can be concluded that the main difference between models and guidelines lies in the different approaches to predict the FRP effective strain at the time of failure. Therefore, the analytical models and design guidelines were classified according to the approach to determine the effective FRP strain. The analytical models and guidelines were categorized into approaches based on a fixed FRP effective strain, approaches based on effective strain as a function of FRP stiffness or based on bond mechanism, and approaches based on non-uniform strain distribution. Some models and guidelines fixed the FRP effective strain to determine the FRP shear contribution. For instance, Chajes et al. (1995) fixed the strain to be the ultimate strain at failure corresponding to the concrete. CSA S806-02 (2002) provides fixed values of effective FRP strain according to wrapping configurations. Empirical models are based directly on the calibration of experimental data and regression analysis to estimate the effective strain in the FRP.

From the regression analysis, relationships to determine the effective FRP strain were derived. Models based on non-uniform strain distribution determine the specific fracture energy of the FRP/concrete interface to estimate the bond strength.

When determining the effective FRP strain, most analytical models, and design guidelines treat separately the mechanisms of FRP debonding and FRP fracture except for Chajes et al. (1995), Triantafillou (1998), JBDPA (1999), JSCE (2001), and CSA S806-02 (2002). Therefore, most models and design standards propose two different approaches that represent the two possible failure modes. When estimating the effective FRP strain, most models and design guidelines, with the exception of Chen and Teng (2003), Cao et al. (2005), Monti and Liotta (2004), and Carolin and Taljsten (2005) determined the effective FRP strain by performing regression analysis of experimental data. Therefore, important parameters that influence the effective FRP strain were not taken into consideration because of the difficulty of accounting all relevant parameters in one single equation. In addition, when estimating the effective FRP strain when debonding controls, models and guidelines based on data regression, did not provide an accurate bond strength model. Therefore, it seems that the models based on fracture mechanics describe more accurately the behavior of RC beams shear strengthened with externally FRP as opposed to the models and guidelines based on test data calibration because the bond strength models were developed by applying fracture mechanics. Bond strength models based on fracture mechanics captures all the crucial parameters relevant to the bond behavior at the FRP/concrete interface. In addition, the bond strength models that apply fracture mechanics recognize the non-uniformity of the FRP stress distribution along a shear crack.

Finally, all analytical models with the exception of Deniaud and Cheng (2004), do not take into consideration the interaction between the concrete, transverse steel reinforcement and FRP reinforcement. Most models add the contributions of concrete, stirrups and FRP to be consistent with the truss approach used in reinforced concrete design codes without taken into account the dependence and interaction between the concrete, stirrups and FRP sheets.

<div align="center">

5. EVALUATION OF EXISTING ANALYTICAL MODELS

</div>

5.1. INTRODUCTION

This section presents a comparative evaluation of the accuracy in predicting the FRP shear contribution, defined as V_f , between the analytical models discussed previously in Section Four. The analytical model developed by Khalifa et al. (1998) has not been considered in the evaluation since a revised version was proposed by Khalifa et al. in 1999. In addition, since this section focuses on the evaluation of analytical models for estimating V_f , the model from Deniaud and Cheng (2004) is not evaluated because this analytical model needs to determine the FRP shear contribution as a function of the concrete and transverse steel reinforcement shear contributions

Before performing the comparative evaluation, the entire database (refer to Table A.1 in the Appendix) was reduced to a subset of data. Only test results corresponding to large and slender beam specimens are included in the comparative evaluation. One reason for not using test results on small and non-slender members is that the fixed development lengths of different FRP strengthening systems is a much larger percentage of the total height of a small member. Therefore by only using test results for which the height is greater than or equal to 300 mm and for which the shear-span to depth ratio a/d was greater than or equal to 2.5, only 142 test results satisfied both of these criteria. Furthermore, test results with other type of strengthening systems such as near-surface mounted (NSM) rebars and prestressed straps are omitted because these types of strengthening systems present a different type of behavior from the externally applied FRP systems. After eliminating tests results in which flexural failures were reported and cases in which insufficient data information was available, there were 127 test results left to be used in the comparative evaluation.

For each analytical model, the predicted shear strength provided by the FRP system, $V_{f,theo}$, is compared with the observed experimental results, $V_{f,\exp}$. The FRP shear capacity ratio, defined as $V_{f,\exp}/V_{f,theo}$, is evaluated in terms of $E_f \rho_f / f'_c{}^{2/3}$, a/d and $\rho_s E_s / \rho_f E_f$. Each analytical model has also been analyzed in terms of failure modes and FRP wrapping schemes. Furthermore, for each analytical model, the predicted total

shear capacity, V_{theo}, is compared with the observed experimental results, V_{exp}. The predictions of total shear capacities are computed as $V_n = V_c + V_s + V_{f,theo}$, where V_c and V_S are computed by applying four RC design codes. These design codes are the ACI 318-05 (2005), Eurocode 2 Part I (2003), CSA A23.3-94 (1994), and AASHTO LRFD Bridge Design Specifications (1998).

As a result, the evaluation for each analytical model yields to fourteen plots for each analytical model. In this section, only the plots corresponding to Chajes et al. (1995) are presented. The plots corresponding to the remaining analytical models are presented in Appendix B. Instead, in this section the mean values and coefficient of variation (COV) values of $V_{f,exp}/V_{f,theo}$ and V_{exp}/V_{theo} are presented in Tables 5.1 through 5.6. These tables also provide statistical results for each mode of failure.

Table 5.1. Comparison of Predictions and Test Results for FRP Capacities ($V_{f,exp}/V_{f,theo}$)

Analytical Model	All		Debonding		Fracture		Other Shear Failure Modes	
	Mean	COV	Mean	COV	Mean	COV	Mean	COV
Chajes et al. (1995)	1.31	1.16	0.78	0.82	3.15	0.69	0.93	1.09
Triantafillou (1998)	0.93	0.77	0.68	0.59	1.73	0.56	0.80	0.64
Khalifa et al. (1999)	1.48	0.78	1.22	0.49	2.65	0.67	1.10	0.69
Triantafillou and Antonopoulos (2000)	0.88	0.50	0.86	0.53	0.98	0.39	0.85	0.53
Pellegrino and Modena (2002)	1.60	0.87	1.28	0.69	2.94	0.67	1.13	0.79
Chaallal et al. (2002)	0.88	0.88	0.89	1.16	1.02	0.41	0.76	0.51
Hsu et al. (2003)	1.04	0.55	1.21	0.54	1.02	0.44	0.79	0.52
Chen and Teng (2003)	1.24	0.47	1.26	0.46	1.27	0.48	1.18	0.51
Monti and Liotta (2005)	1.28	0.71	1.06	0.67	2.07	0.50	1.09	0.75
Cao et al. (2005)	0.81	0.66	0.68	0.58	1.36	0.45	0.66	0.67
Zhang and Hsu (2005)	2.54	0.65	2.51	0.65	2.04	0.49	2.89	0.66
Carolin and Taljsten (2005)	1.26	0.77	1.05	0.75	2.10	0.47	1.06	0.91

Table 5.2. Comparison of Predictions and Test Results for Shear Capacities (V_{exp}/V_{theo})

Analytical Model	ACI 318-05		Eurocode 2		CSA A23.3-94		AASHTO LRFD	
	Mean	COV	Mean	COV	Mean	COV	Mean	COV
Chajes et al. (1995)	1.13	0.46	1.04	0.40	1.04	0.43	1.29	0.38
Triantafillou (1998)	1.09	0.36	0.98	0.34	1.01	0.34	1.18	0.41
Khalifa et al. (1999)	1.34	0.32	1.18	0.28	1.23	0.29	1.48	0.37
Triantafillou and Antonopoulos (2000)	1.15	0.29	1.03	0.27	1.06	0.28	1.23	0.32
Pellegrino and Modena (2002)	1.36	0.32	1.20	0.29	1.24	0.30	1.51	0.38
Chaallal et al. (2002)	1.05	0.33	0.96	0.33	0.99	0.32	1.13	0.36
Hsu et al. (2003)	1.22	0.30	1.10	0.28	1.13	0.29	1.31	0.35
Chen and Teng (2003)	1.33	0.28	1.18	0.25	1.23	0.26	1.45	0.30
Monti and Liotta (2005)	1.28	0.34	1.11	0.31	1.17	0.32	1.38	0.38
Cao et al. (2005)	1.06	0.31	0.97	0.29	0.99	0.29	1.15	0.35
Zhang and Hsu (2005)	1.67	0.32	1.42	0.29	1.50	0.31	1.81	0.36
Carolin and Taljsten (2005)	1.24	0.39	1.15	0.32	1.14	0.36	1.43	0.39

Table 5.3. Comparison of Predictions and Test Results for Shear Capacities (V_{exp}/V_{theo}) by ACI 318-05

Analytical Model	Debonding		Fracture		Other Shear Failure Modes	
	Mean	COV	Mean	COV	Mean	COV
Chajes et al. (1995)	0.96	0.50	1.61	0.31	1.11	0.38
Triantafillou (1998)	0.95	0.40	1.39	0.29	1.13	0.26
Khalifa et al. (1999)	1.32	0.33	1.54	0.30	1.23	0.27
Triantafillou and Antonopoulos (2000)	1.12	0.36	1.14	0.21	1.19	0.21
Pellegrino and Modena (2002)	1.28	0.35	1.59	0.29	1.31	0.27
Chaallal et al. (2002)	1.01	0.42	1.15	0.25	1.06	0.21
Hsu et al. (2003)	1.30	0.32	1.15	0.20	1.13	0.28
Chen and Teng (2003)	1.35	0.31	1.25	0.26	1.37	0.22
Monti and Liotta (2005)	1.20	0.38	1.50	0.24	1.25	0.33
Cao et al. (2005)	0.98	0.33	1.30	0.24	1.03	0.28
Zhang and Hsu (2005)	1.66	0.38	1.59	0.27	1.72	0.26
Carolin and Taljsten (2005)	1.14	0.44	1.54	0.22	1.20	0.36

Table 5.4. Comparison of Predictions and Test Results for Shear Capacities (V_{exp}/V_{theo})
by Eurocode 2

Analytical Model	Debonding		Fracture		Other Shear Failure Modes	
	Mean	COV	Mean	COV	Mean	COV
Chajes et al. (1995)	0.88	0.45	1.38	0.26	1.08	0.28
Triantafillou (1998)	0.85	0.39	1.22	0.24	1.02	0.24
Khalifa et al. (1999)	1.23	0.37	1.33	0.25	1.20	0.28
Triantafillou and Antonopoulos (2000)	1.00	0.34	1.03	0.19	1.10	0.18
Pellegrino and Modena (2002)	1.13	0.31	1.37	0.24	1.15	0.26
Chaallal et al. (2002)	0.92	0.41	1.03	0.21	0.96	0.22
Hsu et al. (2003)	1.16	0.30	1.05	0.20	1.03	0.26
Chen and Teng (2003)	1.18	0.29	1.12	0.23	1.23	0.18
Monti and Liotta (2005)	1.04	0.33	1.31	0.20	1.09	0.30
Cao et al. (2005)	0.90	0.32	1.15	0.20	0.96	0.26
Zhang and Hsu (2005)	1.39	0.33	1.40	0.26	1.49	0.22
Carolin and Taljsten (2005)	1.05	0.39	1.35	0.19	1.18	0.25

Table 5.5. Comparison of Predictions and Test Results for Shear Capacities (V_{exp}/V_{theo})
by CSA A23.3-94

Analytical Model	Debonding		Fracture		Other Shear Failure Modes	
	Mean	COV	Mean	COV	Mean	COV
Chajes et al. (1995)	0.89	0.48	1.42	0.28	1.03	0.34
Triantafillou (1998)	0.89	0.39	1.25	0.27	1.06	0.24
Khalifa et al. (1999)	1.22	0.31	1.36	0.27	1.15	0.24
Triantafillou and Antonopoulos (2000)	1.04	0.35	1.05	0.21	1.12	0.20
Pellegrino and Modena (2002)	1.18	0.33	1.41	0.26	1.21	0.25
Chaallal et al. (2002)	0.95	0.41	1.05	0.24	1.01	0.21
Hsu et al. (2003)	1.20	0.31	1.06	0.20	1.07	0.27
Chen and Teng (2003)	1.24	0.30	1.14	0.25	1.27	0.20
Monti and Liotta (2005)	1.11	0.37	1.34	0.23	1.17	0.30
Cao et al. (2005)	0.92	0.32	1.18	0.23	0.97	0.26
Zhang and Hsu (2005)	1.50	0.36	1.43	0.27	1.57	0.25
Carolin and Taljsten (2005)	1.05	0.43	1.38	0.21	1.11	0.32

Table 5.6. Comparison of Predictions and Test Results for Shear Capacities (V_{exp}/V_{theo}) by AASHTO LRFD

Analytical Model	Debonding		Fracture		Other Shear Failure Modes	
	Mean	COV	Mean	COV	Mean	COV
Chajes et al. (1995)	1.05	0.51	1.90	0.33	1.29	0.38
Triantafillou (1998)	1.00	0.42	1.60	0.31	1.20	0.32
Khalifa et al. (1999)	1.42	0.36	1.81	0.33	1.31	0.33
Triantafillou and Antonopoulos (2000)	1.19	0.39	1.26	0.23	1.28	0.24
Pellegrino and Modena (2002)	1.38	0.38	1.88	0.31	1.39	0.35
Chaallal et al. (2002)	1.09	0.44	1.28	0.26	1.10	0.24
Hsu et al. (2003)	1.40	0.38	1.26	0.22	1.17	0.32
Chen and Teng (2003)	1.45	0.34	1.42	0.28	1.47	0.24
Monti and Liotta (2005)	1.26	0.38	1.75	0.26	1.30	0.39
Cao et al. (2005)	1.04	0.36	1.45	0.25	1.10	0.34
Zhang and Hsu (2005)	1.80	0.43	1.83	0.29	1.84	0.28
Carolin and Taljsten (2005)	1.27	0.45	1.80	0.24	1.43	0.34

5.2. COMPARATIVE EVALUATION

5.2.1. Chajes et al. (1995). Figures 5.1 through 5.3 illustrate the variation of the FRP shear capacity ratio in terms of $E_f \rho_f / f'^{2/3}_c$ for different failure modes and wrapping configurations. From Figure 5.1, the decreasing trendline indicates that if the values of $E_f \rho_f / f'^{2/3}_c$ are smaller than 0.019, this analytical model underestimates the prediction of the FRP shear contribution and overestimates the FRP shear contribution when the values of $E_f \rho_f / f'^{2/3}_c$ are greater than 0.019. From Figure 5.2, it can also be concluded that this analytical model greatly underestimates the FRP shear contribution for lower values of $E_f \rho_f / f'^{2/3}_c$. In addition, Figures 5.1 and 5.2 also indicate that this analytical model tends to greatly underestimate the predictions for the FRP shear contribution for specimens that failed due to FRP fracture in comparison to those that failed due to FRP debonding or other shear failure modes.
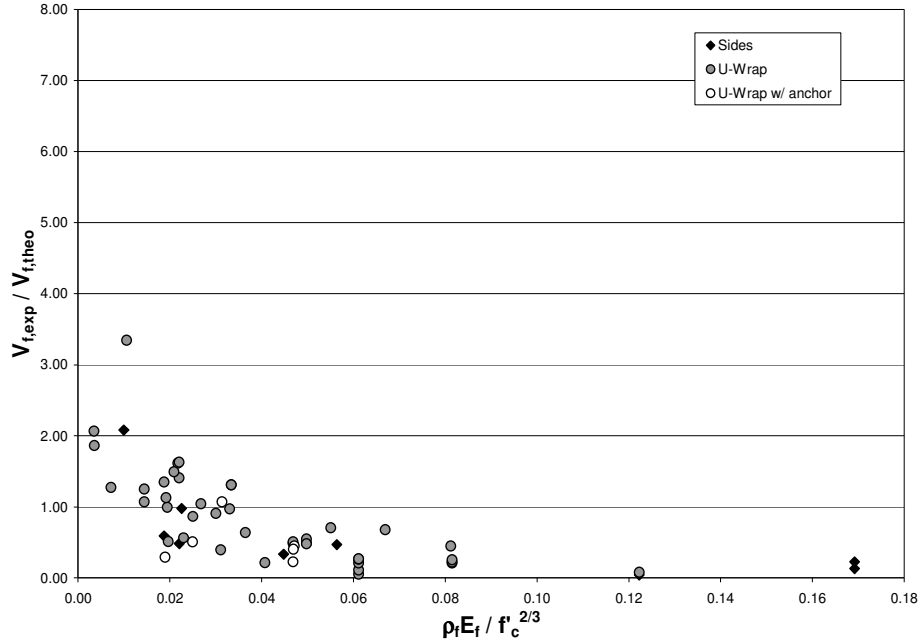
Figure 5.1. $V_{f,\exp}/V_{f,theo}$ in Terms of $E_f\rho_f/f'^{2/3}_c$ - FRP Debonding
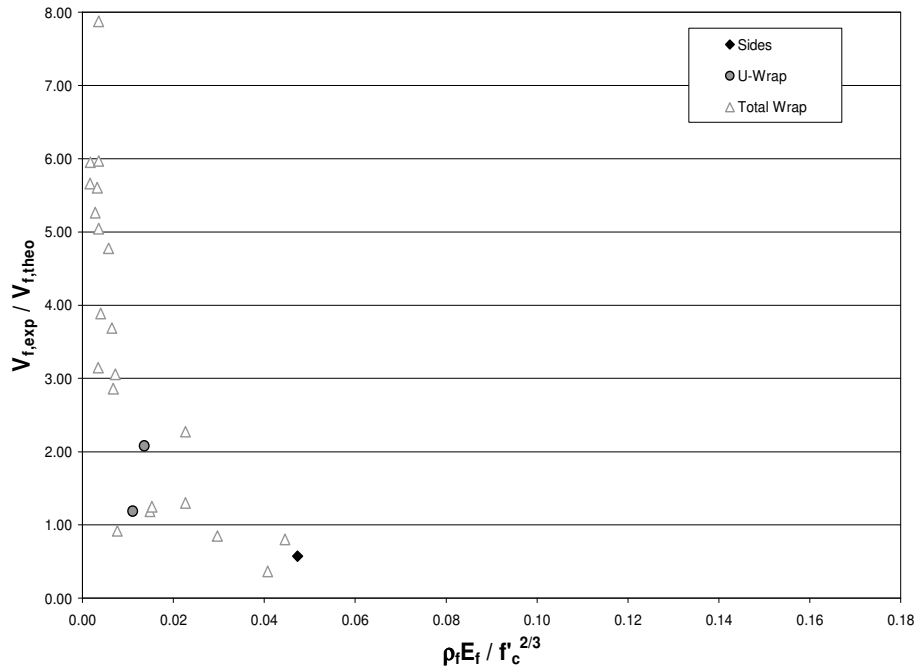
Figure 5.2. $V_{f,\exp}/V_{f,theo}$ in Terms of $E_f\rho_f/f'^{2/3}_c$ - FRP Fracture
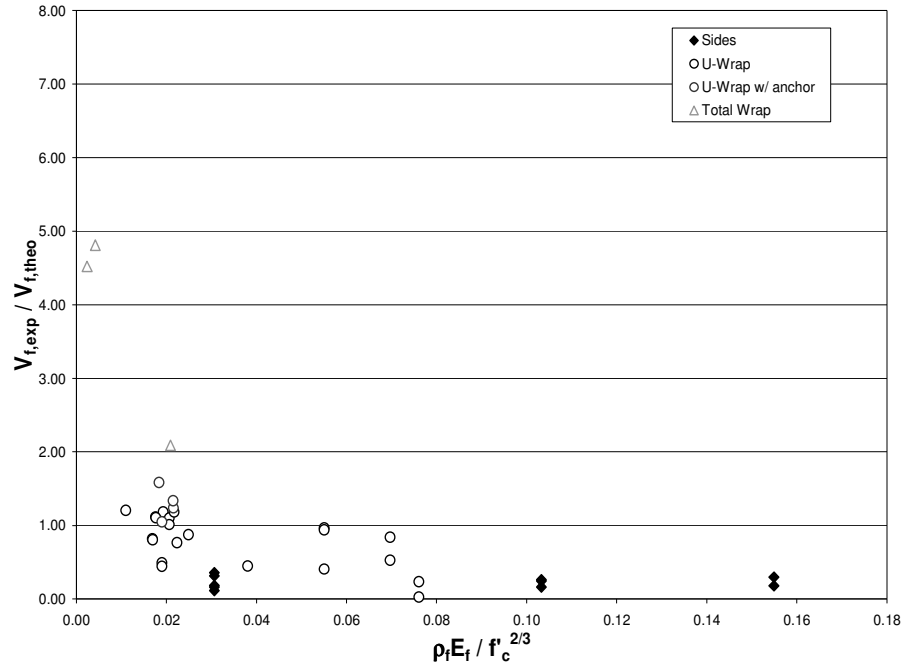
Figure 5.3. $V_{f,\exp}/V_{f,theo}$ in Terms of $E_f\rho_f/f'^{2/3}_c$ - Other Failure Modes

Figures 5.4 through 5.6 illustrate the predictions of FRP shear capacity in terms of a/d for different failure modes. From Figure 5.4, the FRP shear capacity ratio increases up to a/d around 2.69. Afterwards, the FRP shear capacity ratio decreases up to a shear span-to-depth ratio of 3.41. The same trendline is observed for specimens failing in fracture as shown in Figure 5.5. Therefore, it seems that for specimens with a/d less than about 3.0, this analytical model underestimates the FRP shear contribution, and overestimates it for a/d larger than 3.0.

Figures 5.7 through 5.9 illustrate the predictions of FRP shear capacity in terms of the amount of transverse steel reinforcement for different failure modes. From Figure 5.7, it can be observed that when the amount of transverse steel reinforcement increases, the shear capacity ratio of FRP increases up to 2.67 and decreases afterwards. The same trend is exhibited for those specimens that failed due to FRP fracture. Therefore, this analytical model underestimates the FRP shear contribution when the amount of transverse steel reinforcement increases.
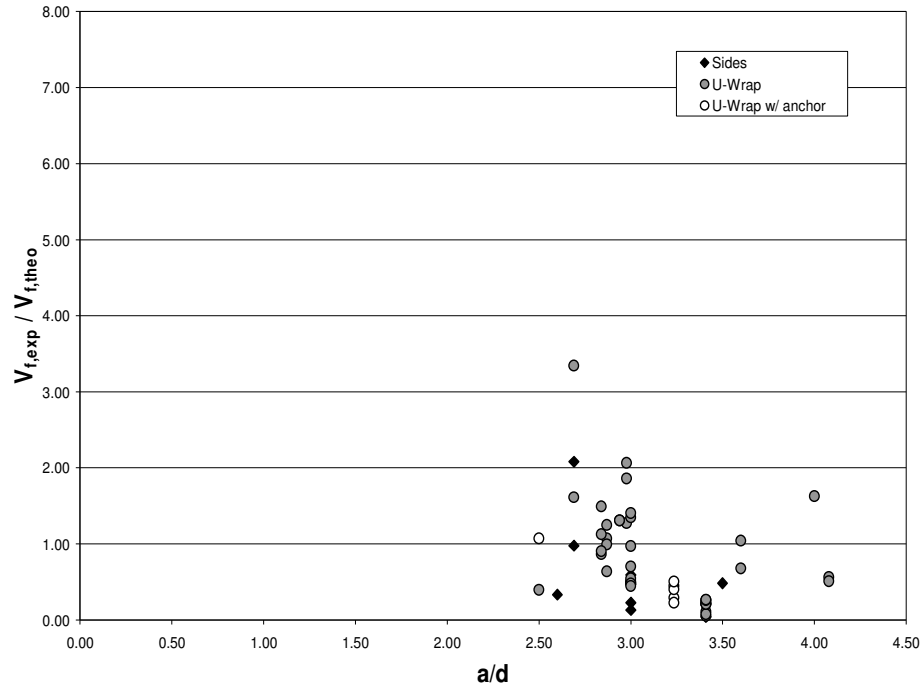
Figure 5.4. $V_{f,\exp}/V_{f,theo}$ in Terms of a/d – FRP Debonding
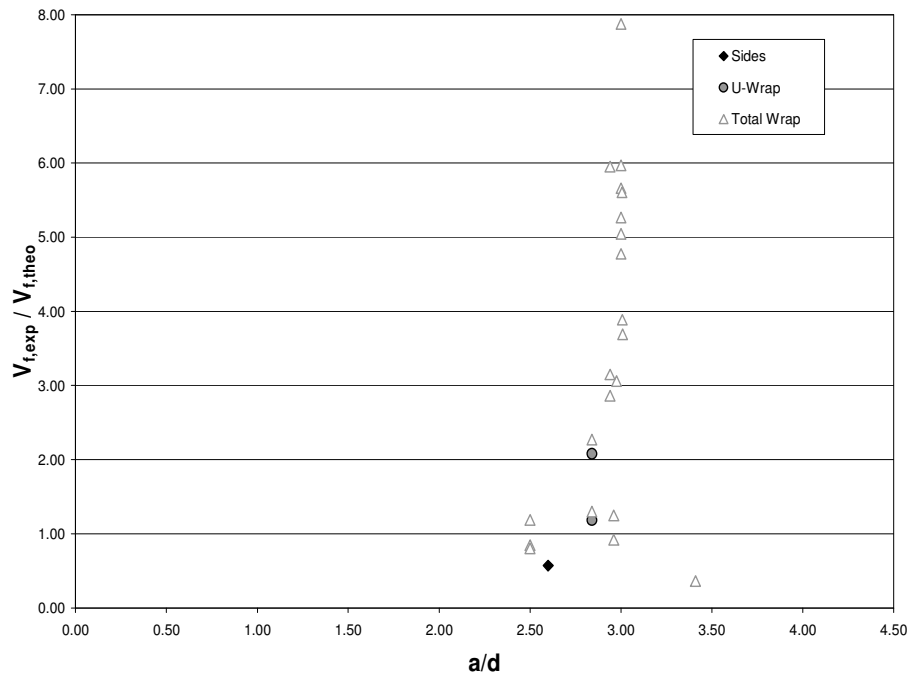
Figure 5.5. $V_{f,\exp}/V_{f,theo}$ in Terms of a/d – FRP Fracture
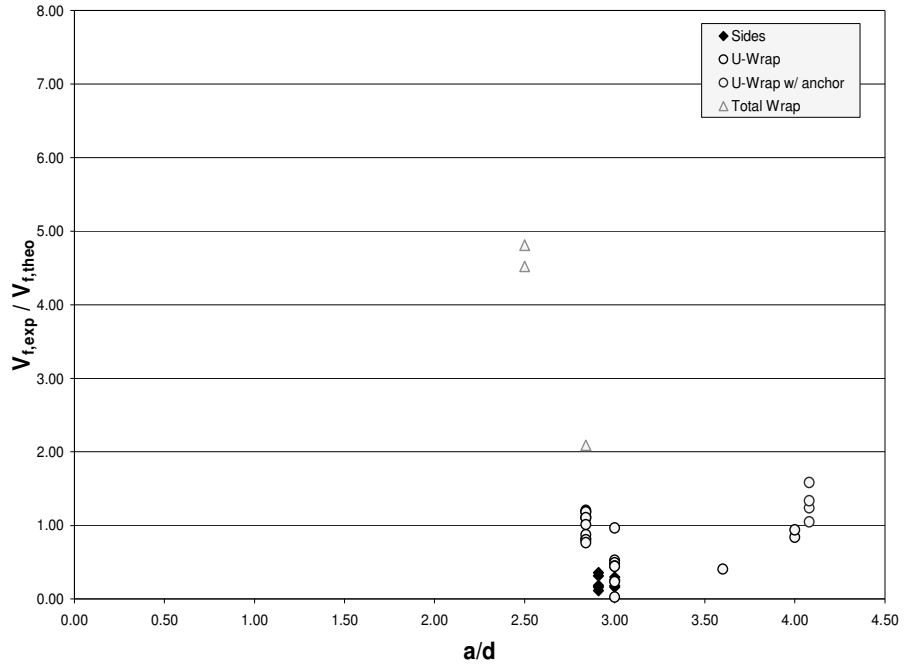
Figure 5.6. $V_{f,\exp}/V_{f,theo}$ in Terms of a/d – Other Failure Modes
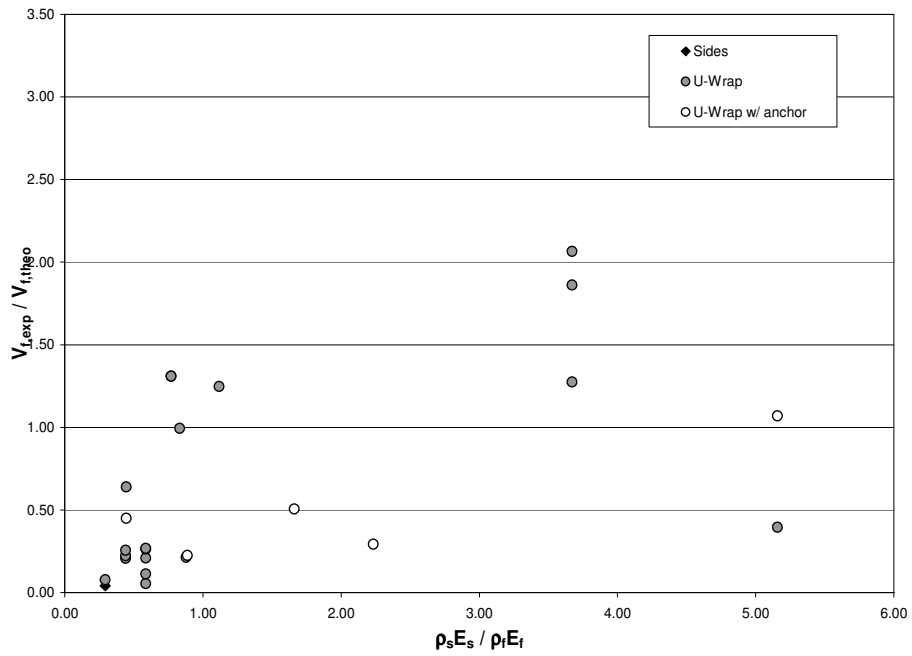
Figure 5.7. $V_{f,\exp}/V_{f,theo}$ in Terms of $\rho_s E_s/\rho_f E_f$ – FRP Debonding
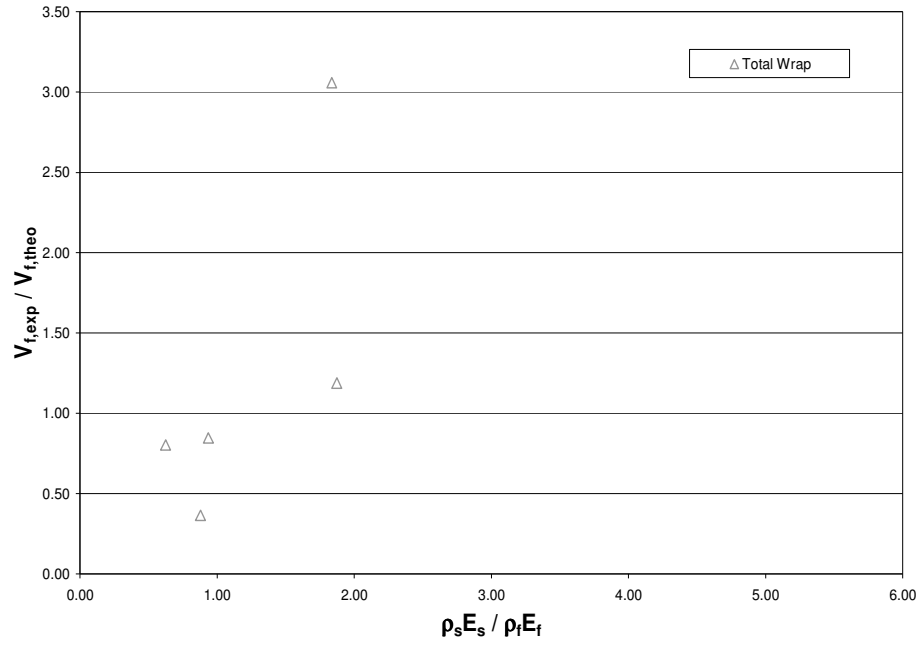
Figure 5.8. $V_{f,\exp}/V_{f,theo}$ in Terms of $\rho_s E_s / \rho_f E_f$ – FRP Fracture
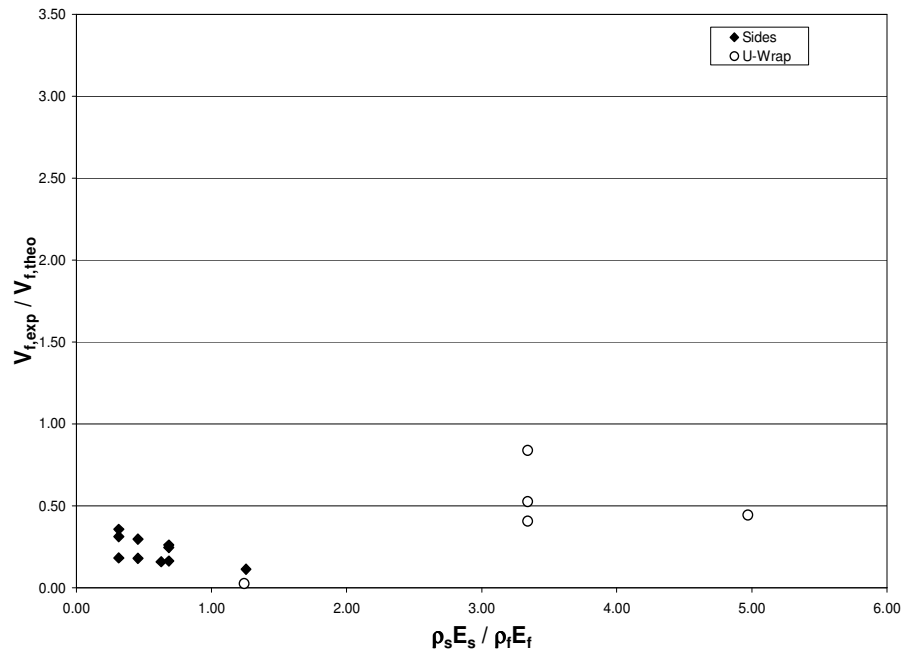
Figure 5.9. $V_{f,\exp}/V_{f,theo}$ in Terms of $\rho_s E_s / \rho_f E_f$ – Other Failure Modes

From the previous analysis, it can be concluded that the analytical approach proposed by Chajes et al. (1995) cannot accurately predict the shear capacity of FRP. This could be attributed to the fact that Chajes et al. (1995) applies a constant ultimate tensile strain, corresponding to the concrete ultimate strain, to calculate the shear capacity of FRP. However, as verified from later studies (Triantafillou, 1998), the ultimate tensile strain of FRP at failure, defined as the effective strain of FRP, decreases as the axial rigidity of FRP, $\rho_f E_f$ increases. In addition, the formulations from this model can only be applied to continuous FRP sheets. The analysis shows that this model predicts more accurately the FRP shear contribution for those specimens that failed in fracture (COV of 69%) than those that failed in debonding (COV of 82 %). However, this model tends to underestimate the FRP shear contribution by more than twice the experimental FRP shear contribution for most test specimens failing in fracture. The inaccuracy in predicting the FRP shear contribution by this analytical model, with a COV of 116%, is also shown in Figure 5.10.
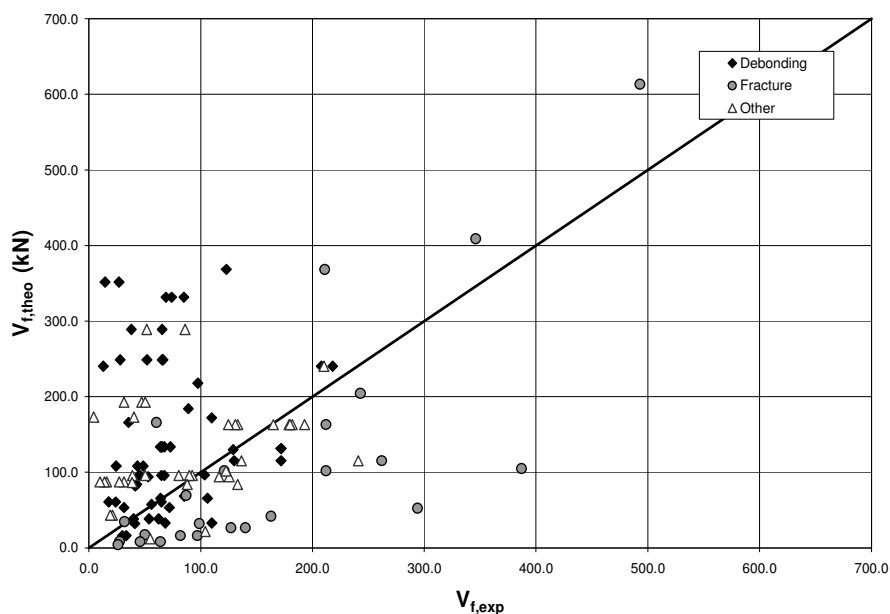
Figure 5.10. Comparison between Analytical Predictions of FRP Shear Contribution and Experimental Results

Finally, the comparison between the predicted total shear capacity by applying four different shear design methodologies and the observed experimental results are illustrated in Figure 5.11. From this analysis, Eurocode 2 exhibits a lower COV of 40% with a mean value of 1.04. Therefore the shear design provisions from Eurocode 2 predict the total shear capacity more accurately than the other design methodologies. For specimens that failed due to FRP fracture and FRP debonding, Eurocode 2 also provides lower COV values than the other design codes.
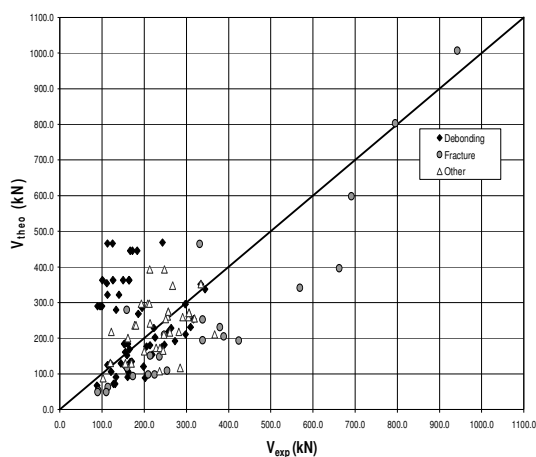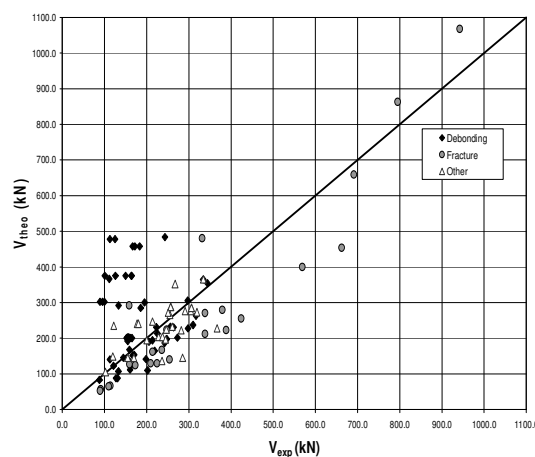
(a) ACI 318-05   (b) Eurocode 2
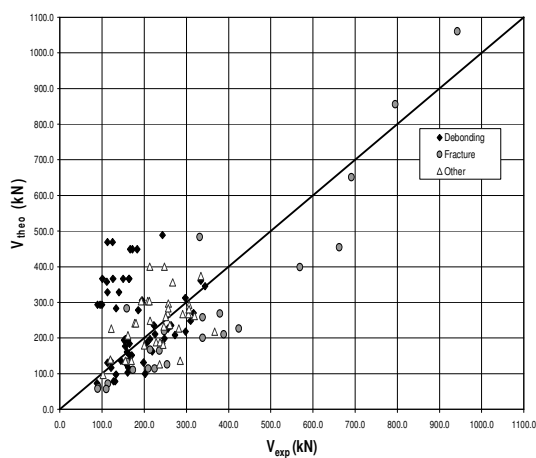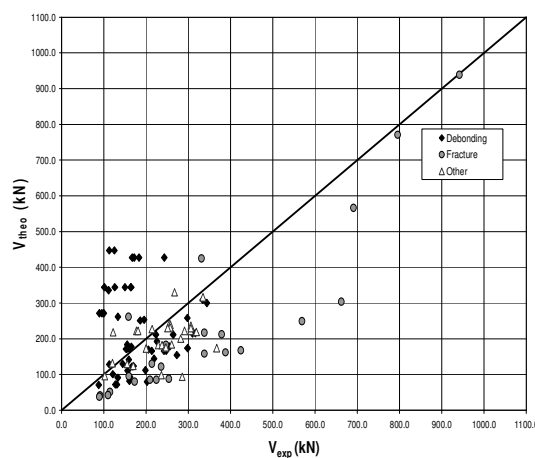
(c) CSA A23.3-94   (d) AASHTO LRFD

Figure 5.11. Comparison between Analytical Predictions of Total Shear Capacity and Experimental Results

5.2.2. Triantafillou (1998). From the analysis of this analytical model (refer to graphs in Appendix B), the analytical model proposed by Triantafillou (1998) predicted the shear capacity of FRP more accurately than the one from Chajes et al. (1995) since it was the first model to determine that the effective strain of the FRP is a function of its axial rigidity. By analyzing the prediction of the FRP shear strength versus $E_f \rho_f /(f_c^{'})^{2/3}$, it was found that as in Chajes et al. (1995) model, this approach overestimates the FRP shear capacity as $E_f \rho_f /(f_c^{'})^{2/3}$ increases. Furthermore, this analytical model predicts the shear capacity of FRP slightly more accurately for specimens that failed due to FRP fracture (COV of 56%) in comparison to those that failed due to FRP debonding (COV of 59 %). However, for debonding and other failure modes, most of the predictions have been overestimated.

In addition, by analyzing the FRP shear strength ratio versus the shear span-to-depth ratio, this analytical model seems to highly underestimate the FRP shear contribution for those specimens that failed due to FRP fracture. On the other hand, for those specimens that failed due to debonding, this analytical model overestimates the FRP shear contribution. Furthermore, from the analysis, it can be observed that the FRP shear capacity ratio increases up to a/d = 3.0 and decreases afterwards. Finally, from analysis of the FRP shear strength ratio versus the effect of transverse steel reinforcement on the FRP shear contribution, it was observed that when the amount of transverse steel reinforcement increases, the shear capacity ratio of FRP increases. The same trend is exhibited for those specimens that failed in fracture and other shear failure modes.

From the analysis, this model predicts the FRP shear capacity more accurately in comparison to Chajes et al. (1995) model because this approach predicts a varying FRP strain. However, this model seems to predict the FRP shear contribution slightly more accurately for specimens that failed due to fracture failure than for those that failed due to debonding or other shear failures. This could be attributed to the fact that this analytical model derived an expression to compute the effective strain of the FRP without considering the different failure mechanisms. As a result, it seems the effective strain of the FRP plays an important role in determining the accuracy of the predictions. In addition, this analytical model provides a COV of 77%, which indicates that this model

predicts the shear capacity due to the FRP more accurate than the model from Chajes et al. (1995).

Finally, from the comparison between the predicted total shear capacity by applying four different design methodologies and the observed experimental results, it can be concluded that both Eurocode 2 and CSA A23.3-94 exhibit a lower COV value of 34%. Therefore the predictions of total shear capacity from Eurocode 2 and CSA A23.3-94 are more accurate than those from other design methodologies when using the analytical model from Triantafillou (1998). For specimens that failed due to FRP fracture, Eurocode 2 design provisions provides less conservative values of $V_{\exp}/V_{theo}$ in comparison to other design methodologies. In addition, for specimens that failed due to FRP fracture and FRP debonding, Eurocode 2 provides lower COV values.

5.2.3. Khalifa et al. (1999). From the analysis of this analytical model (refer to graphs in Appendix B), the analytical model proposed by Khalifa et al. (1999) underestimates the FRP shear capacity for lower values of $E_f \rho_f /(f_c^{'})^{2/3}$ and overestimates it for higher values of $E_f \rho_f /(f_c^{'})^{2/3}$. The predictions of the FRP shear capacity by this model are more conservative for fracture failure (mean value of FRP shear contribution of 2.65) than for debonding (mean value of 1.22) and other shear failures. In contrast to the previously discussed analytical models, this model seems to provide better predictions for specimens that failed in debonding (COV of 49%) probably because the formulation applied to predict the effective FRP strain dominant to fracture failures cannot be applied for higher FRP axial rigidities.

In addition, by analyzing the FRP shear strength ratio versus the shear span-to-depth ratio, for specimens that failed due to fracture failure, this model highly underestimates the FRP shear contribution for test specimens with a shear span-to-depth ratio of 3.0. However, for debonding failure, this model overestimates the FRP shear capacity for most test specimens. Furthermore, this model is more conservative in predicting the FRP shear capacity of specimens that failed due to FRP fracture. From this analysis, it can also be observed that the FRP shear capacity ratio increases up to $a/d = 3.0$ and decreases afterwards. Finally, from analysis of the FRP shear strength ratio versus the effect of transverse steel reinforcement on the FRP shear contribution, it was

observed that the FRP shear capacity ratio increases as the amount of transverse steel reinforcement increases for specimens that failed due to FRP debonding. This increasing trendline is also present for specimens that failed due to FRP fracture.

From the previous analysis, it can be concluded that the analytical model from Khalifa et al. (1999) provides a COV of 78%, thus, this analytical model does not accurately predict the FRP shear capacity in contrast to Triantafillou (1998). However, this is the first analytical model that proposes two different expressions to compute the effective strain of the FRP by taking into consideration the FRP failure mechanisms. In addition, this analytical model gives better prediction for debonding (COV of 49%) because influential parameters to the bond behavior of the FRP/concrete interface are taken into consideration.

Finally, from the comparison between the predicted total shear capacity by applying four different design methodologies and the observed experimental results, it can be concluded that Eurocode 2 exhibits a lower COV value of 24%. Therefore the predictions of total shear capacity from Eurocode 2 are more accurate than those from other design methodologies when using the analytical model from Khalifa et al. (1999). For specimens that failed due to FRP fracture, Eurocode 2 design provisions provides less conservative values of $V_{\exp}/V_{theo}$ in comparison to other design methodologies. In addition Eurocode 2 provides a lower value of COV for specimens that failed due to FRP fracture; however, it exhibits a higher value of COV for specimens that failed due to FRP debonding.

5.2.4. Triantafillou and Antonopoulos (2000). This analytical model is a revision of its earlier version (Triantafillou, 1998). This later version considered the types of FRP, the strengthening scheme of FRP, and the effect of the concrete compressive strength in the formulation of the effective FRP strain. From the analysis of this approach (refer to graphs in Appendix B), this model underestimates the FRP shear capacity for lower values of $E_f\rho_f/(f_c')^{2/3}$ and overestimates it for higher values of $E_f\rho_f/(f_c')^{2/3}$. Moreover, this model provides better predictions of FRP shear contribution for specimens that failed due to FRP fracture (COV of 39%) than for those than failed due to debonding (COV of 53%) or other shear failures modes. This could be

attributed to the fact that this model does not make a clear distinction between side-bonded FRP systems and U-shaped FRP jackets when estimating the effective FRP strain.

Furthermore, by analyzing the FRP shear strength ratio versus the shear span-to-depth ratio, this model tends to overestimate the FRP shear capacity for most data specimens failing due to FRP debonding. On the other hand, for fracture failure, this model underestimates the FRP shear capacity for most test specimens. In addition, from this analysis, it can be observed that the FRP shear capacity ratio increases up to a/d = 3.0, and decreases afterwards. Finally, from the analysis of the FRP shear strength ratio versus the effect of transverse steel reinforcement on the FRP shear contribution, it was observed that for debonding failure, this model underestimates the FRP shear capacity as the amount of transverse steel reinforcement increases. For fracture failure, this model overestimates the FRP shear capacity as the amount of transverse steel reinforcement increases. This analytical model also makes better predictions for specimens than failed due to FRP fracture.

From the previous analysis, the analytical model from Triantafillou and Antonopoulos (2000) provides a lower COV (50 %) than its earlier version. Therefore, this analytical model predicts the FRP shear contribution more accurately than the older version developed by Triantafillou (1998) and the previously discussed models. This could be explained by the fact that this model considers separately the different FRP failure mechanisms when estimating the effective FRP strain as opposed to its earlier version.

Finally, from the comparison between the predicted total shear capacity by applying four different design methodologies and the observed experimental results, it can be concluded that Eurocode 2 exhibits a lower COV value of 27%. Therefore the predictions of total shear capacity from Eurocode 2 are more accurate than those from other design methodologies when using the analytical model from Triantafillou and Antonopoulos (2000). By applying AASHTO LRFD in combination with this analytical model, more conservative values for V_{exp}/V_{theo} are obtained. In addition, for specimens that failed due to FRP fracture and FRP debonding, Eurocode 2 design provisions

provides less conservative values of $V_{\exp}/V_{theo}$ in comparison to those from other design methodologies.

5.2.5. Pellegrino and Modena (2002). The analytical model proposed by Pellegrino and Modena slightly modified the approach proposed by Khalifa et al. (1999) by introducing an additional strain reduction factor, R^*, which accounts for the correlation between the internal steel reinforcement and external FRP reinforcement. From the analysis between the FRP shear capacity ratio and $E_f\rho_f/(f_c')^{2/3}$ (refer to graphs on Appendix B), it can be observed that for all failure modes, this model underestimates the FRP shear capacity for higher values of $E_f\rho_f/(f_c')^{2/3}$ and overestimates the FRP shear capacity for lower values of $E_f\rho_f/(f_c')^{2/3}$. The predictions of the FRP shear capacity by this model are more conservative for fracture failure ($V_{f,\exp}/V_{f,theo}$ of 2.94) than for debonding ($V_{f,\exp}/V_{f,theo}$ of 1.28) and other shear failures modes.

Furthermore, by analyzing the FRP shear capacity ratio in terms of the shear span-to-depth ratio, it can be concluded that for specimens that failed due to FRP debonding, this model tends to overestimate the FRP shear capacity for most data specimens. On the other hand, for those specimens that failed due to FRP fracture, this model tends to highly underestimate the FRP shear capacity for most test specimens. From this analysis, it can also be observed that the FRP shear capacity ratio increases up to a shear span–to-depth ratio of about 3.0, and decreases afterwards. Finally, from the analysis of the FRP shear capacity ratio in terms of the amount of transverse steel reinforcement, it can be observed that the FRP shear contribution predicted by this model decreases as the amount of transverse steel reinforcement increases for specimens failing due to FRP fracture and FRP debonding.

From analysis, this analytical model provides a COV of 87%, thus, in comparison to the previously discussed models, except Chajes et al. (1995) model, this approach does not accurately predict the FRP shear contribution. This model predicts very conservative values of FRP shear capacity ratios for specimens that failed due to FRP fracture. This could be attributed to the fact that the strain reduction factor, R^*, was developed based on test results of specimens strengthened with side bonded FRP, which failed due to FRP

debonding. Therefore, this additional reduction factor needs to be improved by performing additional experimental studies.

Finally, from the comparison between the predicted total shear capacity by applying four different design methodologies and the observed experimental results, it can be concluded that Eurocode 2 exhibits a lower COV value of 29%. Therefore the predictions of total shear capacity from Eurocode 2 are more accurate than those from other design methodologies when using the analytical model from Pellegrino and Modena (2002). By applying AASHTO LRFD in combination with this analytical model, more conservative values for $V_{\exp}/V_{theo}$ and higher COV values are obtained. In addition, for specimens that failed due to FRP fracture and FRP debonding, Eurocode 2 design provisions provides less conservative values of $V_{\exp}/V_{theo}$ in comparison to those from other design methodologies.

5.2.6. Chaallal et al. (2002). This analytical model was developed based on the experimental results of large scale specimens under a low shear span condition. As a consequence, Chaallal et al. proposed that a deep beam coefficient, $f(a/d)$, should be included in the expression to determine the FRP shear contribution. By analyzing the FRP shear capacity ratio in terms of $E_f \rho_f /(f_c^{'})^{2/3}$ (refer to graphs in Appendix B), it can be concluded that this analytical model does not accurately predict the shear contribution of FRP for most data points. As in the previously discussed models, this analytical model under predicts the FRP shear contribution for low values of $E_f \rho_f /(f_c^{'})^{2/3}$, and over predicts the FRP shear capacity for higher values of $E_f \rho_f /(f_c^{'})^{2/3}$.

Furthermore, from the analysis of the FRP shear capacity ratio versus the shear span-to-depth ratio, it can be observed that the FRP shear contribution, predicted by Chaallal et al. (2002), increases as the shear span-to-depth ratio increases for all failure modes. Finally, by analyzing the FRP shear capacity ratio in terms of the amount of transverse steel reinforcement, it can be observed that the FRP shear contribution predicted by this model decreases as the amount of transverse steel reinforcement increases for specimens failing due to FRP fracture and FRP debonding.

From the previous analysis, this analytical model provides a COV of 88%, thus this analytical model inaccurately predicts the FRP shear contribution. This model seems

to make slightly better predictions for specimens that failed in fracture (COV of 41%) than those that failed in debonding (COV of 116%). This inaccuracy in the FRP shear prediction could be attributed to the fact that this analytical model was developed based on the results of the experimental results of large scale specimens under a low shear span condition. Therefore, the formulations for predicting the FRP contribution were derived by analyzing the influence of a deep beam coefficient. When calibrating the formulations to compute both the effective FRP strain and the deep beam coefficient, only data points from this experimental study were used, thus more research work is needed to validate these formulations.

Finally, from the comparison between the predicted total shear capacity by applying four different design methodologies and the observed experimental results, it can be concluded that Eurocode 2 provides a lower COV value of 33% and a lower mean value of 0.96. Therefore the predictions of total shear capacity from Eurocode 2 are more accurate than those from other design methodologies when using the analytical model from Chaallal et al. (2002). By applying AASHTO LRFD in combination with this analytical model, more conservative values for V_{exp}/V_{theo} and higher COV values are obtained. In addition, for specimens that failed due to FRP fracture and FRP debonding, Eurocode 2 design provisions provides less conservative values of V_{exp}/V_{theo} in comparison to those from other design methodologies.

5.2.7. Hsu et al. (2003). From the analysis of this approach (refer to graphs in Appendix B), this analytical model accurately predicts the FRP shear contribution in comparison to the experimental observations (COV of 55%). By analyzing the FRP shear capacity ratio in terms of $E_f \rho_f /(f_c')^{2/3}$, it can be observed that, in contrast to the previously discussed models, this approach does not exhibit a clear trendline between the FRP shear capacity ratio and $E_f \rho_f /(f_c')^{2/3}$ with the exception of specimens strengthened with FRP reinforcement to the sides. The reason behind this may be attributed to the fact that the formulations to compute the FRP shear contribution, were derived from test specimens that failed due to FRP debonding. Moreover, the debonding of FRP seems to occur randomly (COV of 54%). The fracture of FRP also occurs randomly; however, the

data points are slightly less scatter than the ones corresponding to debonding failure (COV of 44%).

By analyzing the FRP shear capacity ratio in terms of the shear span-to-depth ratio, it can be observed that the FRP shear capacity ratio decreases, as the shear span-to-depth ratio increases only for those specimens side bonded with FRP and failing in debonding. For specimens failing due to FRP fracture, no clear trendline can be observed between the FRP shear capacity ratio and the shear span-to-depth ratio. Finally, from the analysis between the FRP shear capacity ratio and the amount of transverse steel reinforcement, it can be observed that, in contrast to the previously discussed models, the FRP shear capacity ratio decreases as the amount of steel stirrups increases.

From the previous analysis, the predictions of the FRP shear contribution by this analytical model are in better agreement to the experimental observations in comparison to the previous models with the exception of the model developed by Triantafillou and Antonopoulos (2000). In fact this analytical model provides a COV of 55% for all failure modes. For debonding and fracture failure, a COV of 54% and 44% respectively are observed from the analysis. For this reason, this model makes more accurate predictions for those specimens that failed due to FRP fracture.

Finally, from the comparison between the predicted total shear capacity by applying four different design methodologies and the observed experimental results, it can be concluded that Eurocode 2 provides a lower COV value of 28% and a lower mean value of 1.10. Therefore the predictions of total shear capacity from Eurocode 2 are more accurate than those from other design methodologies when using the analytical model from Hsu et al. (2003). By applying AASHTO LRFD in combination with this analytical model, more conservative values for V_{exp}/V_{theo} and higher COV values are obtained. In addition, for specimens that failed due to FRP fracture and FRP debonding, Eurocode 2 design provisions provides less conservative values of V_{exp}/V_{theo} in comparison to those from other design methodologies. Finally, in contrast to the previously discussed analytical models, the application of all four design codes with this analytical model provide conservative values of V_{exp}/V_{theo} for specimens failing in debonding.

5.2.8. Chen and Teng (2003). From the analysis of this approach (refer to graphs in Appendix B), this analytical model accurately predicts the FRP shear contribution in comparison to the experimental observations (COV of 47%). By analyzing the FRP shear capacity ratio in terms of $E_f \rho_f /(f_c')^{2/3}$, it can be observed that as in previous models, the FRP shear capacity ratio exhibits a decreasing trend as $E_f \rho_f /(f_c')^{2/3}$ increases. In addition, this analytical model underestimates the FRP shear capacity ratio for low values of $E_f \rho_f /(f_c')^{2/3}$, and overestimates the FRP shear contribution for high values of $E_f \rho_f /(f_c')^{2/3}$. This analytical model approach provides better predictions for the FRP shear contribution for both debonding and fracture failures.

Furthermore, from the analysis of the FRP shear capacity ratio versus the shear span-to-depth ratio, it can be observed that the FRP shear contribution, predicted by Chen and Teng (2003) increases as the shear span-to-depth ratio increases for all failure modes. In addition, from this analysis, it can be observed that the FRP shear capacity ratio increases up to $a/d = 3.0$, and decreases afterwards. Finally, by analyzing the FRP shear capacity ratio in terms of the amount of transverse steel reinforcement, it can be observed that the FRP shear contribution predicted by this model decreases as the amount of transverse steel reinforcement increases for specimens failing due to FRP fracture and FRP debonding.

From the previous analysis, the predictions of the FRP shear contribution by this analytical model are in better agreement to the experimental observations in comparison to the previous models. In fact this analytical model provides a COV of 47% for all failure modes. For debonding and fracture failure, a COV of 46% and 48% respectively are observed from the analysis. For this reason, this model makes accurate predictions for specimens failing due to FRP debonding and FRP fracture.

Finally, from the comparison between the predicted total shear capacity by applying four different design methodologies and the observed experimental results, it can be concluded that Eurocode 2 provides a lower COV value of 25% and a lower mean value of 1.18. Therefore the predictions of total shear capacity from Eurocode 2 are more accurate than those from other design methodologies when using the analytical model from Chen and Teng (2003). By applying AASHTO LRFD in combination with this

analytical model, more conservative values for V_{exp}/V_{theo} and higher COV values are obtained. In addition, for specimens that failed due to FRP fracture and FRP debonding, Eurocode 2 design provisions provides less conservative values of V_{exp}/V_{theo} in comparison to those from other design methodologies. Finally, as in Hsu et al (2003) approach, the application of all four design codes with Chen and Teng (2003) model provide conservative values of V_{exp}/V_{theo} for specimens failing in debonding.

5.2.9. Monti and Liotta (2005). From the analysis between the FRP shear capacity ratio and $E_f \rho_f /(f_c^{'})^{2/3}$ (refer to graphs on Appendix B), it can be observed that the analytical model proposed by Monti and Liotta does not accurately predict the shear capacity of FRP. As in previous models, this analytical model underestimates the FRP shear capacity ratio for low values of $E_f \rho_f /(f_c^{'})^{2/3}$, and overestimates the FRP shear contribution for high values of $E_f \rho_f /(f_c^{'})^{2/3}$. In addition, the debonding of FRP seems to occur randomly for most test specimens (COV of 67%). FRP fracture also seems to occur randomly (COV of 50%); however, the data points are less scattered than the ones corresponding to debonding failure. Therefore, this model tends to underestimate the FRP shear contribution for specimens that failed due to FRP fracture.

Furthermore, by analyzing the FRP shear capacity ratio in terms of the shear span-to-depth ratio, it can be concluded that for specimens that failed due to FRP debonding and FRP fracture, the FRP shear capacity ratio increases up to $a/d = 3.0$, and then decreases up to 3.41. Finally, from the analysis of the FRP shear capacity ratio in terms of the amount of transverse steel reinforcement, it can be observed that for specimens that failed due to FRP debonding, the FRP shear capacity ratio increases as the amount of transverse steel reinforcement increases. The same trendline is observed for specimens that failed due to FRP fracture.

From the analysis, the analytical model by Monti and Liotta (2005) cannot accurately predict the FRP shear contribution in comparison to the previously discussed approaches. This analytical approach provides a COV of 71%. In addition, this model provides conservative values of FRP shear capacity ratio for specimens that failed due to FRP fracture.

This model makes better predictions for specimens that failed due to FRP fracture (COV of 50%), than those that failed due to FRP debonding (COV of 67%). This may be explained by the fact that this model assumes a value of 0.2mm for the interface slip corresponding to full debonding.

Finally, from the comparison between the predicted total shear capacity by applying four different design methodologies and the observed experimental results, it can be concluded that Eurocode 2 provides a lower COV value of 31% and a lower mean value of 1.11. Therefore the predictions of total shear capacity from Eurocode 2 are more accurate than those from other design methodologies when using the analytical model from Monti and Liotta (2005). By applying AASHTO LRFD in combination with this analytical model, a higher mean value of $V_{\exp}/V_{theo}$ and higher COV values are obtained. In addition, for specimens that failed due to FRP fracture and FRP debonding, Eurocode 2 provides more accurate predictions of total shear capacity in comparison to other design codes. Finally, the application of all four design codes with Monti and Liotta (2005) model provide conservative values of $V_{\exp}/V_{theo}$ for specimens failing due to FRP fracture.

5.2.10. Cao et al. (2005). From the analysis of the FRP shear capacity ratio in terms of $E_f \rho_f /(f_c')^{2/3}$, it can be observed that the analytical model proposed by Cao et al. does not accurately predict the shear contribution of FRP. This analytical model predicts the FRP shear contribution more accurately for specimens that failed due to FRP fracture (COV of 45%) than those that failed due to FRP debonding (COV of 58%). As in the previously discussed approaches, the FRP shear capacity ratio exhibits a decreasing trend as $E_f \rho_f /(f_c')^{2/3}$ increases. Therefore, this model underestimates the FRP shear capacity for low values of $E_f \rho_f /(f_c')^{2/3}$ and overestimates the predictions of FRP shear capacity for high values of $E_f \rho_f /(f_c')^{2/3}$.

Furthermore, by analyzing the FRP shear capacity ratio in terms of the shear span-to-depth ratio, it can be observed that for specimens that failed due to FRP debonding, the FRP shear capacity ratio decreases as the shear span-to-depth ratio increases. In addition, this model overestimates the FRP shear contribution for most test specimens. For

specimens failing due to FRP fracture, no clear trend could be observed between the FRP shear capacity ratio and the shear span-to-depth ratio. Finally, from the analysis between the FRP shear capacity ratio and the amount of transverse steel reinforcement, it can be observed that for specimens failing in debonding, the FRP shear capacity increases as the amount of transverse steel reinforcement increases. For specimens failing due to FRP fracture, no clear trend could be observed between the FRP shear capacity ratio and the transverse steel reinforcement.

From the previous analysis, the analytical model by Cao et al. (2005) cannot accurately predict the FRP shear capacity in comparison to the experimental observations. This approach provides a COV of 66%; however this model makes better predictions for fracture failure (COV of 45%), than for debonding failure (COV of 58%). In addition, this model provides conservative values of FRP shear capacity ratio for specimens that failed due to FRP fracture.

Finally, from the comparison between the predicted total shear capacity by applying four different design methodologies and the observed experimental results, it can be concluded that both Eurocode 2 and CSA A23.3-94 provide a lower COV value of 29%. However, CSA A23.3-94 provides a mean value of 0.99; therefore, the predictions of the total shear capacity by this design code are more accurate in comparison to the other design codes. By applying AASHTO LRFD in combination with this analytical model, a higher mean value of V_{exp}/V_{theo} and higher COV values are obtained. In addition, for specimens that failed due to FRP debonding, ACI 318-05 provides more accurate predictions of total shear capacity; however, both Eurocode 2 and CSA A23.3-94 provide lower COV values. For specimens failing in fracture, Eurocode 2 provides more accurate predictions of total shear capacity and a lower COV value. As in the previous analytical models, Cao et al. (2005) approach provides conservative values of V_{exp}/V_{theo} for specimens failing due to FRP fracture.

5.2.11. Zhang and Hsu (2005). This analytical model is an updated version of Hsu et al. (2003) model. The only modification was in the approach to predict the shear contribution of FRP for continuous sheets. This analytical model does not accurately predict the FRP shear contribution in comparison to its previous version (COV of 65%).

From the analysis between the FRP shear capacity ratio $E_f \rho_f / (f_c')^{2/3}$, it can be observed that this analytical model underestimates the FRP shear contribution for most test specimens failing due to FRP debonding or FRP fracture. As in its earlier version, for specimens failing in debonding, no clear trendline between the FRP shear capacity ratio and $E_f \rho_f / (f_c')^{2/3}$ can be observed. However, for specimens that failed due to FRP, the FRP shear capacity ratio increases as $E_f \rho_f / (f_c')^{2/3}$ increases. This increasing trendline is the opposite of the behavior observed in the previous analytical models. Moreover, the debonding of FRP seems to occur randomly (COV of 65%); however this model seems to predict more accurately the FRP shear contribution for those specimens that failed due to FRP fracture (COV of 49%).

In addition, by analyzing the FRP shear capacity ratio and the shear span-to-depth ratio, it can be observed that the FRP shear capacity ratio decreases as the shear span-to-depth ratio increases for specimens that failed due to FRP debonding and FRP fracture. Finally, in contrast to previously discussed models, which exhibit an increasing trend between the FRP shear capacity ratio and the amount of transverse steel reinforcement, this analytical model exhibits a decreasing trendline. Furthermore, this analytical model predicts high conservative values of FRP shear capacity ratios for most test specimens that failed in debonding and fracture.

From the previous analysis, it can be concluded that the analytical model by Zhang and Hsu (2005) cannot accurately predict the FRP shear capacity in comparison to the older version from Hsu et al. (2003). In fact, this analytical model underestimates the FRP shear contribution for most data specimens. This analytical approach provides a COV of 65%; however this model makes better predictions for specimens that failed due to fracture failure (COV of 49%), than those that failed due to FRP debonding (COV of 65%).

Finally, from the comparison between the predicted total shear capacity by applying four different design methodologies and the observed experimental results, it can be concluded that Eurocode 2 provides a lower COV value of 29% and a lower mean value of 1.42. Therefore the predictions of total shear capacity from Eurocode 2 are more accurate than those from other design methodologies when using the analytical model

from Zhang and Hsu (2005). By applying AASHTO LRFD in combination with this analytical model, a higher mean value of V_{exp}/V_{theo} and higher COV values are obtained. In addition, for specimens that failed due to FRP fracture and FRP debonding, Eurocode 2 provides more accurate predictions of total shear capacity in comparison to other design codes.

      5.2.12. Carolin and Taljsten (2005). By comparing the predictions of the total shear capacity by this model to the observed experimental result, it can be concluded that this analytical model does not accurately predict the shear capacity of FRP (COV of 77%). As in previous models, this analytical model underestimates the FRP shear capacity ratio for low values of $E_f \rho_f /(f_c^{'})^{2/3}$, and overestimates the FRP shear contribution for high values of $E_f \rho_f /(f_c^{'})^{2/3}$. In addition, the debonding of FRP seems to occur randomly for most test specimens (COV of 75%). FRP fracture also seems to occur randomly (COV of 47%); however, the data points are less scattered than the ones corresponding to debonding failure. Therefore, this model tends to underestimate the FRP shear contribution for most specimens that failed due to FRP fracture.

      From the analysis of the FRP shear capacity ratio in terms of the shear span-to-depth ratio, it can be observed that the FRP shear capacity ratio increases as the shear span-to-depth ratio increases up to 3.0, and decreases afterwards. In addition, this model tends to provide conservative values of FRP shear capacity ratio for those specimens that failed due to FRP fracture. Finally, by evaluating the FRP shear capacity ratio in terms of the amount of transverse steel reinforcement, the FRP shear capacity ratio increases as the amount of transverse steel reinforcement increases for specimens that failed due to FRP debonding. The same trendline is observed for specimens that failed due to FRP fracture.

      From the analysis, the analytical model by Carolin and Taljsten (2005) cannot accurately predict the FRP shear contribution in comparison to the previously discussed approaches. This analytical approach provides a COV of 77%. This model makes better predictions for specimens that failed due to FRP fracture (COV of 47%), than those that failed due to FRP debonding (COV of 75%). In addition, this analytical model underestimates the FRP shear contribution for most specimens that failed due to FRP

fracture, and overestimates the FRP shear contribution for most specimens failing in debonding.

Finally, from the comparison between the predicted total shear capacity by applying four different design methodologies and the observed experimental results, it can be concluded that Eurocode 2 provides a lower COV value of 32% and a lower mean value of 1.15. Therefore the predictions of total shear capacity from Eurocode 2 are more accurate than those from other design methodologies when using the analytical model from Carolin and Taljsten (2005). By applying AASHTO LRFD in combination with this analytical model, a higher mean value of V_{exp}/V_{theo} and higher COV values are obtained. In addition, for specimens that failed due to FRP fracture and FRP debonding, Eurocode 2 provides more accurate predictions of total shear capacity in comparison to other design codes. Finally, the application of all four design codes with Carolin and Taljsten (2005) model provide conservative values of V_{exp}/V_{theo} for specimens failing due to FRP fracture.

5.3. SUMMARY AND CONCLUDING REMARKS

The purpose of this section was to present a comparative evaluation of the accuracy in predicting the FRP shear contribution between twelve analytical models previously discussed in the literature. For each analytical model, the predicted shear strength of FRP $V_{f,theo}$ was compared with experimental results, $V_{f,exp}$, from the database. In addition, the FRP shear capacity ratio, defined as $V_{f,exp}/V_{f,theo}$, for each analytical model was evaluated in terms of some parameters that affect shear behavior, such as the FRP axial rigidity and concrete compressive strength, the shear span-to-depth ratio, and the interaction between transverse steel reinforcement and FRP. Each analytical model was further evaluated and analyzed in terms of failure modes and FRP wrapping schemes. Finally, for each analytical model, the predicted total shear capacity, V_{theo}, was compared with the observed experimental results, V_{exp}, from the shear database. The predictions of total shear capacities were computed by applying each analytical model in combination with four building codes.

The mean values and coefficient of variation (COV) values of $V_{f,\exp}/V_{f,theo}$ and $V_{\exp}/V_{theo}$ for all analytical models are presented in Tables 5.1 through 5.6. These tables also provide statistical results for each mode of failure. From Tables 5.1 through 5.6, and the graphs presented in this section and in Appendix B, the following conclusions and observations can be drawn:

1. As observed in Table 5.1, the mean values of $V_{f,\exp}/V_{f,theo}$ range from 0.81 through 2.54, with significant scatter as given by the COV values of 0.47 to 1.16. The high scatter in the predictions indicates that the resisting mechanisms of FRP strengthening systems still need to be further investigated.

2. Almost all analytical models underestimate the prediction of FRP shear contribution for low values of $E_f \rho_f /(f_c')^{2/3}$ and overestimate it for high values of $E_f \rho_f /(f_c')^{2/3}$. On the other hand, the analytical models from Hsu et al. (2003) and Zhang and Hsu (2005) exhibit an increasing trend between the FRP shear capacity ratio and $E_f \rho_f /(f_c')^{2/3}$.

3. The predictions of FRP shear contribution for specimens that failed due to FRP fracture are more conservative for most models except for Triantafillou and Antonopoulos (2000), Chaallal et al. (2002), Hsu et al. (2003), Chen and Teng (2003), and Zhang and Hsu (2005). For these models, the mean values of $V_{f,\exp}/V_{f,theo}$ for both debonding and fracture failure are close to each other.

4. The models from Triantafillou and Antonopoulos (2000) and Chen and Teng (2003) provide better predictions for the FRP shear contribution for both debonding and fracture failures. However, the FRP debonding approach from Chen and Teng provides lower COV values than those corresponding to Triantafillou and Antonopoulos (2000).

5. For almost all analytical models, the FRP shear capacity ratio $V_{f,\exp}/V_{f,theo}$ increases as the shear span-to-depth ratio increases up to 3.0, and decreases afterwards. However, from the analytical models of Chaallal et al. (2002), Cao et al. (2005) and Zhang and Hsu (2005), a decreasing trend is observed.

6. For almost all analytical models, the FRP shear capacity ratio $V_{f,\exp}/V_{f,theo}$ increases as the amount of transverse steel reinforcement increases. However, from the analytical models of Hsu et al. (2003) and Zhang and Hsu (2005), a decreasing trend is observed.

7. From Table 5.2, for all building codes, the combination of the analytical model from Cao et al. (2005) and Chaallal et al. (2002) with the CSA A23.3-94 design code, provide the most accurate prediction of total shear capacity. However, the combination of Chen and Teng (2003) analytical model with Eurocode 2 provides less scatter in the data points.

8. Both AASHTO specifications and ACI 318-05 provide higher conservative values of $V_{\exp}/V_{theo}$ and higher COV values than the other design codes when applied in combination with all analytical models.

9. Eurocode 2 provides lower COV values and predicts the total shear capacity more accurately when applied in combination with most analytical models.

10. The application of the analytical model from Triantafillou and Antonopoulos (2000) in combination with Eurocode 2 provides the most accurate predictions of total shear capacity for both debonding and fracture failures. In addition, the analytical model from Chen and Teng (2003) in combination with Eurocode 2 provides the lower COV values for both debonding and fracture failures.

11. The predictions of total shear capacities for specimens that failed due to FRP fracture are more conservative for all models and design codes, except for the models of Triantafillou and Antonopoulos (2000), Chen and Teng (2003), and Zhang and Hsu (2005). For these three models, the mean values of $V_{\exp}/V_{theo}$ for both debonding and fracture failure are close to each other.

6. EVALUATION OF EXISTING DESIGN GUIDELINES

6.1. INTRODUCTION

This section presents a comparative evaluation of the accuracy in predicting the FRP shear contribution, defined as V_f, between design guidelines discussed previously in Section Four. The design guideline developed by JBDPA (1999) is not considered for evaluation since the formulation to determine the FRP shear contribution is dependent of the shear contribution from the transverse steel reinforcement. In addition, any partial safety factors and strength reduction factors have not been considered when calculating the shear contribution of FRP for comparison purposes.

Before performing the comparative evaluation, the entire database (refer to Table A.1 in the Appendix) was reduced to a subset of data. Only test results corresponding to large and slender beam specimens are included in the comparative evaluation. Furthermore, test results with other type of strengthening systems such as near-surface mounted (NSM) rebars and prestressed straps are omitted because these types of strengthening systems present a different type of behavior from the externally applied FRP systems. After eliminating tests results in which flexural failures were reported and cases in which insufficient data information was available, there were 127 test results left to be used in the comparative evaluation.

For each design guideline, the predicted shear strength of FRP $V_{f,theo}$ was compared with experimental results, $V_{f,\exp}$, from the shear database. The FRP shear capacity ratio, defined as $V_{f,\exp}/V_{f,theo}$, for each design guideline is evaluated in terms of non-dimensional parameters that affect the shear behavior, such as $E_f \rho_f / f'^{2/3}_c$, a/d, and $\rho_s E_s / \rho_f E_f$. In addition, each design guideline has been evaluated in terms of failure modes and FRP wrapping schemes. Finally, the predictions of total shear capacities, V_{theo}, with the observed test results $V_{\exp}$ are also compared. The predictions of the total shear capacities are computed as $V_n = V_c + V_s + V_{f,theo}$, where V_c and V_s are computed using the respective RC design codes from each design guideline

As a result, the evaluation for each design guideline yields to 11 plots for each design guideline. In this section, only the plots corresponding to the Great Britain Technical Report No.55 (2004) are presented. The plots corresponding to the remaining design guidelines are presented in Appendix C. Instead, in this section, the mean values and coefficient of variation (COV) values of $V_{f,\exp}/V_{f,theo}$ and $V_{\exp}/V_{theo}$ are presented in Tables 6.1 and 6.2. These tables also provide statistical results for each mode of failure

Table 6.1. Comparison of Prediction and Test Result for FRP Capacities ($V_{f,\exp}/V_{f,theo}$)

Design Guideline	All		Debonding		Fracture		Shear Failure	
	Mean	COV	Mean	COV	Mean	COV	Mean	COV
Technical Report No.55 (2004)	1.92	0.94	1.41	0.56	4.00	0.66	1.31	0.90
fib TG 9.3 (2001)	0.88	0.50	0.86	0.53	0.98	0.39	0.85	0.53
JSCE Recommendations (2001)	0.49	0.77	0.41	0.72	0.81	0.52	0.41	0.88
ISIS Design Manual 4 (2001)	1.82	1.01	1.22	0.60	3.94	0.69	1.33	0.93
ACI 440.2R-02 (2002)	1.89	0.96	1.32	0.55	3.94	0.69	1.39	0.87
CSA-S806-02 (2002)	1.78	1.02	1.23	0.78	3.78	0.69	1.32	0.89

Table 6.2. Comparison of Prediction and Test Result for Shear Capacities ($V_{\exp}/V_{theo}$)

Design Guideline	All		Debonding		Fracture		Shear Failure	
	Mean	COV	Mean	COV	Mean	COV	Mean	COV
Technical Report No.55 (2004)	1.27	0.28	1.19	0.32	1.48	0.21	1.25	0.22
fib TG 9.3 (2001)	1.02	0.28	0.99	0.36	1.02	0.18	1.08	0.19
JSCE Recommendations (2001)	0.75	0.43	0.67	0.49	0.95	0.30	0.74	0.40
ISIS Design Manual 4 (2001)	1.23	0.32	1.15	0.34	1.49	0.26	1.19	0.26
ACI 440.2R-02 (2002)	1.39	0.32	1.31	0.33	1.70	1.60	1.33	0.91
CSA-S806-02 (2002)	1.22	0.35	1.12	0.42	1.49	0.26	1.21	0.24

6.2. COMPARATIVE EVALUATION OF SHEAR DESIGN GUIDELINES

6.2.1. Great Britain Technical Report No. 55 (2004). As illustrated in Figures 6.1 through 6.3, the analytical predictions proposed by the Great Britain Technical Report No.55 (2004) cannot accurately predict the shear contribution provided by the FRP. From these figures, it can be observed that as $E_f \rho_f /(f_c^{'})^{2/3}$ increases, the shear capacity ratio of the FRP exhibits a decreasing trend. This trendline shows that for lower values of $E_f \rho_f /(f_c^{'})^{2/3}$, Technical Report No 55 underestimates the prediction of the FRP shear contribution; while for higher values of $E_f \rho_f /(f_c^{'})^{2/3}$, this design guideline overestimates the prediction of the FRP shear contribution Furthermore, from analyzing Figures 6.1 and 6.2 illustrate, this design guideline provides conservative values for the FRP shear capacity ratio. Therefore, Technical Report No. 55 tends to underestimate the FRP shear contribution for most data points, especially for those that failed due to FRP fracture.
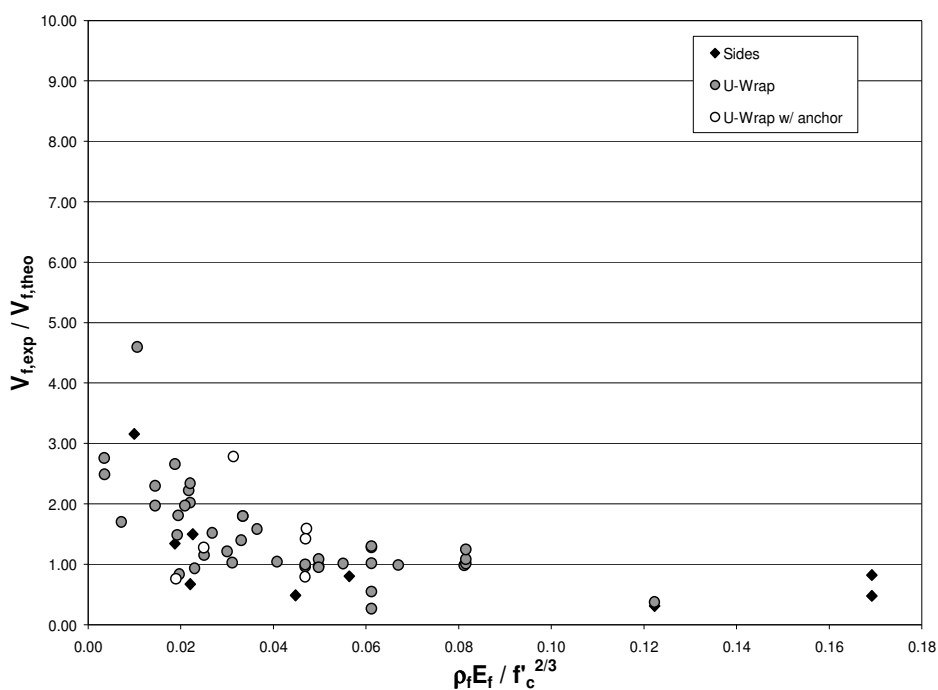
Figure 6.1. $V_{f,\exp} / V_{f,theo}$ in Terms of $E_f \rho_f /(f_c^{'})^{2/3}$ - FRP Debonding
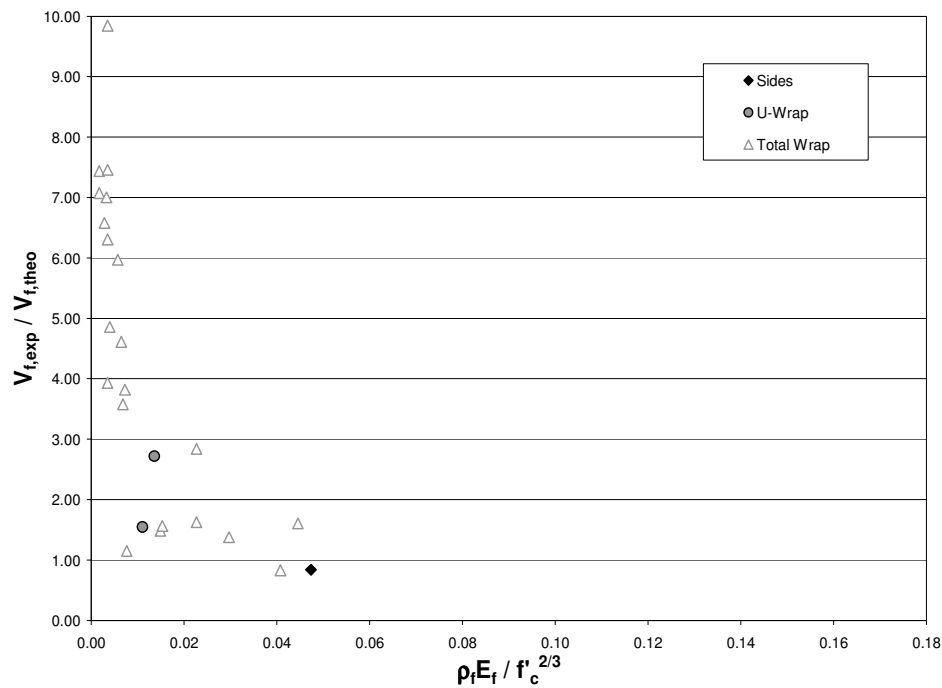
Figure 6.2. $V_{f,\exp} / V_{f,theo}$ in Terms of $E_f \rho_f / (f_c^{'})^{2/3}$ - FRP Fracture
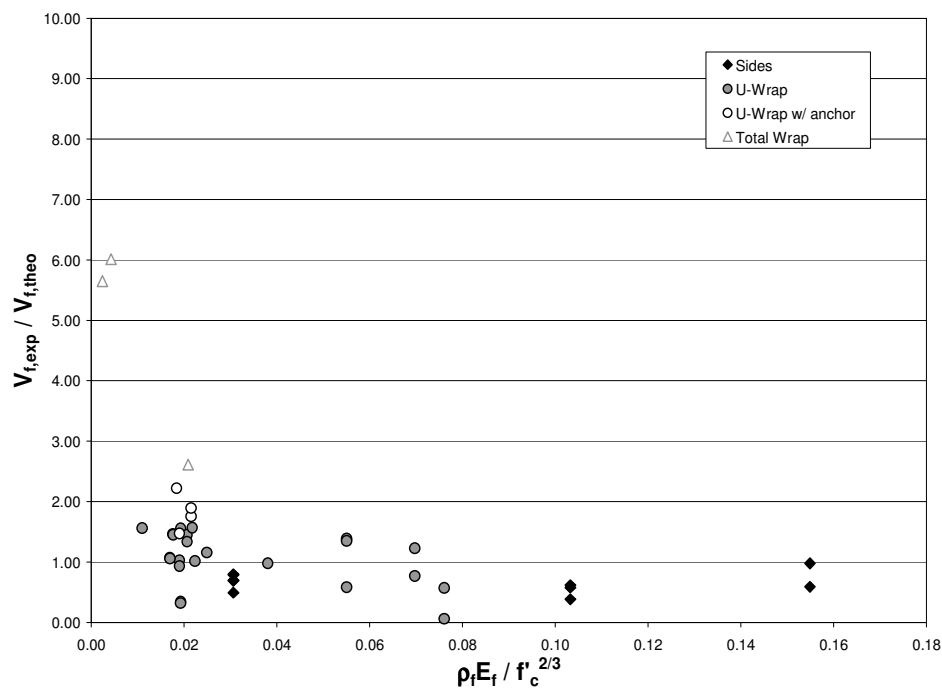
Figure 6.3. $V_{f,\exp} / V_{f,theo}$ in Terms of $E_f \rho_f / (f_c^{'})^{2/3}$ - Other Failure Modes

Figures 6.4 through 6.6 illustrate the predictions of the FRP shear contribution in terms of the shear span-to-depth ratio for different modes of failures. From Figures 6.4 and 6.5, it can be observed that the FRP shear capacity ratio increases up to values of shear span-to depth ratio of 3.0, and decreases afterwards. Moreover, as shown in Figures 6.4 and 6.5, the predictions for specimens that failed due to FRP debonding are relatively more accurate (COV of 56%) in comparison to those that failed due to FRP fracture (COV of 66 %). In addition, this design guideline provides a very conservative mean value of $V_{f,\text{exp}}/V_{f,theo}$ for specimens failing in fracture. Figures 6.7 through 6.9 illustrate the effect of the transverse steel reinforcement on the FRP shear contribution for different modes of failure. From Figure 6.7, it can be observed that when the amount of transverse steel reinforcement increases, the shear capacity ratio of FRP increases. The same trend is exhibited for those specimens that failed in fracture and other shear failure modes.
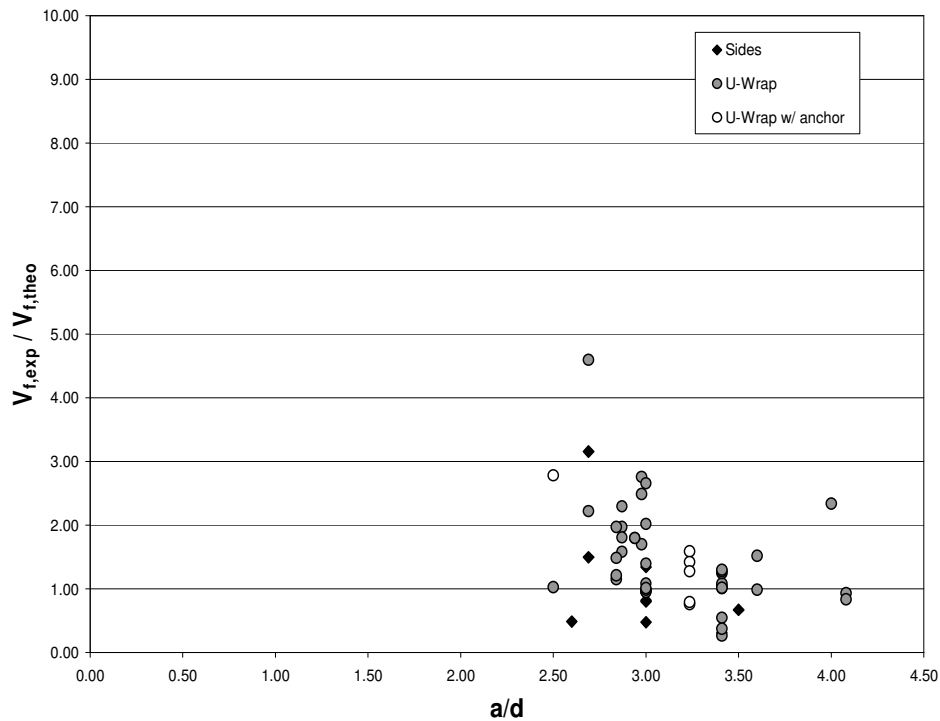
Figure 6.4. $V_{f,\text{exp}}/V_{f,theo}$ in Terms of a/d - FRP Debonding
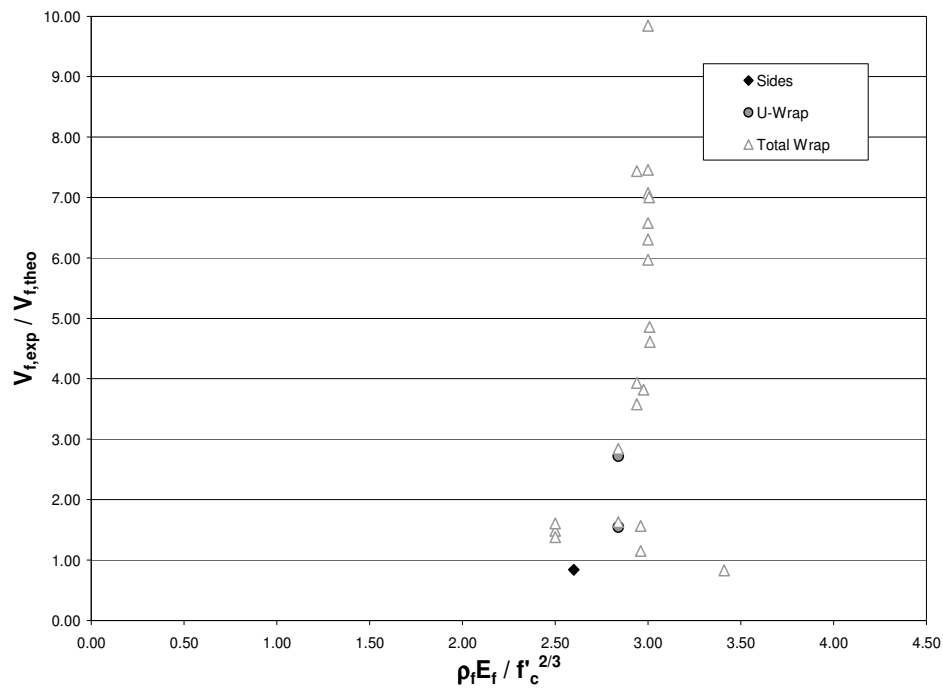
Figure 6.5. $V_{f,\exp}/V_{f,theo}$ in Terms of a/d - FRP Fracture
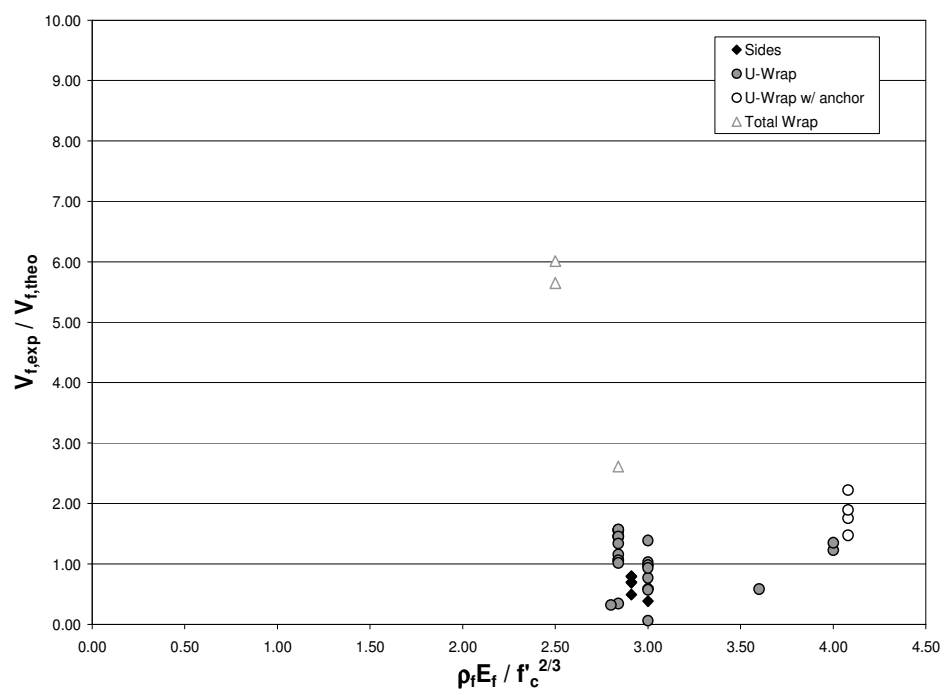
Figure 6.6. $V_{f,\exp}/V_{f,theo}$ in Terms of a/d - Other Failure Modes
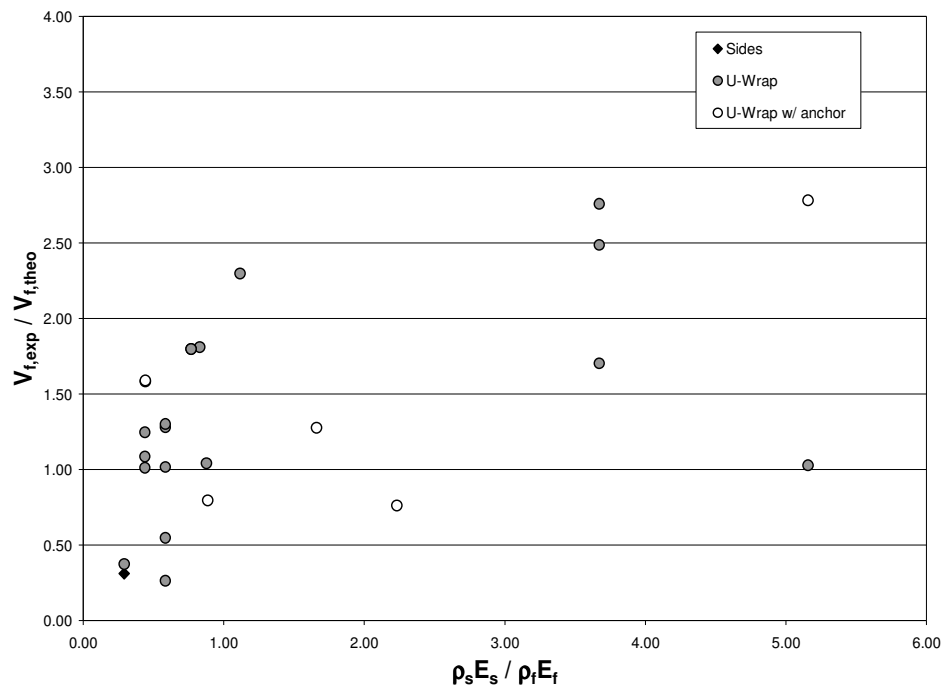
Figure 6.7. $V_{f,\exp}/V_{f,theo}$ in Terms of $\rho_s E_s / \rho_f E_f$ - FRP Debonding
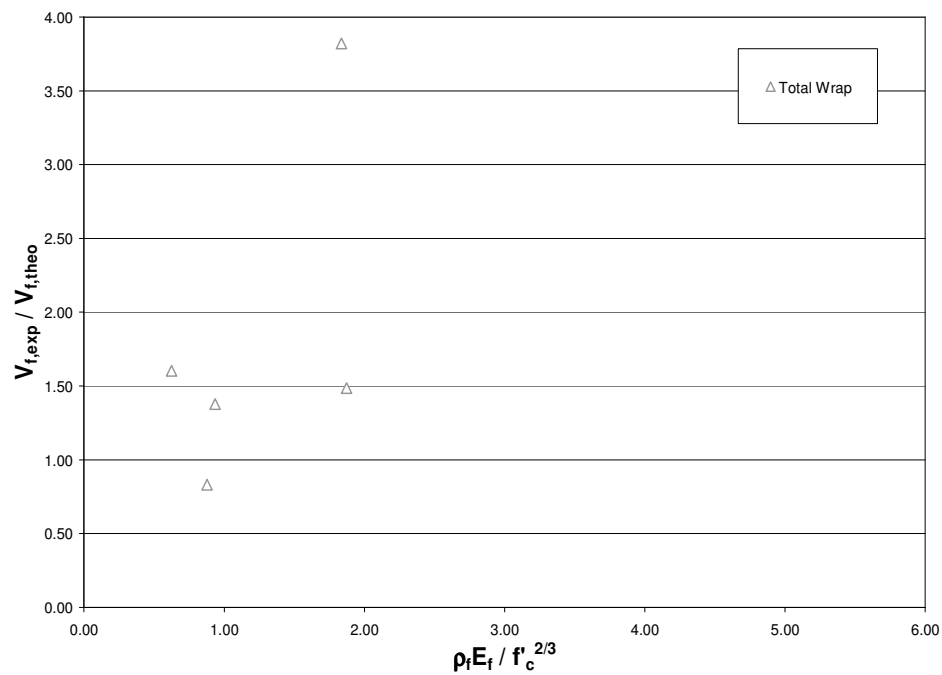
Figure 6.8. $V_{f,\exp}/V_{f,theo}$ in Terms of $\rho_s E_s / \rho_f E_f$ - FRP Fracture
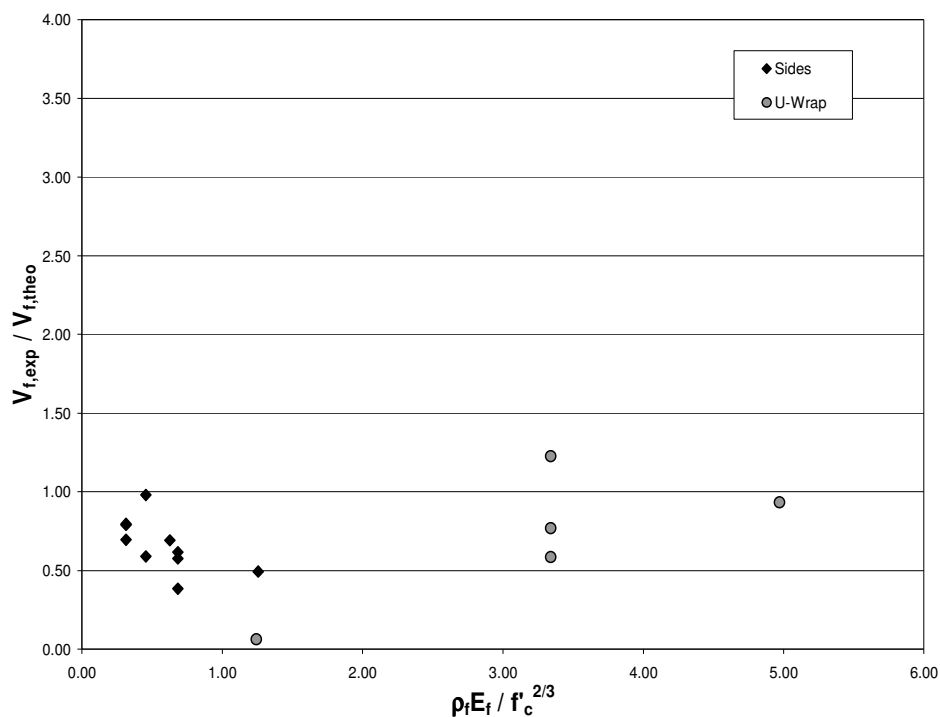
Figure 6.9. $V_{f,\exp}/V_{f,theo}$ in Terms of $\rho_s E_s / \rho_f E_f$ - Other Failure Modes

In conclusion, from the previous analysis, Technical Report No. 55 does not accurately predict the shear capacity due to the FRP (COV of 94%). In fact, the substantial majority of test specimens lie on the safe side, with the experimentally measured values exceeding those determined using the proposed design method. The analysis shows that this model predicts more accurately the FRP shear contribution for those specimens that failed in debonding (COV of 56%) to those that failed due to FRP fracture (COV of 66 %). However, this model tends to underestimate the FRP shear contribution by more than twice the experimental FRP shear contribution for most observed test specimens. The inaccuracy in predicting the FRP shear contribution by this design guideline is also shown in Figure 6.10. Finally, the analytical predictions for the shear capacity provided by the Technical Report No. 55 design guideline are also evaluated and compared to the experimental results as shown in Figure 6.11. The mean value of $V_{n,\exp}/V_{n,theo}$ for all specimens is around 1.27 with a COV of 28%.
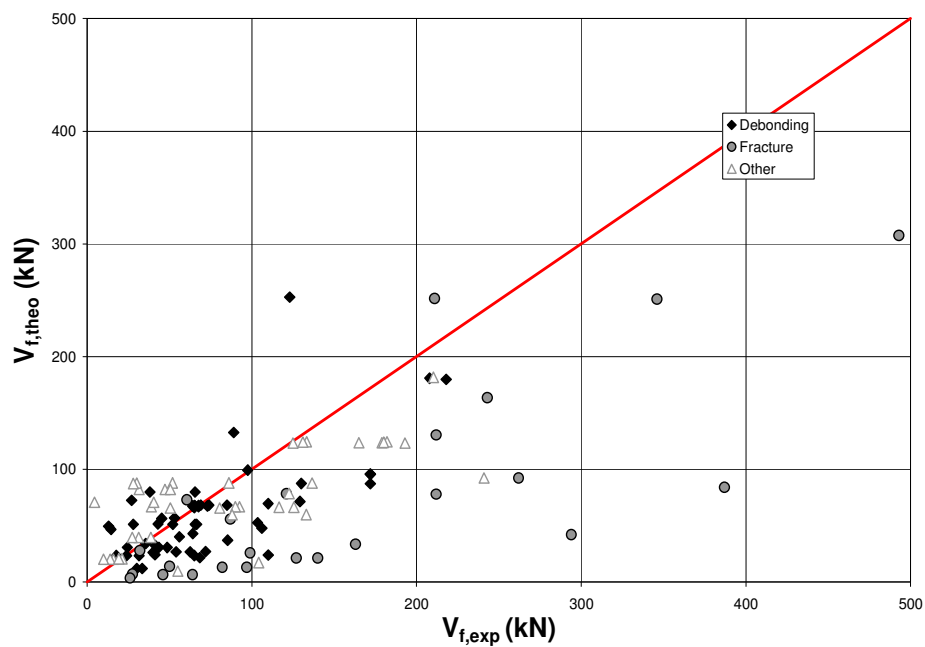
Figure 6.10. Comparison between Analytical Predictions of FRP Shear Contribution and Experimental Results
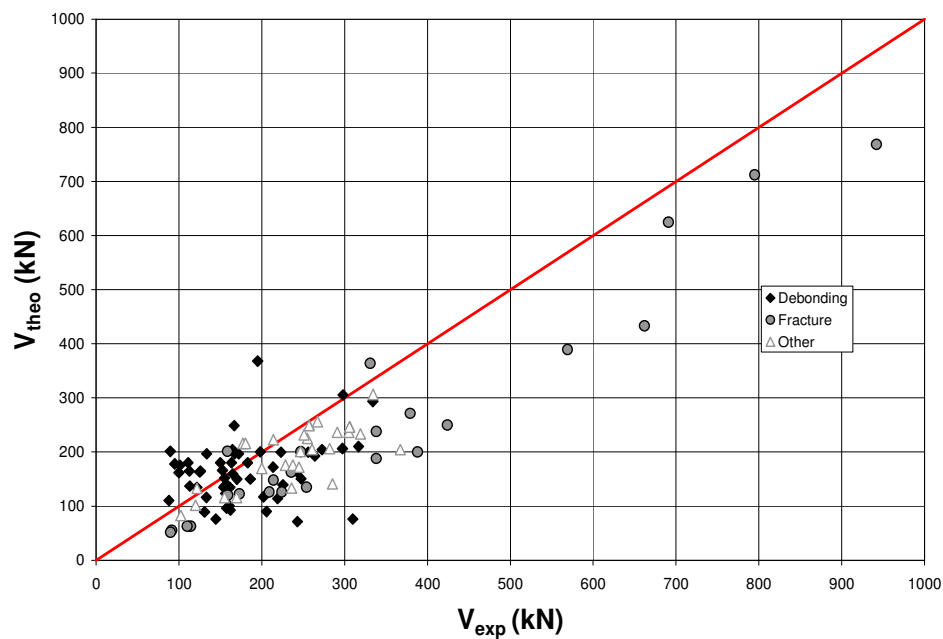
Figure 6.11. Comparison between Analytical Predictions of Total Shear Capacity and Experimental Results

6.2.2. fib-TG 9.3 Bulletin 14 (2001). From the analysis of this design guideline (refer to graphs of Appendix B), the shear design guidelines proposed by fib TG 9.3 predicted the shear capacity of FRP more accurately than the Technical Report No. 55 since it proposes an equation to determine the effective strain of FRP when fracture failure controls as opposed to providing a fixed value. By analyzing the prediction of the FRP shear strength versus $E_f \rho_f / (f_c')^{2/3}$, it was found that as in Technical Report No. 55 design guideline, fib-TG 9.3 overestimates the FRP shear capacity as $E_f \rho_f / (f_c')^{2/3}$ increases. In addition, fib TG 9.3 predicts the shear capacity of FRP relatively accurately for the case of FRP fracture. However, for debonding and other failure modes, most of the predictions have been overestimated.

In addition, by analyzing the FRP shear strength ratio versus the shear span-to-depth ratio, fib TG 9.3 seems to predict more accurately for fracture failure (COV of 39%) than for debonding (COV of 53%). For specimens that failed due to FRP debonding, the FRP shear capacity ratio increases up to $a/d = 3.0$, and then decreases up to 3.41. For specimens that failed in fracture, the same trend is observed. Finally, from analysis of the FRP shear strength ratio versus the effect of transverse steel reinforcement on the FRP shear contribution, it was observed that for specimens that failed in FRP debonding, the FRP shear capacity ratio increases as the amount of transverse steel reinforcement increases up to around 1.0. For specimens failing due to FRP fracture, the FRP shear capacity ratio increases as the amount of transverse steel reinforcement increases.

In conclusion, from the analysis, fib TG 9.3 predicts the FRP shear capacity more accurately in comparison to Technical Report No.55 because fib TG 9.3 proposes an equation to determine the effective strain of FRP when fracture failure controls as opposed to providing a fixed value for the effective strain. However, fib TG 9.3 seems to predict the FRP shear contribution more accurately when fracture failure governs than for debonding or other shear failures. This could be attributed to the fact that fib TG 9.3 does not make a clear distinction between side and U-shaped FRP jackets, which usually tend to fail in debonding, when estimating the effective FRP strain. As a result, it seems the effective strain of the FRP plays an important role in determining the accuracy of the predictions of FRP shear contribution. From analysis, fib TG 9.3 provides a COV of

50%, which indicates that this design guideline predicts the shear capacity due to the FRP more accurate than Technical Report No.55.

Finally, the analytical predictions for the total shear resistance provided by fib-TG 9.3 design guideline are also evaluated and compared to the experimental results. From the analysis, the mean value of $V_{n,\exp}/V_{n,theo}$ for all test specimens is around 1.02 with a COV of 28%. This means that the predicted total shear capacity is slightly conservative, but provides better predictions in comparison to Technical Report No. 55. In addition, the FRP system provides higher values of FRP shear contribution to the total shear resistance in comparison to Technical Report No. 55.

6.2.3. JSCE Design Recommendations (2001). From the analysis of this design guideline (refer to graphs in Appendix B), the predictions of the FRP shear contribution are overestimated; therefore, JSCE exhibit very low values of $V_{f,exp}/V_{f,theo.}$ This can be explained by the fact that this design guideline recommends the effective FRP stress to be between 0.4 and 0.8 times the fracture stress of FRP, which leads to high predictions of the FRP shear contribution. By analyzing the prediction of the FRP shear strength versus $E_f \rho_f /(f_c')^{2/3}$, it was found that for all failure modes, the FRP shear capacity ratio decreases as $E_f \rho_f /(f_c')^{2/3}$ increases. In addition, JSCE design recommendations predicts the FRP shear capacity more accurately for specimens that failed in fracture (COV of 52%) than for those than failed in debonding (COV of 72%) or other shear failures. This could be attributed to the fact that the JSCE design recommendations treats only the case of fully-wrapped FRP laminates, which usually tend to fail in fracture.

Furthermore, by analyzing the FRP shear strength ratio versus the shear span-to-depth ratio, it can be observed that for FRP debonding failure, the FRP shear capacity ratio increases as the shear span-to-depth ratio increases up to a/d equal to 3.0 and decreases afterwards up to 3.41. This same trend is observed for those specimens failing due to FRP fracture. Finally, from analysis of the FRP shear strength ratio versus the effect of transverse steel reinforcement on the FRP shear contribution, it was observed that for specimens failing due to FRP debonding and fracture, the FRP shear capacity ratio increases as the amount of transverse steel reinforcement increases.

From analysis, JSCE design recommendations provides a COV of 77%, thus, in comparison to fib TG 9.3, this analytical model does not accurately predict the FRP shear capacity. This model seems to make better predictions for specimens that failed in fracture than those that failed in debonding. This could be attributed to the fact that the JSCE design recommendations treats only the case of fully-wrapped FRP laminates. In addition, this code recommends the effective stress of FRP to be between 0.4 and 0.8 times the FRP ultimate strength, which leads to high predictions of FRP shear contribution. For this reason, the JSCE design recommendations overestimate the FPR shear contribution for almost all test specimens. Finally, the analytical predictions for the total shear resistance provided by JSCE design recommendations are also evaluated and compared to the experimental results. From the analysis, the mean value of $V_{n,\exp}/V_{n,theo}$ for all test specimens is around 0.75 with a COV of 43%. This means that the predicted total shear capacity is overestimated. This could be explained by the fact that JSCE recommendations provide very high values of FRP shear contribution to the total shear resistance in comparison to both Technical Report No.55 and fib TG 9.3 design guidelines.

6.2.4. ISIS Design Manual 4 (2001). This design guideline proposes similar shear formulations to both ACI 440.2R-02 and fib TG 9.3. By analyzing the predictions of the FRP shear strength versus $E_f \rho_f /(f_c')^{2/3}$, it was found that as in previous shear design protocols, the ISIS design manual underestimates the FRP shear capacity for lower values of $E_f \rho_f /(f_c')^{2/3}$ and overestimates the FRP shear contribution for higher values of $E_f \rho_f /(f_c')^{2/3}$. This design model provides very conservative values for the FRP shear capacity ratio in the case of FRP fracture failure. This could be attributed to the fact that this design manual fixes the effective strain of FRP to a value of around 0.004 for cases of fully-wrapped FRP laminates, which usually tend to fail in fracture.

Furthermore, by analyzing the FRP shear strength ratio versus the shear span-to-depth ratio, for specimens that failed due to FRP debonding, the FRP shear capacity ratio increases up to $a/d = 3.0$, and then decreases up to 3.41. For specimens that failed in fracture, the same trend is observed. In addition, from analysis of the FRP shear strength ratio versus the effect of transverse steel reinforcement on the FRP shear contribution, it

was observed that for both debonding and fracture failure, it can be observed that the FRP shear capacity ratio increases as the amount of transverse steel reinforcement increases.

In conclusion, from the analysis, ISIS does not accurately predict the FRP shear capacity. This design manual provides very conservative values for the prediction of FRP shear capacity, especially in the case of FRP fracture failure. This could be explained by the fact that ISIS provides a fixed value for the effective strain for totally-wrapped FRP laminates, which tend to fail in fracture. From analysis, ISIS provides a COV of 101%, which indicates that this design guideline does not accurately predict the shear capacity due to the FRP. Finally, the analytical predictions for the total shear resistance provided by ISIS design manual are also evaluated and compared to the experimental results. From the analysis, the mean value of $V_{n,\exp}/V_{n,theo}$ for all test specimens is around 1.23 with a COV of 32%. This means that the predicted total shear capacity is typically conservative, but provides better predictions in comparison to Technical Report No. 55 and JSCE recommendations.

6.2.5. ACI 440.2R-02 (2002). From the analysis of this design guideline (refer to graphs in Appendix B), the analytical predictions proposed by ACI 440.2R-02 (ACI, 2002) cannot accurately predict the shear capacity of FRP. It can be observed that as $E_f \rho_f /(f_c^{'})^{2/3}$ increases, the shear capacity ratio of the FRP exhibits a decreasing trend. This trendline shows that for low values of $E_f \rho_f /(f_c^{'})^{2/3}$, ACI 440.2R-02 underestimates the prediction of the shear capacity of FRP; while for high values of $E_f \rho_f /(f_c^{'})^{2/3}$, this design guideline overestimates the prediction of the shear capacity of FRP. Furthermore, the predictions for specimens that failed in fracture are more conservative than those that failed in debonding or other shear failure modes. This can be explained by the fact that for cases when fracture failure is likely to govern, ACI 440.2R-02 provides a fixed value of FRP effective strain around 0.004; therefore, this suggests that a fixed value of effective strain is conservative for fracture failure.

Furthermore, by analyzing the FRP shear strength ratio versus the shear span-to-depth ratio, for specimens that failed due to FRP debonding, the FRP shear capacity ratio increases up to $a/d = 3.0$, and then decreases up to 3.41. For specimens that failed in fracture, the same trend is observed. Finally, from analysis of the FRP shear strength

ratio versus the effect of transverse steel reinforcement on the FRP shear contribution, it was observed that for specimens failing due to FRP debonding and fracture, the FRP shear capacity ratio increases as the amount of transverse steel reinforcement increases.

From the analysis, ACI 440.2R-02 provides very conservative predictions of the FRP shear contribution. ACI 440.2R-02 provides more conservative predictions for fracture failure with a mean value of 3.94 than for debonding failure. This could be attributed to the fact that ACI 440.2R-02 provides a fixed value of FRP effective strain; therefore, suggesting that a fixed value of effective strain is conservative for fracture failure. ACI 440.2R-02 provides a COV of 96%, which indicates that this design guideline does not accurately predict the shear capacity provided by the FRP. Finally, the analytical predictions for the total shear resistance provided by ACI 440.2R-02 design guideline are also evaluated and compared to the experimental results. The mean value of $V_{n,\exp}/V_{n,theo}$ for all specimens is around 1.39 with a COV of 32%. This means that the predicted total shear capacity is typically conservative. A significant portion of this conservatism is likely due to the conservative characteristics of the relationships for evaluating V_c and V_s.

6.2.6. CAN/CSA-S806-02 (2002). From the analysis of this design code (refer to graphs in Appendix B), the predictions of the FRP shear contribution are underestimated for the majority of data points probably because this design code fixes a conservative value of FRP effective strain. By analyzing the prediction of the FRP shear strength versus $E_f \rho_f /(f_c^{'})^{2/3}$, it was found that as in previous shear design protocols, CSA-S806-02 underestimates the FRP shear capacity for lower values of $E_f \rho_f /(f_c^{'})^{2/3}$ and overestimates the FRP shear contribution for higher values of $E_f \rho_f /(f_c^{'})^{2/3}$. However, both CSA-S806-02 and ACI 440.2R-02 provide high values for the FRP shear capacity ratio, especially for FRP fracture failure. Therefore, the predictions of the FRP shear capacity by this design guideline are more conservative for fracture failure than for debonding and other shear failures.

Furthermore, by analyzing the FRP shear strength ratio versus the shear span-to-depth ratio, it can be observed that for fracture failure, this design code tends to underestimate the FRP shear capacity for most slender beams. For both debonding and

fracture failure, the FRP shear capacity ratio increases up to $a/d = 3.0$, and then decreases up to 3.41. Finally, from analysis of the FRP shear strength ratio versus the effect of transverse steel reinforcement on the FRP shear contribution, it was observed that for debonding failure, it can be observed that the FRP shear capacity ratio increases as the amount of transverse steel reinforcement increases. This increasing trendline is also present for specimens that failed in fracture

From analysis, CSA-S806-02 provides a COV of 102%, thus, this analytical model does not accurately predict the FRP shear capacity in contrast to the previously discussed design guidelines. This design guideline tends to predict conservative FRP shear contributions for specimens that failed due to FRP fracture than those failing in debonding. This could be attributed to the fact that CSA-S806-02 fixes values of effective strains of 0.004 and 0.002 for both FRP fracture and debonding respectively. For fracture failure, CSA-S806-02 produces high values of $V_{f,exp}/V_{f,theo}$. This suggests that a fixed value of effective strain around 0.004 is conservative for fracture failure. The results for debonding failure suggests that if a fixed value of effective strain is used for debonding failure, then it should be less than 0.004. Finally, the analytical predictions for the total shear resistance provided by CSA-S806-02 are also evaluated and compared to the experimental results. The mean value of $V_{n,\exp}/V_{n,theo}$ for all specimens is around 1.22 with a COV of 35%. This means that the predicted total shear capacity is typically conservative.

6.3. SUMMARY AND CONCLUDING REMARKS

The predictions for the FRP shear contribution and total shear resistance provided by Technical Report No.55, fib TG9.3, JSCE 2001, ISIS 4, ACI 440.2R-02, and CSA-S806-02 design guidelines for beams strengthened with FRP systems were evaluated and compared. The analytical predictions for the FRP shear contribution from each shear design provision were compared to the experimental results observed from the shear database. Each design guideline was also independently analyzed in detail by evaluating the influence of some of the parameters on the behavior of RC members shear strengthened with FRP systems such as the FRP axial rigidity, concrete compressive strength, shear span-to-depth ratio, and transverse steel reinforcement.

    The FRP shear capacity predictions for each design guideline discussed are presented in Table 6.1. The total shear capacity predictions by each design guideline are shown in Table 6.2. Both tables provide the mean values and coefficient of variation of $V_{f,\exp}/V_{f,theo}$ and $V_{n,\exp}/V_{n,theo}$ for all shear design guidelines. The mean and coefficient of variation (COV) are divided by the different failure mechanisms. From Tables 6.1 and 6.2, and the plots discussed in the previous section, the following observations can be drawn:

1. As presented in Table 6.1, the mean values of $V_{f,\exp}/V_{f,theo}$ range from 0.49 through 1.92, with significant scatter as given by the COV values of 0.50 to 1.02. The high scatter in the predictions indicates that the mechanisms of FRP strengthening are still poorly understood.

2. From Table 6.2, the mean values of $V_{n,\exp}/V_{n,theo}$ range from 0.75 through 1.39, with significant scatter as given by the COV values of 0.28 to 0.43. The data points are less scattered because the predictions indicate that the predicted values for the total shear resistance are in good agreement with the experimental results.

3. For all design guidelines, the FRP shear capacity ratio $V_{f,\exp}/V_{f,theo}$ decreases as $E_f \rho_f /(f_c')^{2/3}$ increases. For this reason, all design guidelines underestimate the prediction of FRP shear capacity for low values of $E_f \rho_f /(f_c')^{2/3}$ and overestimate the FRP shear contribution for high values of $E_f \rho_f /(f_c')^{2/3}$.

4. For all design guidelines, the FRP shear capacity ratio $V_{f,\exp}/V_{f,theo}$ increases as the shear span-to-depth ratio increases up to a/d equal to 3.0, and decreases afterwards up to 3.41. Therefore, all design guidelines tend to overestimate the FRP shear contribution for higher a/d ratios.

5. For all design guidelines, the FRP shear capacity ratio $V_{f,\exp}/V_{f,theo}$ increases as the amount of transverse steel reinforcement increases for both specimens failing due to FRP debonding and fracture.

6. The predictions of FRP shear capacity for fracture failure are more conservative for all design guidelines except for fib TG9.3 (2001). For this design guideline, the

mean values of $V_{f,\exp}/V_{f,theo}$ for both debonding and fracture failure are close to each other.

7. The fib TG9.3 (2001) provides better predictions for the FRP and total shear capacities for both debonding and fracture failures. This design guideline also provides smaller COV values.

8. Technical Report No.55 (2004), ISIS Design Manual 4 (2001), ACI 440.2R-02 (2002), and CSA-S806-02 (2002) provide very conservative predictions of the FRP contribution and total shear capacities for both FRP debonding and fracture failures.

9. JSCE design recommendations overestimate the FRP shear contribution for almost all test specimens because this code recommends the effective stress of FRP to be between 0.4 and 0.8 times the FRP ultimate strength, which leads to high predictions of FRP shear contribution.

7. APPLICATION EXAMPLES OF ANALYTICAL APPROACHES ON SHEAR STRENGTHENING WITH FRP

7.1. INTRODUCTION

As previously discussed in Section Five and Section Six, most analytical and design approaches were not able to provide reliable predictions of FRP shear contribution for all of the 127 RC members presented in the database. The high scatter in the predictions (COV) of the FRP shear contribution indicates that the resisting mechanisms of FRP strengthening systems still need to be further investigated. This is further exemplified by the large differences in the predictions by the examined analytical and design approaches. Furthermore, as mentioned in Section Four, most RC members collected in the shear database (refer to Table A.1 in the Appendix), correspond to slender, rectangular cross-sections without internal transverse reinforcement. Therefore, the members in the evaluation database do not exactly reflect the types of RC members usually found in practice. By contrast, most RC members in real practice are large, slender, have a T-cross section, and contain internal transverse reinforcement. Therefore, due to the complexity of the analytical approaches examined, and the limited database, the FRP shear contribution predicted by these approaches can be more effectively compared by providing specific examples. Before performing the comparative evaluation, it is important to note that the analytical model from Triantafillou and Antonopoulos (2000) is omitted from the evaluation because of its similarity to the fib TG9.3 (2001) design approach. In addition, since the examples provided consist of externally applied CFRP strips, the analytical models from Hsu et al (2003), and Zhang and Hsu (2005) are essentially the same.

7.2. EXAMPLES TO COMPARE THE FRP SHEAR CONTRIBUTION

This section provides three different application examples with different type of cross-sections. The first example deals with RC T-beams, which usually are used in building structures. The second one deals with RC T-girders used in small bridges or highway overpass. The last one deals with prestressed (PC) I-cross section representing a large bridge girder. The three examples provided are used to compare the FRP shear contribution, V_f, among all the analytical and design approaches discussed in the

literature. The comparison of the magnitude of V_f is performed in terms of the axial rigidity of FRP, $\rho_f E_f$. In all the relationships for estimating V_f, the shear crack angle is assumed to be 45 degree, and all partial safety factors are assumed to be equal to 1.0.

7.2.1. RC T-Beam. Figure 7.1 illustrates the cross-section of a T-beam having a shear span-to-depth ratio of 3.5. The concrete compressive strength is 27.6 MPa. The longitudinal steel reinforcement consists of three 36 mm diameter at the bottom of the beam section. The transverse steel reinforcement consists of 9.5M bars ($A_{sv} = 142$ mm^2) with a yield strength of 276 MPa and a modulus of elasticity of 200 GPa. The spacing between steel stirrups is of 305 mm. The FRP strengthening system consists of CFRP strips with a width of 254 mm and spacing between strips of 305 mm. The angle of fiber orientation is 90 degrees. The thickness of the CFRP is 0.167 mm, the modulus of elasticity of the CFRP is 228 GPa, and the ultimate tensile strength of the CFRP is 3792 MPa. This example is evaluated by applying two types of strengthening schemes: side-bonded and U-wrapped CFRP sheets
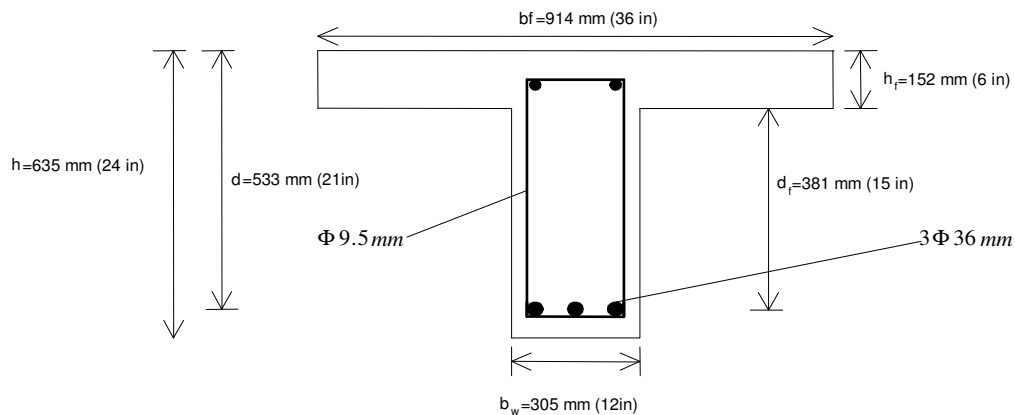
Figure 7.1. T-Beam Cross-Section

Figure 7.2 compares the magnitude of V_f computed by the analytical and design approaches in terms of $\rho_f E_f$. This figure illustrates the magnitude of V_f by applying a side-bonded CFRP strengthening configuration.
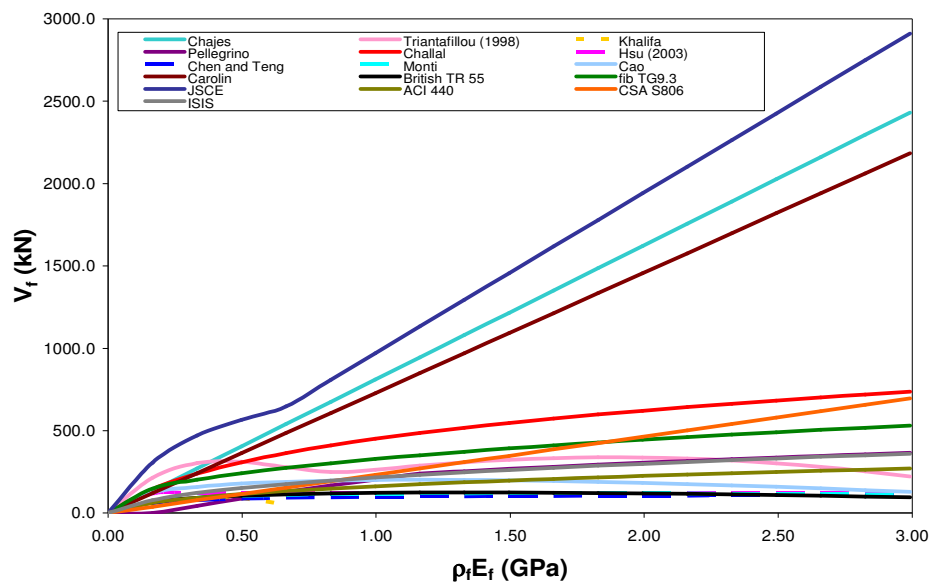
Figure 7.2. FRP Shear Contribution in Terms of Axial Rigidity – Side-Bonded
T-Beam Cross-Section

From Figure 7.2, it can be observed that the prediction of V_f, by Chajes et al.
(1995) analytical approach, linearly increases as the amount of FRP reinforcement
increases. This behavior is explained by the fact that this analytical model fixes a value
for the strain in the FRP. As a result, the predictions of the FRP shear contribution by
this analytical model are conservative.

From the analytical approach by Triantafillou (1998), it can be observed that for
values of $\rho_f E_f$ up to about 0.43 GPa, the FRP shear contribution increases with $\rho_f E_f$
reaching a maximum, beyond which it drops slightly and then increases again slightly.
This suggests that the value of 0.43 GPa can be used to determine the limiting amount of
FRP reinforcement, beyond which the effectiveness of strengthening ceases to be
positive. This observed particular behavior could be attributed to the fact that
Triantafillou (1998) derived the effective FRP strain based on limited experimental data.
As a result, Triantafillou (1998) derived a single expression for determining the effective
FRP strain without taking into consideration the different failure modes.

Khalifa et al. (1999) analytical approach indicates that for values of $\rho_f E_f$ up to
about 0.40 GPa, the FRP shear contribution increases almost linearly with $\rho_f E_f$ reaching a

maximum, beyond which it drops up to $\rho_f E_f$ equal to 0.7. This suggests that the value of 0.40 GPa can be used to determine the limiting amount of FRP reinforcement, beyond which the effectiveness of strengthening ceases to be positive. For values of $\rho_f E_f > 0.7$ GPa, additional amount of FRP results on negative values of FRP shear contribution. This means, that this analytical model is only valid for low values of FRP axial rigidity.

From the analytical approach by Pellegrino and Modena (2002), additional shear gain due to the FRP contribution is not observed for axial rigidities lower than 0.17 GPa. For values of $\rho_f E_f$ up to 1.16 GPa, the FRP shear contribution linearly increases in proportion to $\rho_f E_f$. However, after this limit, the FRP shear contribution increases less than in proportion to the axial rigidity. Therefore, the effectiveness of the FRP system seems to reduce as the amount of FRP reinforcement increases beyond 1.16 GPa. This behavior confirms the observations reported by Pellegrino and Modena (2002) that the effectiveness of the FRP systems decreases as the amount of additional FRP reinforcement increases.

The same trend is observed in Chaallal et al. (2002) analytical approach. The FRP shear contribution increases as the axial rigidity of FRP increases; however, after $\rho_f E_f > 1.0$ GPa, the FRP shear contribution increases less than in proportion to $\rho_f E_f$. Therefore, the effectiveness of the FRP system seems to reduce as the amount of FRP reinforcement increases beyond 1.0 GPa. This behavior confirms the observations reported by Chaallal etl al. (2002) that the FRP shear contribution depends on the amount of FRP and transverse steel reinforcement.

Hsu et al. (2003) analytical approach indicates that the FRP shear contribution increases linearly up to about $\rho_f E_f$ equal to 0.17 GPa, beyond which a constant shear gain due to the FRP contribution is observed. This behavior is explained by the fact that the effective FRP strain predicted by this analytical model decreases in propotion to the FRP axial rigidity. This means that as the FRP axial rigidity increases, its effective FRP strain decreases at a decreasing rate.

From the analytical approach by Chen and Teng (2003a-b), for values of $\rho_f E_f$ up to 1.0 GPa, the FRP shear contribution increases in proportion to $\rho_f E_f$. However, after this limit, the FRP shear contribution increases less than in proportion to the axial

rigidity. Therefore, the effectiveness of the FRP system seems to reduce as the amount of FRP reinforcement increases beyond 1.0 GPa.

Monti and Liotta (2005) analytical approach indicates that for values of $\rho_f E_f$ up to about 1.5 GPa, the FRP shear contribution increases with $\rho_f E_f$ reaching a maximum, beyond which it drops slightly. Therefore, the effectiveness of the FRP system seems to reduce as the amount of FRP reinforcement increases beyond 1.5 GPa.

The same trend is observed in the Cao et al. (2005) approach. The FRP shear contribution increases as the axial rigidity of FRP increases; however, after $\rho_f E_f > 1.16$ GPa, the FRP shear contribution starts to decrease. Therefore, the effectiveness of the FRP system seems to reduce as the amount of FRP reinforcement increases beyond 1.16 GPa.

From the Carolin and Taljsten (2005) analytical approach, it can be observed that the FRP shear contribution increases linearly in proportion to the FRP axial rigidity. This behavior is explained by the fact that this analytical model fixes a value for the strain in the FRP, which is equal to the ultimate FRP strain. As a result, the predictions of the FRP shear contribution by this analytical model are conservative.

The design approach from the British Technical Report No. 55 (2000) indicates that for values of $\rho_f E_f$ up to about 1.33 GPa, the FRP shear contribution increases with $\rho_f E_f$ reaching a maximum, beyond which it starts to decrease. Therefore, the effectiveness of the FRP system seems to reduce as the amount of FRP reinforcement increases beyond 1.33 GPa.

From the design approach by fib TG 9.3 (2001), for values of $\rho_f E_f$ up to 1.0 GPa, the FRP shear contribution increases in proportion to $\rho_f E_f$. However, after this limit, the FRP shear contribution increases less than in proportion to the axial rigidity. Therefore, the effectiveness of the FRP system seems to reduce as the amount of FRP reinforcement increases beyond 1.0 GPa.

From the JSCE recommendations (2001) design approach, for values of $\rho_f E_f$ up to 0.66 GPa, the FRP shear contribution increases as $\rho_f E_f$ increases. Beyond this limit, the FRP shear contribution increases linearly in proportion to the FRP axial rigidity. This behavior can be attributed to the fact that the effective FRP strain remains constant after 0.66 GPa. The predictions of FRP shear contribution by the JSCE recommendations are

observed to be the least conservative in comparison to all analytical and design approaches examined.

Both design approaches from ACI 440.2R (2002) and ISIS 4 (2002) indicate that for values of $\rho_f E_f$ up to 1.0 GPa, the magnitude of V_f increases in proportion to $\rho_f E_f$. However, after this limit, the FRP shear contribution increases less than in proportion to the axial rigidity. Therefore, the effectiveness of the FRP system for both approaches seems to reduce as the amount of FRP reinforcement increases beyond 1.0 GPa.

Finally, from the CSA S806 (2002) design approach, it can be observed that the FRP shear contribution increases linearly in proportion to the FRP axial rigidity. This behavior is explained by the fact that this design approach fixes a value for the effective strain in the FRP, which is equal to 0.002 for side-bonded strengthening schemes. As a result, the predictions of the FRP shear contribution by this design approach are conservative.

Figure 7.3 compares the magnitude of V_f computed by the analytical and design approaches in terms of $\rho_f E_f$. Figure 7.3 shows the magnitude of V_f by applying a U-wrapped CFRP strengthening configuration
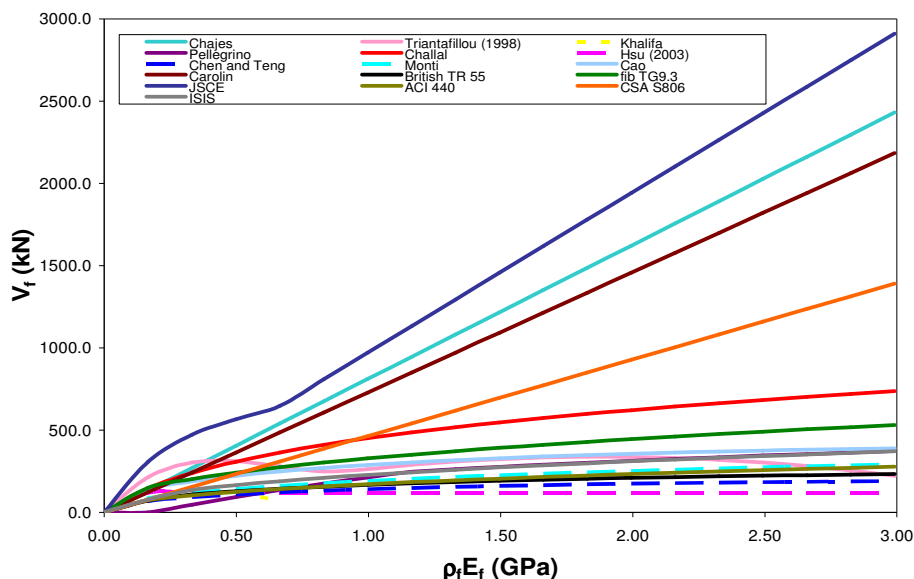
Figure 7.3. FRP Shear Contribution in Terms of Axial Rigidity – U-Wrapped T-Beam Cross-Section

From Figure 7.3, the approaches from Chajes et al., Triantafillou, Chaallal et al., Hsu et al., Carolin and Taljsten, fib TG 9.3, and JSCE do not make a distinction, in the formulations to determine V_f between side-bonded and U-wrapped configurations. Therefore, the predictions of V_f are the same for both strengthening configurations. The predictions of V_f by the remaining approaches are higher in the case of U-wrapped configuration than those of side-bonded configuration. The trend between V_f and the FRP axial rigidity, for most approaches, exhibits the same behavior as in the case of side-bonded configuration. However, for the approaches from Monti and Liotta, Cao et al., and the British TR 55, the magnitude of V_f increases in proportion to $\rho_f E_f$ up to 1.0 GPa. After this limit, the magnitude of V_f increases less than in proportion to the axial rigidity.

7.2.2. RC T-Girder. Figure 7.4 illustrates the cross-section of a T-girder with a shear span-to-depth ratio of 2.4. The concrete compressive strength is 34.5 MPa. The longitudinal steel reinforcement consists of four 25 mm diameter at the bottom of the cross-section. Transverse steel reinforcement consists of 9.5M bars (A_{sv} = 142 mm^2) with a yield strength of 276 MPa and a modulus of elasticity of 200 GPa. The spacing between steel stirrups is of 305 mm. The FRP strengthening system consists of CFRP strips with a width of 610 mm and spacing between strips of 864 mm. The angle of fiber orientation is 90 degrees. The thickness of the CFRP is 0.165 mm, the modulus of elasticity of the CFRP is 228 GPa, and the ultimate tensile strength of the CFRP is 3868 MPa.
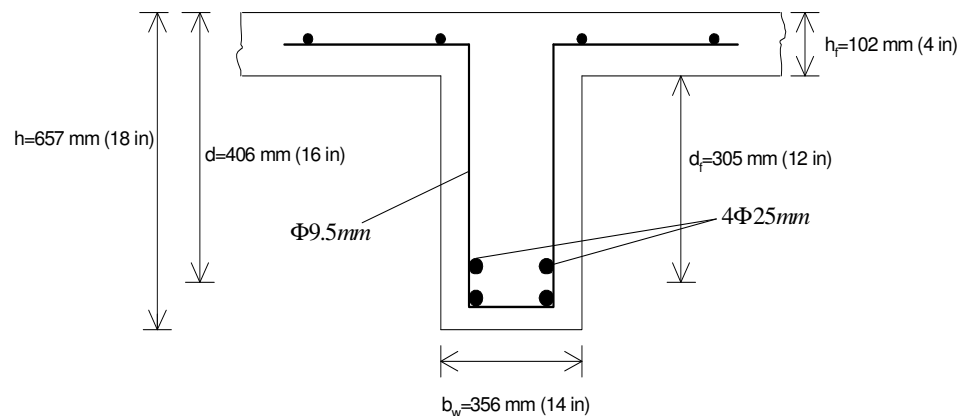
Figure 7.4. T-Girder Cross-Section

Figure 7.5 compares the magnitude of V_f computed by the analytical and design approaches in terms of $\rho_f E_f$. Figure 7.5 shows the magnitude of V_f by applying a side-bonded CFRP strengthening configuration.
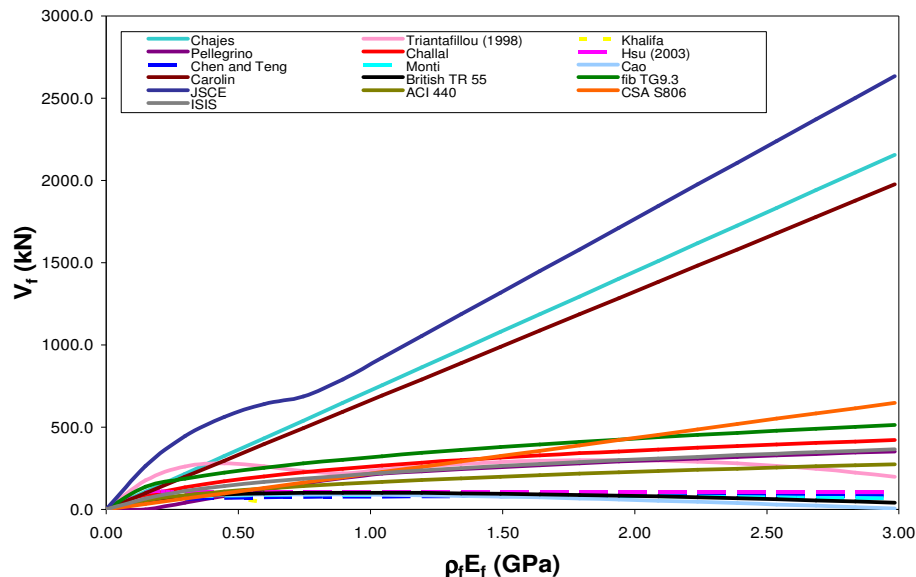
Figure 7.5. FRP Shear Contribution in Terms of Axial Rigidity – Side-Bonded T-Girder

From Figure 7.5, it can be observed that the predictions of V_f, by Chajes et al. (1995) analytical approach, linearly increases as the amount of FRP reinforcement increases. This behavior is explained by the fact that this analytical model fixes a value for the strain in the FRP. As a result, the predictions of the FRP shear contribution by this analytical model are conservative.

From the analytical approach by Triantafillou (1998), it can be observed that for values of $\rho_f E_f$ up to about 0.45 GPa, the FRP shear contribution increases almost linearly with $\rho_f E_f$ reaching a maximum, beyond which it drops slightly and then increases again slightly. This suggests that the value of 0.45 GPa can be used to determine the limiting amount of FRP reinforcement, beyond which the effectiveness of strengthening ceases to

be positive. This observed particular behavior could be attributed to the fact that Triantafillou (1998) derived the effective FRP strain based on limited experimental data. As a result, Triantafillou (1998) derived a single expression for determining the effective FRP strain without taking into consideration the different failure modes.

Khalifa et al. (1999) analytical approach indicates that for values of $\rho_f E_f$ up to about 0.36 GPa, the FRP shear contribution increases almost linearly with $\rho_f E_f$ reaching a maximum, beyond which it drops up to $\rho_f E_f$ equal to 0.7. This suggests that the value of 0.36 GPa can be used to determine the limiting amount of FRP reinforcement, beyond which the effectiveness of strengthening ceases to be positive. For values of $\rho_f E_f > 0.7$ GPa, additional amount of FRP results on negative values of FRP shear contribution. This means, that this analytical model is only valid for low values of FRP axial rigidity.

From the analytical approach by Pellegrino and Modena (2002), additional shear gain due to the FRP contribution is not observed for axial rigidities lower than 0.15 GPa. For values of $\rho_f E_f$ up to 1.0 GPa, the FRP shear contribution increases in proportion to $\rho_f E_f$. However, after this limit, the FRP shear contribution increases less than in proportion to the axial rigidity. Therefore, the effectiveness of the FRP system reduces as the amount of FRP reinforcement increases beyond 1.0 GPa.

The same trend is observed in Chaallal et al. (2002) analytical approach. The FRP shear contribution increases as the axial rigidity of FRP increases; however, after $\rho_f E_f > 1.0$ GPa, the FRP shear contribution increases less than in proportion to $\rho_f E_f$. Therefore, the effectiveness of the FRP system seems to reduce as the amount of FRP reinforcement increases beyond 1.0 GPa.

Hsu et al. analytical approach (2003) indicates that the FRP shear contribution increases linearly up to about $\rho_f E_f$ equal to 0.15 GPa, beyond which a constant shear gain due to the FRP contribution is observed. This behavior is explained by the fact that the effective FRP strain predicted by this analytical model decreases in propotion to the FRP axial rigidity. This means that as the FRP axial rigidity increases, its effective FRP strain decreases at a decreasing rate.

From the analytical approach by Chen and Teng (2003a-b), for values of $\rho_f E_f$ up to 1.0 GPa, the FRP shear contribution increases in proportion to $\rho_f E_f$. However, after

this limit, the FRP shear contribution increases less than in proportion to the axial rigidity. Therefore, the effectiveness of the FRP system seems to reduce as the amount of FRP reinforcement increases beyond 1.0 GPa.

Monti and Liotta (2005) analytical approach indicates that for values of $\rho_f E_f$ up to about 1.0 GPa, the FRP shear contribution increases with $\rho_f E_f$ reaching a maximum, beyond which it drops slightly. Therefore, the effectiveness of the FRP system seems to reduce as the amount of FRP reinforcement increases beyond 1.0 GPa.

The same trend is observed in the Cao et al. (2005) approach. The FRP shear contribution increases as the axial rigidity of FRP increases reaching a maximum at $\rho_f E_f$ equal to 0.75 GPa, afterwards the FRP shear contribution starts to decrease. Therefore, the effectiveness of the FRP system seems to reduce as the amount of FRP reinforcement increases beyond 0.75 GPa.

From the Carolin and Taljsten (2005) analytical approach, it can be observed that the FRP shear contribution increases linearly in proportion to the FRP axial rigidity. This behavior is explained by the fact that this analytical model fixes a value for the strain in the FRP, which is equal to the ultimate FRP strain. As a result, the predictions of the FRP shear contribution by this analytical model are conservative.

The design approach from the British Technical Report No. 55 (2000) indicates that for values of $\rho_f E_f$ up to about 1.0 GPa, the FRP shear contribution increases with $\rho_f E_f$ reaching a maximum, beyond which it starts to decrease. Therefore, the effectiveness of the FRP system seems to reduce as the amount of FRP reinforcement increases beyond 1.0 GPa.

From the design approach by fib TG 9.3 (2001), for values of $\rho_f E_f$ up to 1.0 GPa, the FRP shear contribution increases in proportion to $\rho_f E_f$. However, after this limit, the FRP shear contribution increases less than in proportion to the axial rigidity. Therefore, the effectiveness of the FRP system seems to reduce as the amount of FRP reinforcement increases beyond 1.0 GPa.

From the JSCE recommendations (2001) design approach, for values of $\rho_f E_f$ up to 0.60 GPa, the FRP shear contribution increases as $\rho_f E_f$ increases. Beyond this limit, the FRP shear contribution increases linearly in proportion to the FRP axial rigidity. This behavior can be attributed to the fact that the effective FRP strain remains constant after

0.60 GPa. The predictions of FRP shear contribution by the JSCE recommendations are observed to be the least conservative in comparison to all analytical and design approaches examined.

Both design approaches from ACI 440.2R (2002) and ISIS 4 (2002) indicate that for values of $\rho_f E_f$ up to 1.0 GPa, the magnitude of V_f increases in proportion to $\rho_f E_f$. However, after this limit, the FRP shear contribution increases less than in proportion to the axial rigidity. Therefore, the effectiveness of the FRP system for both approaches seems to reduce as the amount of FRP reinforcement increases beyond 1.0 GPa.

Finally, from the CSA S806 (2002) design approach, it can be observed that the FRP shear contribution increases linearly in proportion to the FRP axial rigidity. This behavior is explained by the fact that this design approach fixes a value for the effective strain in the FRP. As a result, the predictions of the FRP shear contribution by this design approach are conservative.

Figure 7.6 compares the magnitude of V_f computed by the analytical and design approaches in terms of $\rho_f E_f$. Figure 7.6 shows the magnitude of V_f by applying a U-wrapped CFRP strengthening configuration
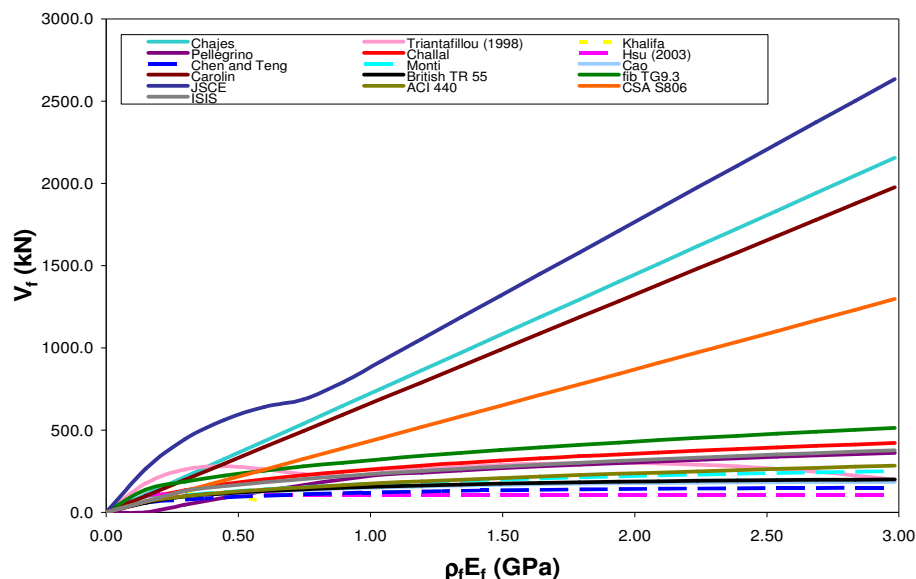
Figure 7.6. FRP Shear Contribution in Terms of Axial Rigidity – U-Wrapped T-Girder

From Figure 7.6, it can be observed that the the predictions of V_f by the approaches from Chajes et al., Triantafillou, Chaallal et al., Hsu et al., Carolin and Taljsten, fib TG 9.3, and JSCE are the same for both strengthening schemes. The predictions of V_f by the remaining approaches are higher in the case of U-wrapped configuration. The trend between V_f and the FRP axial rigidity, for most approaches, exhibits the same behavior as in the case of side-bonded configuration. However, the analytical and design approaches from Monti and Liotta, Cao et al., and the British TR 55, the FRP shear contribution keeps increasing as the FRP axial rigidity increases.

7.2.3. PC I-Girder. Figure 7.7 illustrates the cross-section of an I-girder with a shear span-to-depth ratio of 2.57. The concrete compressive strength is 48.3 MPa. The longitudinal reinforcement consists of twenty 15.2 mm diameter prestressed tendons at the bottom of the cross-section. Transverse steel reinforcement consists of 10M bars with a yield strength of 420 MPa and a modulus of elasticity of 200 GPa. The spacing between steel stirrups is of 305 mm. The FRP strengthening system consists of CFRP strips with a width of 254 mm and spacing between strips of 305 mm. The angle of fiber orientation is 90 degrees. The thickness of the CFRP is 0.165 mm, the modulus of elasticity of the CFRP is 228 GPa, and the ultimate tensile strength of the CFRP is 3792 MPa.
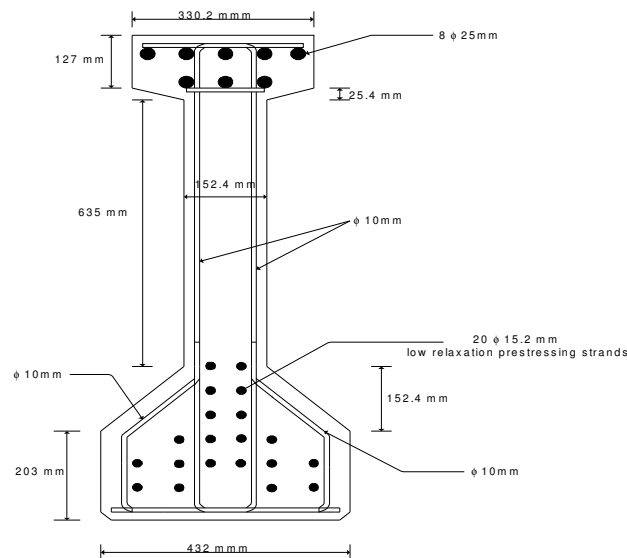
Figure 7.7. I-Girder Cross-section

Figure 7.8 compares the magnitude of V_f computed by the analytical and design approaches in terms of $\rho_f E_f$. Figure 7.8 shows the magnitude of V_f by applying a side-bonded CFRP strengthening configuration.
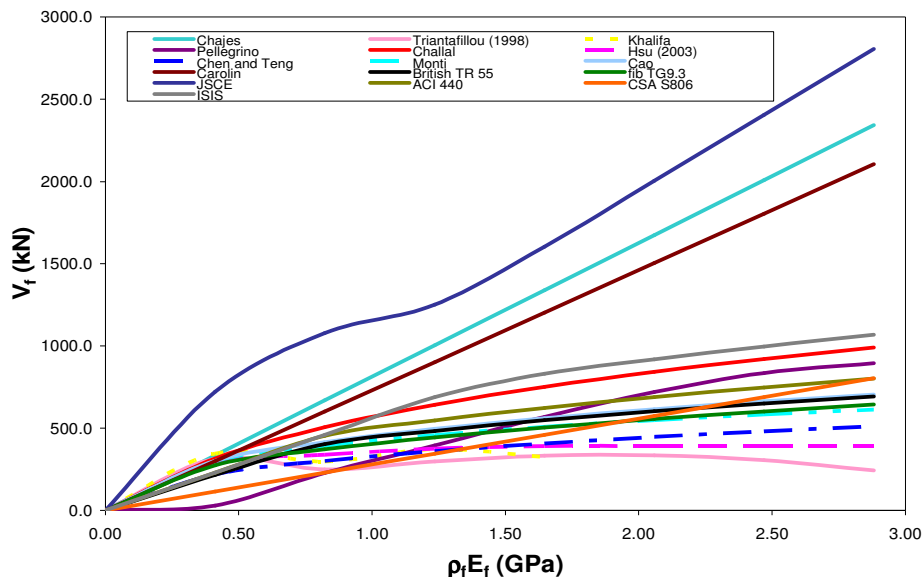
Figure 7.8. FRP Shear Contribution in Terms of Axial Rigidity – Side-Bonded I-Girder

From Figure 7.8, it can be observed that the predictions of V_f, by Chajes et al. (1995) analytical approach, linearly increases as the amount of FRP reinforcement increases. This behavior is explained by the fact that this analytical model fixes a value for the strain in the FRP. As a result, the predictions of the FRP shear contribution by this analytical model are conservative.

From the analytical approach by Triantafillou (1998), it can be observed that for values of $\rho_f E_f$ up to about 0.45 GPa, the FRP shear contribution increases almost linearly with $\rho_f E_f$ reaching a maximum, beyond which it drops slightly and then increases again slightly. This suggests that the value of 0.45 GPa can be used to determine the limiting amount of FRP reinforcement, beyond which the effectiveness of strengthening ceases to

be positive. This observed particular behavior could be attributed to the fact that Triantafillou (1998) derived the effective FRP strain based on limited experimental data. As a result, Triantafillou (1998) derived a single expression for determining the effective FRP strain without taking into consideration the different failure modes.

Khalifa et al. (1999) analytical approach indicates that for values of $\rho_f E_f$ up to about 0.50 GPa, the FRP shear contribution increases almost linearly with $\rho_f E_f$ reaching a maximum, beyond which it drops slightly and then increases again slightly. FRP shear contribution for values beyond $\rho_f E_f$ of about 1.65 GPa could not be estimated because negative values of V_f are obtained.

From the analytical approach by Pellegrino and Modena (2002), for values of $\rho_f E_f$ up to 2.5 GPa, the FRP shear contribution increases in proportion to $\rho_f E_f$. However, after this limit, the FRP shear contribution increases less than in proportion to the axial rigidity. Therefore, the effectiveness of the FRP system reduces as the amount of FRP reinforcement increases beyond 2.5 GPa.

The same trend is observed in Chaallal et al. (2002) analytical approach. The FRP shear contribution increases as the axial rigidity of FRP increases; however, after $\rho_f E_f > 2.5$ GPa, the FRP shear contribution increases less than in proportion to $\rho_f E_f$. Therefore, the effectiveness of the FRP system seems to reduce as the amount of FRP reinforcement increases beyond 2.5 GPa.

Hsu et al. (2003) analytical approach indicates that the FRP shear contribution increases up to about $\rho_f E_f$ equal to 1.5 GPa, beyond which a constant shear gain due to the FRP contribution is observed. This behavior is explained by the fact that the effective FRP strain predicted by this analytical model decreases in propotion to the FRP axial rigidity. This means that as the FRP axial rigidity increases, its effective FRP strain decreases at a decreasing rate.

From the analytical approach by Chen and Teng (2003a-b), for values of $\rho_f E_f$ up to 2.5 GPa, the FRP shear contribution increases in proportion to $\rho_f E_f$. However, after this limit, the FRP shear contribution increases less than in proportion to the axial rigidity. Therefore, the effectiveness of the FRP system seems to reduce as the amount of FRP reinforcement increases beyond 2.5 GPa. The same type of behavior is exhibited by the analytical models from Monti and Liotta (2005) and Cao et al. (2005).

From the Carolin and Taljsten (2005) analytical approach, it can be observed that the FRP shear contribution increases linearly in proportion to the FRP axial rigidity. This behavior is explained by the fact that this analytical model fixes a value for the strain in the FRP, which is equal to the ultimate FRP strain. As a result, the predictions of the FRP shear contribution by this analytical model are conservative.

The design approach from the British Technical Report No. 55(2000) indicates that for values of $\rho_f E_f$ up to about 2.5 GPa, the magnitude of V_f increases; however, after this limit, the FRP shear contribution increases less than in proportion to the axial rigidity. This same type of trend between the FRP shear contribution and the FRP axial rigidity is observed in the fib TG 9.3 (2001) design approach.

From the JSCE recommendations (2001) design approach, for values of $\rho_f E_f$ up to 1.4 GPa, the FRP shear contribution increases as $\rho_f E_f$ increases. Beyond this limit, the FRP shear contribution increases linearly in proportion to the FRP axial rigidity. This behavior can be attributed to the fact that the effective FRP strain remains constant after 1.4 GPa. The predictions of FRP shear contribution by the JSCE recommendations are observed to be the least conservative in comparison to all analytical and design approaches examined.

Both design approaches from ACI 440.2R (2002) and ISIS 4 (2002) indicate that for values of $\rho_f E_f$ up to 2.5 GPa, the FRP shear contribution increases in proportion to $\rho_f E_f$. However, after this limit, the FRP shear contribution increases less than in proportion to the axial rigidity. Therefore, the effectiveness of the FRP system for both approaches seems to reduce as the amount of FRP reinforcement increases beyond 2.5 GPa.

Finally, from the CSA S806 (2002) design approach, it can be observed that the FRP shear contribution increases linearly in proportion to the FRP axial rigidity. This behavior is explained by the fact that this design approach fixes a value for the effective strain in the FRP. As a result, the predictions of the FRP shear contribution by this design approach are conservative.

Figure 7.9 compares the magnitude of V_f computed by the analytical and design approaches in terms of $\rho_f E_f$. Figure 7.9 shows the magnitude of V_f by applying a side-bonded CFRP strengthening configuration.
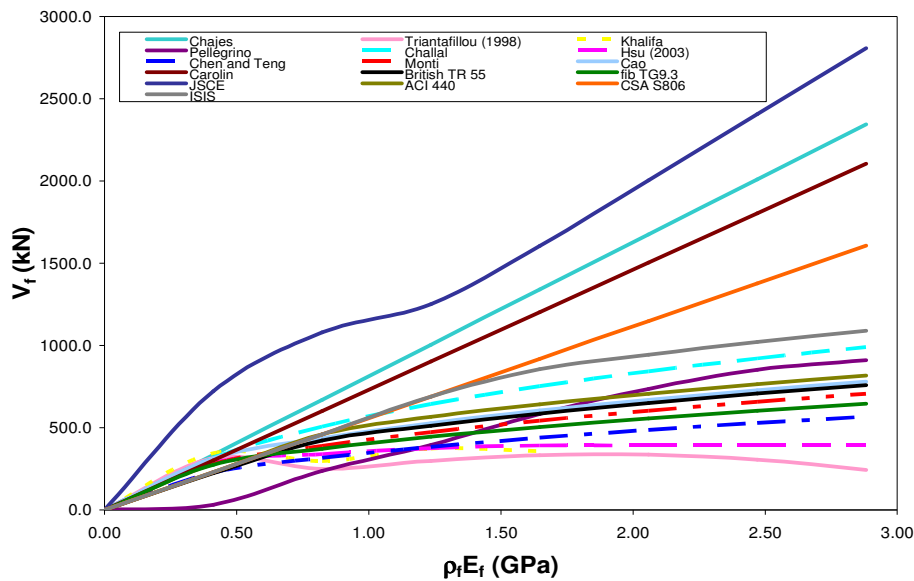
Figure 7.9. FRP Shear Contribution in Terms of Axial Rigidity – U-Wrapped
I-Girder

Figure 7.9 illustrates the comparison of the FRP shear contribution by applying a
U-wrapped strengthening configuration. The analytical and design approaches from
Chajes et al., Triantafillou, Chaallal et al., Hsu et al., Carolin and Taljsten, fib TG 9.3,
and JSCE do not make a distinction, in the formulations to determine the FRP shear
contribution, between side-bonded and U-wrapped configurations. Therefore, the
predictions of FRP shear contribution are the same for both strengthening configurations.
The predictions of V_f by the remaining analytical and design approaches are higher in the
case of U-wrapped configuration than those of side-bonded configuration. The trend
between V_f and the FRP axial rigidity, for most analytical and design approaches, exhibits
the same behavior as in the case of side-bonded configuration.

7.3. SUMMARY AND CONCLUDING REMARKS

Due to the complexity of the analytical approaches examined and the limited
database presented in Section Three and Section Five, the FRP shear contribution
predicted by these approaches was effectively compared by providing specific examples.
The first example consisted of a RC T-cross section representing a beam. The second

example consisted of a RC T-cross-section representing a small bridge girder. The last example consisted of a prestressed (PC) I-cross section representing a large bridge girder.

The three examples provided were applied to compare the FRP shear contribution, V_f, among all the analytical and design approaches evaluated in Section Five and Section Six. The comparison of the magnitude of V_f was performed in terms of the axial rigidity of the provided FRP reinforcement, $\rho_f E_f$. In all the relationships for estimating V_f, the shear crack angle was assumed to be 45 degree, and all partial safety factors were assumed to be equal to 1.0.

From the comparative evaluation presented in the plots discussed in the previous section, the following observations can be drawn:

1. All three examples showed that there are very significant differences in the prediction of V_f by the examined analytical and design approaches for a given level of axial rigidity of FRP.

2. For all three examples, the JSCE Recommendations (2001) approach was observed to be the least conservative. The most conservative approach was different for any given level of $\rho_f E_f$ among all the examples.

3. For all three examples, the analytical and design approaches from Chajes et al, Triantafillou, Chaallal et al., Hsu et al., Carolin and Taljsten, fib TG 9.3, and JSCE do not make a distinction, in the formulations to determine the FRP shear contribution, between side-bonded and U-wrapped configurations. Therefore, the magnitude of V_f is the same for both strengthening configurations.

4. The predictions of V_f, by the approaches from Khalifa et al., Pellegrino and Modena, Chen and Teng, Monti and Liotta, Cao et al., British TR 55, ACI 440.2R, CSA S806 and ISIS, are higher in the case of U-wrapped configuration than those of side-bonded configuration.

5. The predictions of V_f for the PC I-girder are higher, for both wrapping configurations, than those corresponding to the RC T-beam and RC T-girder.

6. The predictions of V_f estimated by Chajes et al., Carolin and Taljsten, JSCE and CSA S806 linearly increased in proportion to the FRP axial rigidity for all three types of cross-section and both wrapping configurations.

7. The approaches from Triantafillou, Khalifa et al., Monti and Liotta, Cao et al., and British TR 55 established a limit on the FRP shear contribution for both the RC T-beam and T-girder with side-bonded configuration. For U-wrapped configuration, only the approaches from Triantafillou and Khalifa et al. placed a limit on the FRP shear contribution.

8. For both the RC T-beam and T-girder with side-bonded configuration, V_f predicted by Pellegrino and Modena, Chaallal et al., Chen and Teng, fib TG 9.3, ACI 440.2R, and ISIS increased less in proportion to the FRP axial rigidity, for values of $\rho_f E_f$ >1.0 GPa. For U-wrapped configuration, V_f predicted by the approaches mentioned above, in addition to the approaches from Monti and Liotta, Cao et al., and British TR 55, increased less in proportion to the FRP axial rigidity, for values of $\rho_f E_f$ >1.0 GPa.

9. For the PC I-girder with both strengthening configurations, the same approaches showed a linear increase in the magnitude of V_f in proportion with the FRP axial rigidity. The approaches from Triantafillou and Khalifa et al., established a limit on the FRP shear contribution. The FRP shear contribution, predicted by Pellegrino and Modena, Chaallal et al., Chen and Teng, fib TG 9.3, ACI 440.2R, ISIS, Monti and Liotta, Cao et al., and British TR 55, increased less than in proportion to the FRP axial rigidity, especially after $\rho_f E_f$ >2.5 GPa.

8. CONCLUSIONS AND RECOMMENDATIONS FOR FUTURE RESEARCH

8.1. SUMMARY OF RESEARCH WORK

FRP composite materials have emerged as one of the most promising materials in the use of external reinforcement for repair and strengthening of RC structures. Their application in structural engineering has become increasingly popular due to their resistance to corrosion, excellent high strength, ease in manufacturing, handling and installation, and cost-effectiveness.

Extensive research to investigate the behavior of RC members strengthened in shear with FRP composite materials has been developed over the last 20 years. However, the results obtained thus far are scarce and sometimes controversial. This is in essence due to the intrinsic difficulty of shear behavior of reinforced concrete (RC) members. Therefore, the overall objective of this study was to investigate previous analytical studies and design guidelines on shear strengthening of RC members with externally-bonded FRP laminates, and their assessment with experimental data collected from the literature.

This study was organized in three main parts: review and summary of analytical and design approaches, parametric study of the experimental data, and comparative evaluation of analytical and design approaches. The first part consisted on a summary and discussion of existing analytical models and design guidelines to determine the shear strength of RC members strengthened with FRP systems. These analytical models and design guidelines investigated were classified according to the approach adopted to predict the FRP effective strain at the time of failure. The second part consisted of the identification and evaluation of parameters that influence the behavior of RC members shear strengthened with FRP systems. For this purpose, an extensive and detailed database was developed for data analysis. The last part consisted of a comparative evaluation of the accuracy in predicting the FRP shear contribution between the analytical and design approaches. Furthermore, due to the complexity and variety of the analytical and design approaches, the comparative evaluation was also performed through specific examples. These examples consist on different type of RC members, with different FRP strengthening schemes.

8.2. CONCLUSIONS

      8.2.1. Review and Summary of Analytical and Design Approaches. The following conclusions can be drawn from the review of the analytical and design approaches.

1.   The main difference between the analytical models and design guidelines examined adopted in the different approaches to predict the FRP effective strain at the time of failure. Therefore, the analytical models and design guidelines were classified into approaches based on a fixed FRP effective strain, empirical approaches, and approaches based on non-uniform strain distribution.

2.   Some models and guidelines fixed the effective FRP strain to determine the FRP shear contribution. For instance, Chajes et al. (1995) fixed the strain to be the ultimate strain at failure corresponding to the concrete. CSA S806-02 (2002) provided fixed values of effective FRP strain according to wrapping configurations.

3.   Empirical approaches were based directly on the calibration of experimental data and regression analysis to estimate the effective strain in the FRP. These models basically estimated experimental values for the effective FRP strain by back calculating from the experimental values of the FRP shear contribution. Then, a relationship for the effective FRP strain in terms of the FRP stiffness was obtained by regression analysis. Additionally, in this category were classified analytical models that were based on empirical bond mechanism approaches

4.   Analytical models, based on non-uniform strain distribution, were derived from bond strength approaches, which were based on fracture mechanics at the FRP/concrete interface. The specific fracture energy of the FRP/concrete interface was used to determine the bond strength.

5.   Most analytical models and design guidelines treated separately the mechanisms of FRP debonding and FRP fracture except for Chajes et al. (1995), Triantafillou (1998), JBDPA (1999), JSCE (2001), and CSA S806-02 (2002). Therefore, most models and design standards proposed two different approaches that represent the two possible failure modes.

6.   Most models and design guidelines, with the exception of Chen and Teng (2003), Cao et al. (2005), Monti and Liotta (2004), and Carolin and Taljsten (2005)

determined the effective FRP strain by performing regression analysis of experimental data. Therefore, important parameters that influence the effective FRP strain were not taken into consideration because of the difficulty of accounting all relevant parameters in one single equation.

7. Models and guidelines based on data regression did not provide an accurate bond strength model. Therefore, it seems that the models based on fracture mechanics described more accurately the behavior of RC beams shear strengthened with externally FRP because the bond strength models were developed by applying fracture mechanics. Bond strength models that apply fracture mechanics recognize the non-uniformity of the FRP stress distribution along a shear crack.

8. Most analytical models, added the shear contributions of concrete, stirrups and FRP to be consistent with the truss approach used in RC design codes, without taken into account the dependence and interaction between the concrete, stirrups and FRP sheets. The exception was the analytical model from Deniaud and Cheng (2004).

8.2.2. Parametric Study of the Experimental Data. The following conclusions were drawn from the parametric study.

1. No clear trendline was observed between the shear gain and $E_f \rho_f / f'^{2/3}_c$ for specimens that failed due to FRP debonding. However, for specimens failing due to FRP fracture, additional shear gains were observed as the amount of FRP reinforcement increases.

2. Test specimens that failed due to FRP debonding were more frequent in members with higher a/d ratios. Furthermore the effect of transverse steel reinforcement on additional shear gain due to FRP systems was observed. This additional shear gain was smaller in beam specimens with transverse steel reinforcement than in beam specimens without transverse steel.

3. The influence of the transverse steel reinforcement was confirmed in the present study. The gain in shear resistance due to FRP decreased as the ratio of $\rho_s E_s / \rho_f E_f$ increased. However, additional experimental and analytical investigations are needed to provide a better understanding of the mechanisms involved in the interaction between transverse steel and FRP reinforcements.

8.2.3. Comparative Evaluation of Analytical and Design Approaches. The comparative evaluation was performed in three parts: evaluation of analytical models, evaluation of design guidelines, and comparison of the analytical and design approaches by means of specific examples.

The comparative evaluation of the analytical models was conducted by comparing the predicted shear strength of FRP $V_{f,theo}$ with the experimental results, $V_{f,exp}$. In addition, for each analytical model, the predicted total shear capacity, V_{theo}, was compared with the observed experimental results, V_{exp}. The predictions of total shear capacities were computed by applying each analytical model in combination with four RC design codes. From this comparative evaluation, the following conclusions were drawn:

1. Almost all analytical models, underestimated the prediction of FRP shear contribution for low values of $E_f \rho_f / (f_c')^{2/3}$, and overestimated it for high values of $E_f \rho_f / (f_c')^{2/3}$. On the other hand, the analytical models from Hsu et al. (2003) and Zhang and Hsu (2005) exhibited an increasing trend between the FRP shear capacity ratio and $E_f \rho_f / (f_c')^{2/3}$.

2. The predictions of FRP shear contribution for specimens that failed due to FRP fracture were more conservative for most models except for Triantafillou and Antonopoulos (2000), Hsu et al. (2003), and Chen and Teng (2003). For these three models, the mean values of $V_{f,exp} / V_{f,theo}$ for both debonding and fracture failure were close to each other.

3. The models from Hsu et al. (2003) and Chen and Teng (2003) provided better predictions for the FRP shear contribution for both debonding and fracture failures. However, the FRP debonding approach from Chen and Teng provided lower COV values.

4. For almost all analytical models, the FRP shear capacity ratio $V_{f,exp} / V_{f,theo}$ increases as the shear span-to-depth ratio increases up to 3.0, and decreases afterwards. However, from the analytical models of Chaallal et al. (2002), Cao et al. (2005) and Zhang and Hsu (2005), a decreasing trend is observed.

5.   For almost all analytical models, the FRP shear capacity ratio $V_{f,exp}/V_{f,theo}$

increases as the amount of transverse steel reinforcement increases. However, from
the analytical models of Hsu et al. (2003) and Zhang and Hsu (2005), a decreasing
trend is observed.

6.   For all RC design codes, the combinations of the analytical model from Cao et al.
(2005) and Chaallal et al. (2002) with the CSA A23.3-94 design code provided the
most accurate prediction of total shear capacity. However, the combination of Chen
and Teng (2003) analytical model with Eurocode 2 provided less scatter in the data
points.

7.   Both AASHTO specifications and ACI 318-05 provided higher conservative values

of V_{exp}/V_{theo} and higher COV values than the other design codes when applied in

combination with all analytical models. Eurocode 2 provided lower COV values
and predicts the total shear capacity more accurately when applied in combination
with all analytical models.

8.   The application of the analytical model from Triantafillou and Antonopoulos (2000)
in combination with Eurocode 2 provided the most accurate predictions of total
shear capacity and lower COV values for both debonding and fracture failures.

9.   The predictions of total shear capacities for specimens that failed due to FRP
fracture were more conservative for all models and design codes, except for the
models of Triantafillou and Antonopoulos (2000), Chen and Teng (2003), and

Zhang and Hsu (2005). For these three models, the mean values of V_{exp}/V_{theo} for

both debonding and fracture failure are close to each other.

The comparative evaluation of the design guidelines was performed by comparing
the predicted shear strength of FRP $V_{f,theo}$ with the observed experimental results, $V_{f,exp}$.
In addition, for each design guideline, the predicted total shear capacity, V_{theo}, was
compared with the observed experimental results, V_{exp} for total shear capacity. The
predictions of total shear capacities were computed by applying each design guideline
with its corresponding RC design code. From this comparative evaluation, the following
conclusions were drawn:

1. For all design guidelines, the FRP shear capacity ratio $V_{f,\exp}/V_{f,theo}$ decreased as

    $E_f \rho_f /(f_c')^{2/3}$ increases. For this reason, it was found that all design guidelines

    underestimated the prediction of FRP shear capacity for low values of

    $E_f \rho_f /(f_c')^{2/3}$, and overestimated the FRP shear contribution for high values of

    $E_f \rho_f /(f_c')^{2/3}$.

2. For all design guidelines, the FRP shear capacity ratio $V_{f,\exp}/V_{f,theo}$ increased as the

    shear span-to-depth ratio increased up to a/d equal to 3.0, and decreased afterwards

    up to 3.41. Therefore, all design guidelines tended to overestimate the FRP shear

    contribution for higher a/d ratios.

3. For all design guidelines, the FRP shear capacity ratio $V_{f,\exp}/V_{f,theo}$ increased as the

    amount of transverse steel reinforcement increased for both specimens failing due

    to FRP debonding and fracture.

4. The predictions of FRP shear capacity for fracture failure were more conservative

    for all design guidelines except for fib TG 9.3 (2001). For this design guideline, the

    mean values of $V_{f,\exp}/V_{f,theo}$ for both debonding and fracture failure were close to

    each other.

5. The fib TG 9.3 (2001) provided better predictions for the FRP and total shear

    capacities for both debonding and fracture failures. This design guideline also

    provided smaller COV values.

6. Technical Report No.55 (2004) , ISIS Design Manual 4 (2001), ACI 440.2R-02

    (2002), and CSA-S806-02 (2002) provided very conservative predictions of the

    FRP contribution and total shear capacities for both FRP debonding and fracture

    failures.

7. JSCE design recommendations overestimated the FRP shear contribution for almost

    all test specimens because this code recommended the effective stress of FRP to be

    between 0.4 and 0.8 times the FRP ultimate strength, which leaded to high

    predictions of FRP shear contribution.

    Finally, the comparison of the magnitude of V_f was performed in terms of the

axial rigidity of the provided FRP reinforcement, $\rho_f E_f$. This comparative evaluation was

performed by means of three examples that represent three different types of cross-sections: RC T-beam, RC T-girder, and PC I-girder. From the comparative evaluation, the following observations can be drawn:

1. All three examples showed that there are very significant differences in the prediction of V_f by the examined analytical and design approaches for a given level of axial rigidity of FRP.

2. For all three examples, the JSCE Recommendations (2001) approach was observed to be the least conservative. The most conservative approach was observed to be different for any given level of $\rho_f E_f$ among all the examples.

3. The predictions of V_f, by the approaches from Khalifa et al., Pellegrino and Modena, Chen and Teng, Monti and Liotta, Cao et al., British TR 55, ACI 440.2R, CSA S806 and ISIS, were higher in the case of U-wrapped configuration than those of side-bonded configuration. The predictions of V_f for the PC I-girder were higher, for both wrapping configurations, than those corresponding to the RC T-beam and RC T-girder.

4. The predictions of V_f estimated by Chajes et al., Carolin and Taljsten, JSCE and CSA S806 linearly increased in proportion to the FRP axial rigidity for all three types of cross-section and both wrapping configurations.

5. The approaches from Triantafillou, Khalifa et al., Monti and Liotta, Cao et al., and British TR 55 established a limit on the FRP shear contribution for both the RC T-beam and T-girder with side-bonded configuration. For U-wrapped configuration, only the approaches from Triantafillou and Khalifa et al. placed a limit on the FRP shear contribution.

6. For both the RC T-beam and T-girder with side-bonded configuration, V_f predicted by Pellegrino and Modena, Chaallal et al., Chen and Teng, fib TG 9.3, ACI 440.2R, and ISIS increased less in proportion to the FRP axial rigidity, for values of $\rho_f E_f$ >1.0 GPa. For U-wrapped configuration, V_f predicted by the approaches mentioned above, in addition to the approaches from Monti and Liotta, Cao et al., and British TR 55, increased less in proportion to the FRP axial rigidity, for values of $\rho_f E_f$ >1.0 GPa.

7. For the PC I-girder with both wrapping configurations, the approaches from Triantafillou and Khalifa et al., established a limit on the FRP shear contribution. The FRP shear contribution, predicted by Pellegrino and Modena, Chaallal et al., Chen and Teng, fib TG9.3, ACI 440.2R, ISIS, Monti and Liotta, Cao et al., and British TR 55, increased less than in proportion to the FRP axial rigidity, especially after $\rho_f E_f > 2.0$ GPa.

8.3. RECOMMENDATIONS FOR FUTURE RESEARCH

It is recommended that the following research be pursued as an extension of the present study.

1. Additional experimental investigations are recommended to address the influence of transverse steel reinforcement, with emphasis on the mechanisms which can explain the experimentally observed interaction between external FRP shear strengthening and internal transverse steel reinforcement. The size effect also needs to be addressed since the available experimental data are mainly based on relatively small specimens.

2. Further experimental investigations need to carefully monitor and record strain data in the different components (concrete, FRP, longitudinal and transverse steel reinforcement). This will provide a better understanding of the mechanisms involved and thus, more rational and accurate design methods and guidelines can be developed.

3. From previous studies, the anchorage systems appeared to be very helpful to increase the shear capacity provided by FRP by changing the failure mode from FRP debonding to FRP fracture. Therefore, the effect of anchorage systems needs to be further experimentally investigated.

4. The bond strength between the FRP and concrete surface depends on the compressive strength of concrete. However, the effect of concrete strength has not been thoroughly evaluated and analyzed. Therefore, the influence of this parameter needs to be further evaluated and analyzed.

5. The inclination of shear crack influences the shear strengthening provided by the FRP sheet. Some analytical models take into consideration the angle of inclined

cracks. However, experimental investigations do not provide information on the magnitude of the angle of shear crack inclination, which is necessary to critique the different models. This problem should be address for further analysis and future research.

6. From the comparative evaluation in this study, none of the analytical and design approaches that were examined were able to provide reliable estimates of shear strengthening for all of the members in the database. This indicates that the mechanisms of FRP strengthening are still poorly understood. This is further demonstrated by the very significant differences in the predictions by the examined models. Therefore, additional parameter that are not taken into account in these approaches, but that affect the behavior of members strengthened in shear with FRP need to be further investigated.

APPENDIX A.

EXPERIMENTAL DATA ON
SHEAR STRENGTHENING WITH FRP SYSTEMS

Table A.1. Experimental Shear Data on Shear Strengthening with FRP Systems

Table A.1. Experimental Shear Data on Shear Strengthening with FRP Systems (Contd.)

Table A.1. Experimental Shear Data on Shear Strengthening with FRP Systems (Contd.)

APPENDIX B

COMPARISON BETWEEN EXPERIMENTAL OBSERVATIONS
AND ANALYTICAL PREDICTIONS
BY ANALYTICAL MODELS
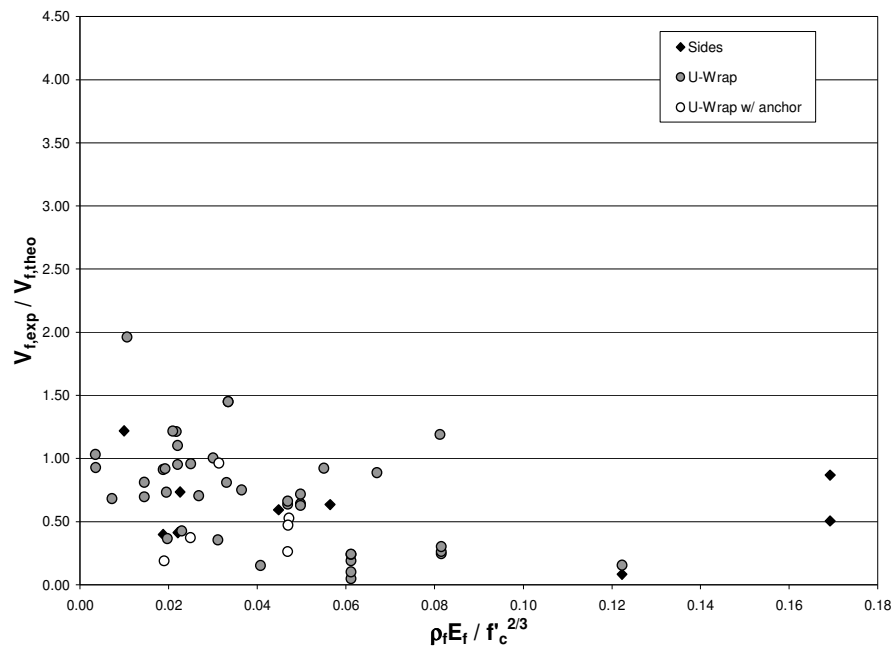
Figure B.1. $V_{f,\exp} / V_{f,theo}$ in terms of $E_f \rho_f / (f_c^{'})^{2/3}$ - FRP Debonding
Triantafillou (1998)
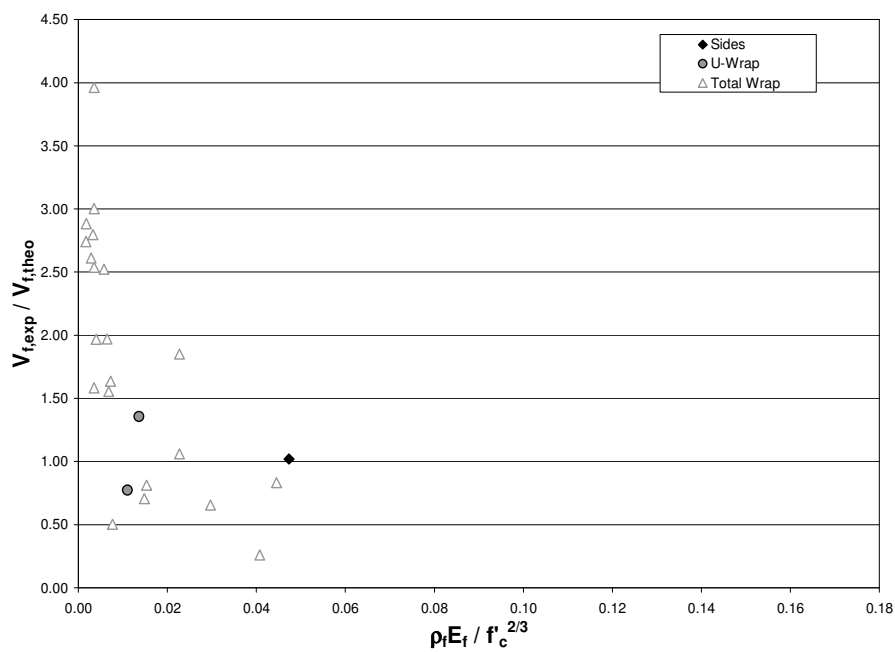
Figure B.2. $V_{f,\exp} / V_{f,theo}$ in terms of $E_f \rho_f / (f_c^{'})^{2/3}$ - FRP Fracture
Triantafillou (1998)
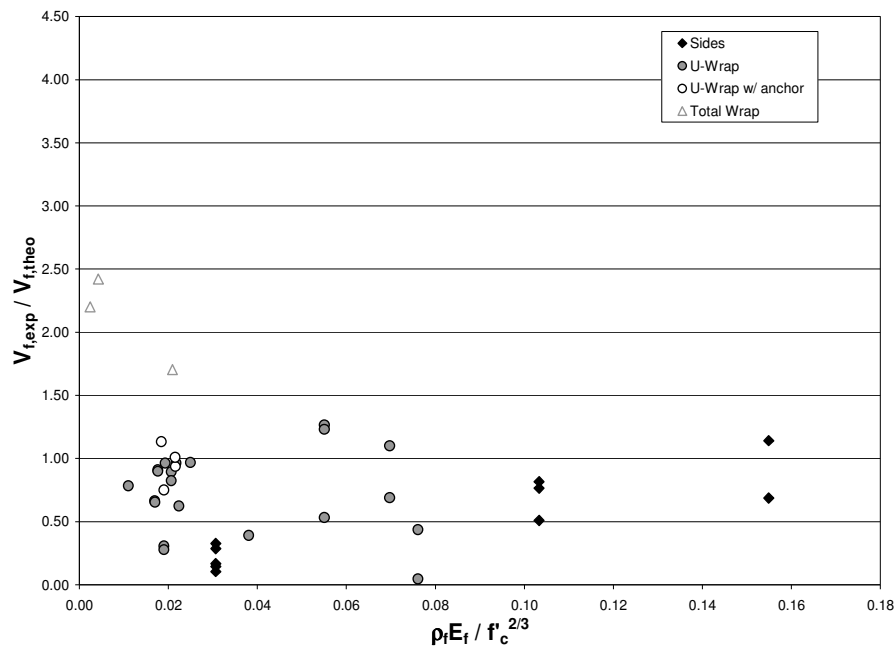
Figure B.3. $V_{f,\exp}/V_{f,theo}$ in terms of $E_f\rho_f/(f_c')^{2/3}$ - Other Failure Modes
Triantafillou (1998)
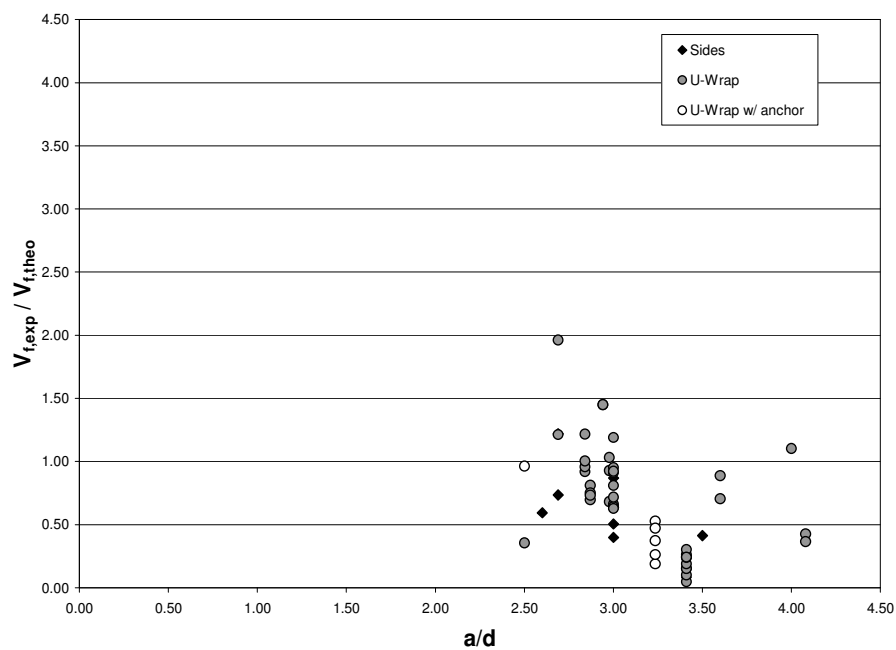
Figure B.4. $V_{f,\exp}/V_{f,theo}$ in terms of a/d – FRP Debonding
Triantafillou (1998)
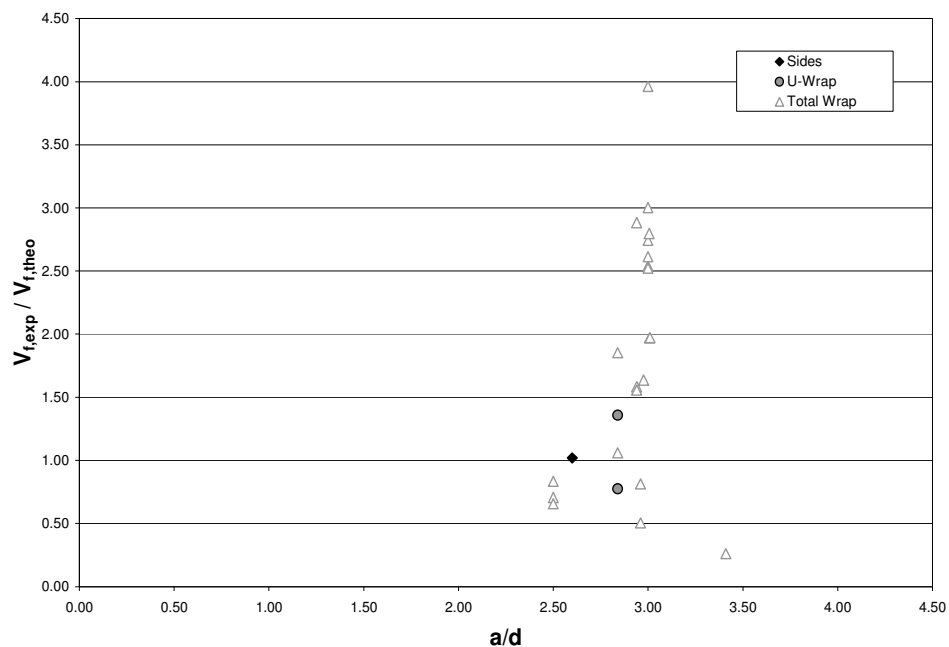
Figure B.5. $V_{f,\exp}/V_{f,theo}$ in terms of a/d – FRP Fracture
Triantafillou (1998)
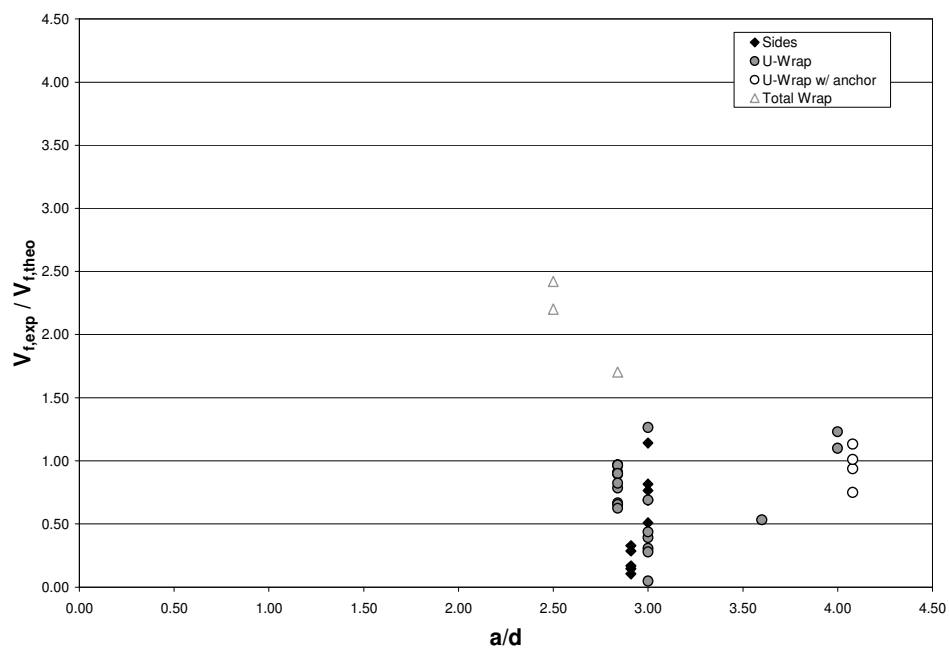
Figure B.6. $V_{f,\exp}/V_{f,theo}$ in terms of a/d – Other Failure Modes
Triantafillou (1998)
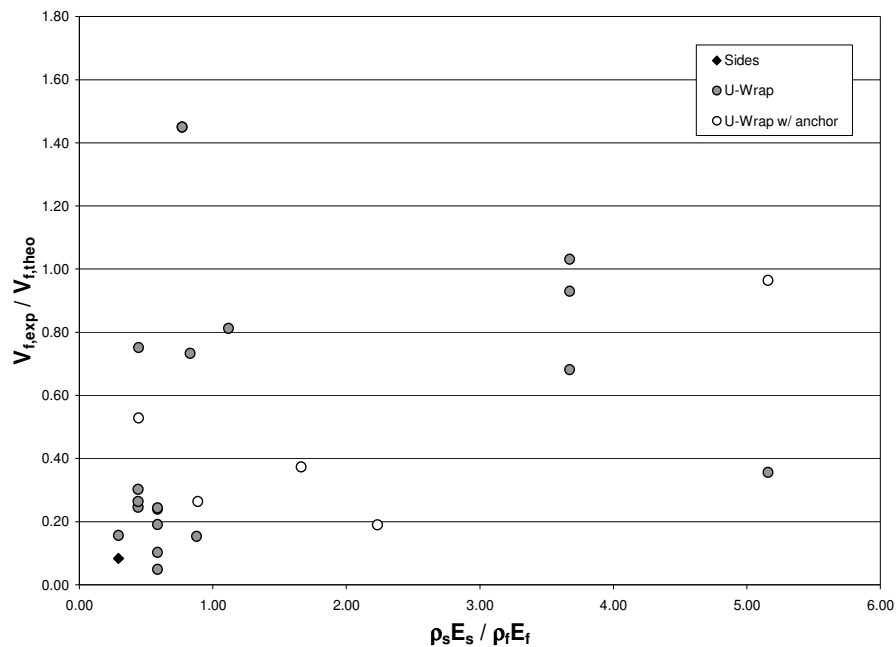
Figure B.7. $V_{f,\exp}/V_{f,theo}$ in terms of $\rho_s E_s / \rho_f E_f$ – FRP Debonding
Triantafillou (1998)
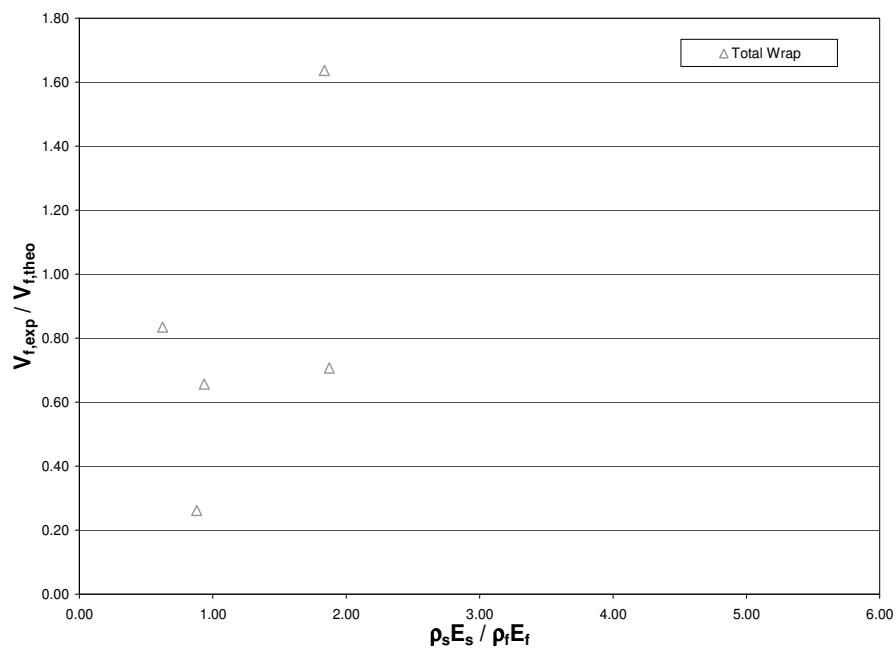
Figure B.8. $V_{f,\exp}/V_{f,theo}$ in terms of $\rho_s E_s / \rho_f E_f$ – FRP Fracture
Triantafillou (1998)
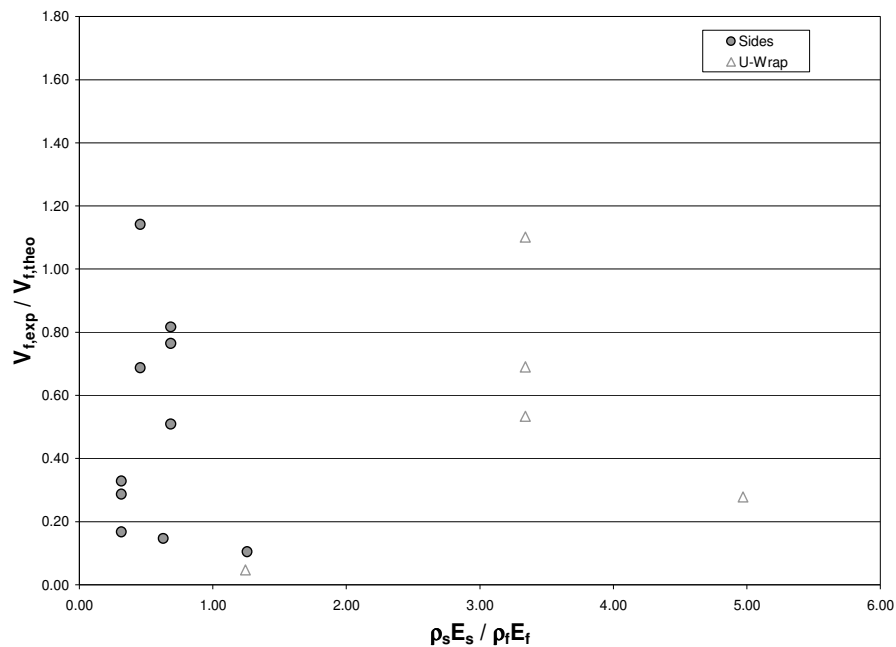
Figure B.9. $V_{f,\exp}/V_{f,theo}$ in terms of $\rho_s E_s / \rho_f E_f$ – Other Failure Modes
Triantafillou (1998)
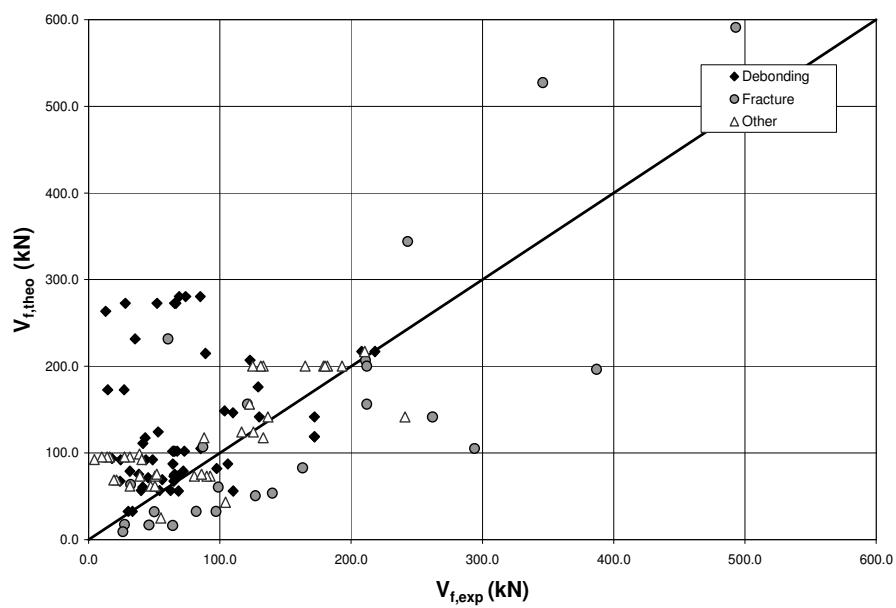
Figure B.10. Comparison between Predictions by Triantafillou (1998) and Experimental
Results
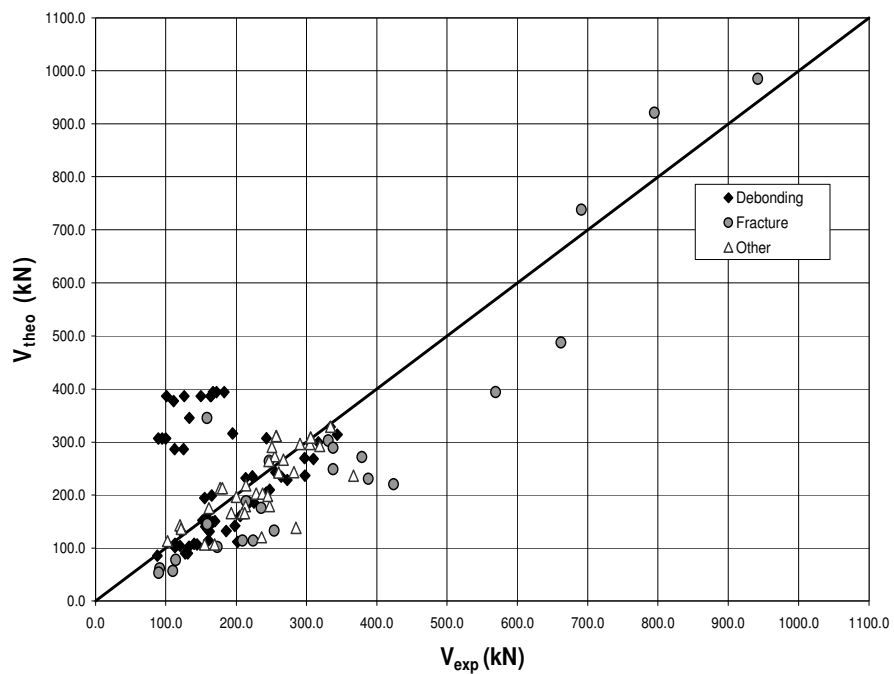
(a) ACI 318-05
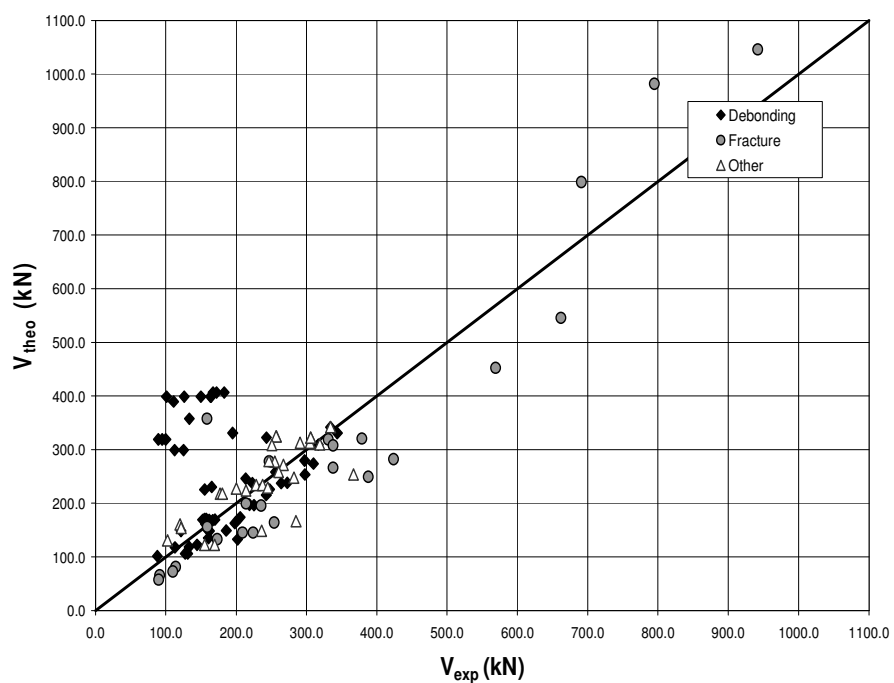
(b) Eurocode 2

Figure B.11. Comparison between Analytical Predictions of total shear capacity by Triantafillou (1998) and Experimental Results
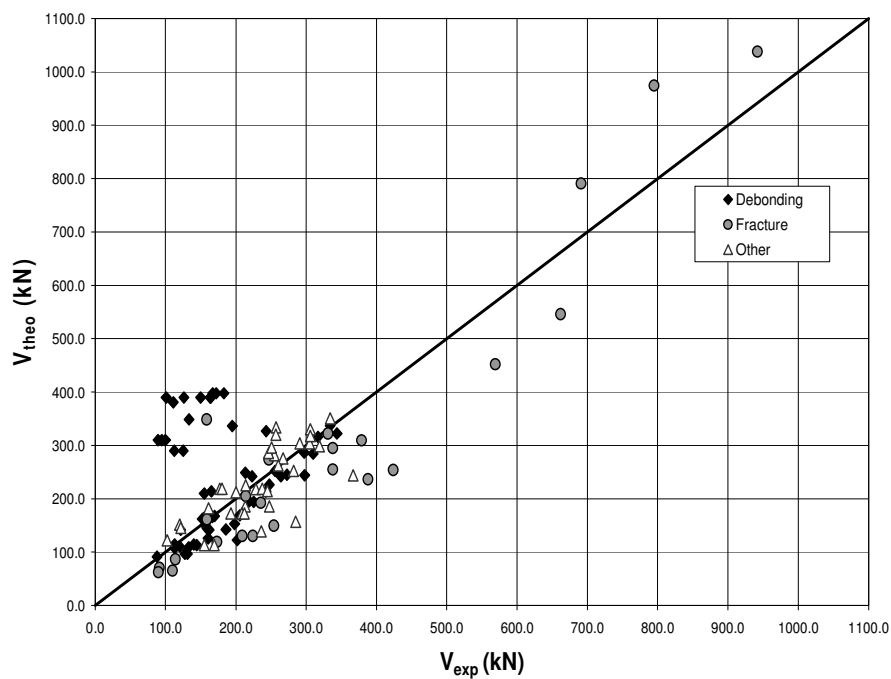
(c) CSA A23.3-94
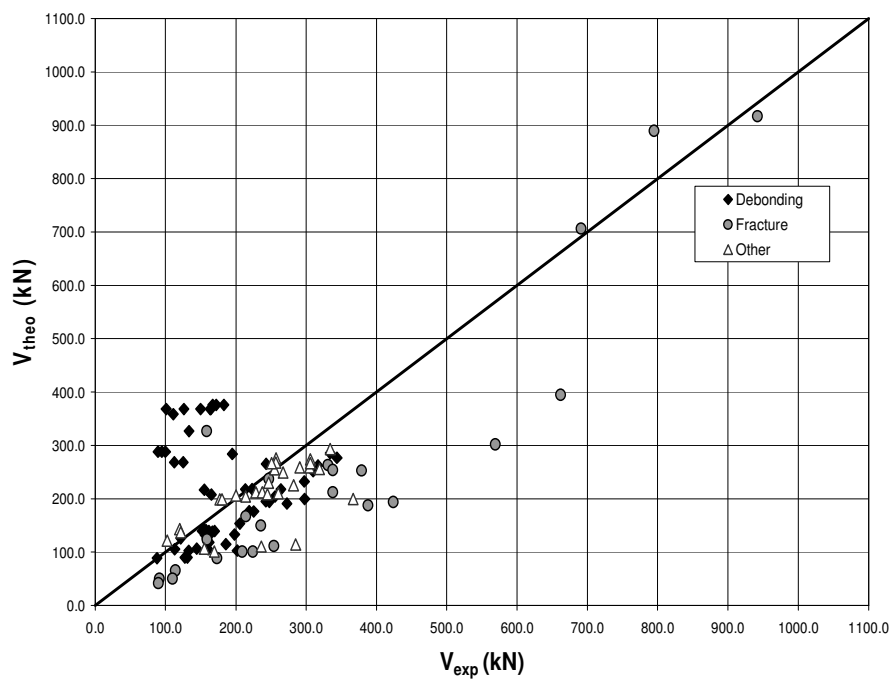
(d) AASHTO LRFD

Figure B.12. Comparison between Analytical Predictions of total shear capacity by Triantafillou (1998) and Experimental Results
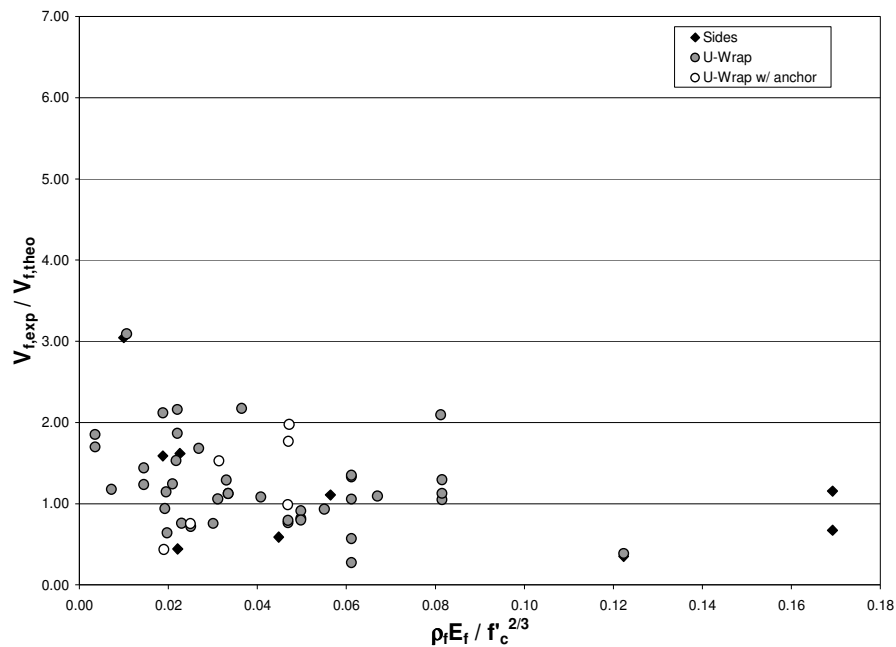
Figure B.13. $V_{f,\exp} / V_{f,theo}$ in terms of $E_f \rho_f / (f_c^{'})^{2/3}$ - FRP Debonding
Khalifa et al. (1999)
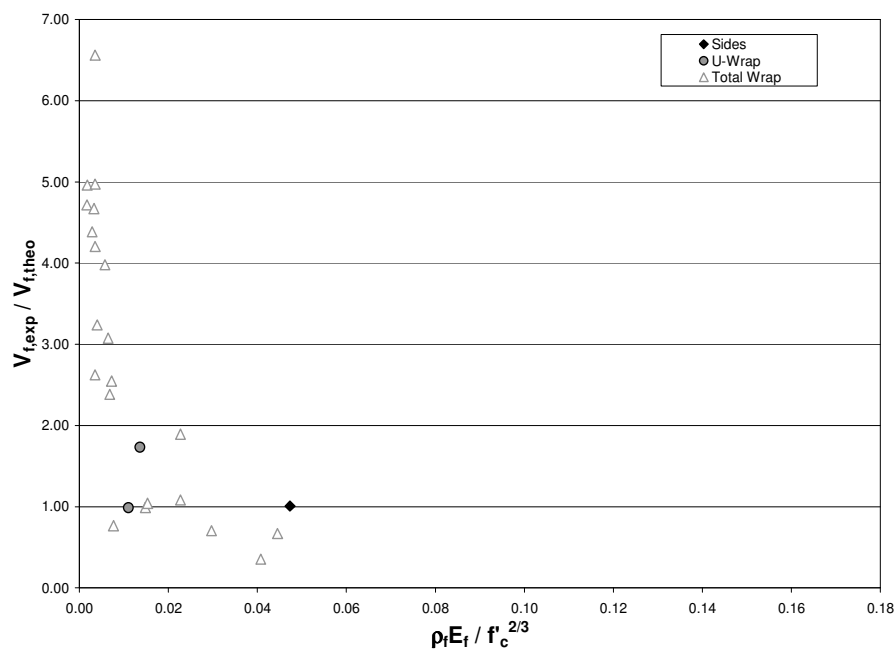
Figure B.14. $V_{f,\exp} / V_{f,theo}$ in terms of $E_f \rho_f / (f_c^{'})^{2/3}$ - FRP Fracture
Khalifa et al. (1999)
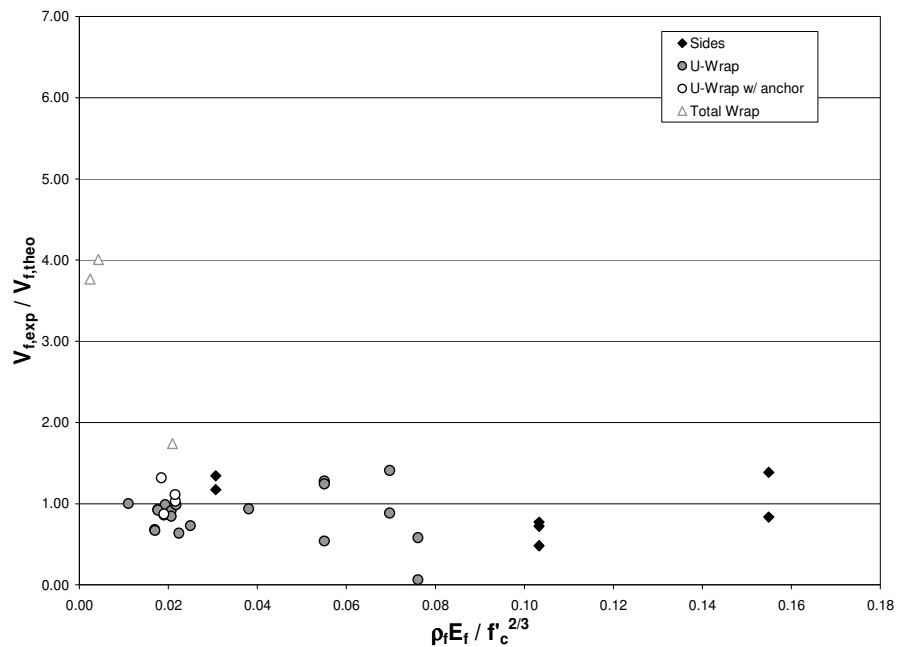
Figure B.15. $V_{f,\exp}/V_{f,theo}$ in terms of $E_f \rho_f /(f_c^{'})^{2/3}$ - Other Failure Modes
Khalifa et al. (1999)
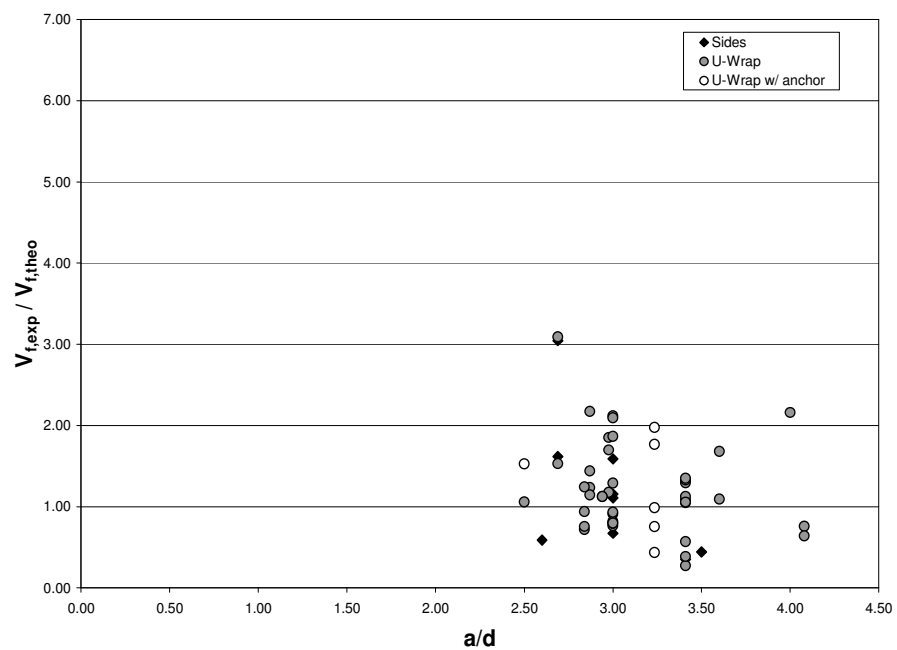
Figure B.16. $V_{f,\exp}/V_{f,theo}$ in terms of a/d – FRP Debonding
Khalifa et al. (1999)
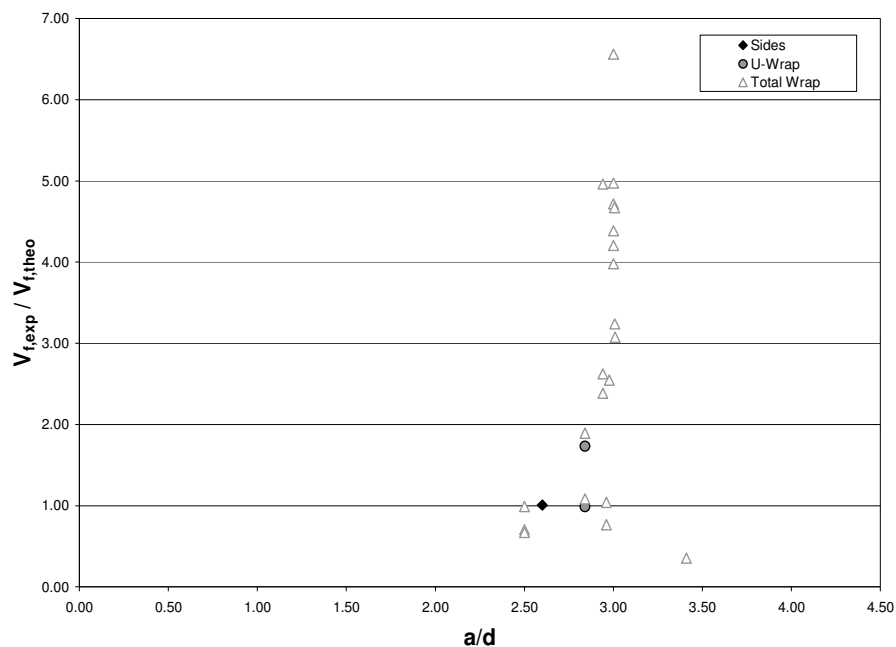
Figure B.17. $V_{f,\exp}/V_{f,theo}$ in terms of a/d – FRP Fracture
Khalifa et al. (1999)
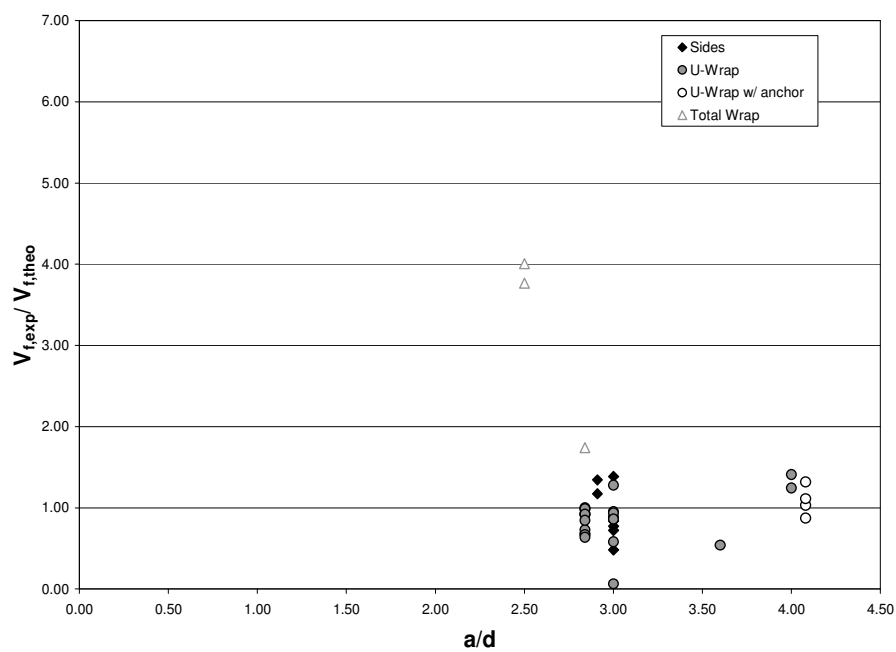
Figure B.18. $V_{f,\exp}/V_{f,theo}$ in terms of a/d – Other Failure Modes
Khalifa et al. (1999)
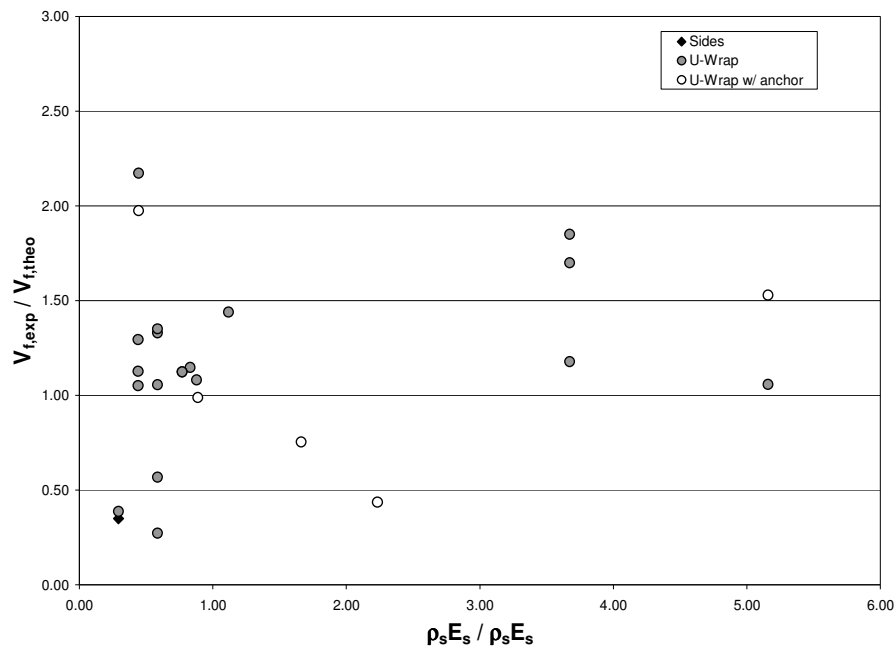
Figure B.19. $V_{f,\exp}/V_{f,theo}$ in terms of $\rho_s E_s / \rho_f E_f$ – FRP Debonding Khalifa et al. (1999)
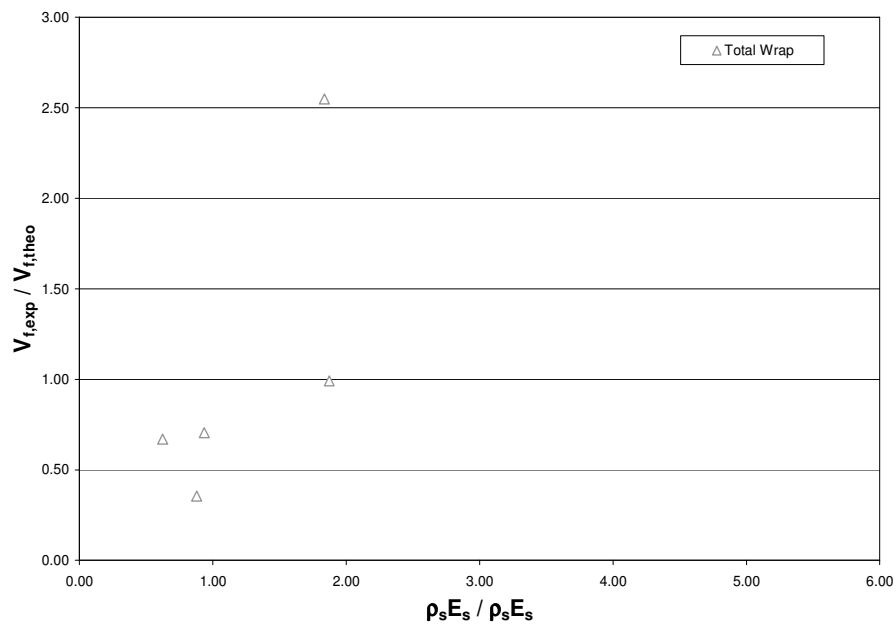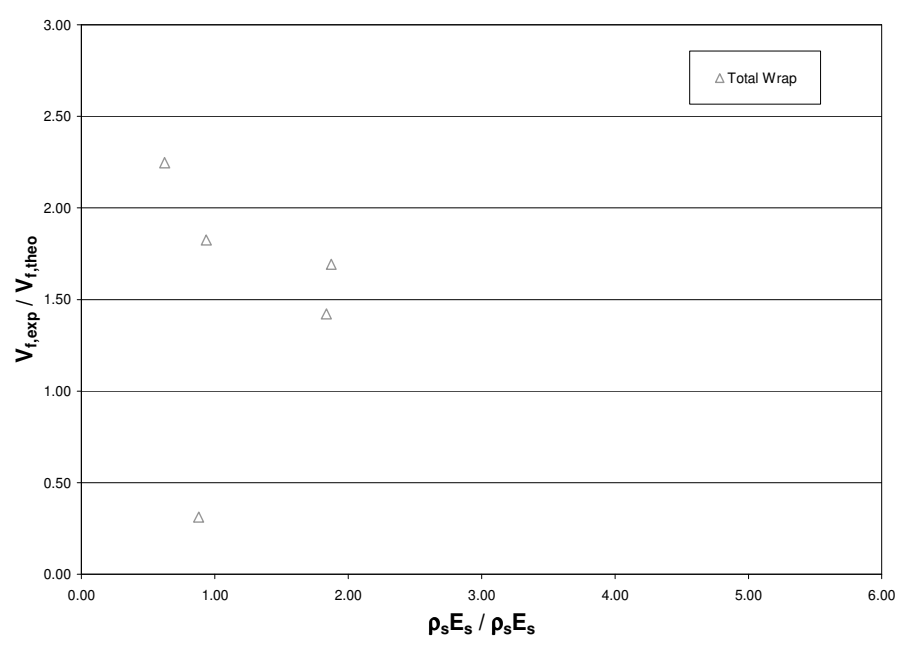

Figure B.20. $V_{f,\exp}/V_{f,theo}$ in terms of $\rho_s E_s / \rho_f E_f$ – FRP Fracture Khalifa et al. (1999)
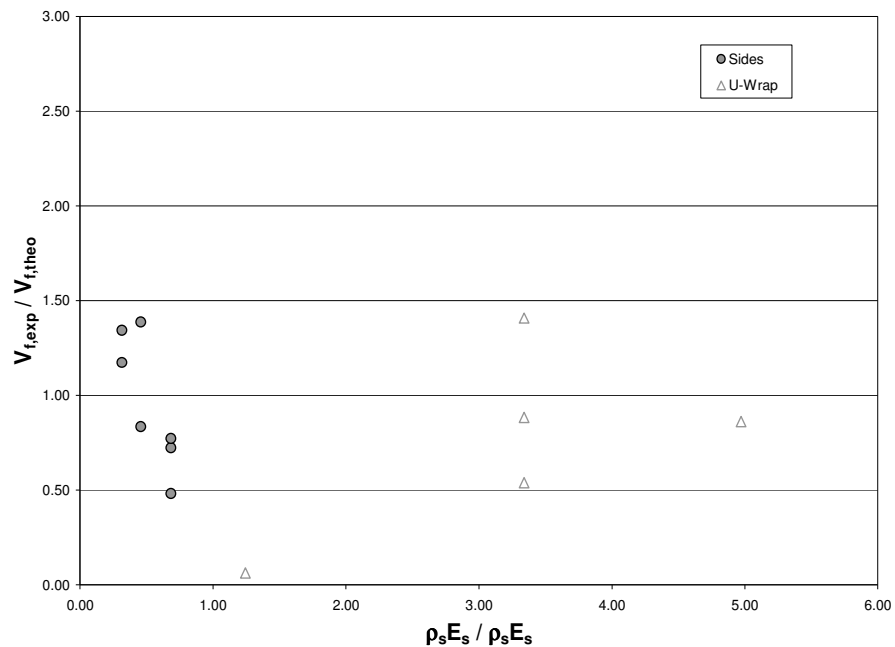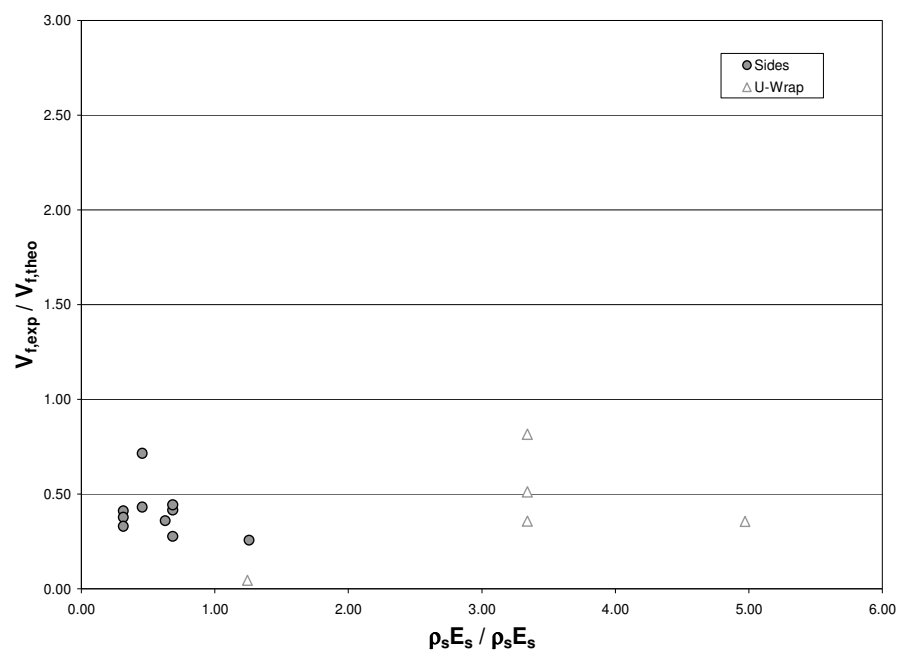
Figure B.21. $V_{f,\exp}/V_{f,theo}$ in terms of $\rho_s E_s / \rho_f E_f$ – Other Failure Modes
Khalifa et al. (1999)
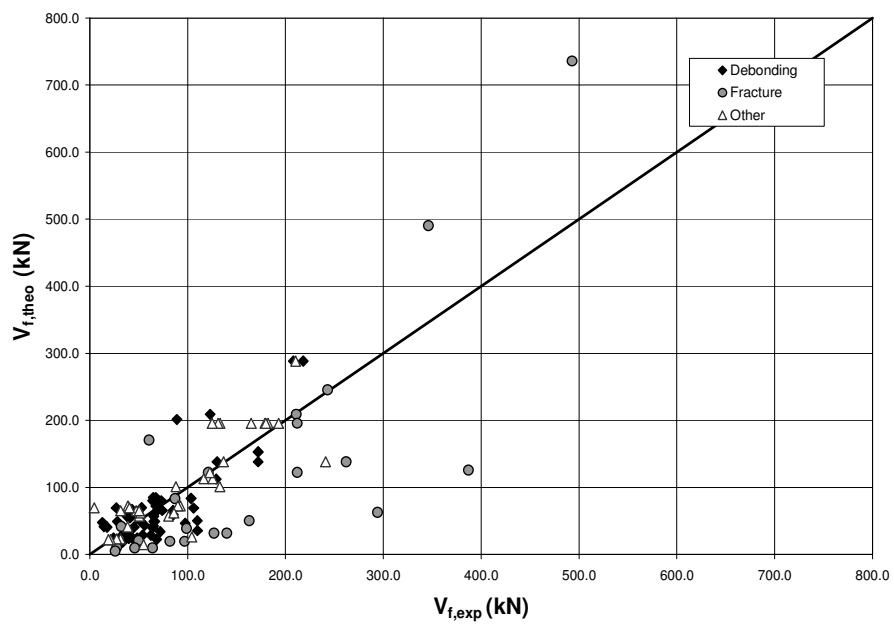
Figure B.22. Comparison between Predictions by Khalifa et al (1999) and Experimental
Results
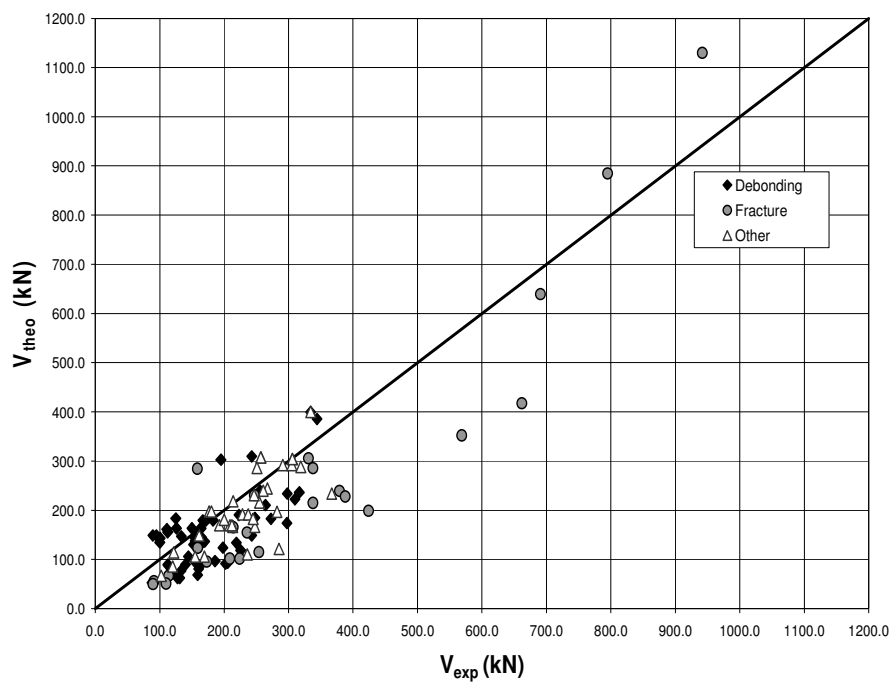
(a) ACI 318-05
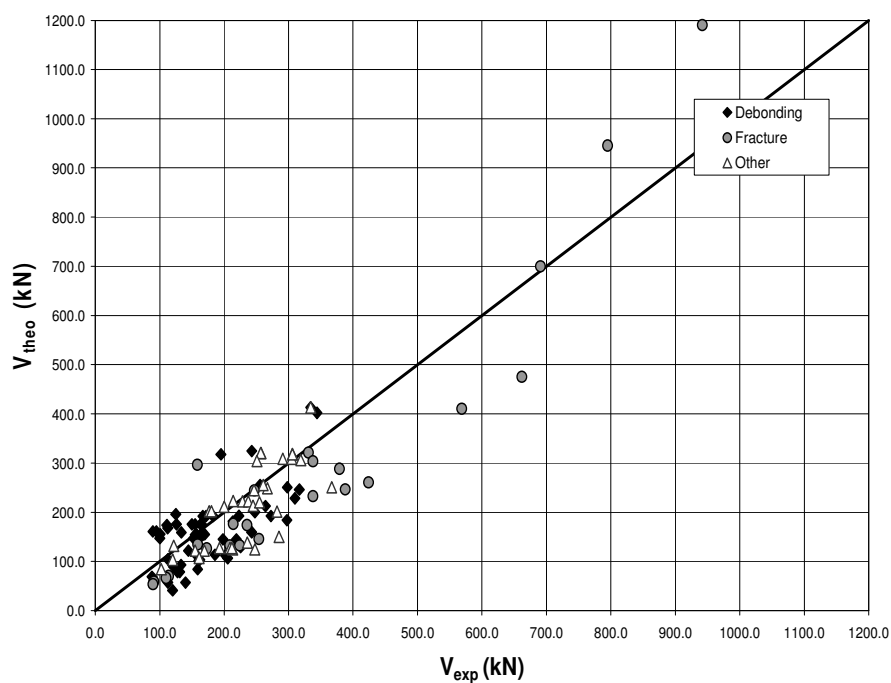
(b) Eurocode 2

Figure B.23. Comparison between Analytical Predictions of total shear capacity by
Khalifa et al. (1999) and Experimental Results
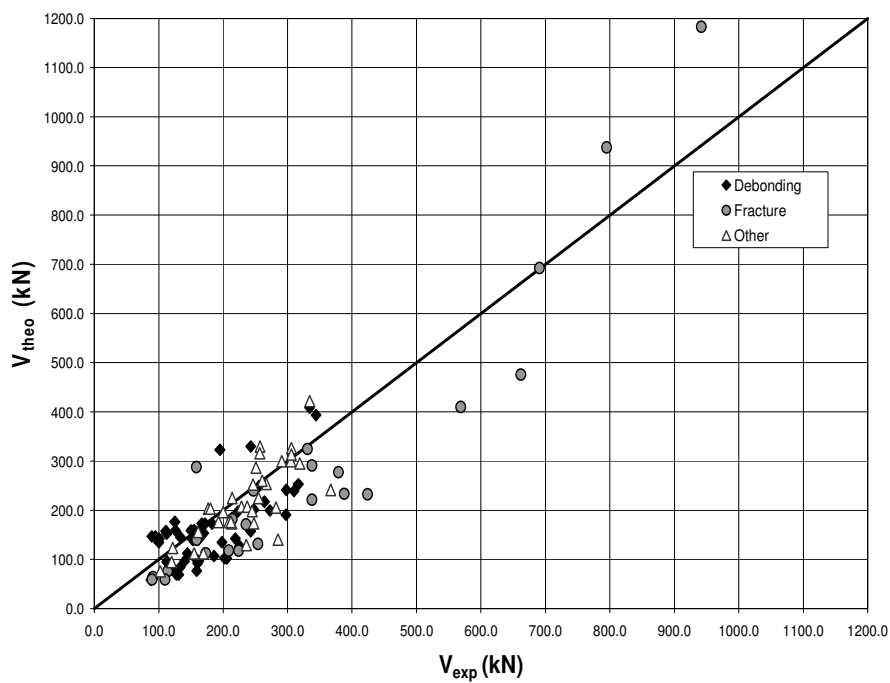
(c) CSA A23.3-94
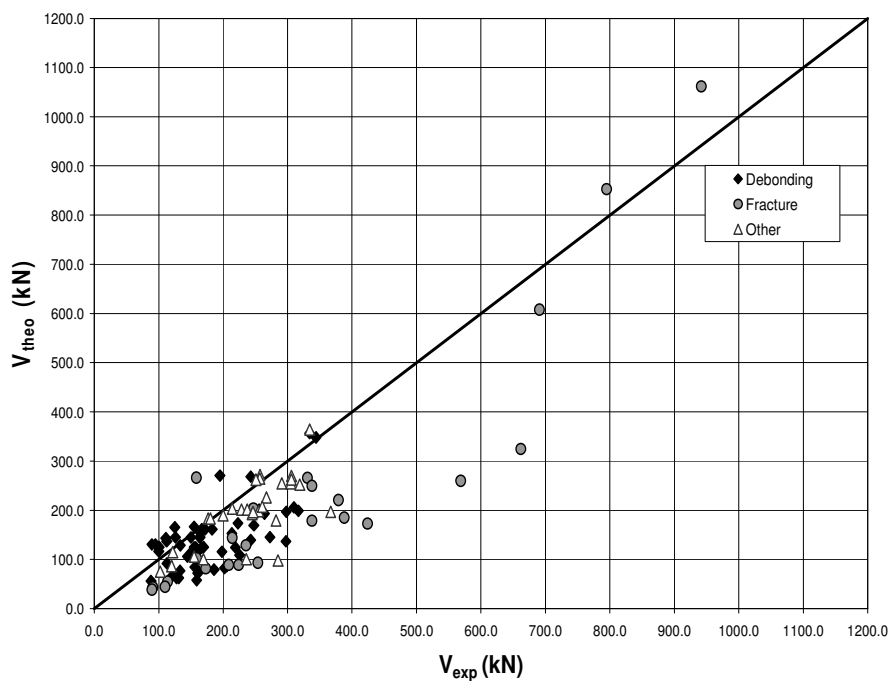
(d) AASHTO LRFD

Figure B.24. Comparison between Analytical Predictions of total shear capacity by
Khalifa et al. (1999) and Experimental Results
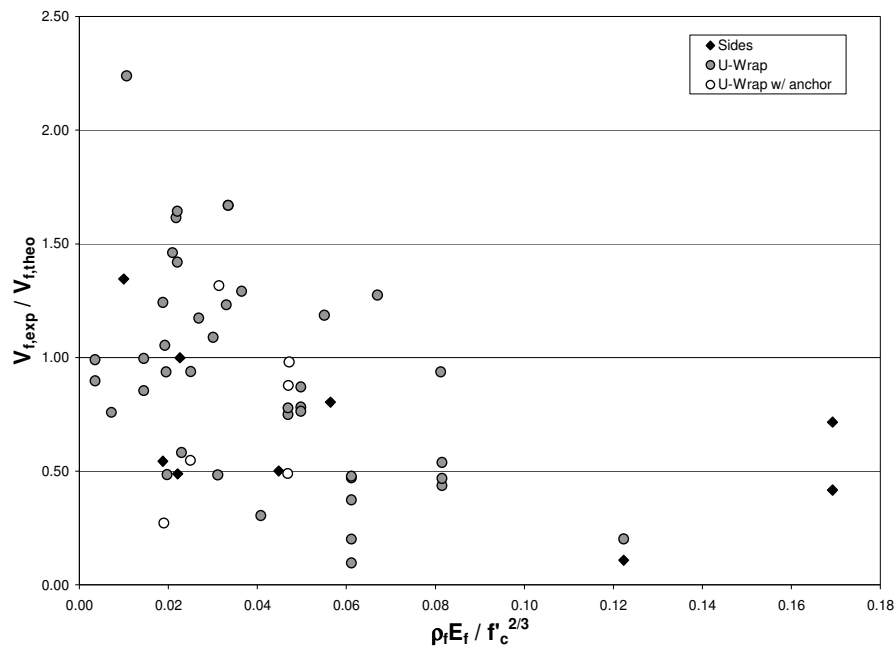
Figure B.25. $V_{f,\exp}/V_{f,theo}$ in terms of $E_f \rho_f /(f_c^{'})^{2/3}$ - FRP Debonding
Triantafillou and Antonopoulos (2000)
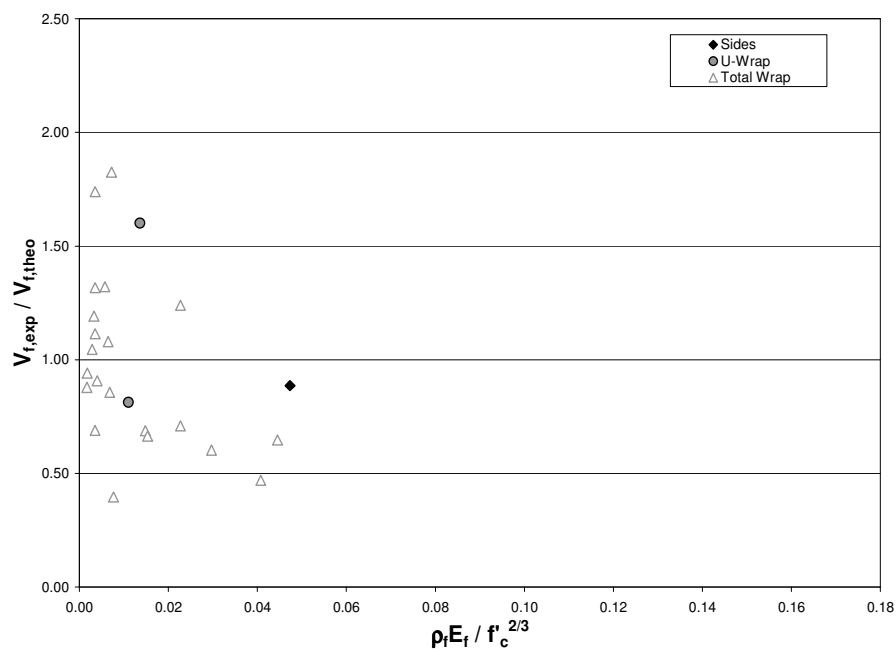
Figure B.26. $V_{f,\exp}/V_{f,theo}$ in terms of $E_f \rho_f /(f_c^{'})^{2/3}$ - FRP Fracture
Triantafillou and Antonopoulos (2000)
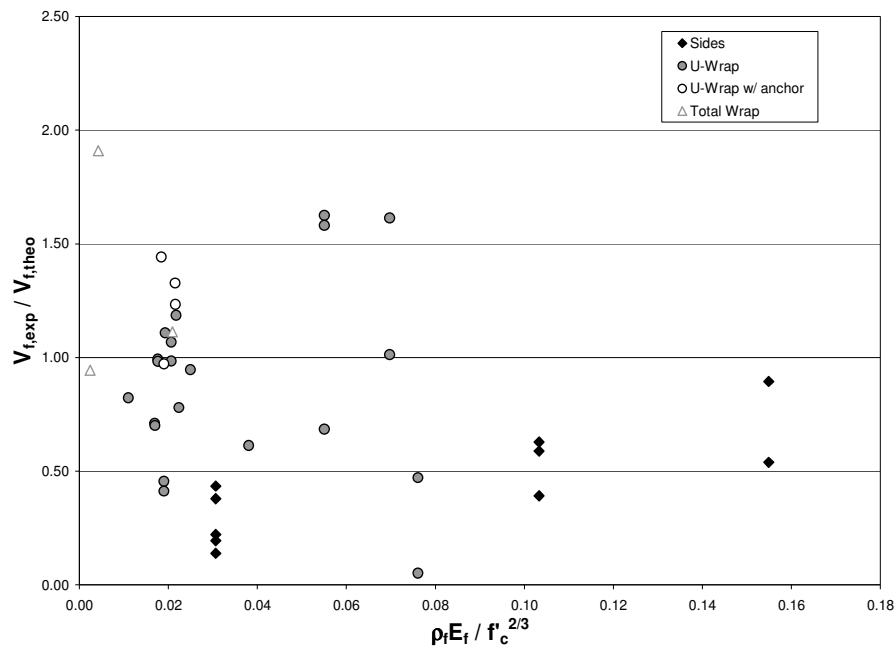
Figure B.27. $V_{f,\exp}/V_{f,theo}$ in terms of $E_f\rho_f/(f_c^{'})^{2/3}$ - Other Failure Modes
Triantafillou and Antonopoulos (2000)
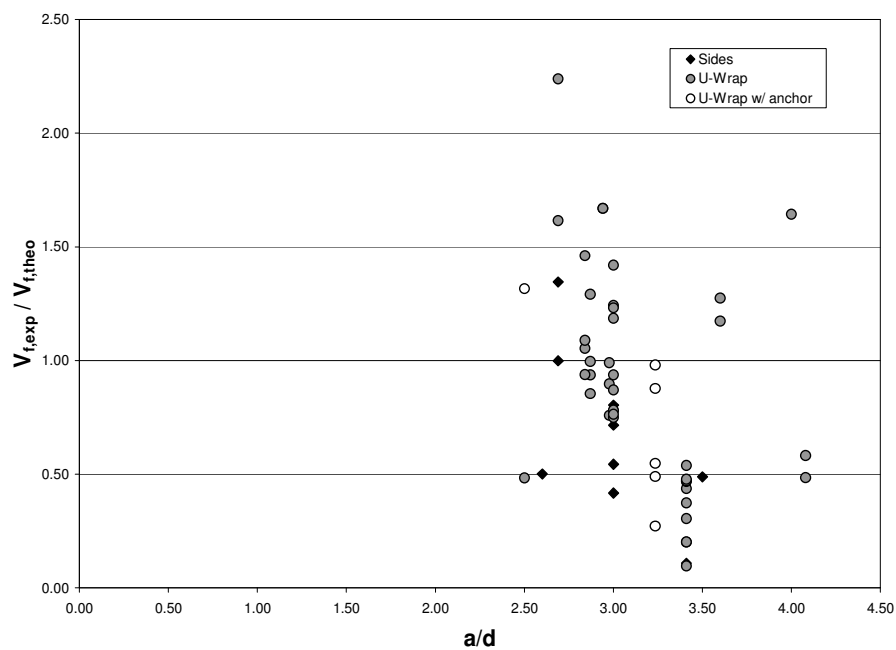
Figure B.28. $V_{f,\exp}/V_{f,theo}$ in terms of a/d – FRP Debonding
Triantafillou and Antonopoulos (2000)
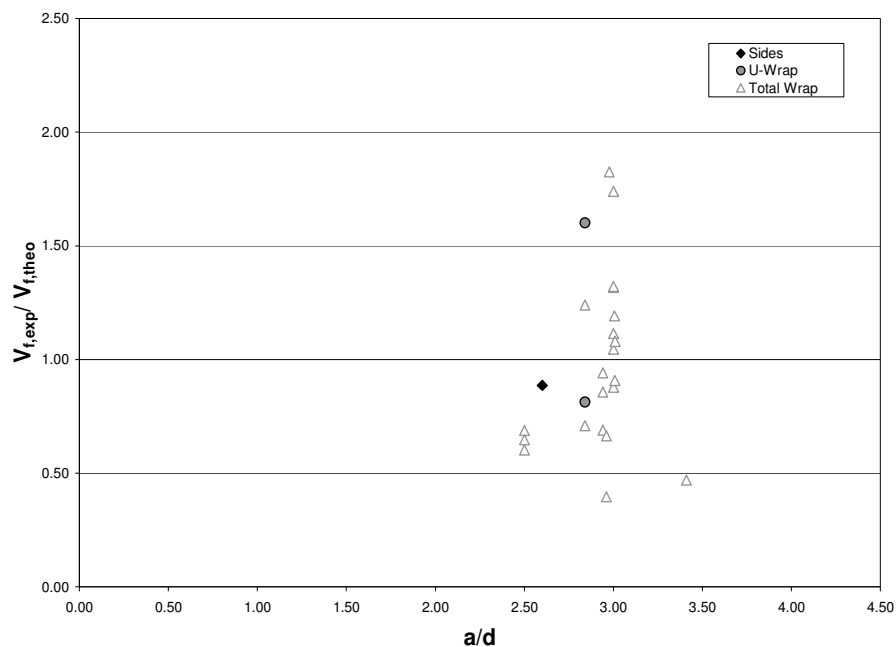
Figure B.29. $V_{f,\exp}/V_{f,theo}$ in terms of a/d – FRP Fracture
Triantafillou and Antonopoulos (2000)

Figure B.30. $V_{f,\exp}/V_{f,theo}$ in terms of a/d – Other Failure Modes
Triantafillou and Antonopoulos (2000)

180

Figure B.31. $V_{f,\exp}/V_{f,theo}$ in terms of $\rho_s E_s / \rho_f E_f$ – FRP Debonding
Triantafillou and Antonopoulos (2000)

Figure B.32. $V_{f,\exp}/V_{f,theo}$ in terms of $\rho_s E_s / \rho_f E_f$ – FRP Fracture
Triantafillou and Antonopoulos (2000)
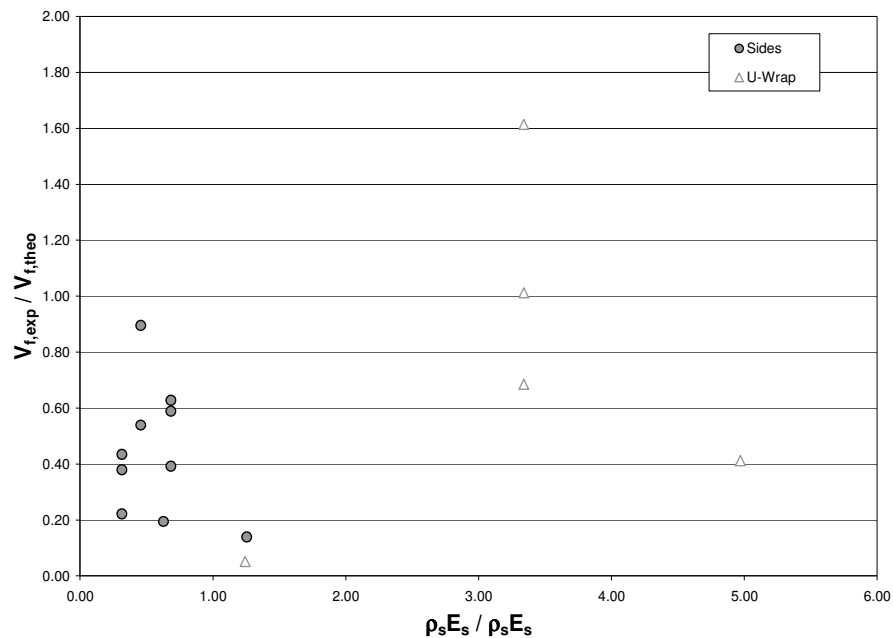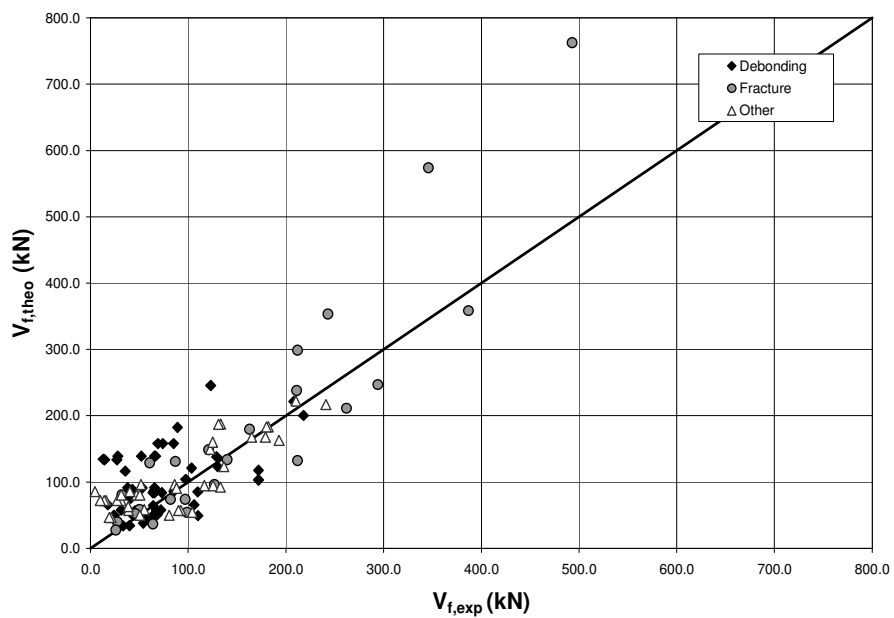
(a) ACI 318-05

(b) Eurocode 2

Figure B.35. Comparison between Analytical Predictions of total shear capacity by Triantafillou and Antonopoulos (2000) and Experimental Results
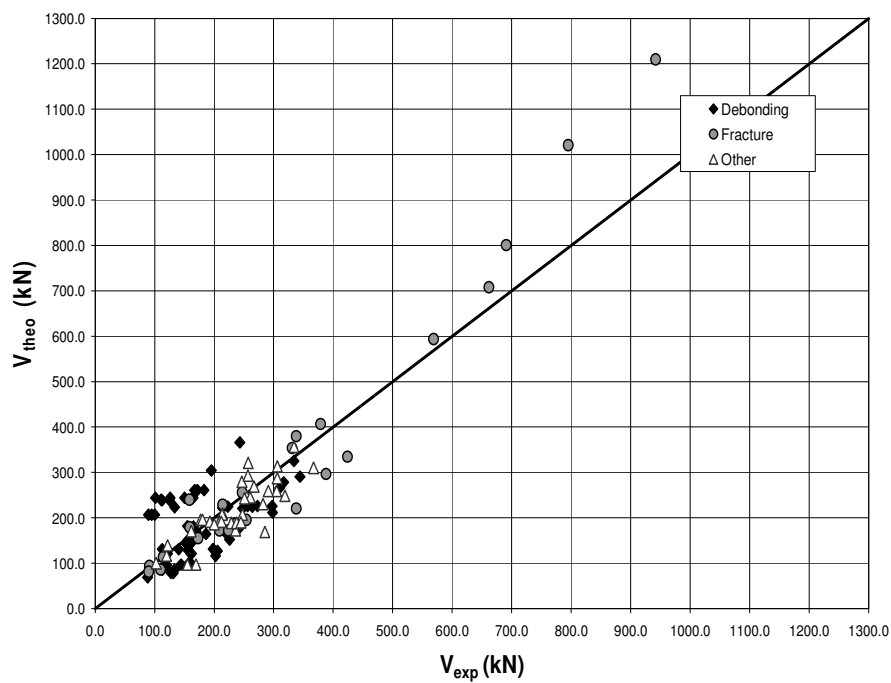
(c) CSA A23.3-94
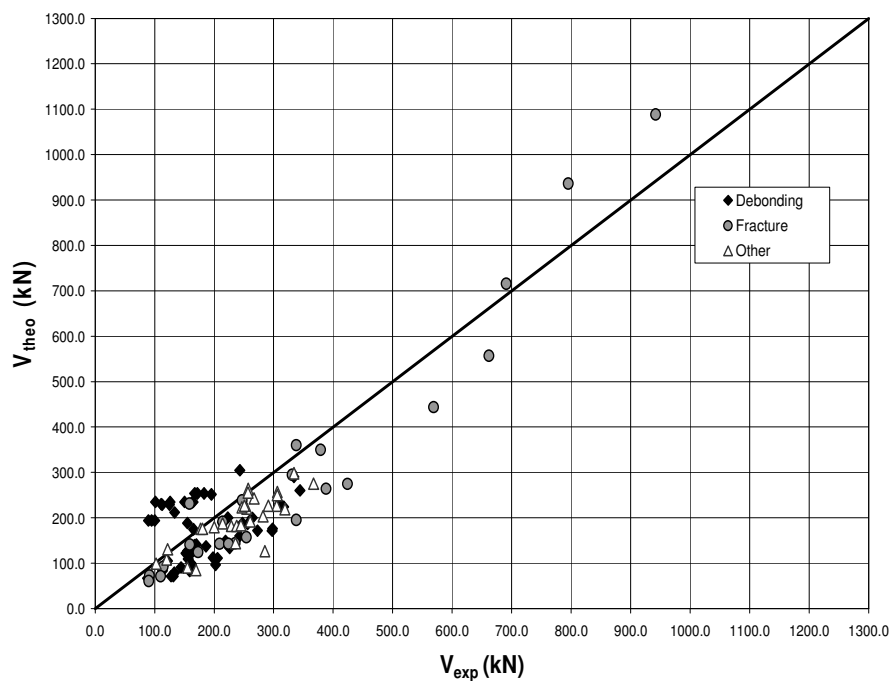
(d) AASHTO LRFD

Figure B.36. Comparison between Analytical Predictions of total shear capacity by Triantafillou and Antonopoulos (2000) and Experimental Results
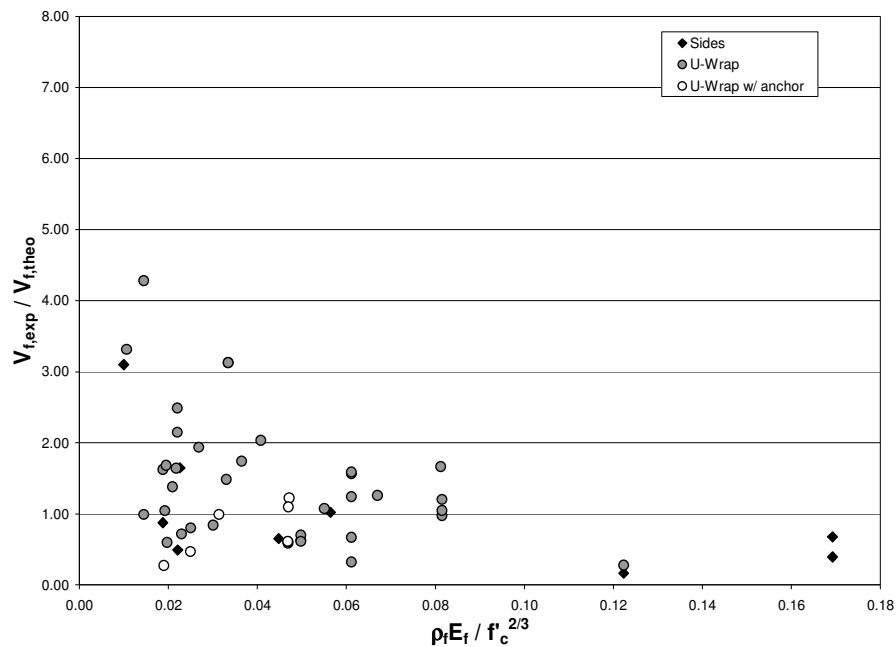
Figure B.37. $V_{f,\exp}/V_{f,theo}$ in terms of $E_f\rho_f/(f_c^{'})^{2/3}$ - FRP Debonding
Pellegrino and Modena (2002)
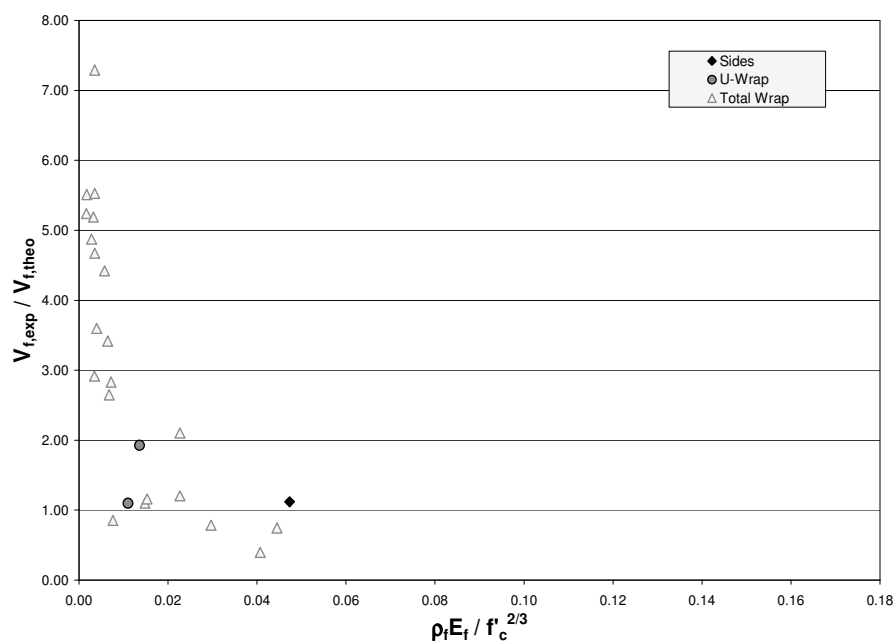
Figure B.38. $V_{f,\exp}/V_{f,theo}$ in terms of $E_f\rho_f/(f_c^{'})^{2/3}$ - FRP Fracture
Pellegrino and Modena (2002)
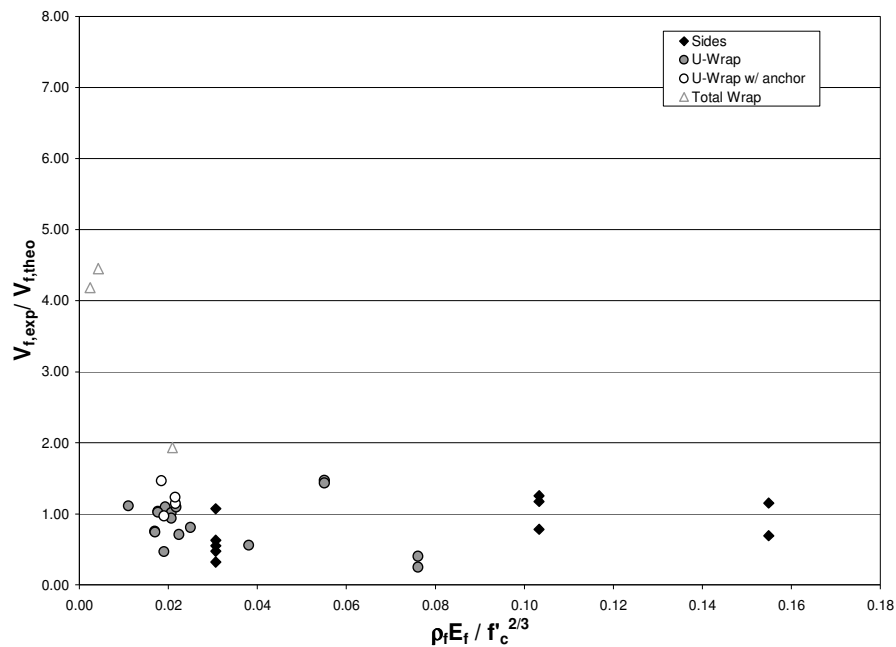
Figure B.39. $V_{f,\exp}/V_{f,theo}$ in terms of $E_f \rho_f /(f_c^{'})^{2/3}$ - Other Failure Modes
Pellegrino and Modena (2002)
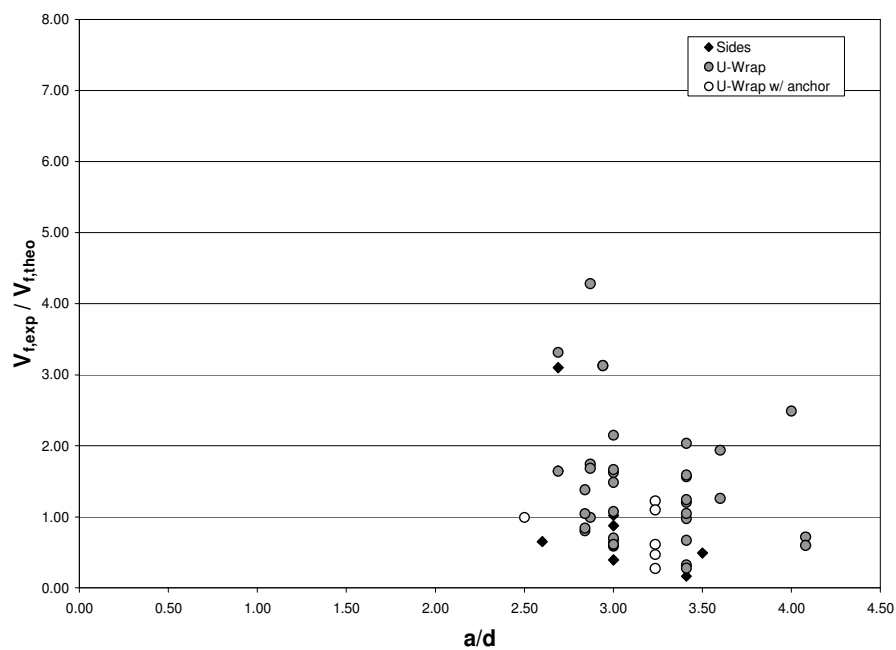
Figure B.40. $V_{f,\exp}/V_{f,theo}$ in terms of a/d – FRP Debonding
Pellegrino and Modena (2002)
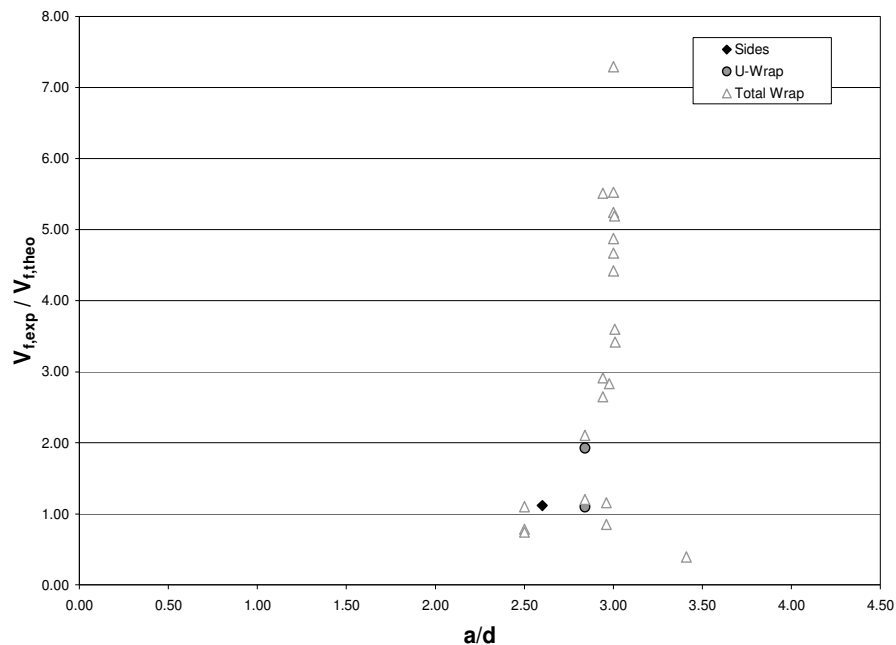
Figure B.41. $V_{f,\exp}/V_{f,theo}$ in terms of a/d – FRP Fracture
Pellegrino and Modena (2002)
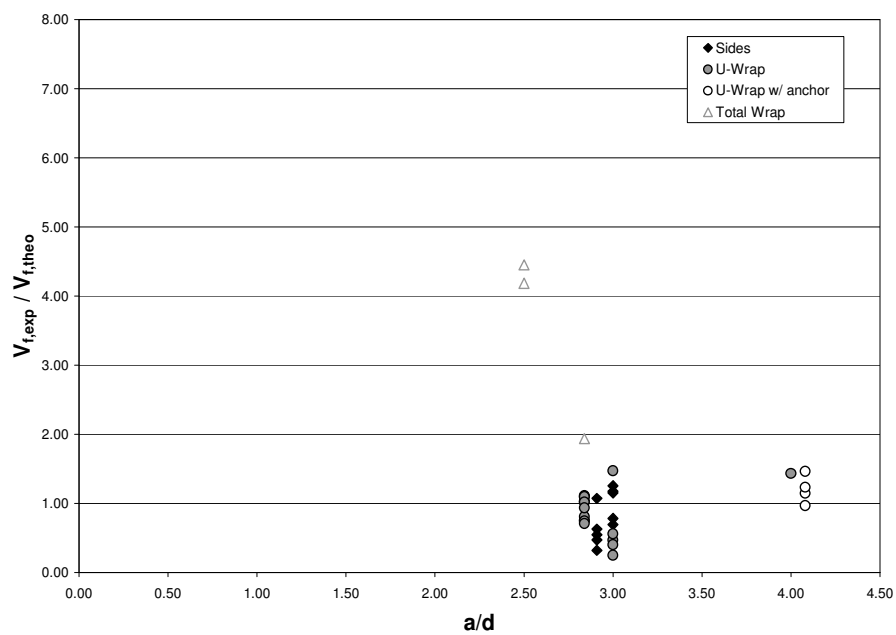
Figure B.42. $V_{f,\exp}/V_{f,theo}$ in terms of a/d – Other Failure Modes
Pellegrino and Modena (2002)
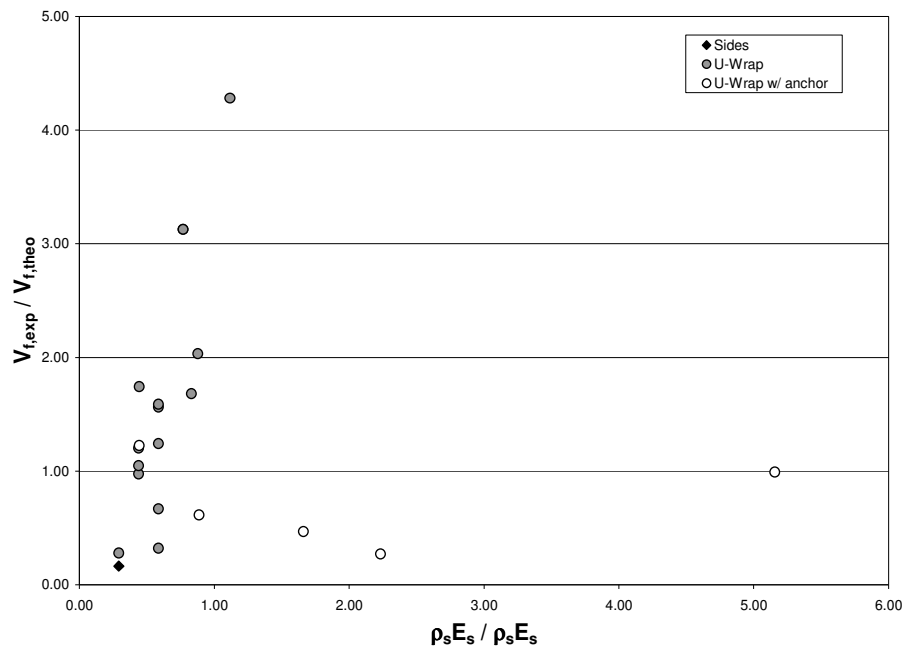
Figure B.43. $V_{f,\exp}/V_{f,theo}$ in terms of $\rho_s E_s / \rho_f E_f$ – FRP Debonding
Pellegrino and Modena (2002)
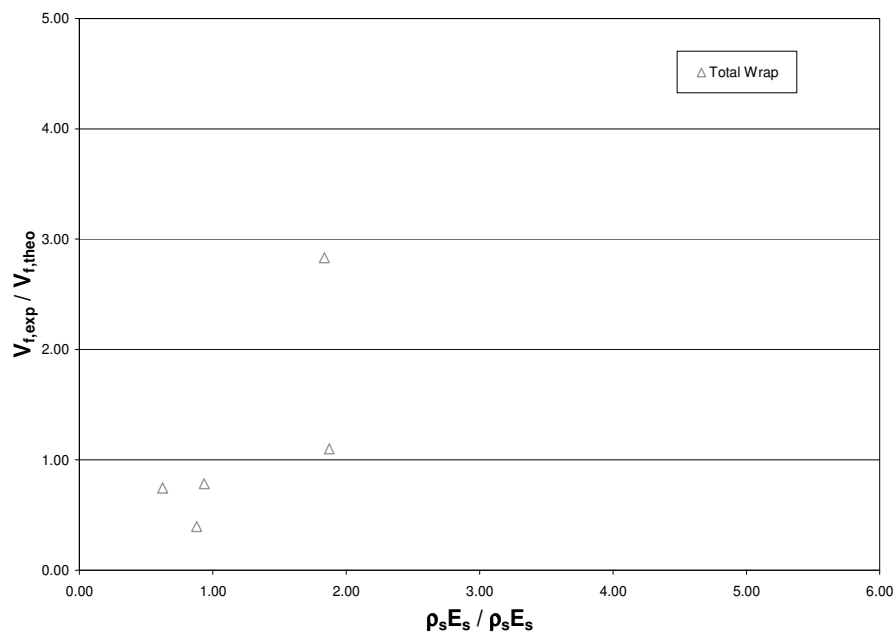
Figure B.44. $V_{f,\exp}/V_{f,theo}$ in terms of $\rho_s E_s / \rho_f E_f$ – FRP Fracture
Pellegrino and Modena (2002)
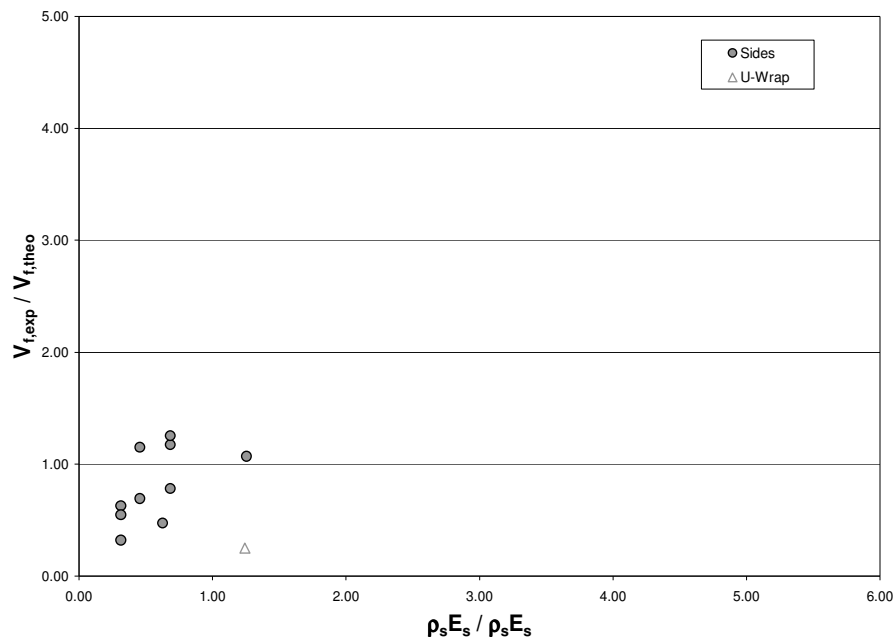
Figure B.45. $V_{f,\exp}/V_{f,theo}$ in terms of $\rho_s E_s / \rho_f E_f$ – Other Failure Modes Pellegrino and Modena (2002)
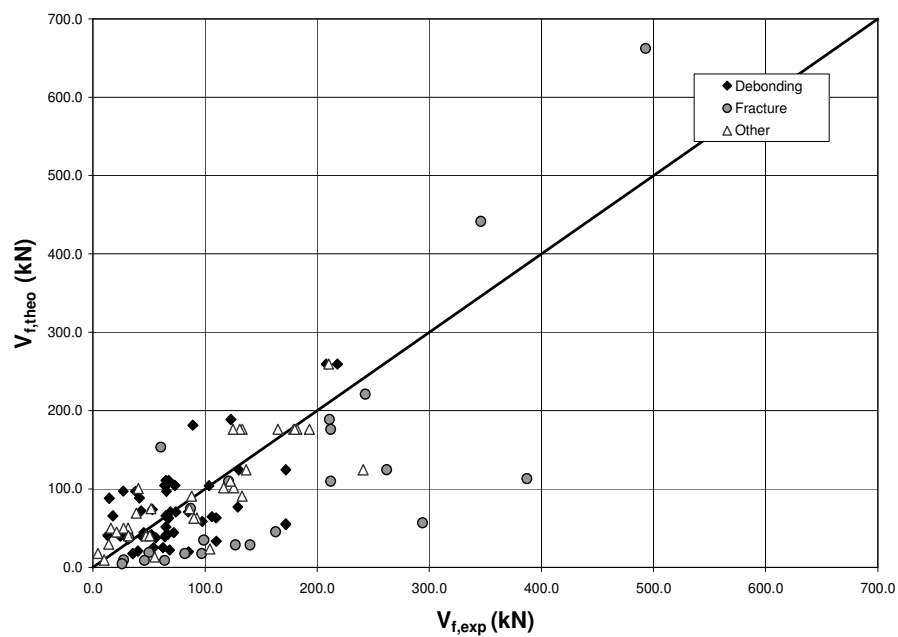
Figure B.46. Comparison between Predictions by Pellegrino and Modena (2002) and Experimental Results
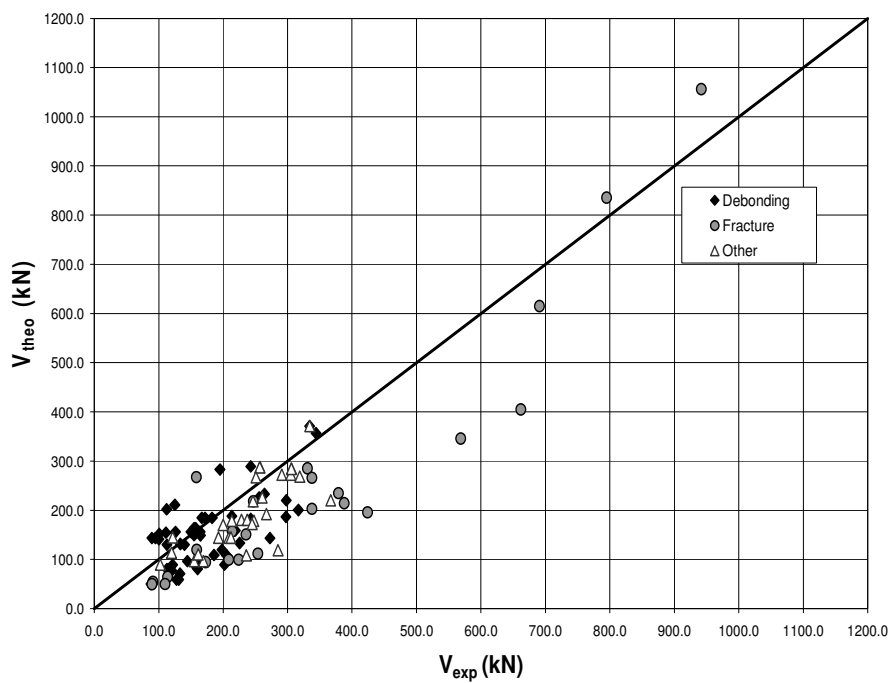
(a) ACI 318-05
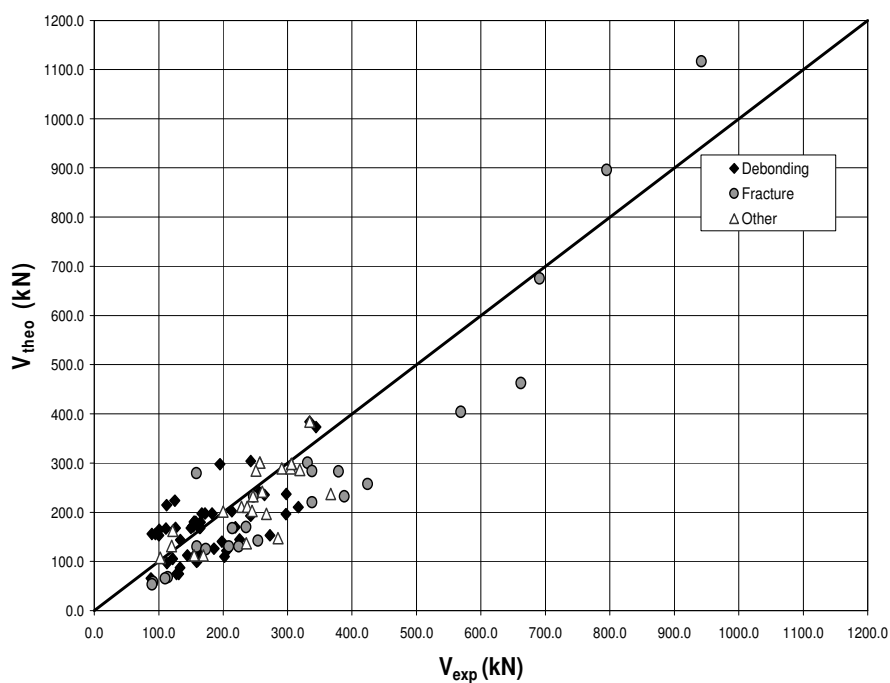
(b) Eurocode 2

Figure B.47. Comparison between Analytical Predictions of total shear capacity by
Pellegrino and Modena (2002) and Experimental Results
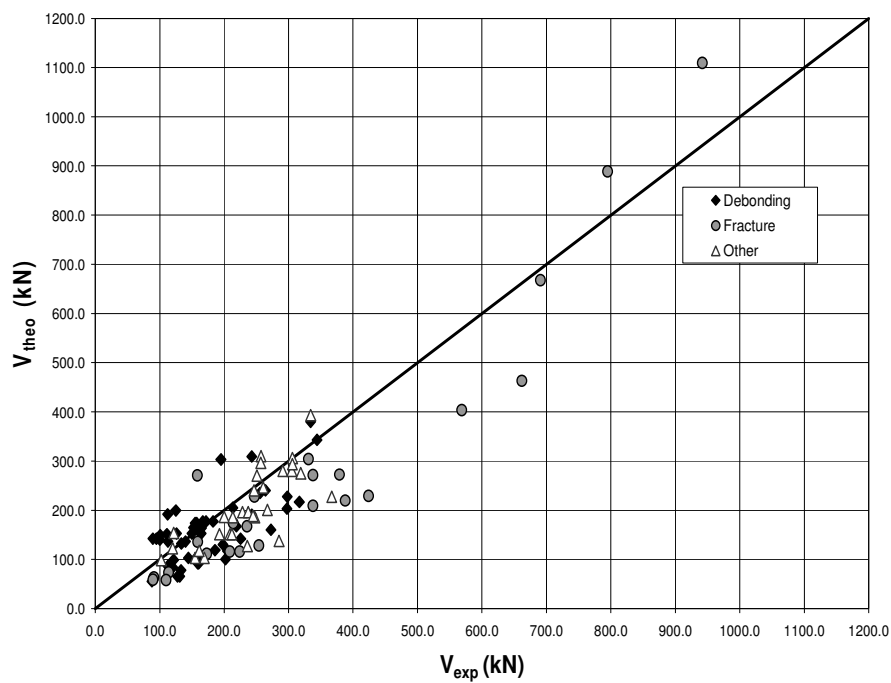
(c) CSA A23.3-94
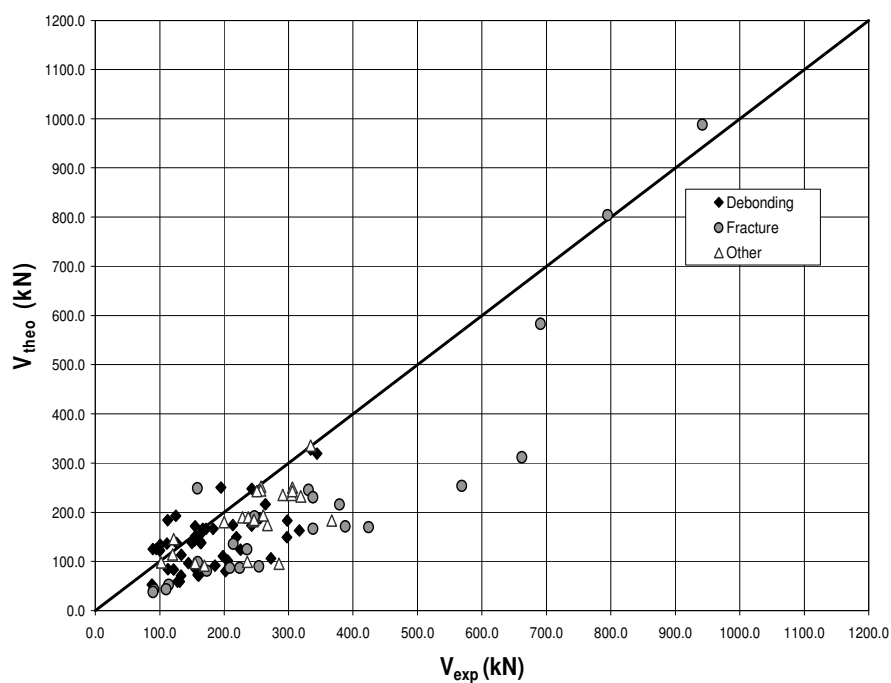
(d) AASHTO LRFD

Figure B.48. Comparison between Analytical Predictions of total shear capacity by
Pellegrino and Modena (2002) and Experimental Results
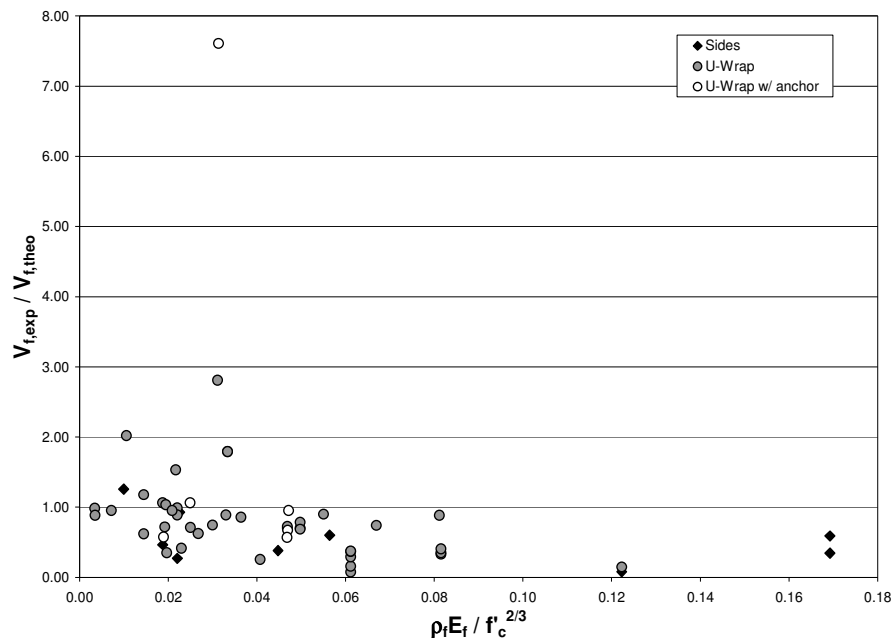
Figure B.49. $V_{f,\exp}/V_{f,theo}$ in terms of $E_f\rho_f/(f_c^{'})^{2/3}$ - FRP Debonding
Chaallal et al. (2002)
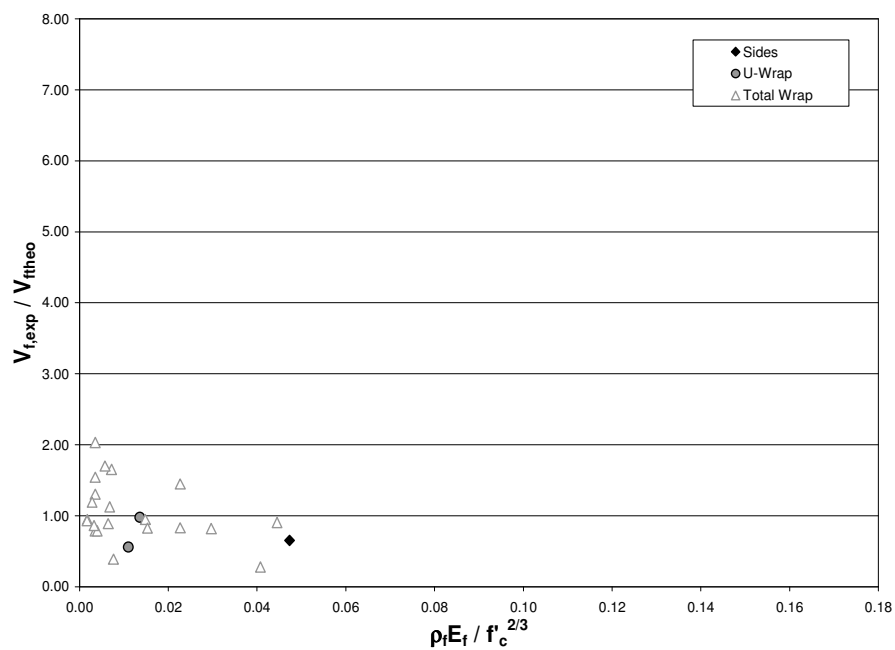
Figure B.50. $V_{f,\exp}/V_{f,theo}$ in terms of $E_f\rho_f/(f_c^{'})^{2/3}$ - FRP Fracture
Chaallal et al. (2002)
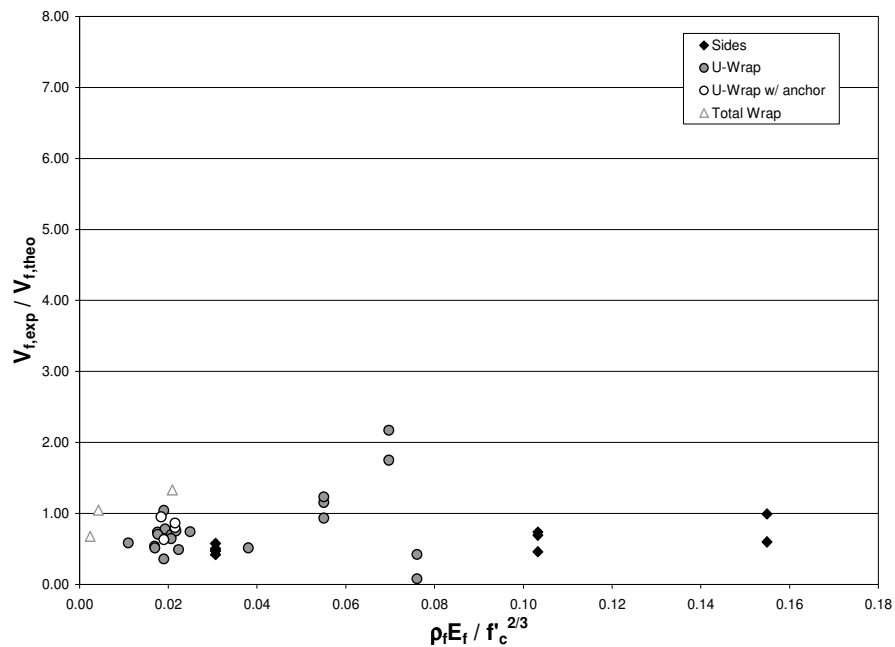
Figure B.51. $V_{f,\exp}/V_{f,theo}$ in terms of $E_f \rho_f /(f_c^{'})^{2/3}$ - Other Failure Modes
Chaallal et al. (2002)
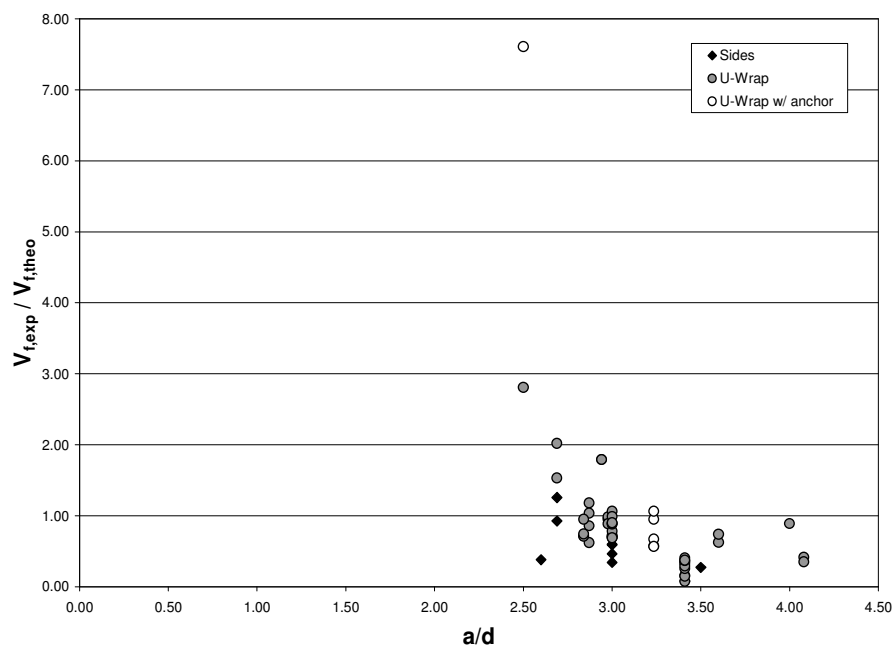
Figure B.52. $V_{f,\exp}/V_{f,theo}$ in terms of a/d – FRP Debonding
Chaallal et al. (2002)
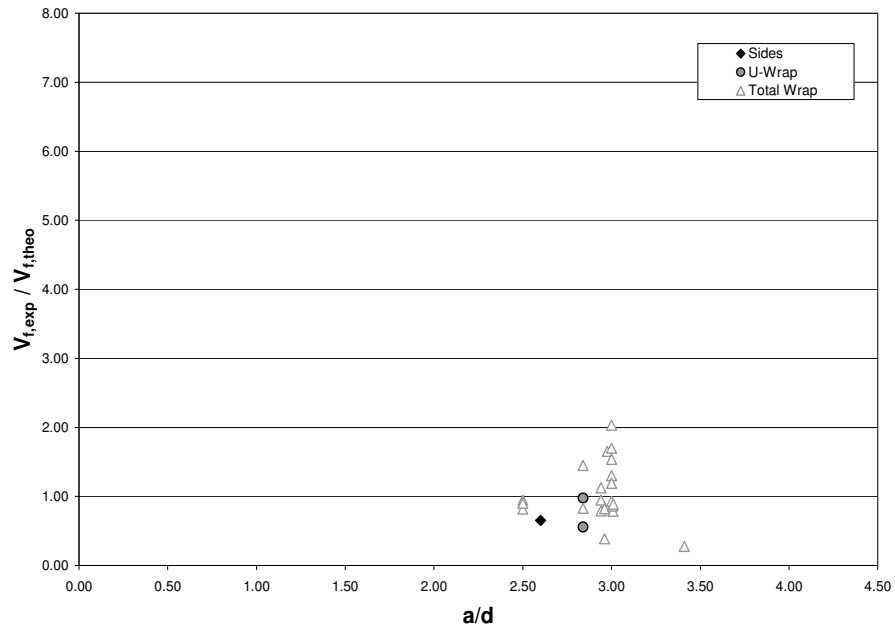
Figure B.53. $V_{f,\exp}/V_{f,theo}$ in terms of a/d – FRP Fracture
Chaallal et al. (2002)
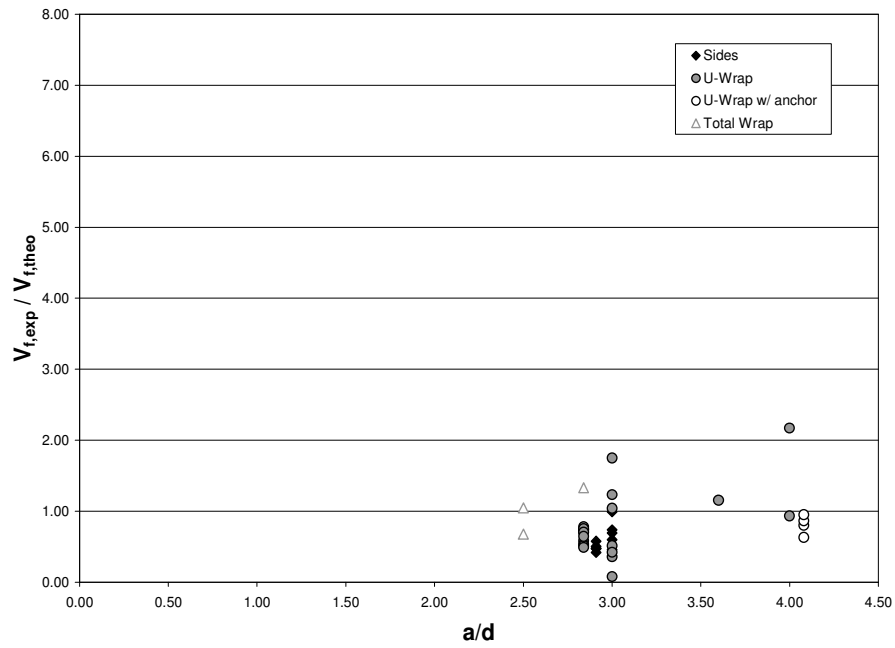
Figure B.54. $V_{f,\exp}/V_{f,theo}$ in terms of a/d – Other Failure Modes
Chaallal et al. (2002)
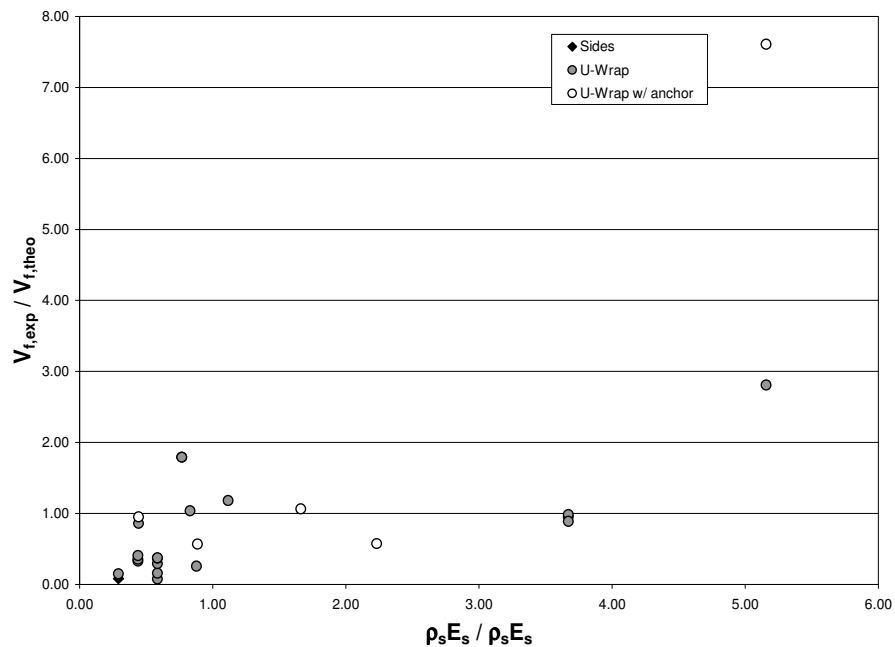
Figure B.55. $V_{f,\exp}/V_{f,theo}$ in terms of $\rho_s E_s / \rho_f E_f$ – FRP Debonding
Chaallal et al. (2002)
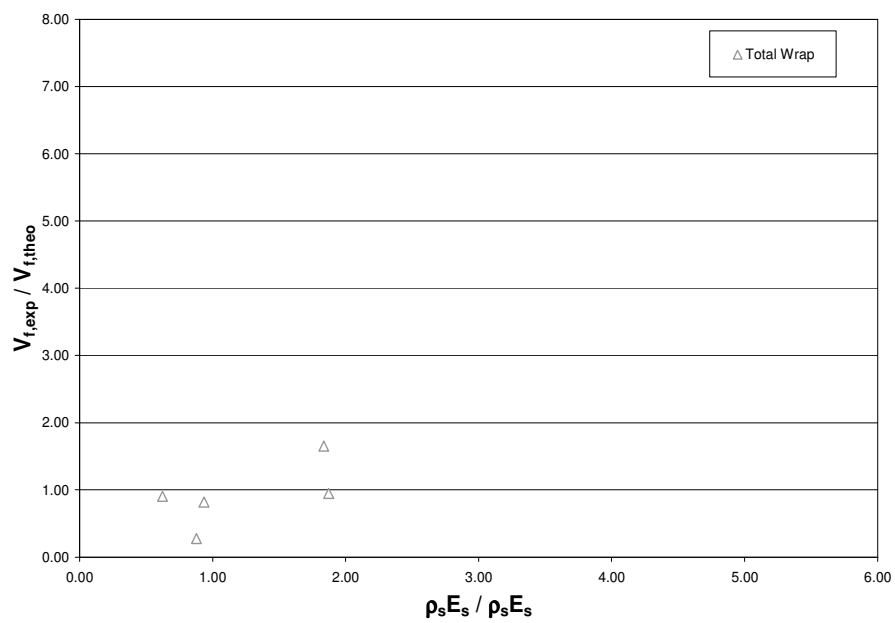
Figure B.56. $V_{f,\exp}/V_{f,theo}$ in terms of $\rho_s E_s / \rho_f E_f$ – FRP Fracture
Chaallal et al. (2002)
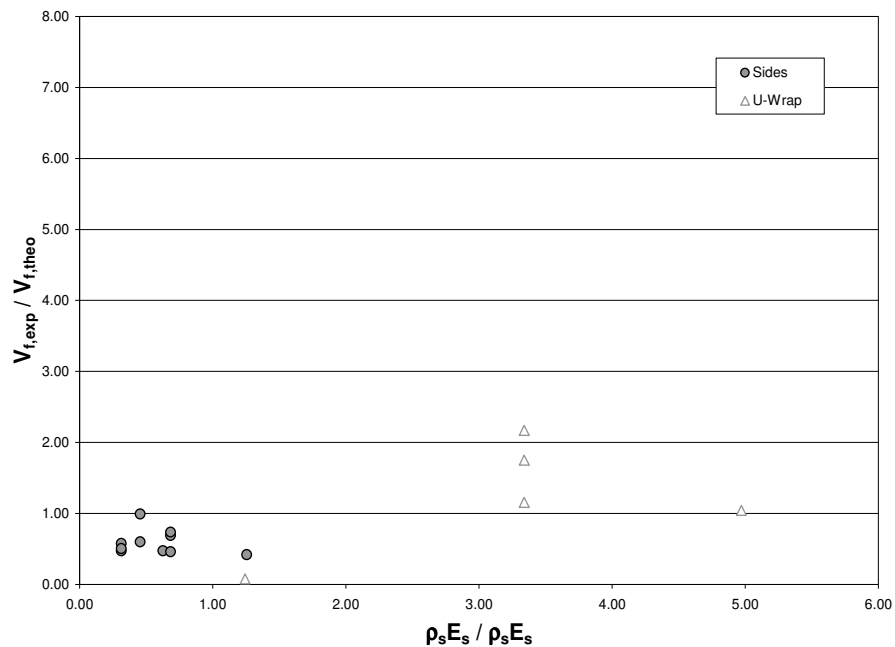
Figure B.57. $V_{f,\exp}/V_{f,theo}$ in terms of $\rho_s E_s / \rho_f E_f$ – Other Failure Modes
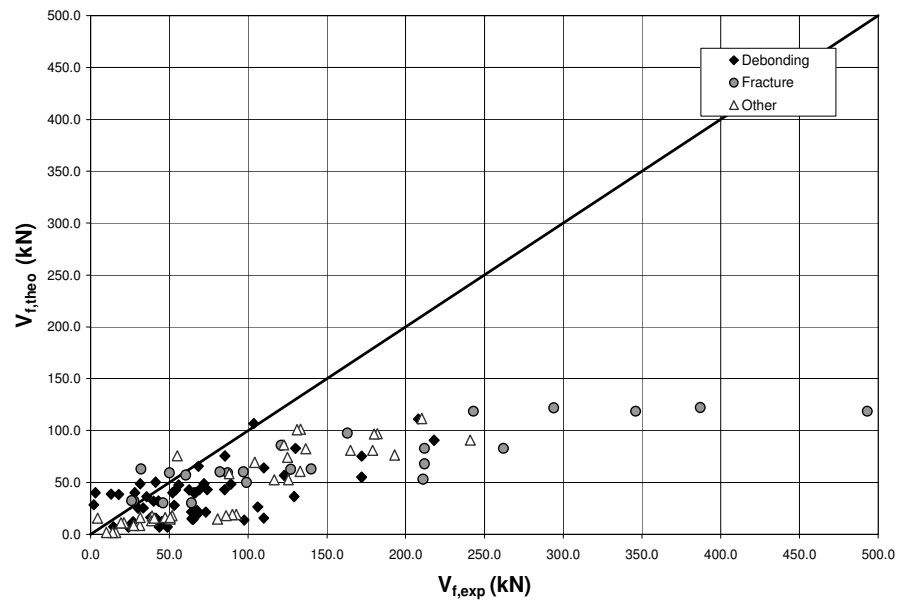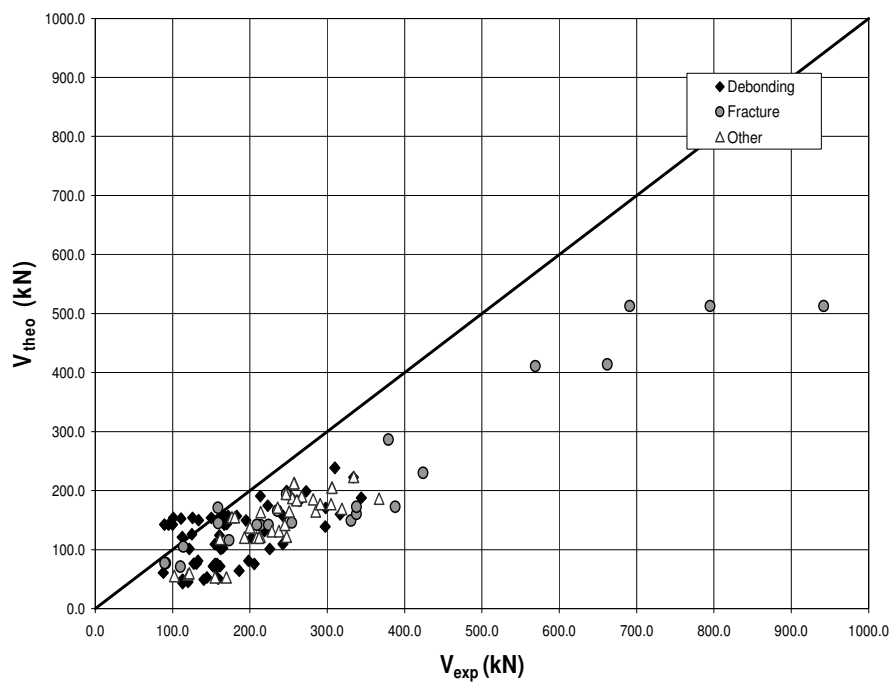Chaallal et al. (2002)
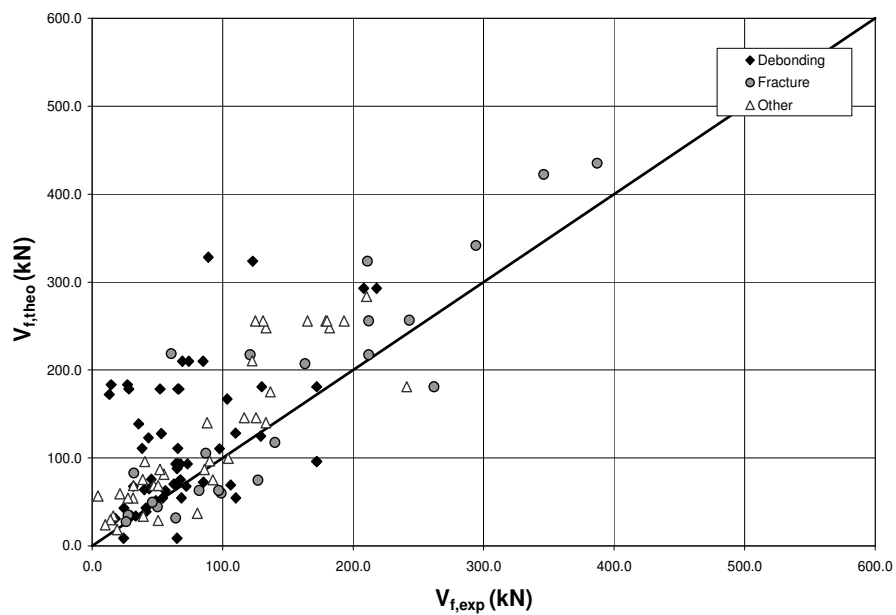
Figure B.58. Comparison between Predictions by Chaallal et al. (2002) and
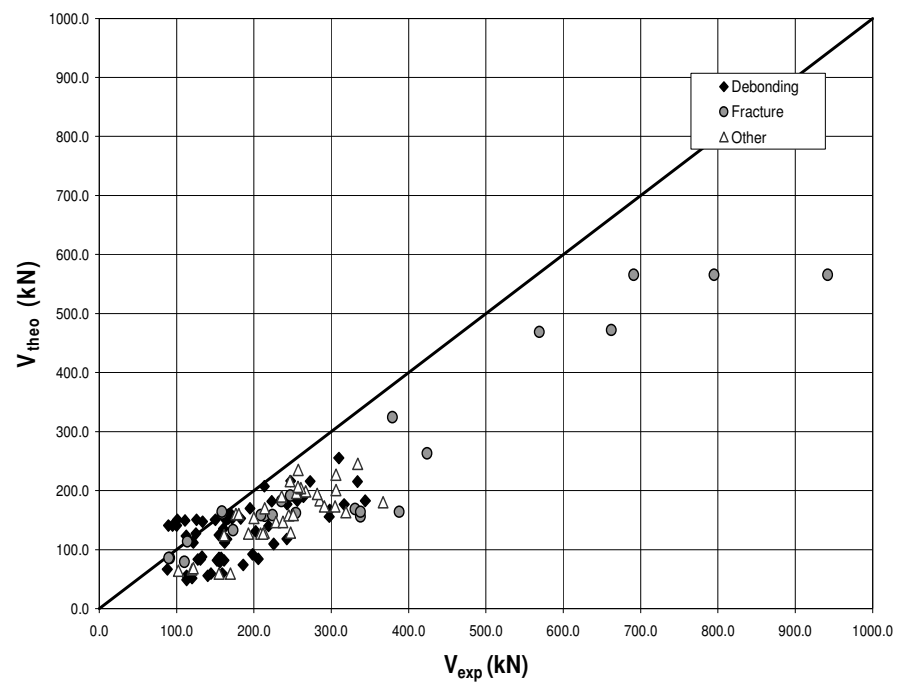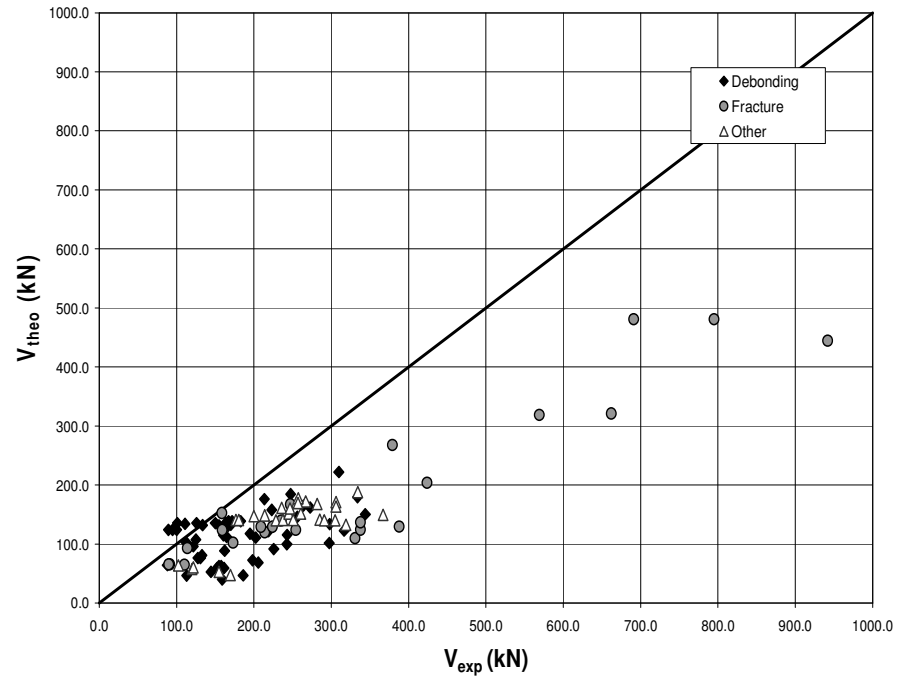Experimental Results
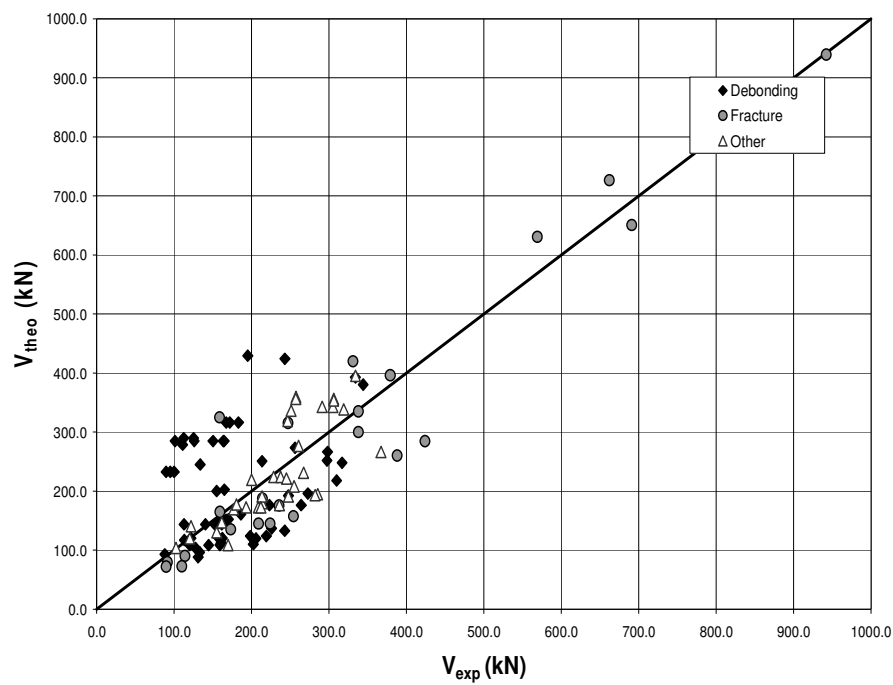
(a) ACI 318-05
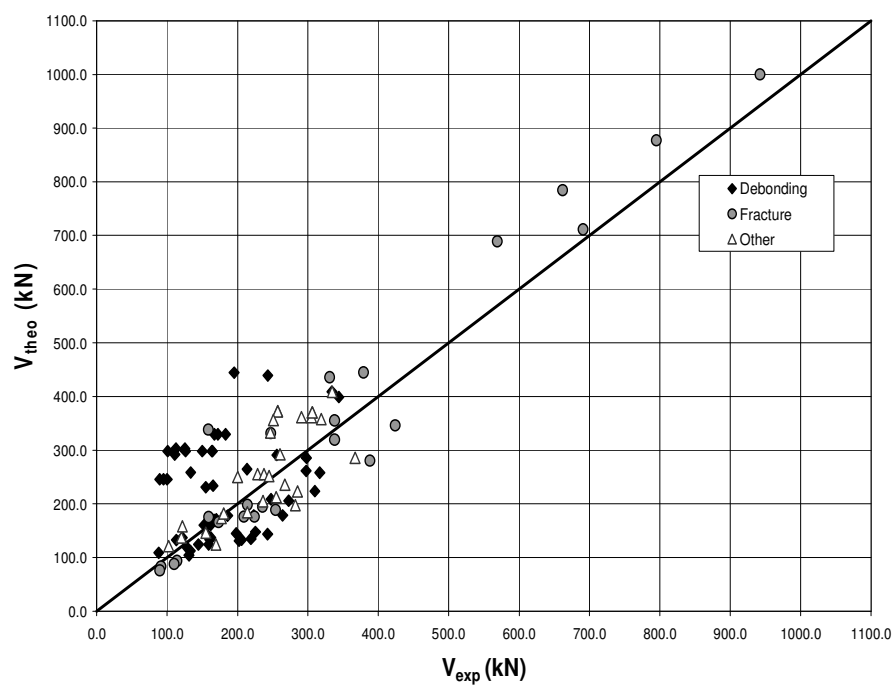
(b) Eurocode 2

Figure B.59. Comparison between Analytical Predictions of total shear capacity by
Chaallal et al. (2002) and Experimental Results
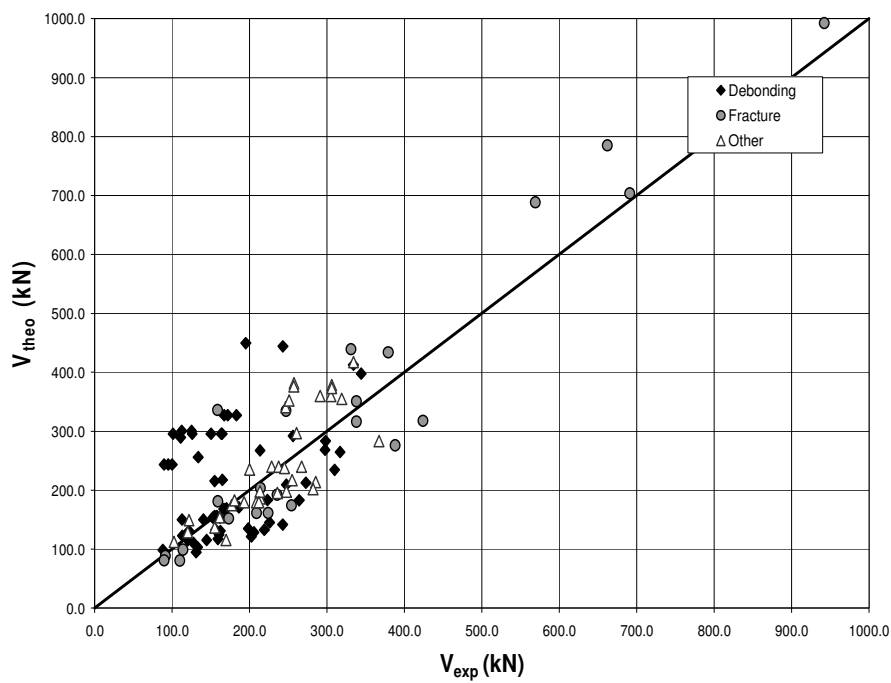
(c) CSA A23.3-94
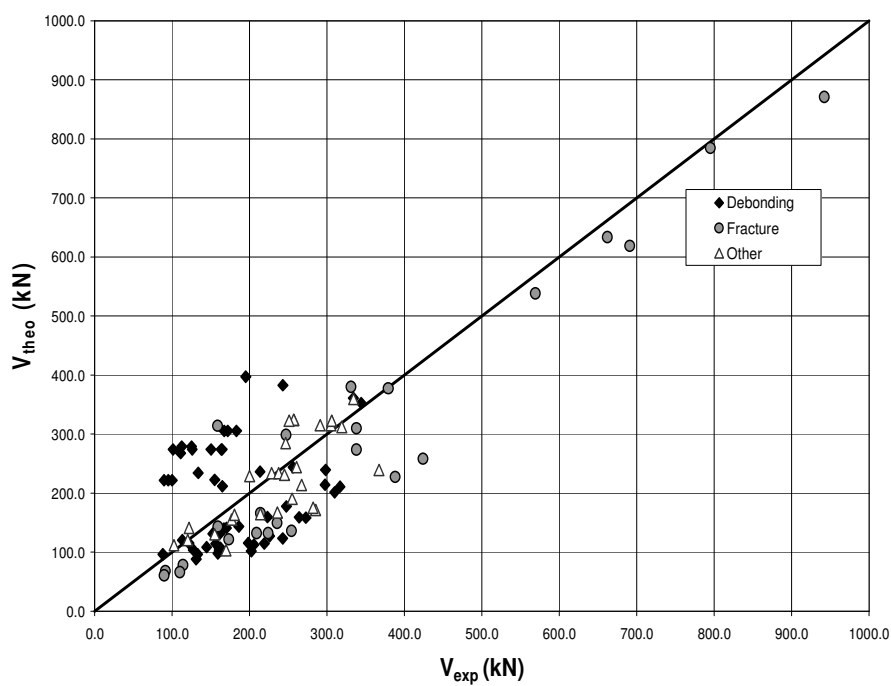
(d) AASHTO LRFD

Figure B.60. Comparison between Analytical Predictions of total shear capacity by Chaallal et al. (2002) and Experimental Results
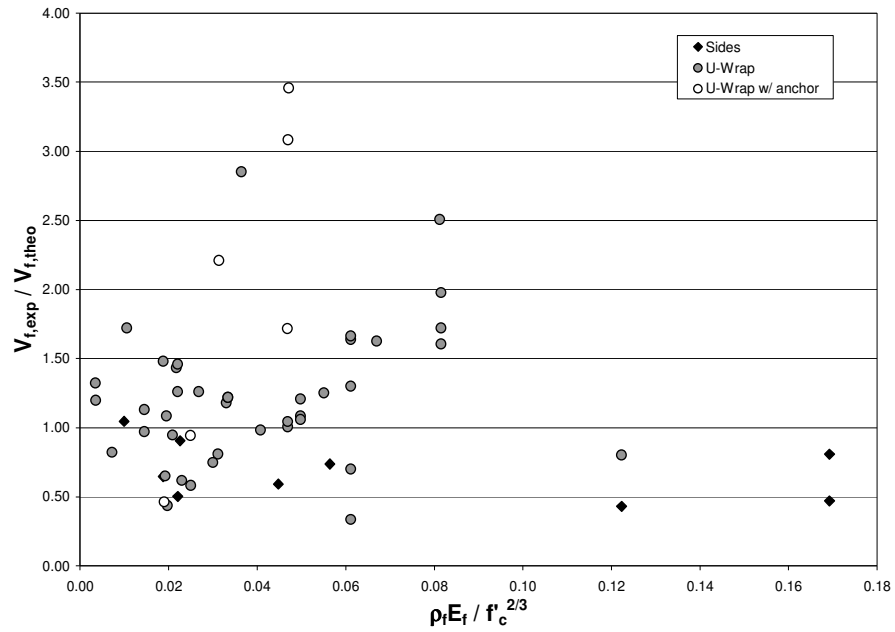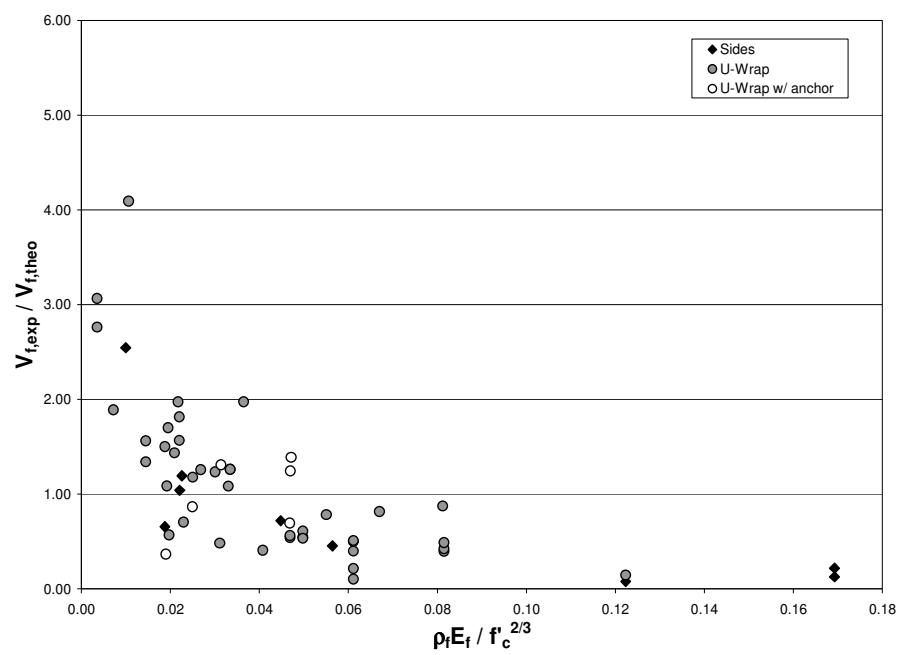
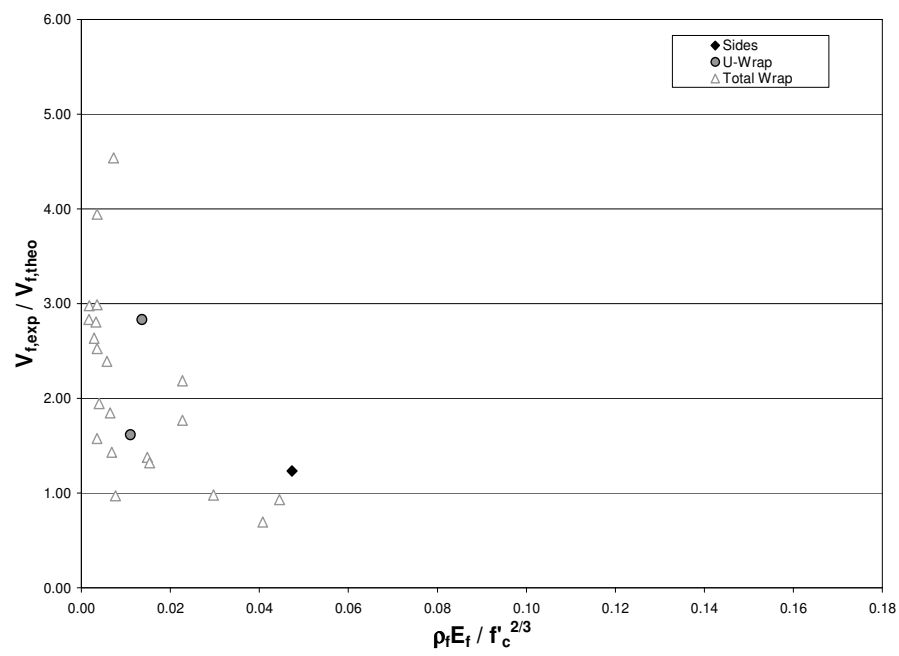Figure B.61. $V_{f,\exp}/V_{f,theo}$ in terms of $E_f \rho_f /(f_c^{'})^{2/3}$ - FRP Debonding
Hsu et al. (2003)
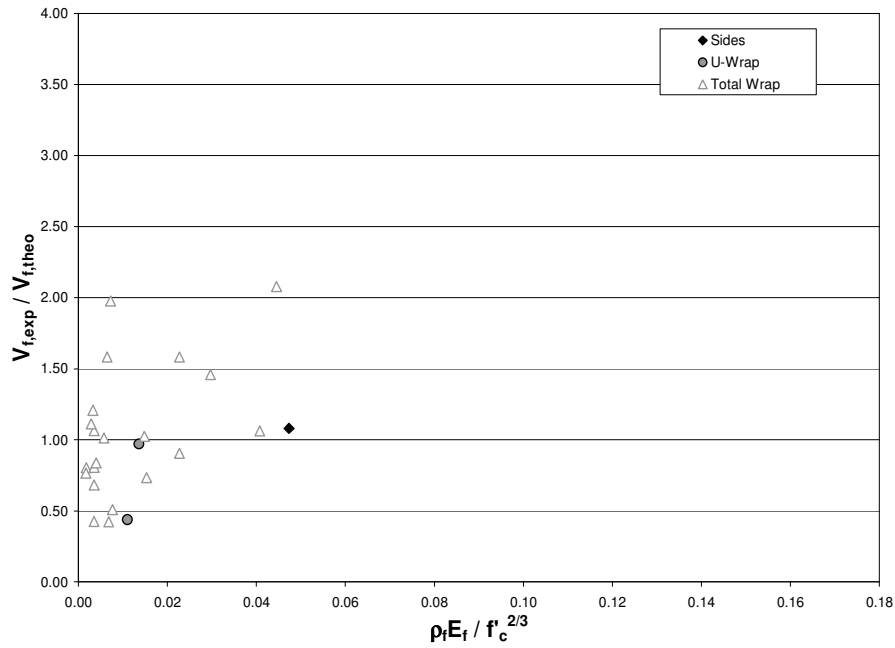
Figure B.62. $V_{f,\exp}/V_{f,theo}$ in terms of $E_f \rho_f /(f_c^{'})^{2/3}$ - FRP Fracture
Hsu et al. (2003)
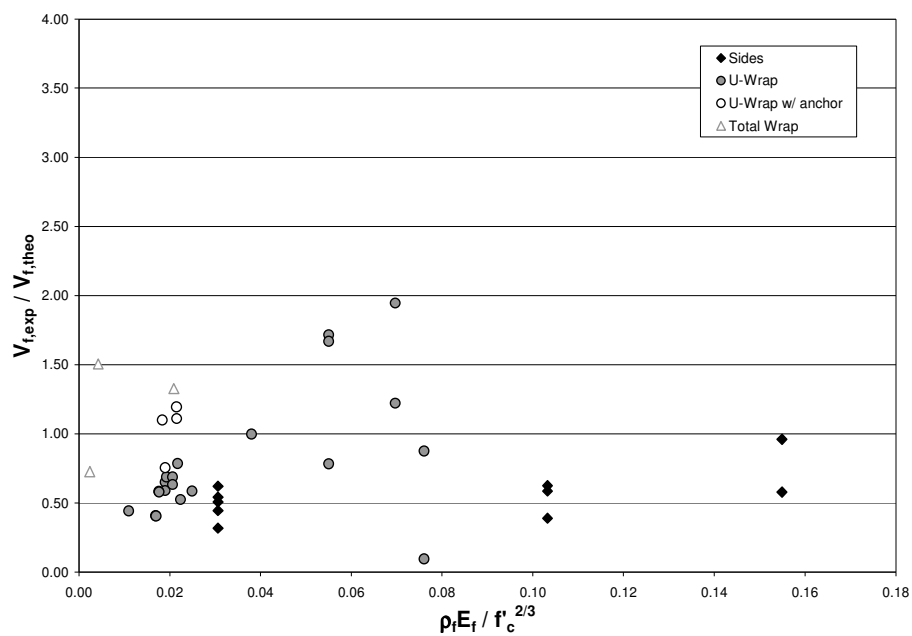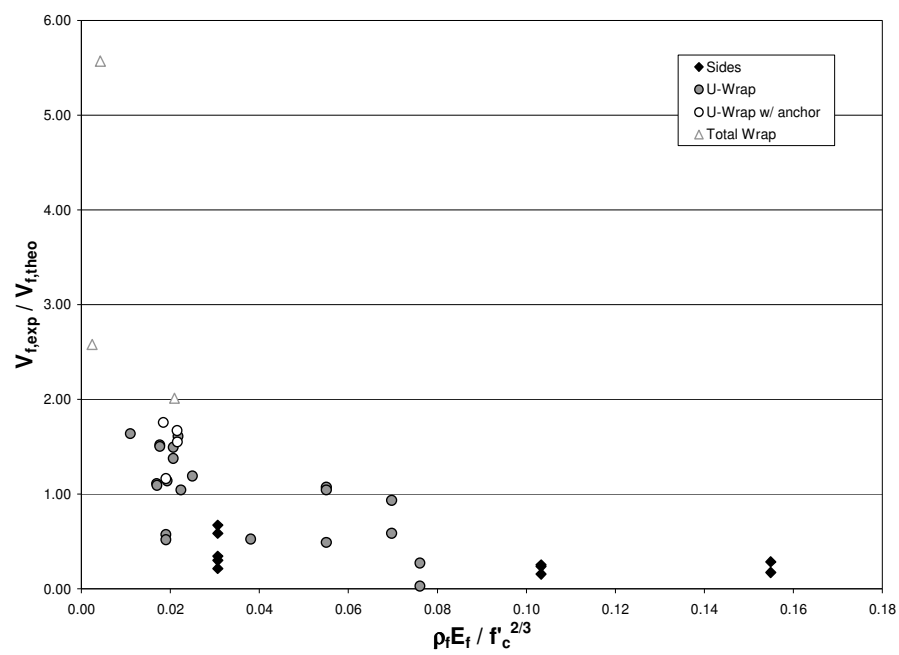
Figure B.63. $V_{f,\exp}/V_{f,theo}$ in terms of $E_f\rho_f/(f_c')^{2/3}$ - Other Failure Modes
Hsu et al. (2003)
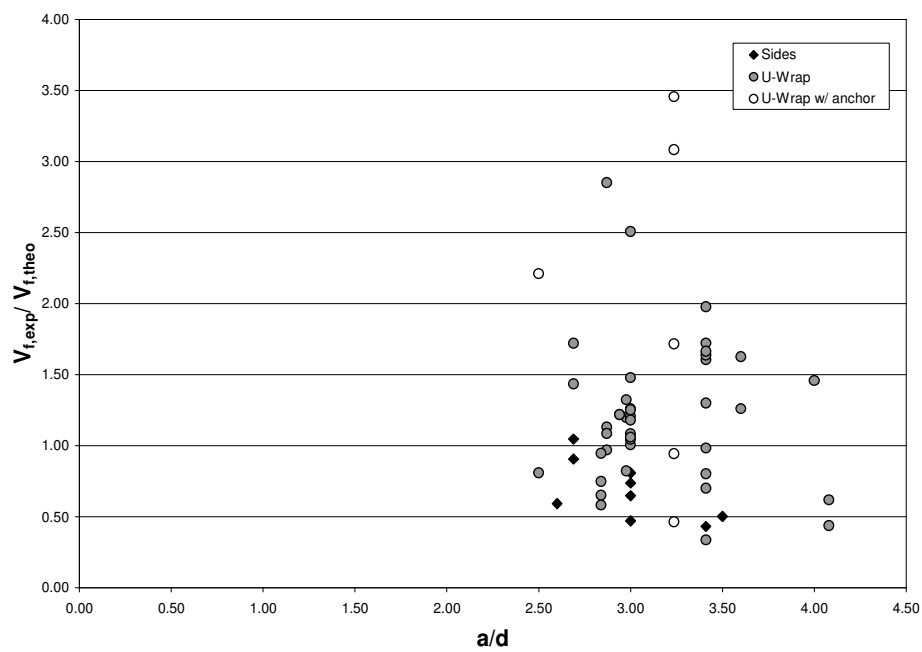
Figure B.64. $V_{f,\exp}/V_{f,theo}$ in terms of a/d - FRP Debonding
Hsu et al. (2003)
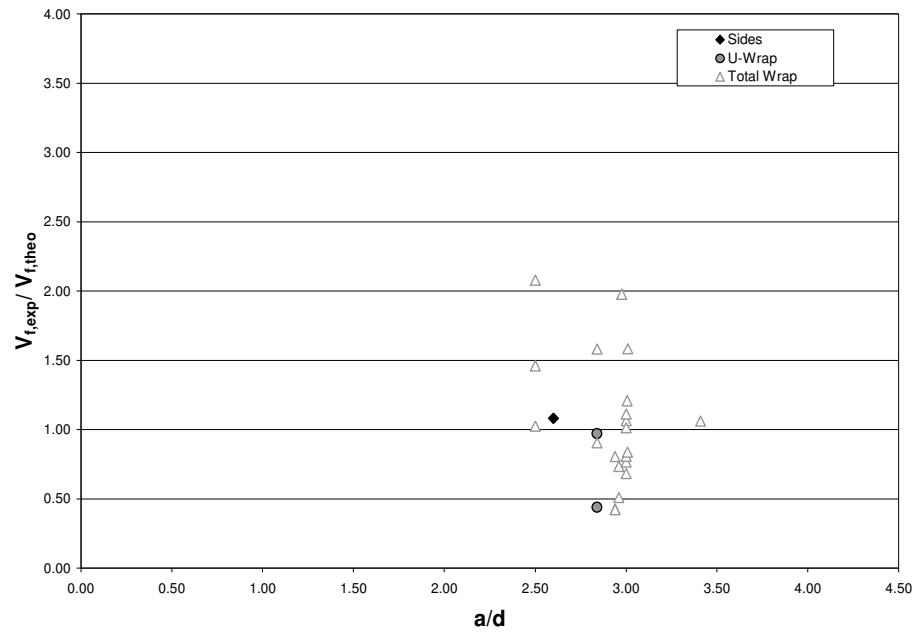
Figure B.65. $V_{f,\exp}/V_{f,theo}$ in terms of a/d - FRP Fracture
Hsu et al. (2003)
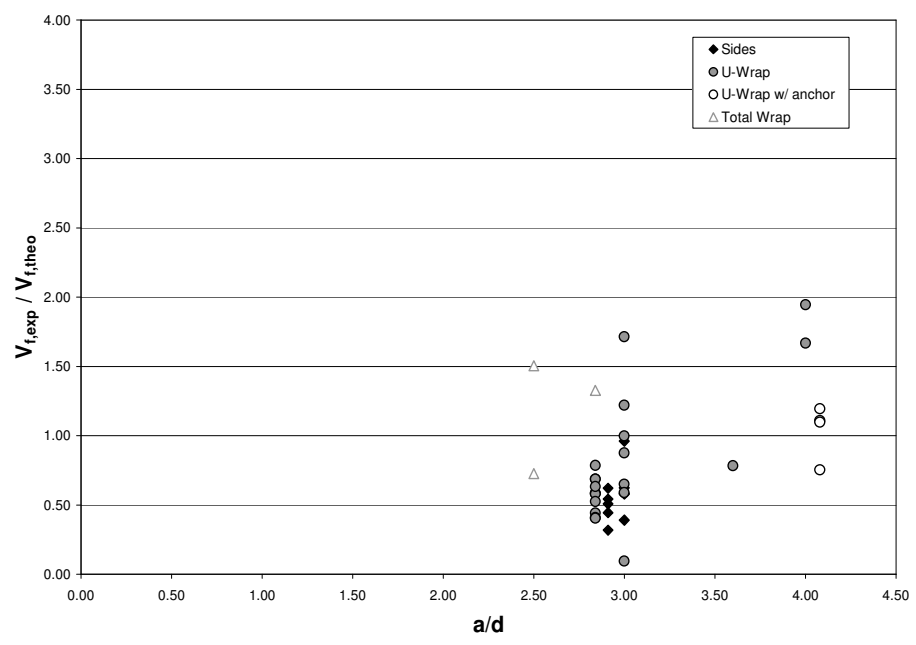
Figure B.66. $V_{f,\exp}/V_{f,theo}$ in terms of a/d – Other Failure Modes
Hsu et al. (2003)
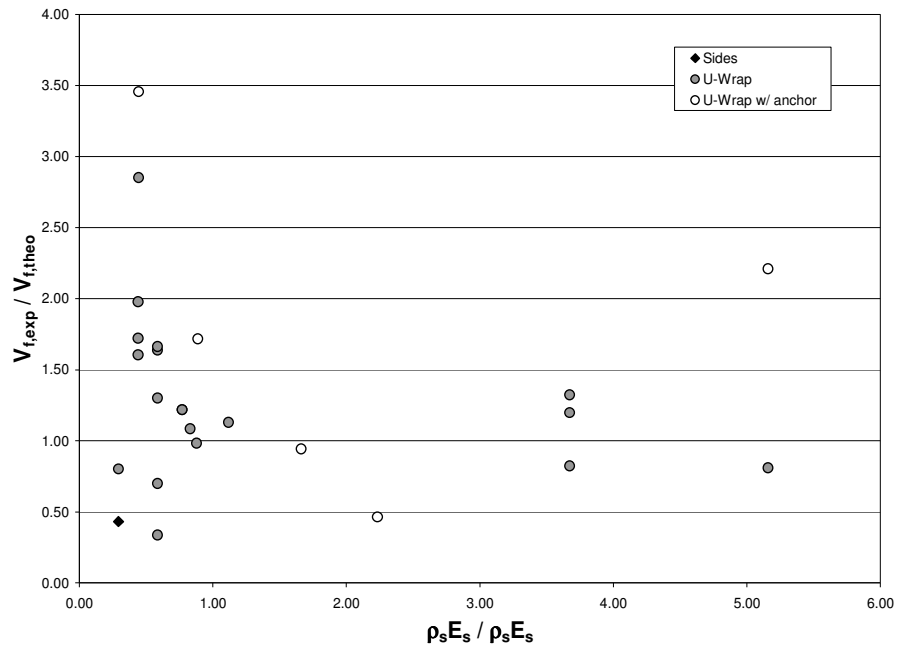
Figure B.67. $V_{f,\exp}/V_{f,theo}$ in terms of $\rho_s E_s / \rho_f E_f$ – FRP Debonding
Hsu et al. (2003)
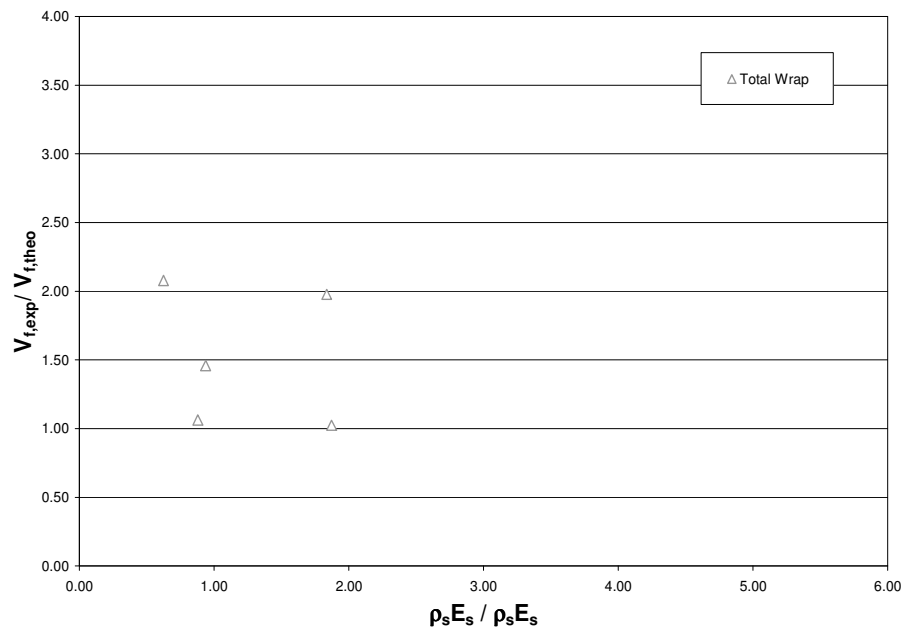
Figure B.68. $V_{f,\exp}/V_{f,theo}$ in terms of $\rho_s E_s / \rho_f E_f$ – FRP Fracture
Hsu et al. (2003)
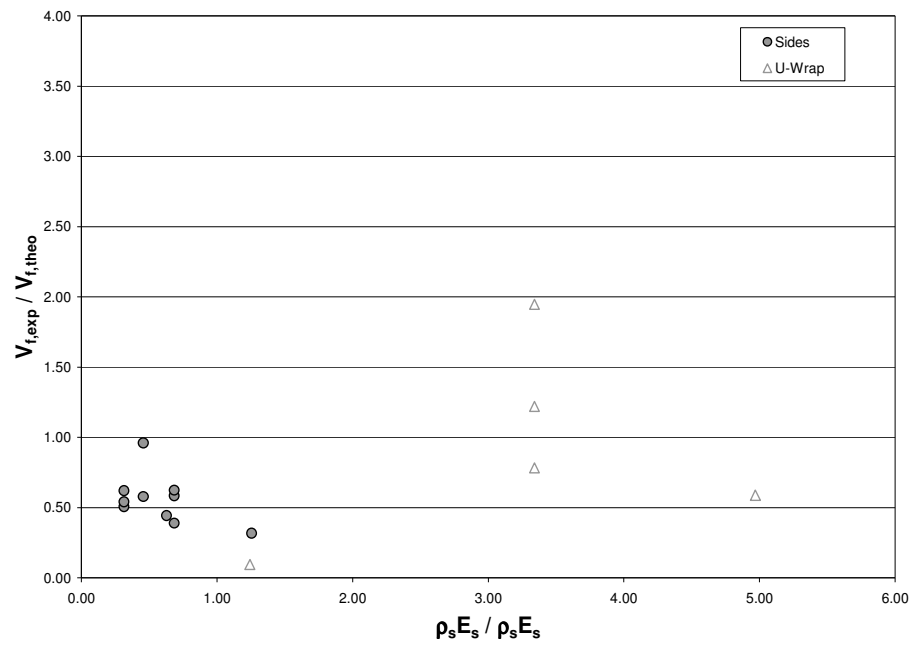
Figure B.69. $V_{f,\exp}/V_{f,theo}$ in terms of $\rho_s E_s / \rho_f E_f$ – Other Failure Modes Hsu et al. (2003)
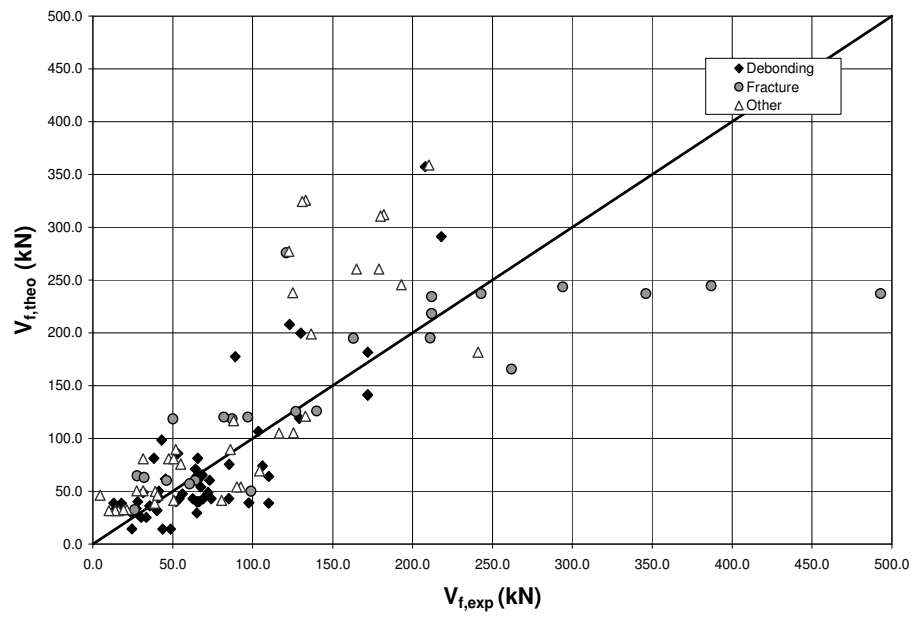
Figure B.70. Comparison between Predictions by Hsu et al. (2003) and Experimental Results
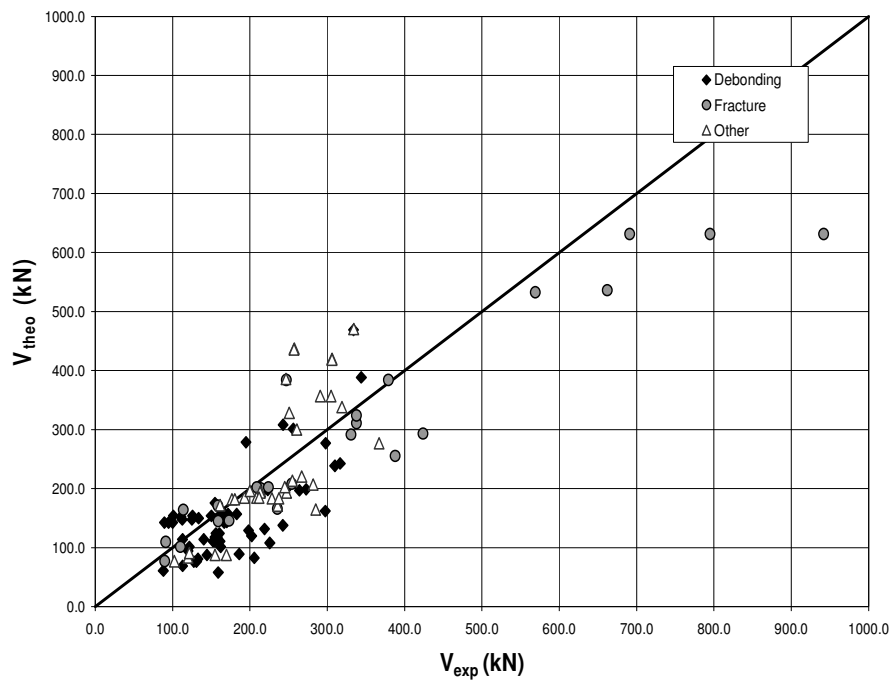
(a) ACI 318-05
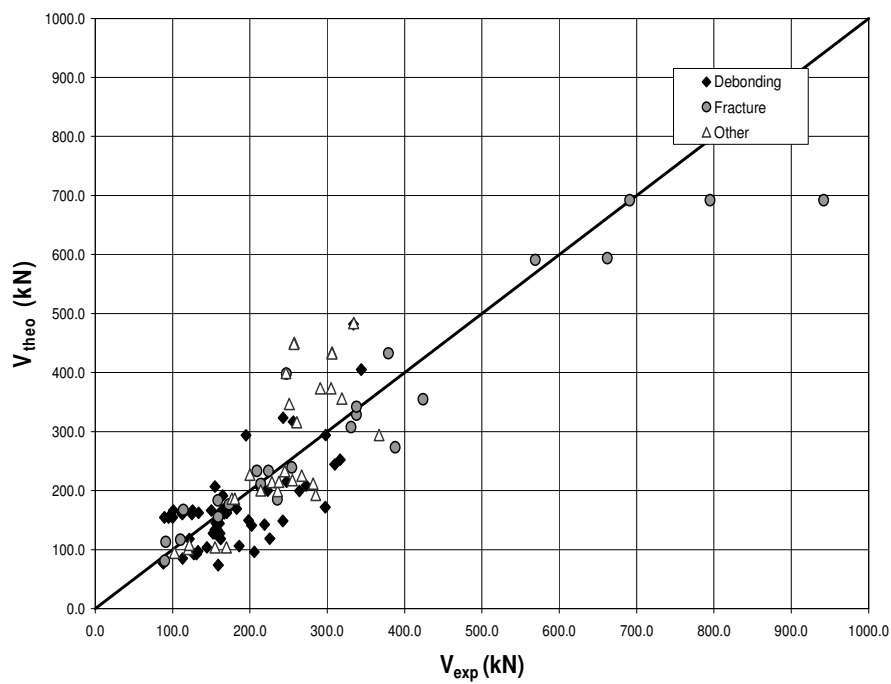
(b) Eurocode 2

Figure B.71. Comparison between Analytical Predictions of total shear capacity by Hsu et al. (2003) and Experimental Results
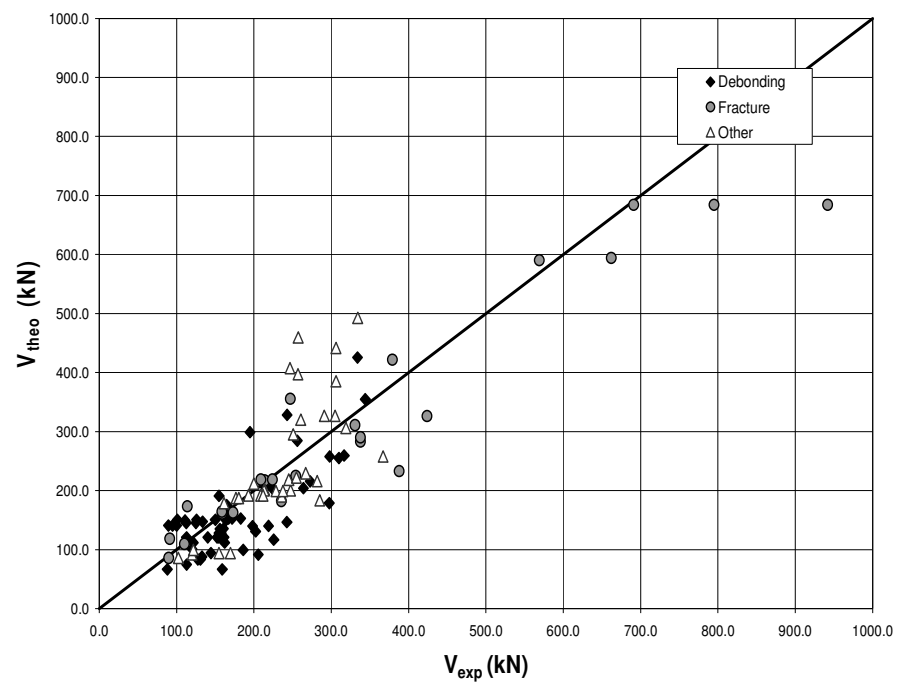
(c) CSA A23.3-94
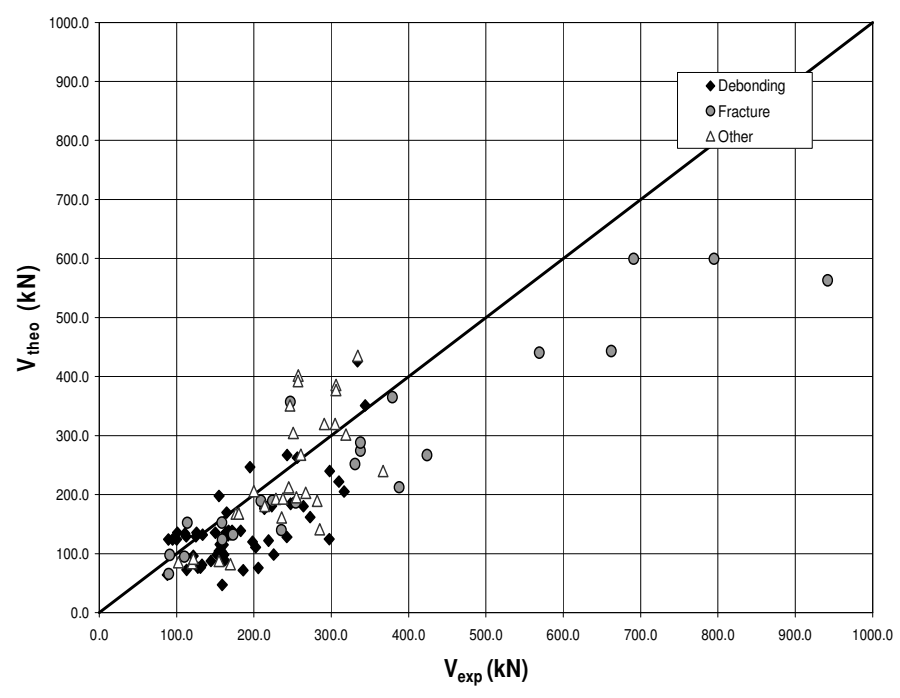
(d) AASHTO LRFD

Figure B.72. Comparison between Analytical Predictions of total shear capacity by Hsu et al. (2002) and Experimental Results
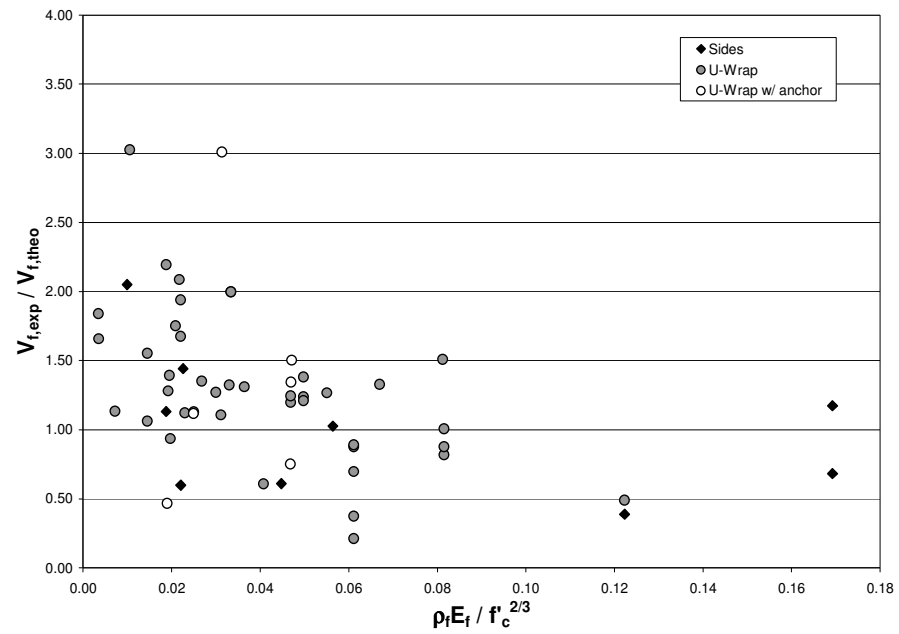
Figure B.73. $V_{f,\exp}/V_{f,theo}$ in terms of $E_f \rho_f /(f_c^{'})^{2/3}$ – FRP Debonding
Chen and Teng (2003)
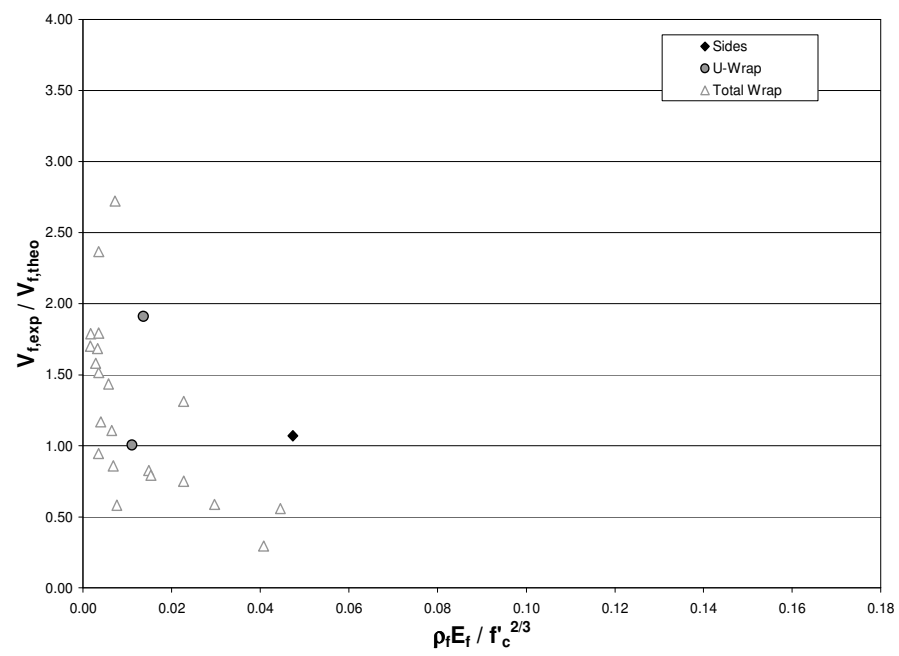
Figure B.74. $V_{f,\exp}/V_{f,theo}$ in terms of $E_f \rho_f /(f_c^{'})^{2/3}$ – FRP Fracture
Chen and Teng (2003)
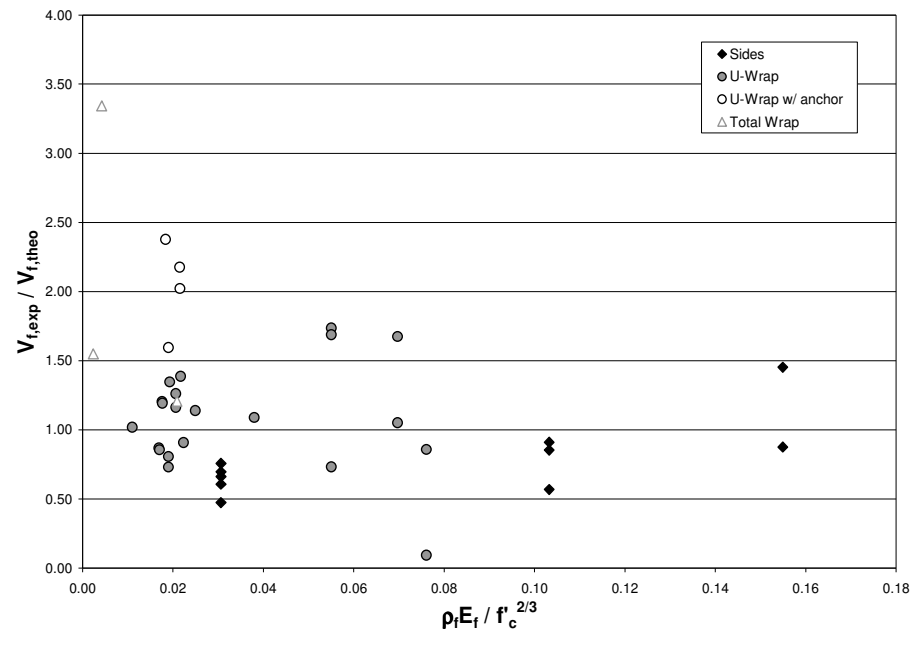
Figure B.75. $V_{f,\exp}/V_{f,theo}$ in terms of $E_f \rho_f /(f_c^{'})^{2/3}$ – Other Failure Modes
Chen and Teng (2003)
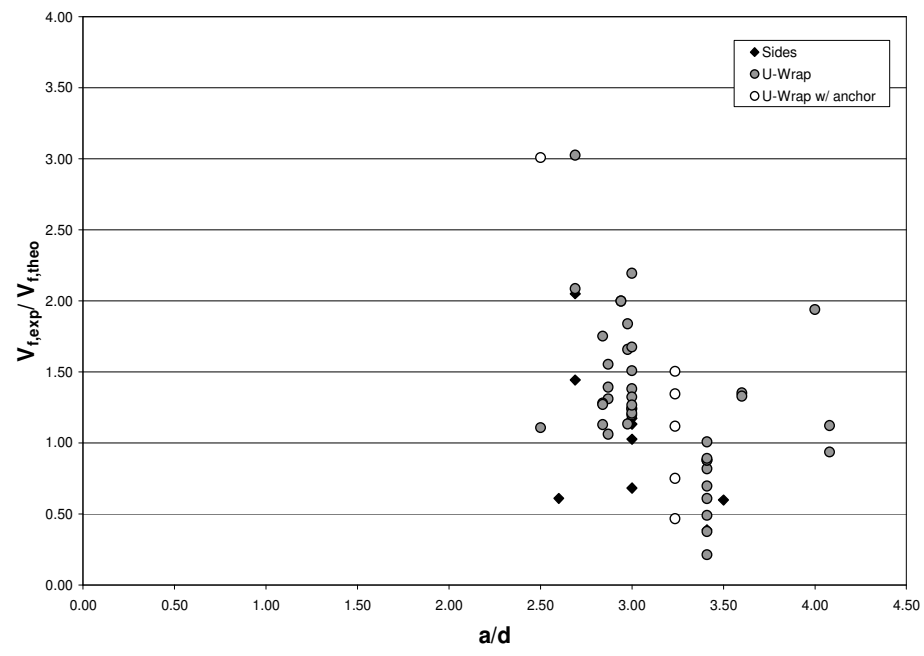
Figure B.76. $V_{f,\exp}/V_{f,theo}$ in terms of a/d – FRP Debonding
Chen and Teng (2003)
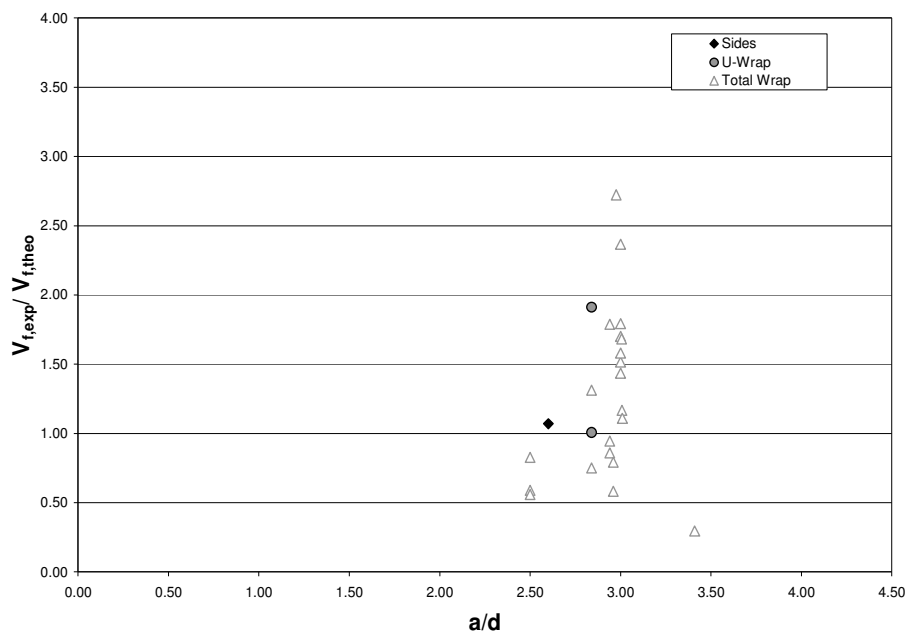
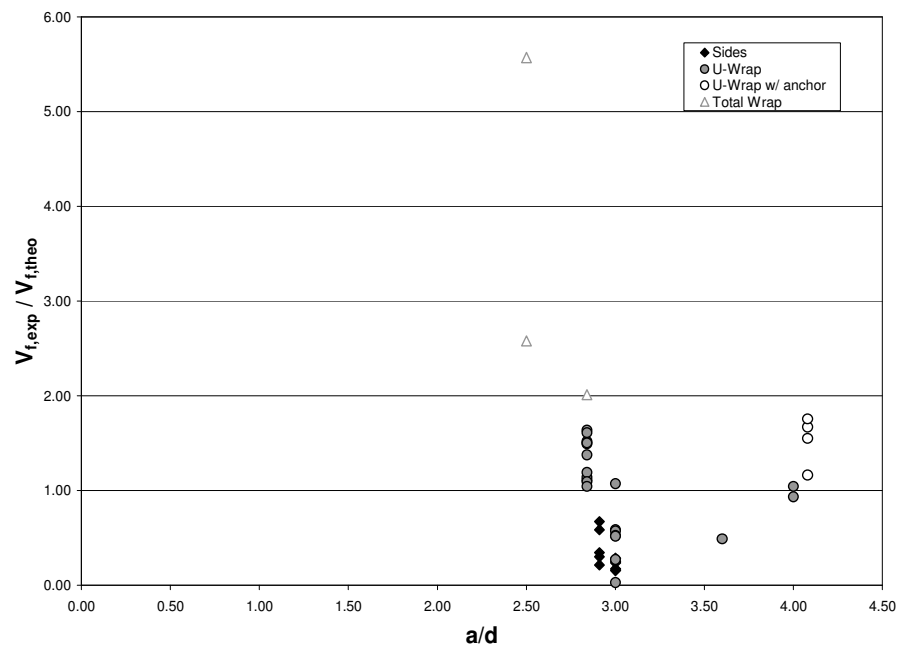Figure B.77. $V_{f,\exp} / V_{f,theo}$ in terms of a/d – FRP Fracture
Chen and Teng (2003)
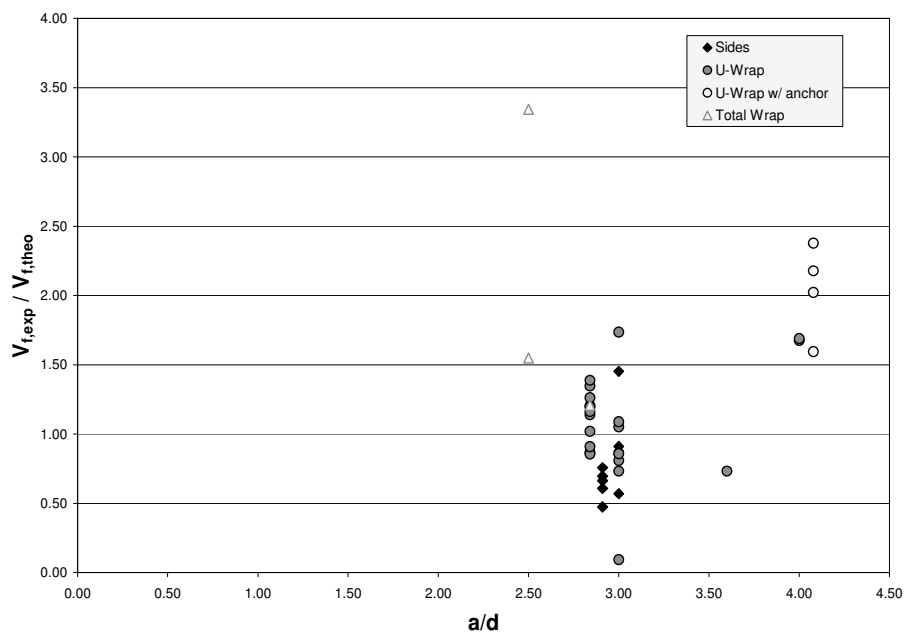
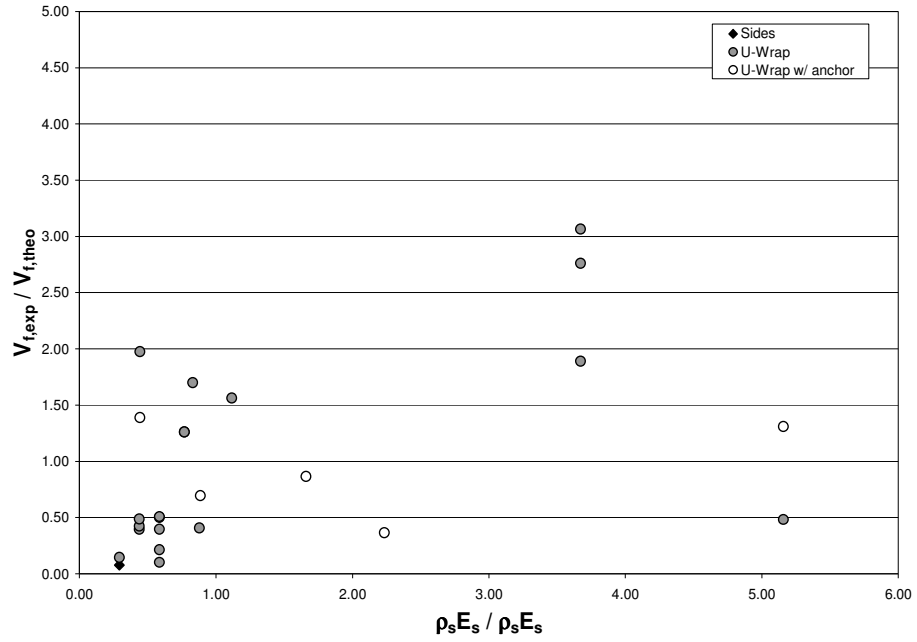Figure B.78. $V_{f,\exp} / V_{f,theo}$ in terms of a/d – Other Failure Modes
Chen and Teng (2003)
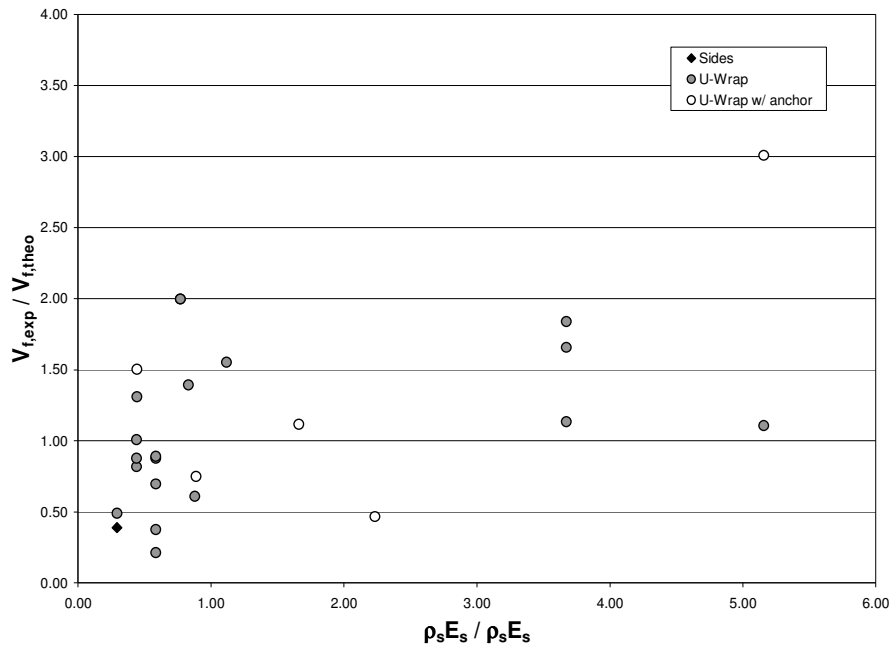
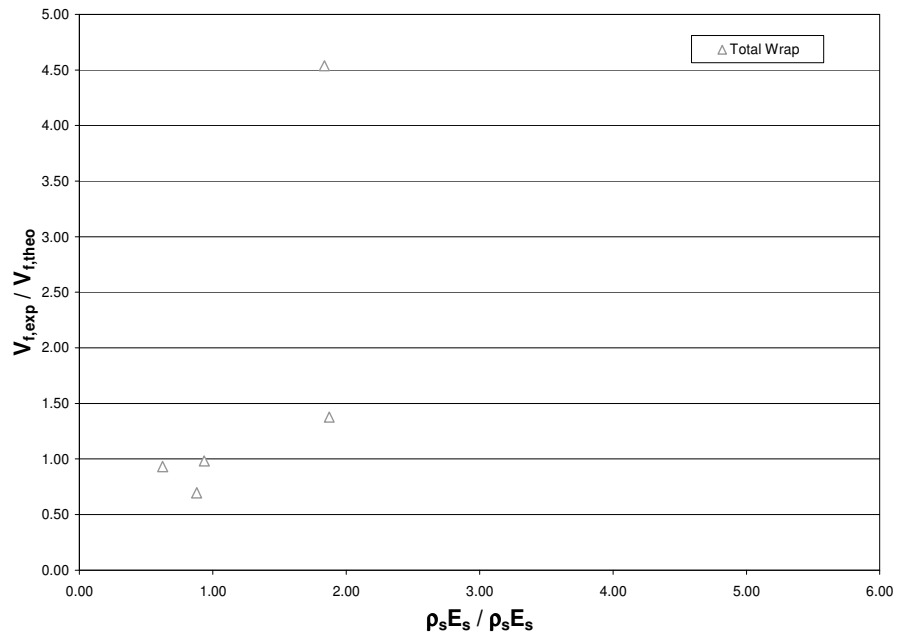Figure B.79. $V_{f,\exp}/V_{f,theo}$ in terms of $\rho_s E_s / \rho_f E_f$ – FRP Debonding Chen and Teng (2003)
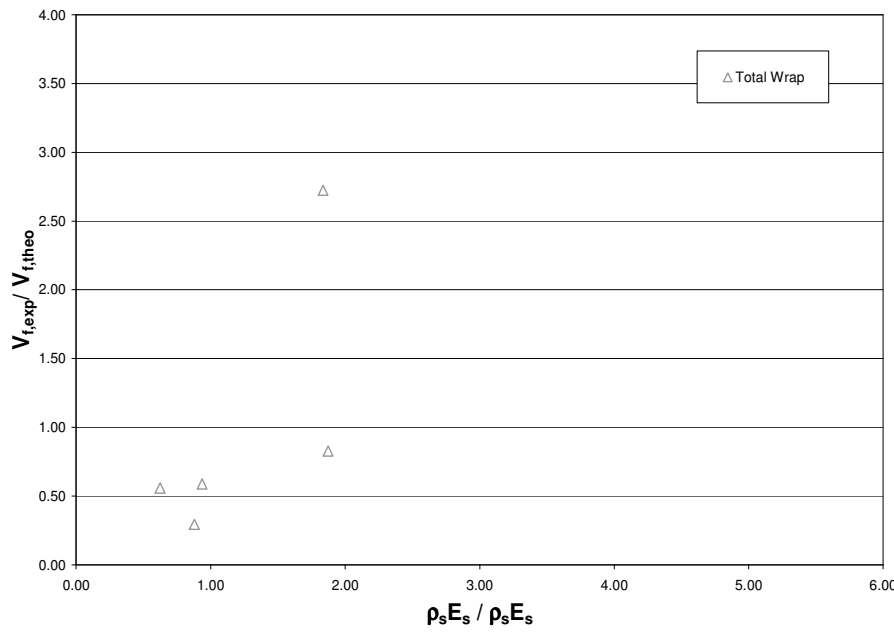
Figure B.80. $V_{f,\exp}/V_{f,theo}$ in terms of $\rho_s E_s / \rho_f E_f$ – FRP Fracture Chen and Teng (2003)
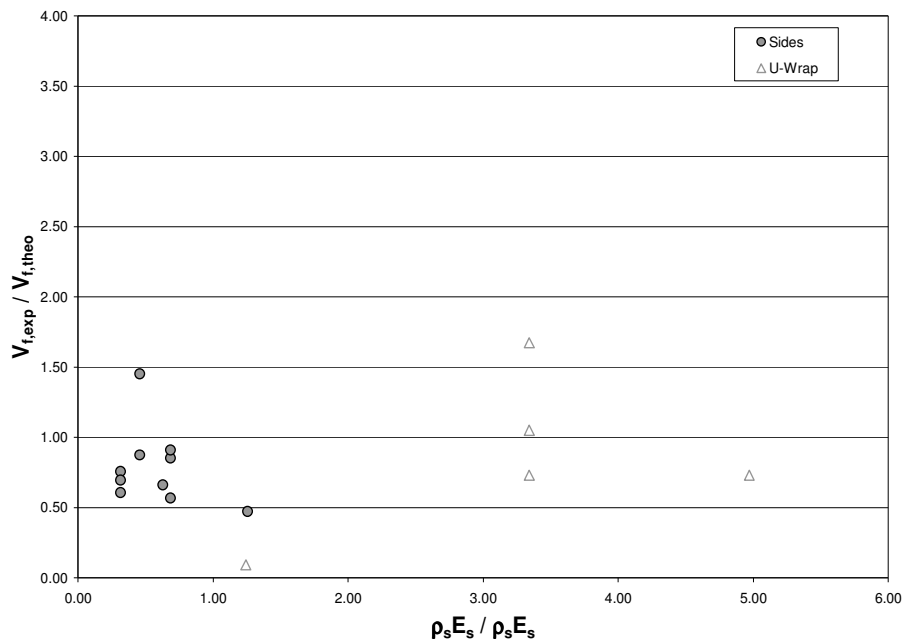
Figure B.81. $V_{f,\exp} / V_{f,theo}$ in terms of $\rho_s E_s / \rho_f E_f$ – Other Failure Modes
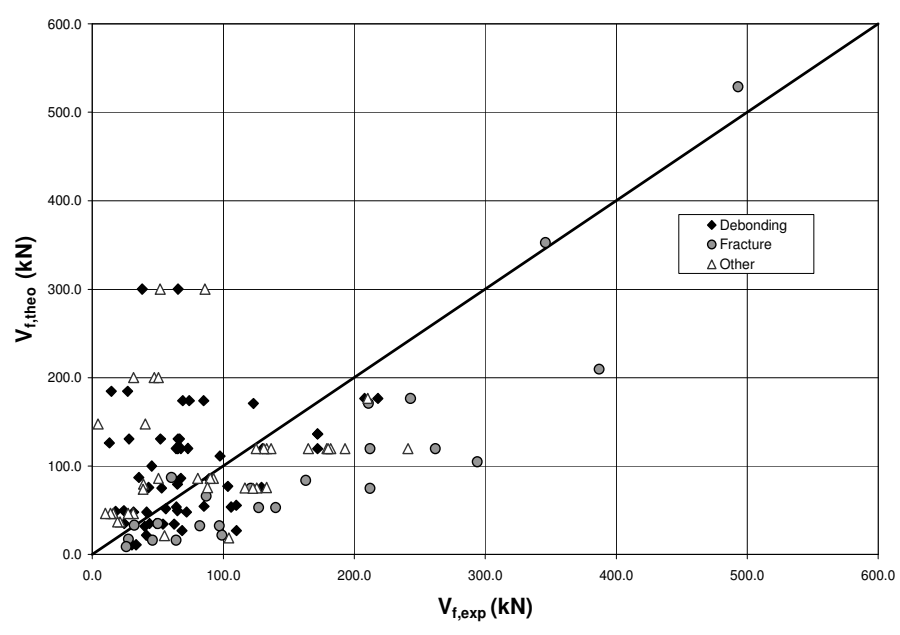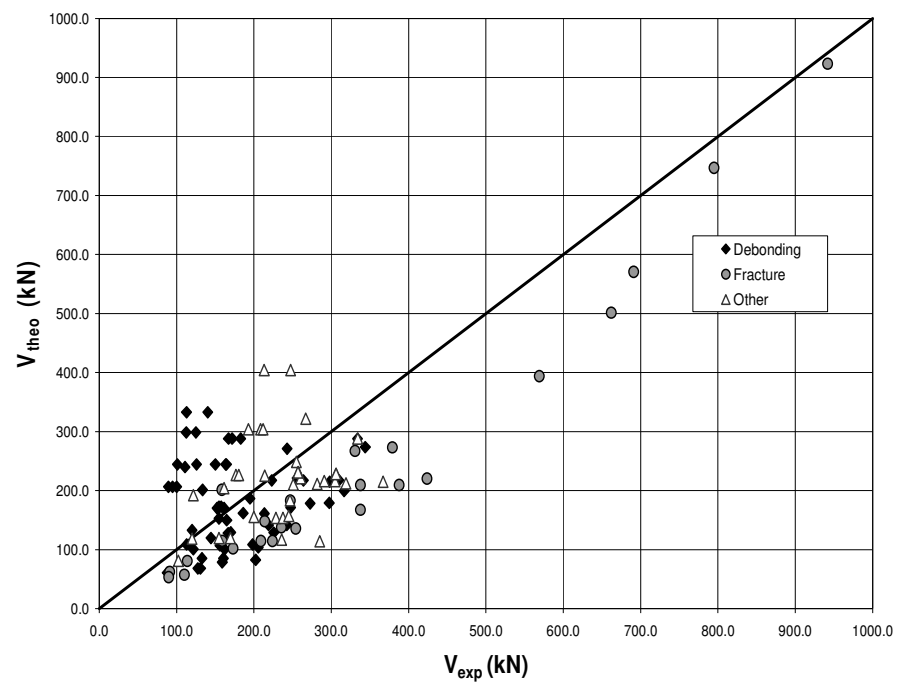Chen and Teng (2003)
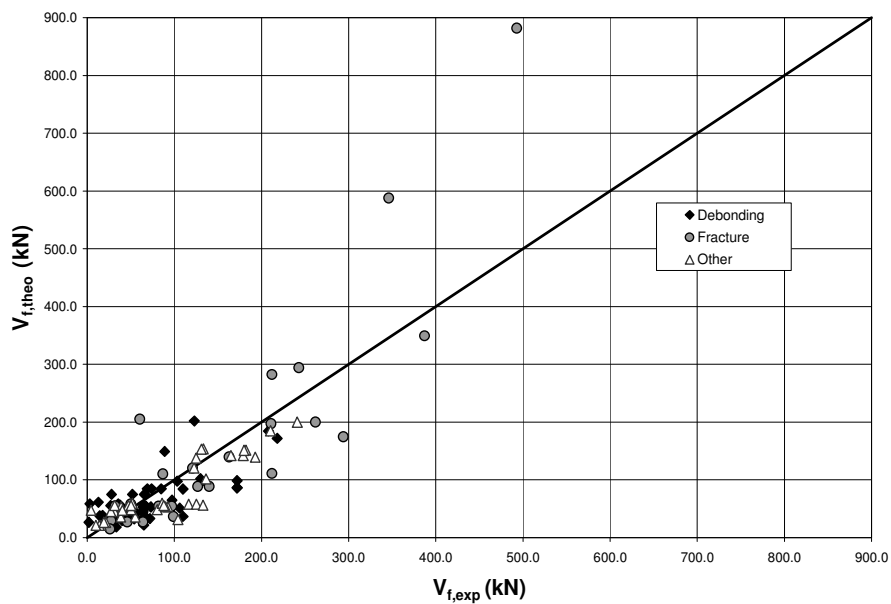
Figure B.82. Comparison between Predictions by Chen and Teng (2003) and
Experimental Results
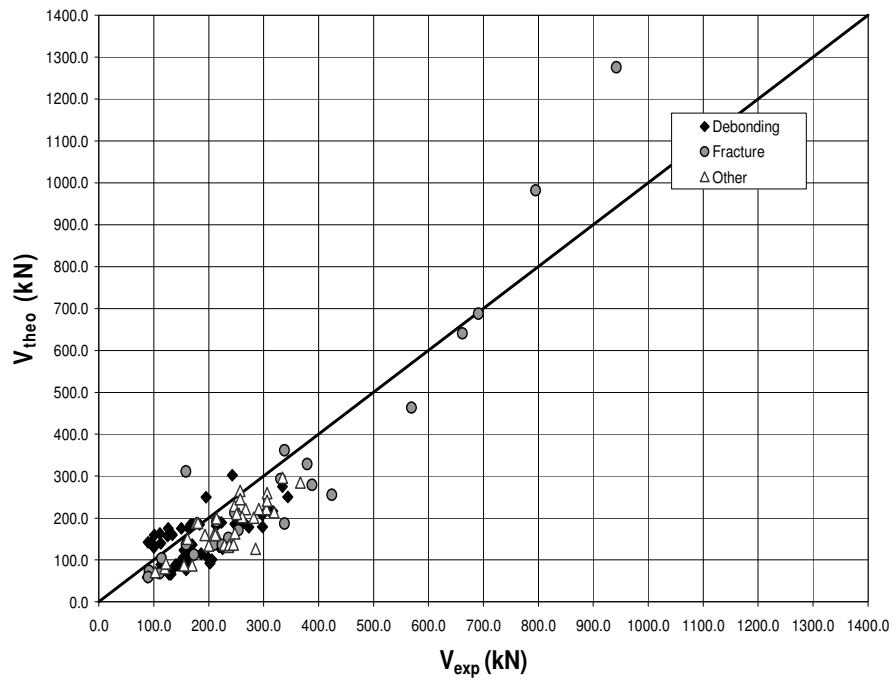
(a) ACI 318-05
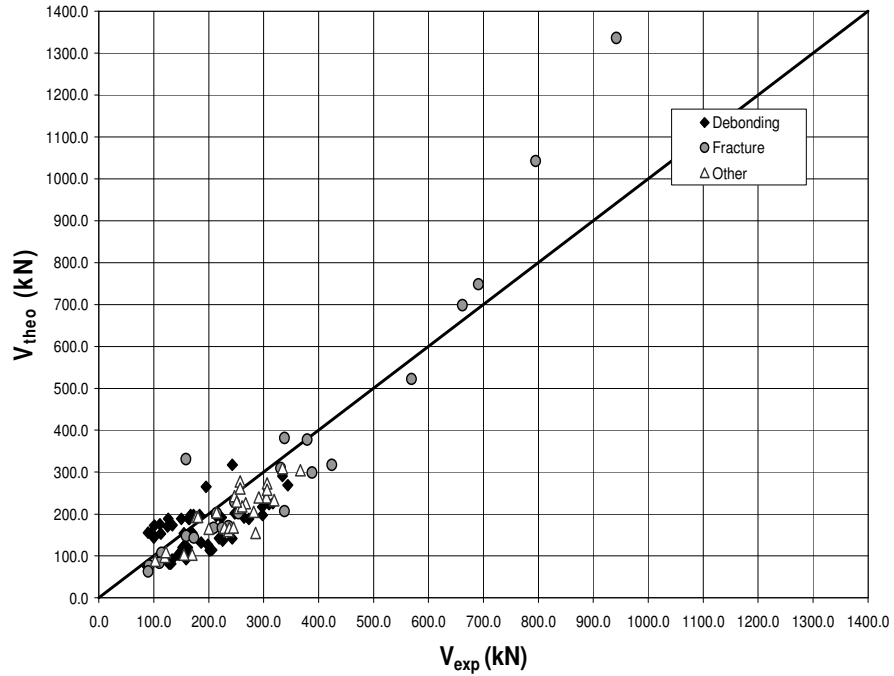
(b) Eurocode 2

Figure B.83. Comparison between Analytical Predictions of total shear capacity by Chen and Teng (2003) and Experimental Results
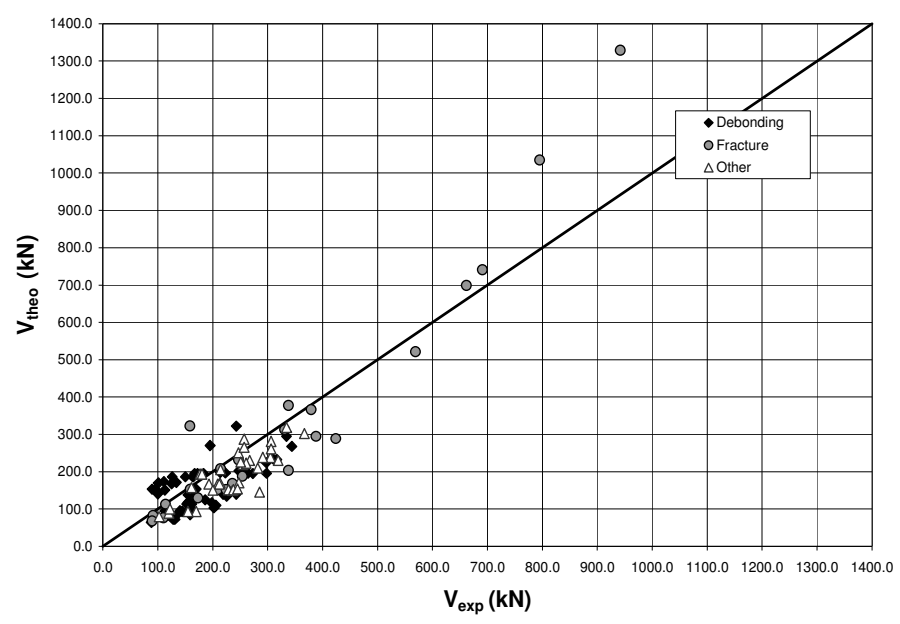
(c) CSA A23.3-94
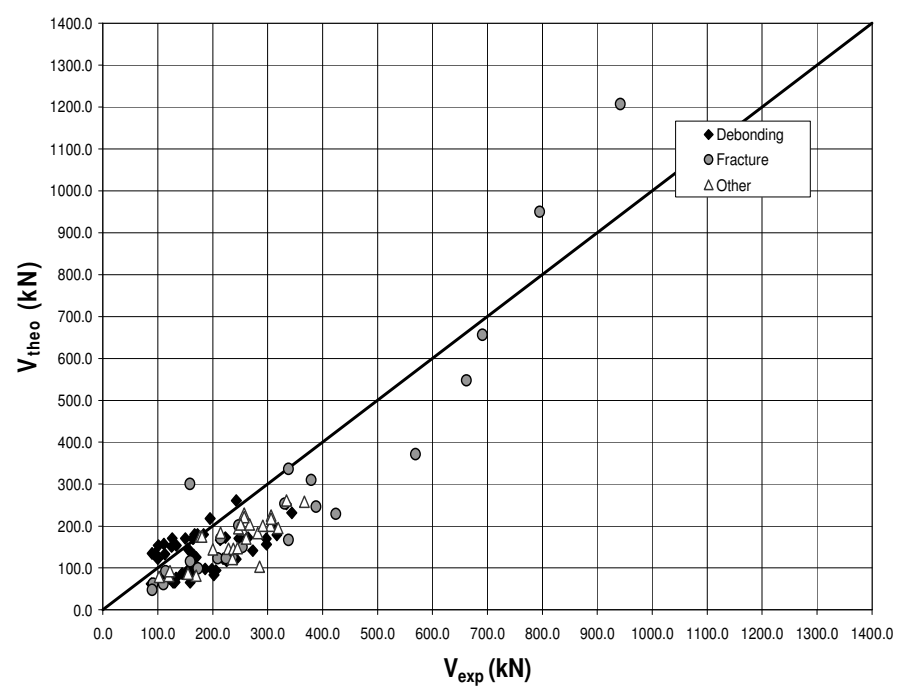
(d) AASHTO LRFD
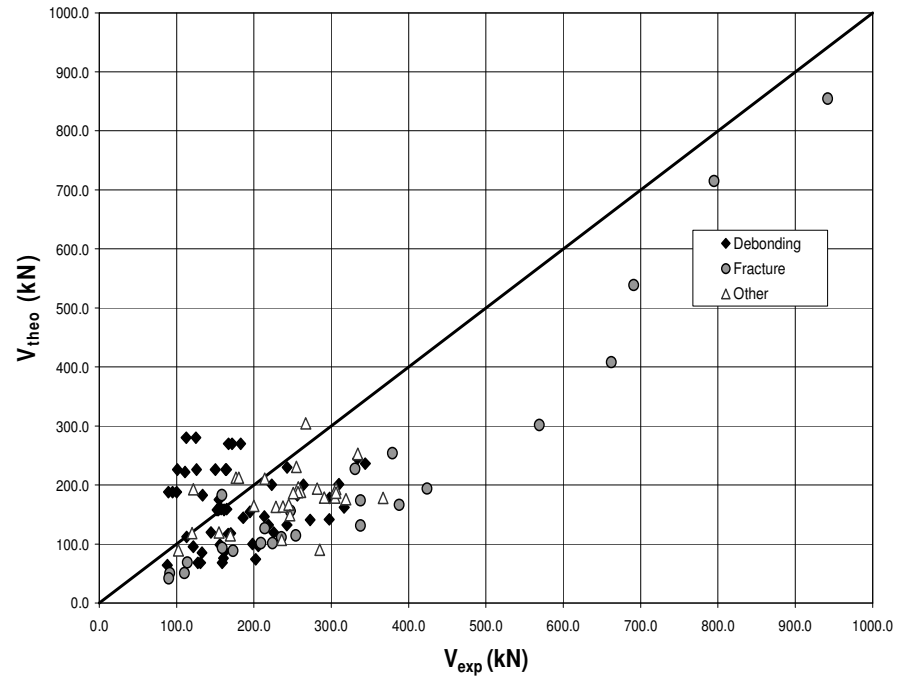
Figure B.84. Comparison between Analytical Predictions of total shear capacity by Chen and Teng (2003) and Experimental Results

212
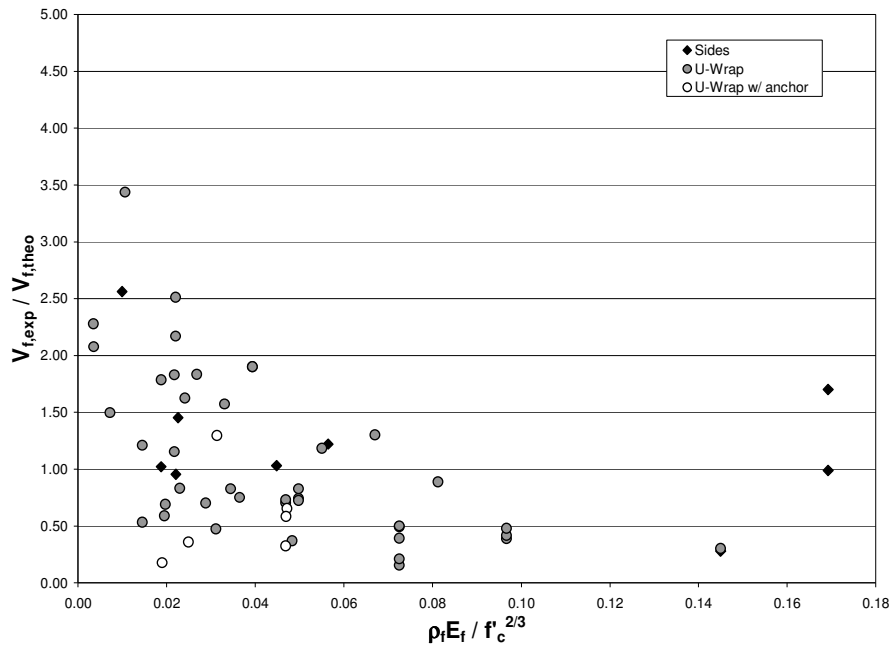
Figure B.85. $V_{f,\exp}/V_{f,theo}$ in terms of $E_f\rho_f/(f_c^{'})^{2/3}$ – FRP Debonding
Monti and Liotta (2005)
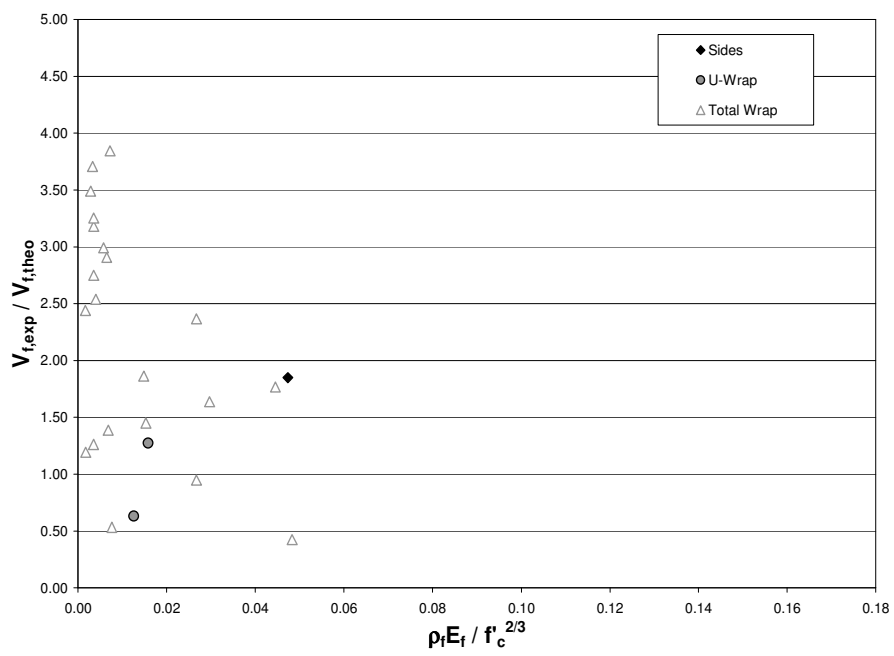
Figure B.86. $V_{f,\exp}/V_{f,theo}$ in terms of $E_f\rho_f/(f_c^{'})^{2/3}$ – FRP Fracture
Monti and Liotta (2005)
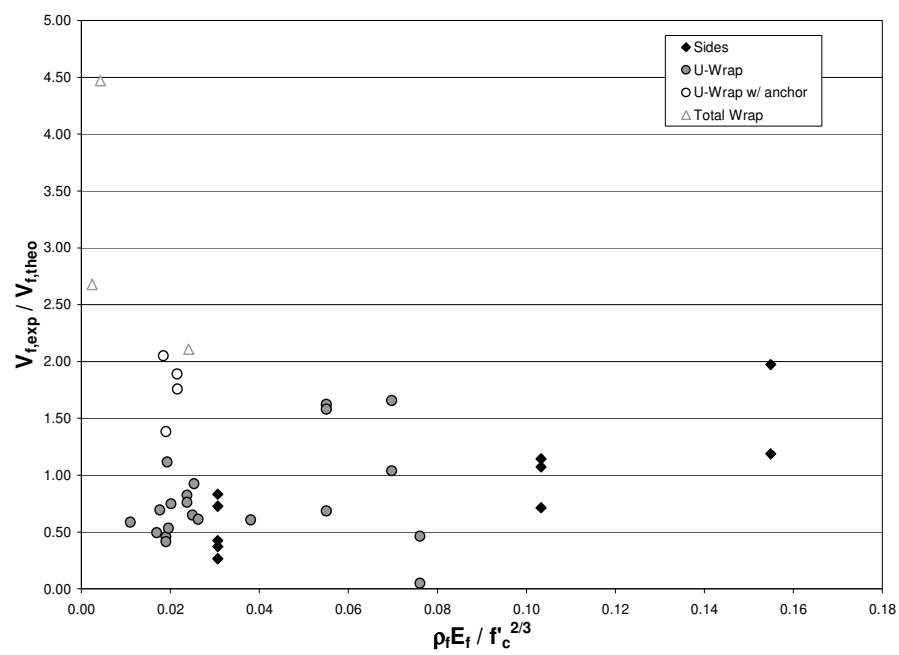
Figure B.87. $V_{f,\exp}/V_{f,theo}$ in terms of $E_f \rho_f /(f_c^{'})^{2/3}$ – Other Failure Modes
Monti and Liotta (2005)
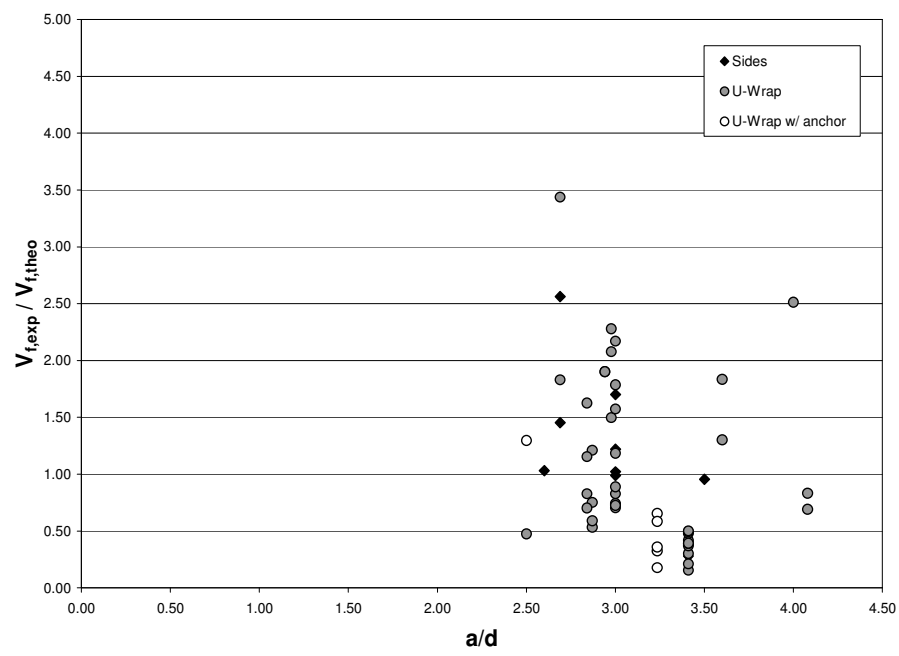
Figure B.88. $V_{f,\exp}/V_{f,theo}$ Results in terms of a/d – FRP Debonding
Monti and Liotta (2005)
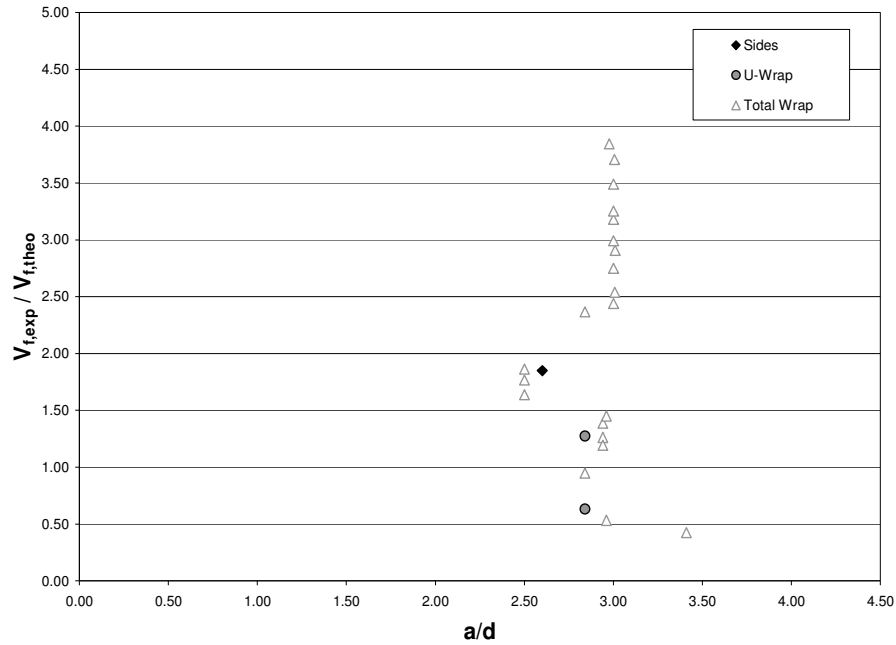
Figure B.89. $V_{f,\exp}/V_{f,theo}$ in terms of a/d – FRP Fracture
Monti and Liotta (2005)
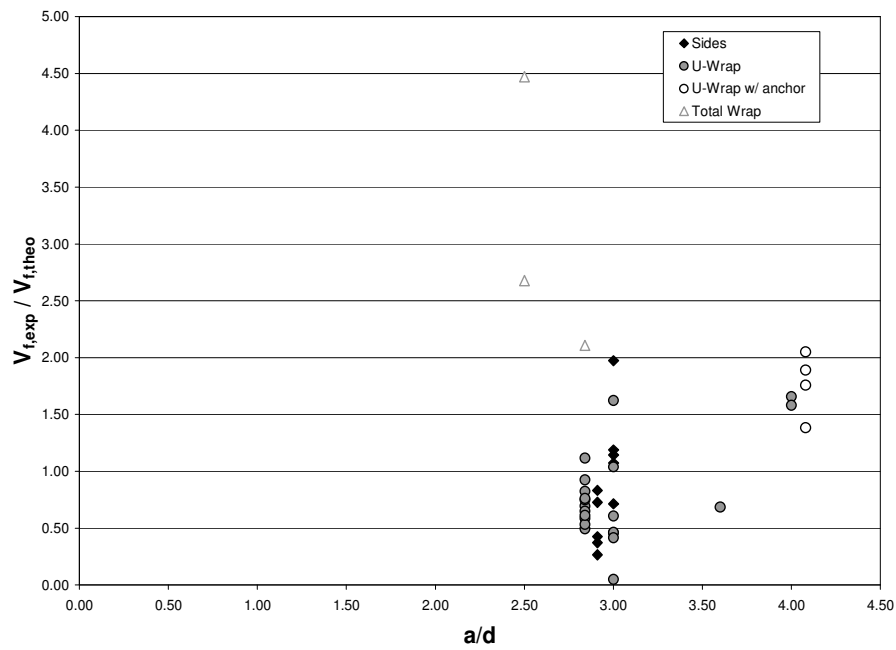
Figure B.90. $V_{f,\exp}/V_{f,theo}$ in terms of a/d – Other Failure Modes
Monti and Liotta (2005)
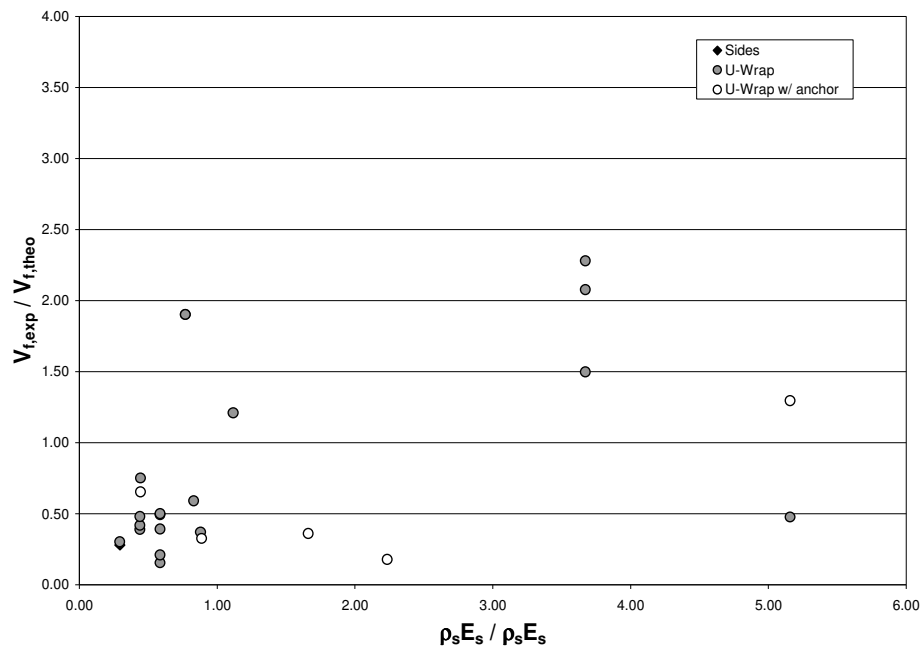
Figure B.91. $V_{f,\exp}/V_{f,theo}$ in terms of $\rho_s E_s / \rho_f E_f$ – FRP Debonding
Monti and Liotta (2005)
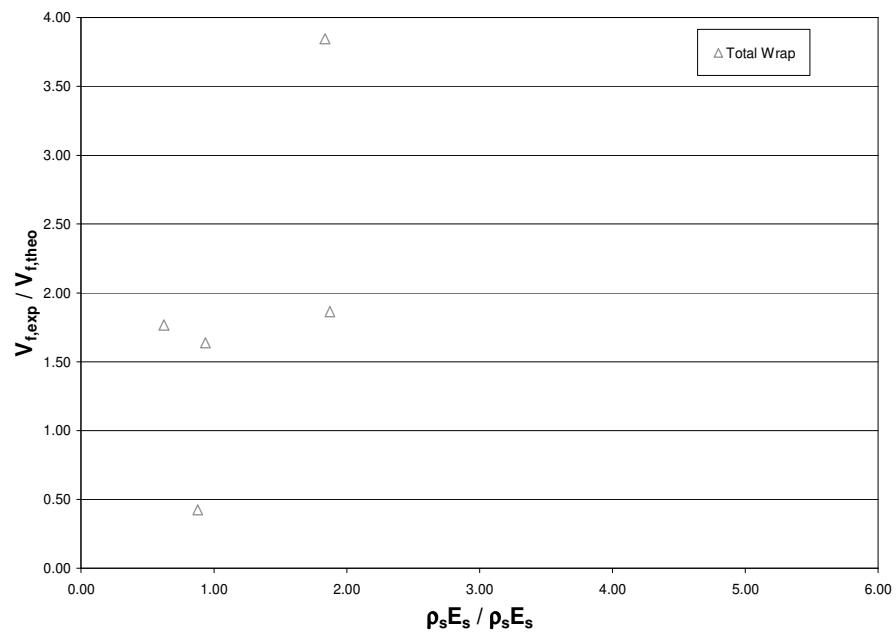
Figure B.92. $V_{f,\exp}/V_{f,theo}$ in terms of $\rho_s E_s / \rho_f E_f$ – FRP Fracture
Monti and Liotta (2005)
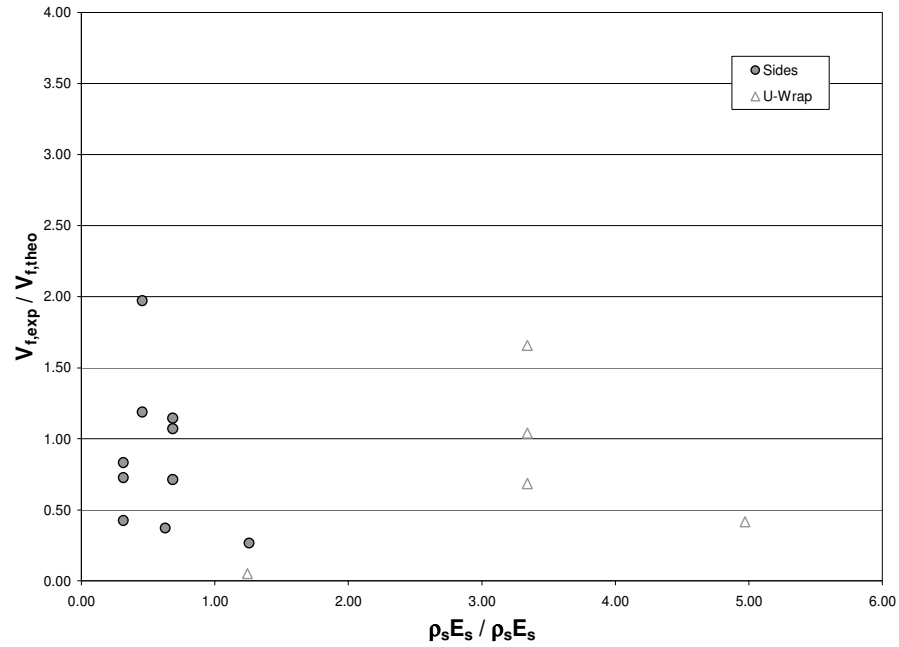
Figure B.93. $V_{f,\exp}/V_{f,theo}$ in terms of $\rho_s E_s / \rho_f E_f$ – Other Failure Modes
Monti and Liotta (2005)
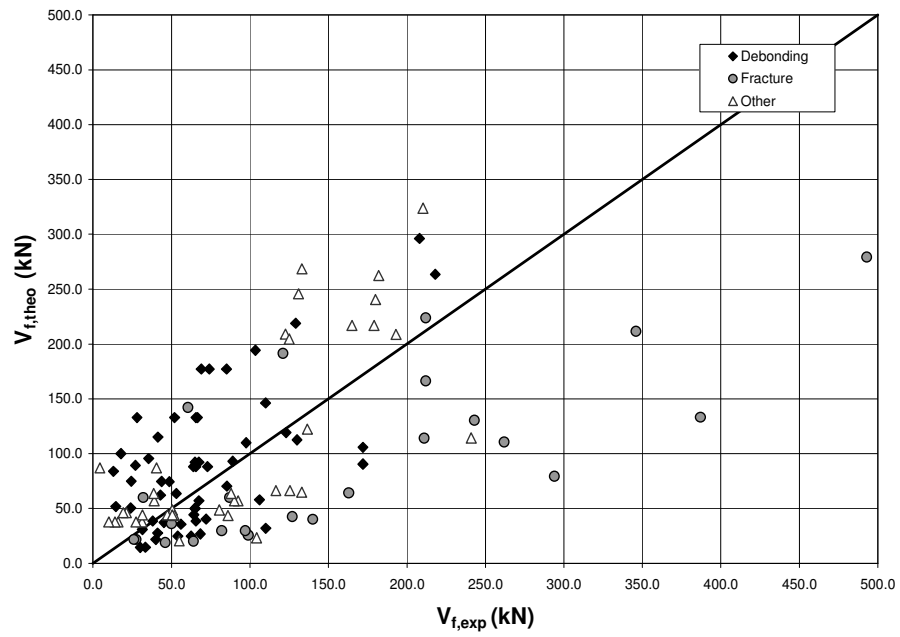
Figure B.94. Comparison between Predictions by Monti and Liotta (2005) and
Experimental Results
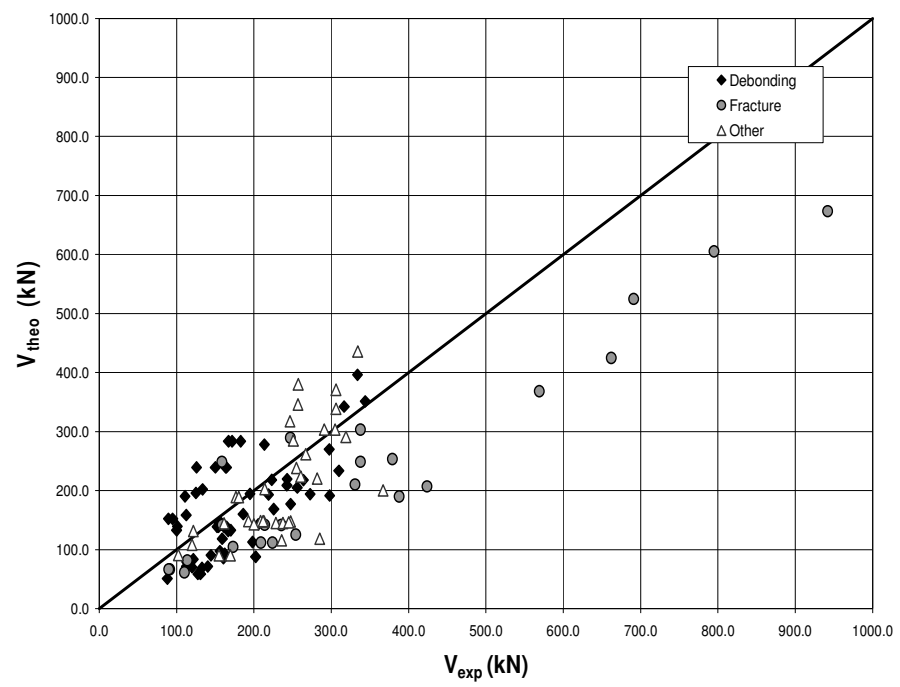
(a) ACI 318-05
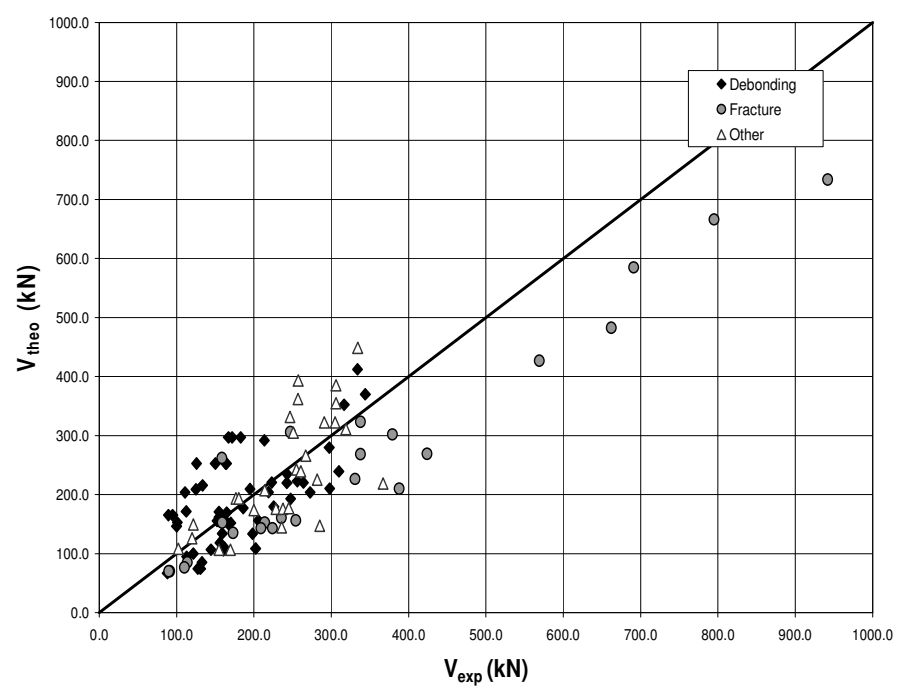
(b) Eurocode 2

Figure B.95. Comparison between Analytical Predictions of total shear capacity by
Monti and Liotta (2005) and Experimental Results
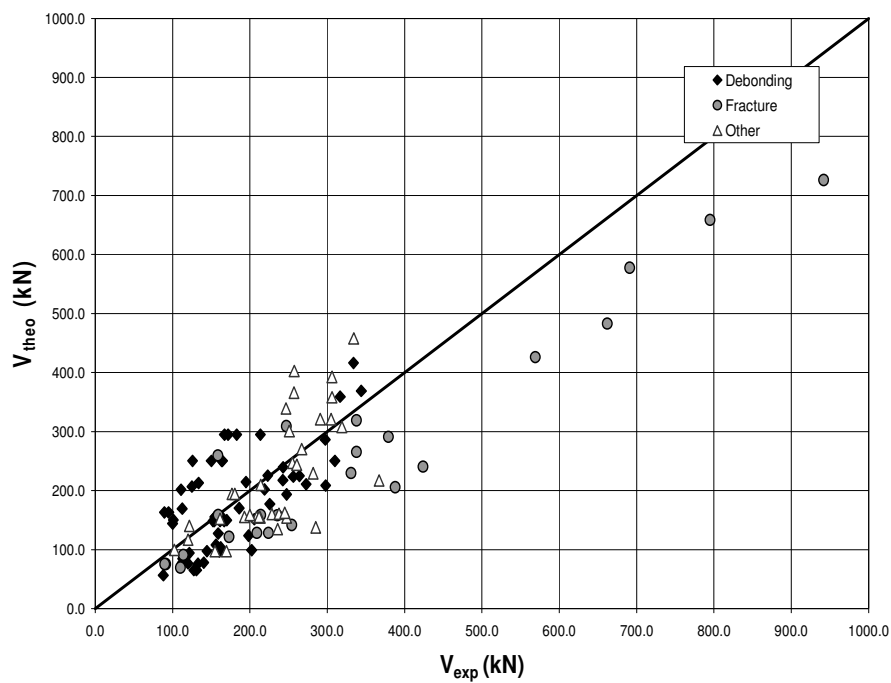
(c) CSA A23.3-94
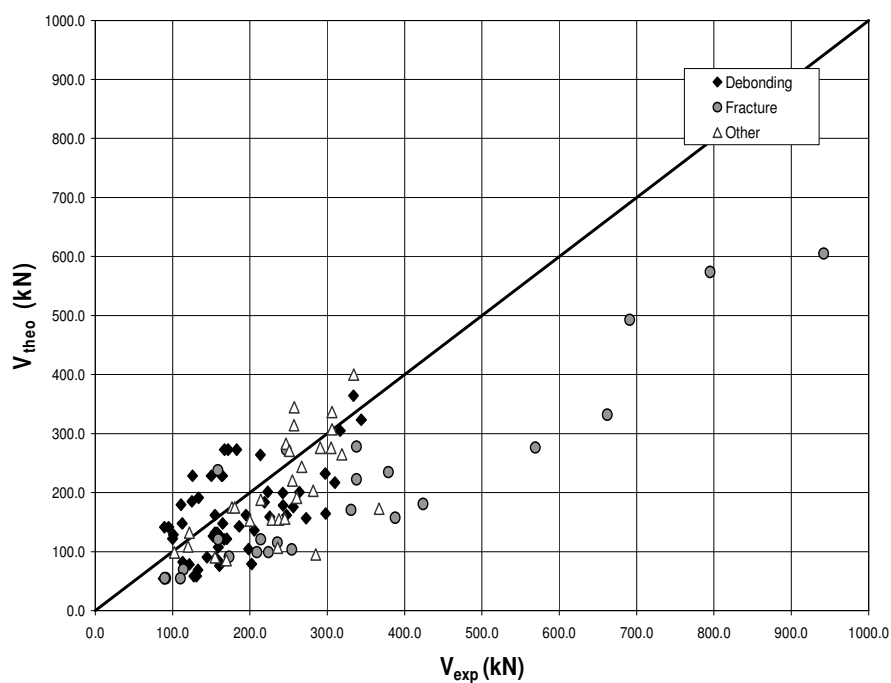
(d) AASHTO LRFD

Figure B.96. Comparison between Analytical Predictions of total shear capacity by
Monti and Liotta (2005) and Experimental Results
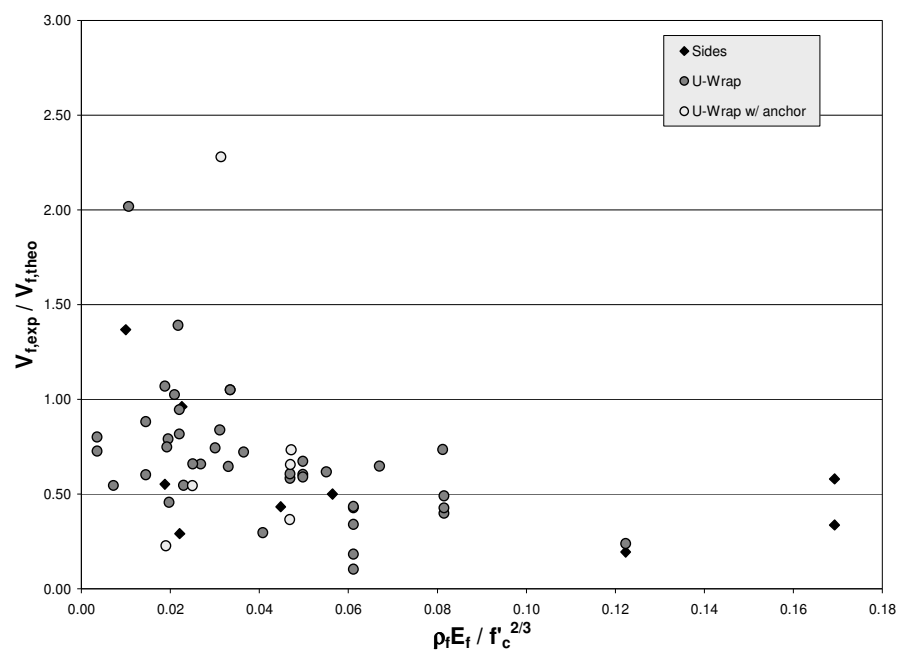
Figure B.97. $V_{f,\exp}/V_{f,theo}$ in terms of $E_f \rho_f /(f_c^{'})^{2/3}$ - FRP Debonding
Cao et al. (2005)
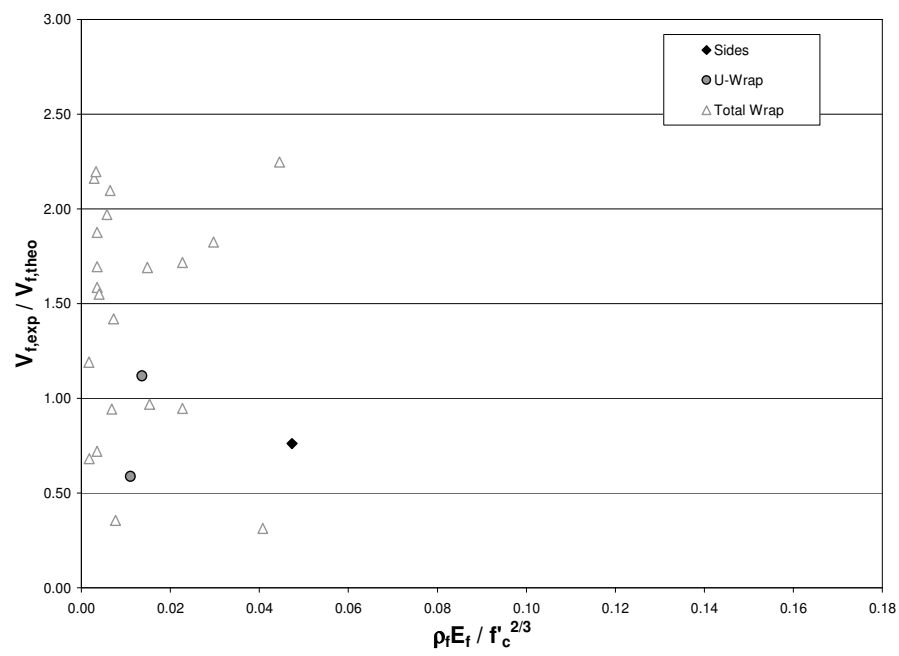
Figure B.98. $V_{f,\exp}/V_{f,theo}$ in terms of $E_f \rho_f /(f_c^{'})^{2/3}$ - FRP Fracture
Cao et al. (2005)
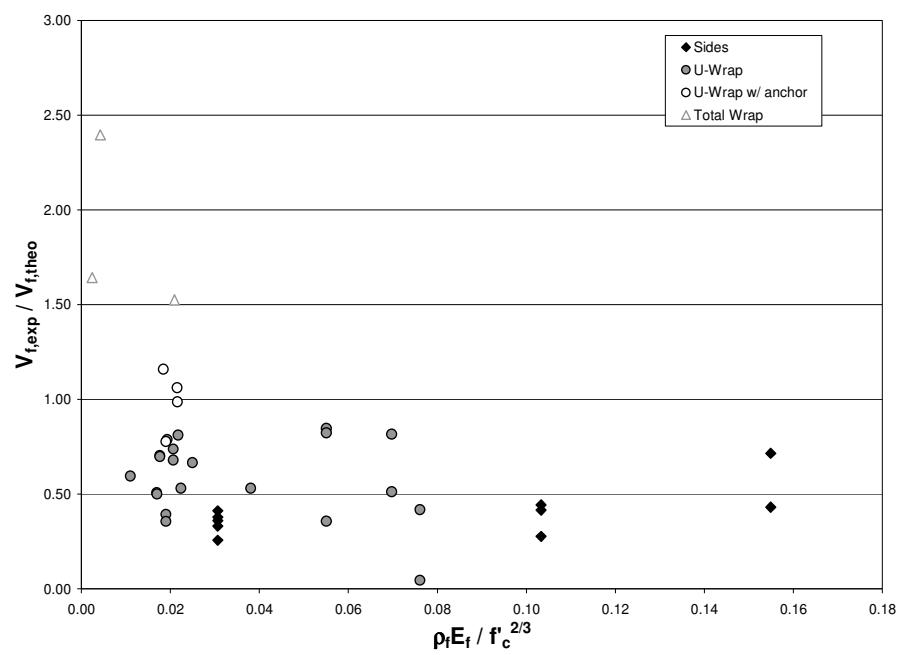
Figure B.99. $V_{f,\exp}/V_{f,theo}$ in terms of $E_f \rho_f /(f_c^{'})^{2/3}$ - Other Failure Modes
Cao et al. (2005)
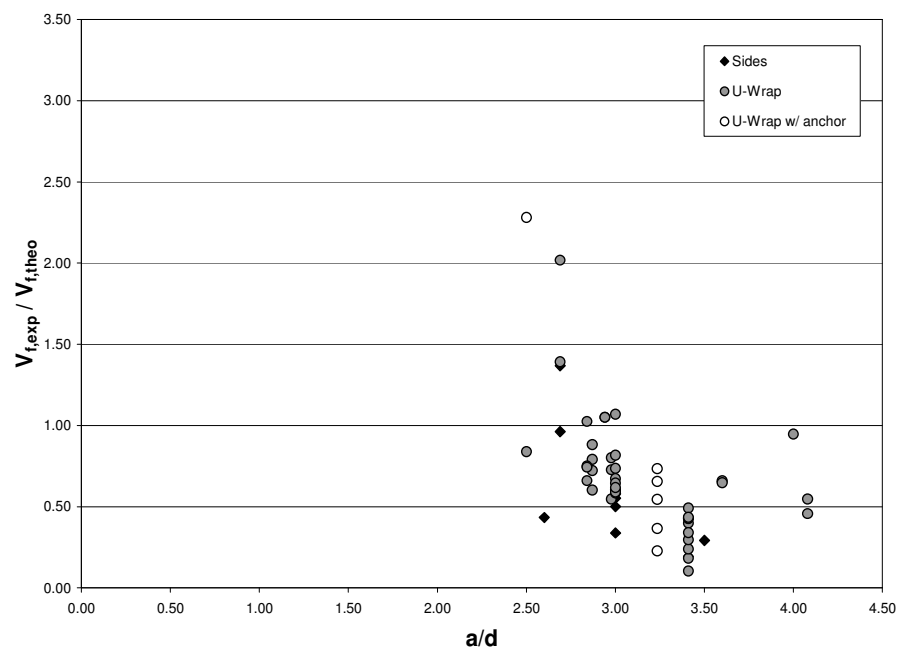
Figure B.100. $V_{f,\exp}/V_{f,theo}$ in terms of a/d – FRP Debonding
Cao et al. (2005)
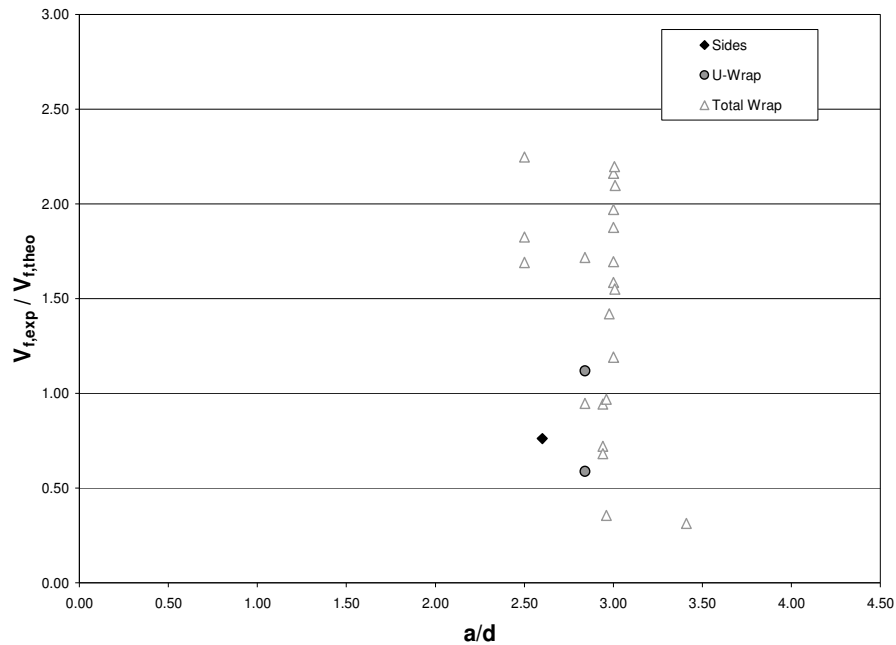
Figure B.101. $V_{f,\exp}/V_{f,theo}$ in terms of a/d – FRP Fracture
Cao et al. (2005)
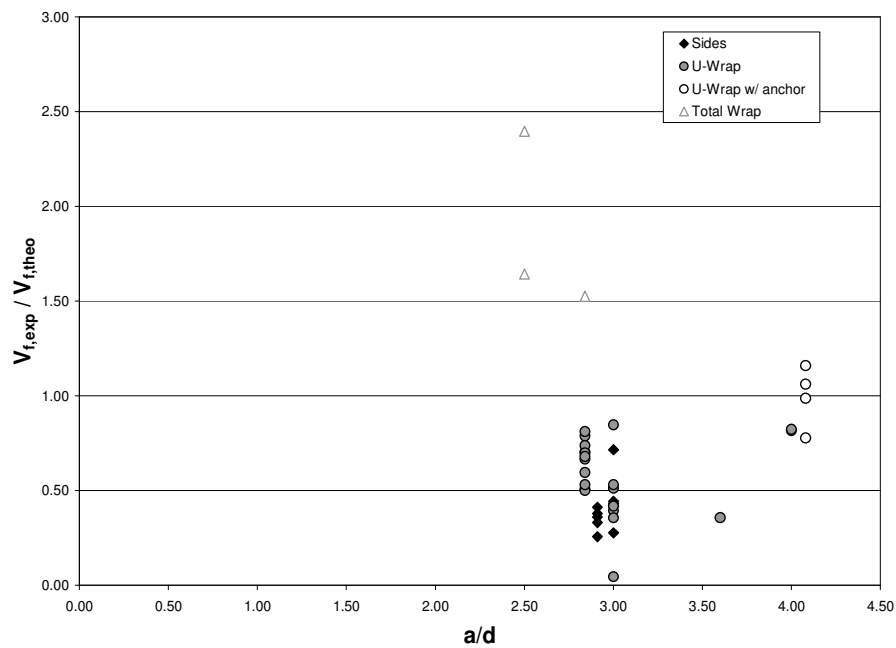
Figure B.102. $V_{f,\exp}/V_{f,theo}$ in terms of a/d – Other Failure Modes
Cao et al. (2005)
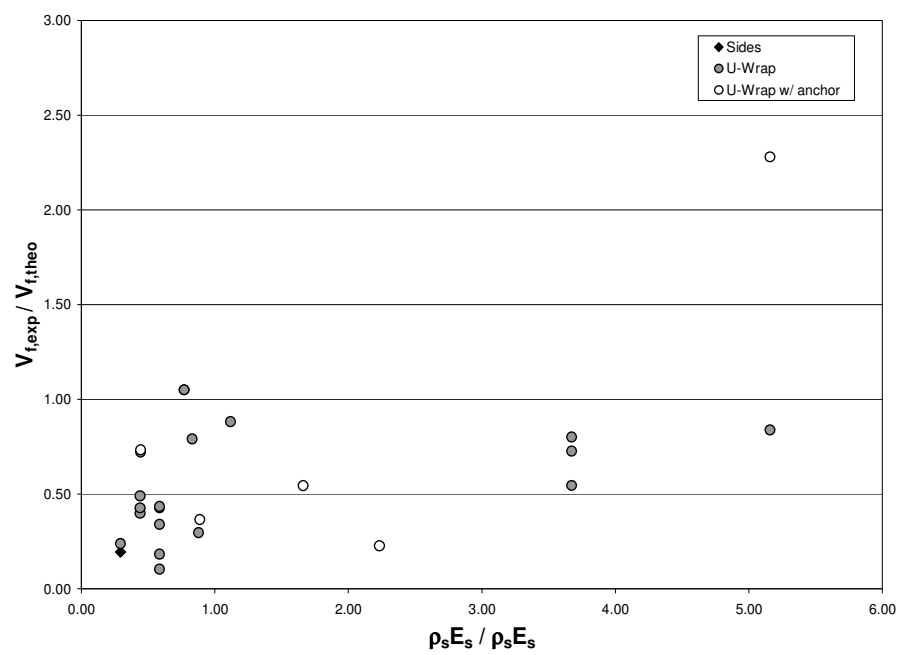
Figure B.103. $V_{f,\exp}/V_{f,theo}$ in terms of $\rho_s E_s / \rho_f E_f$ – FRP Debonding
Cao et al. (2005)

Figure B.104. $V_{f,\exp}/V_{f,theo}$ in terms of $\rho_s E_s / \rho_f E_f$ – FRP Fracture
Cao et al. (2005)

Figure B.105. $V_{f,\exp}/V_{f,theo}$ in terms of $\rho_s E_s/\rho_f E_f$ – Other Failure Modes
Cao et al. (2005)
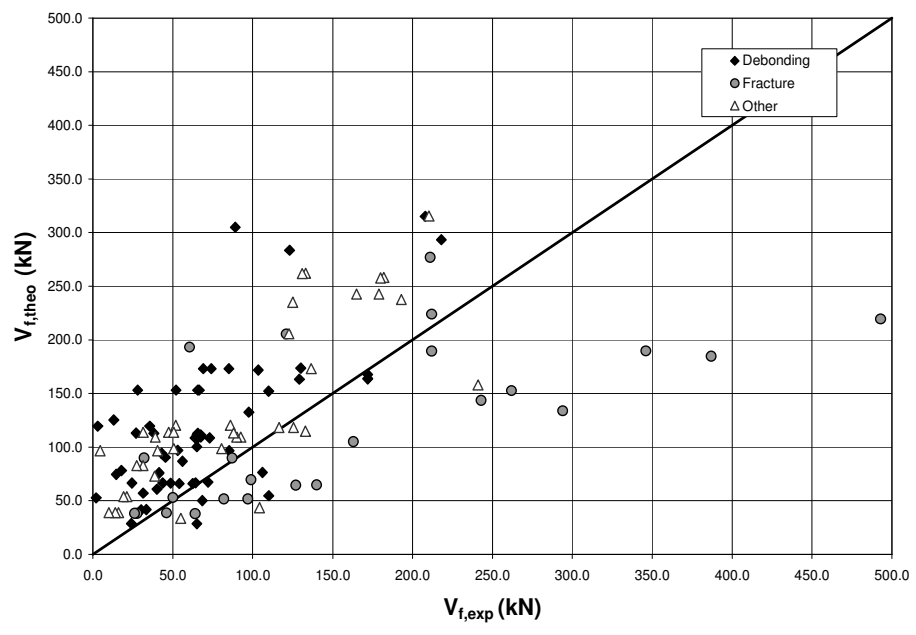
Figure B.106. Comparison between Predictions by Cao et al. (2005) and Experimental
Results
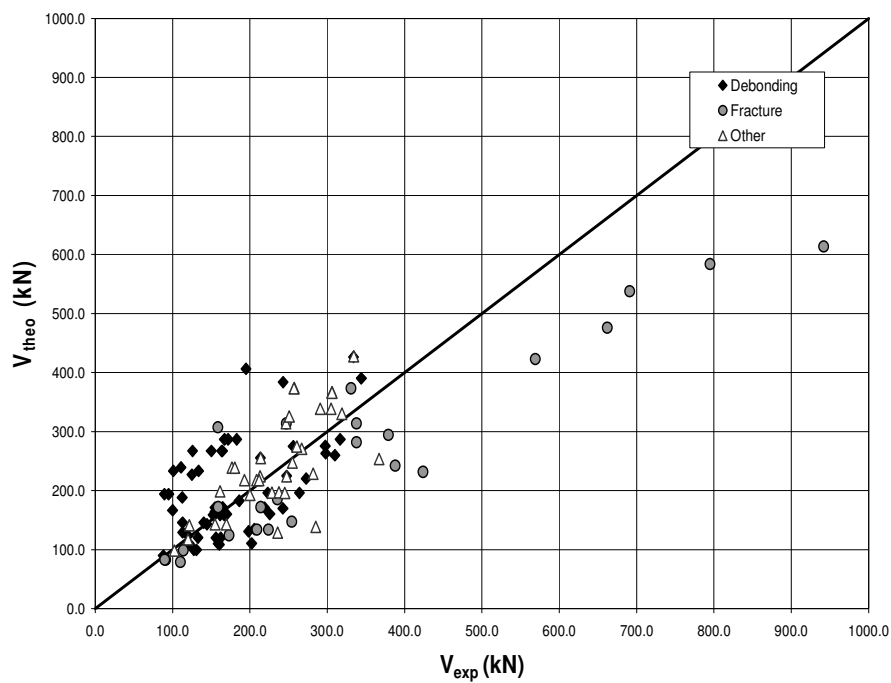
(a) ACI 318-05
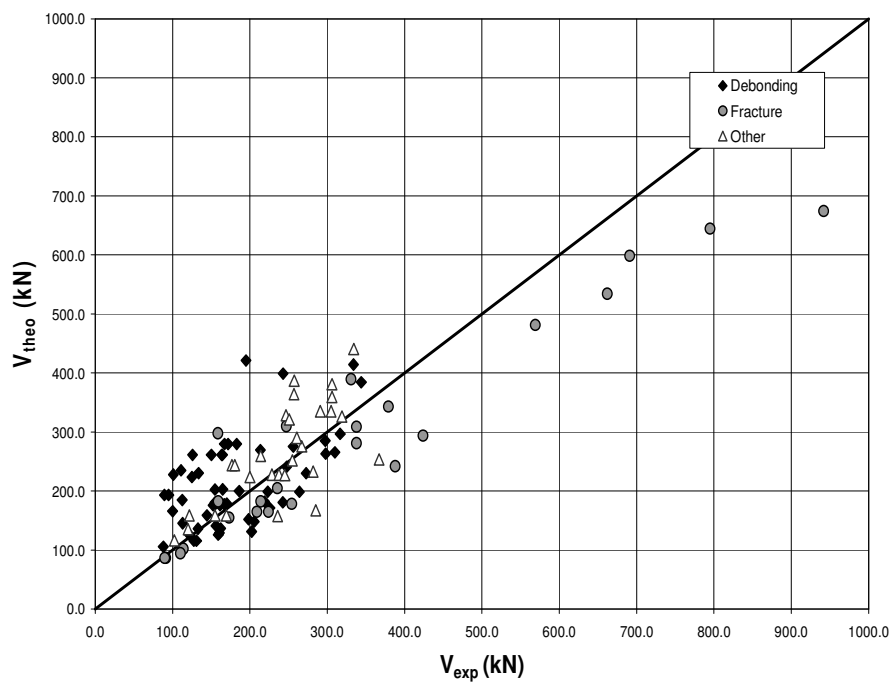
(b) Eurocode 2

Figure B.107. Comparison between Analytical Predictions of total shear capacity by Cao et al. (2005) and Experimental Results
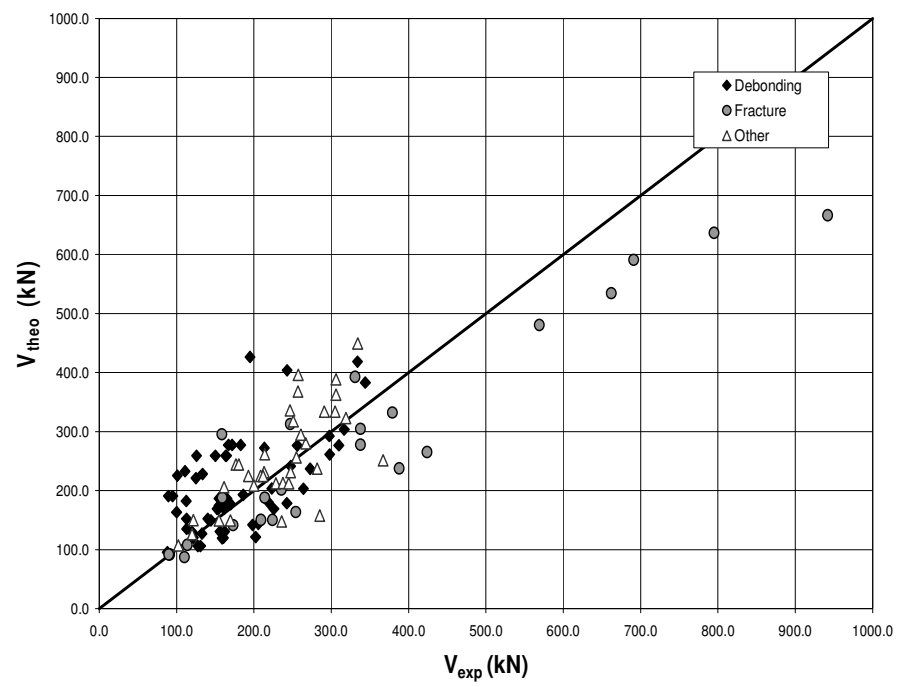
(c) CSA A23.3-94
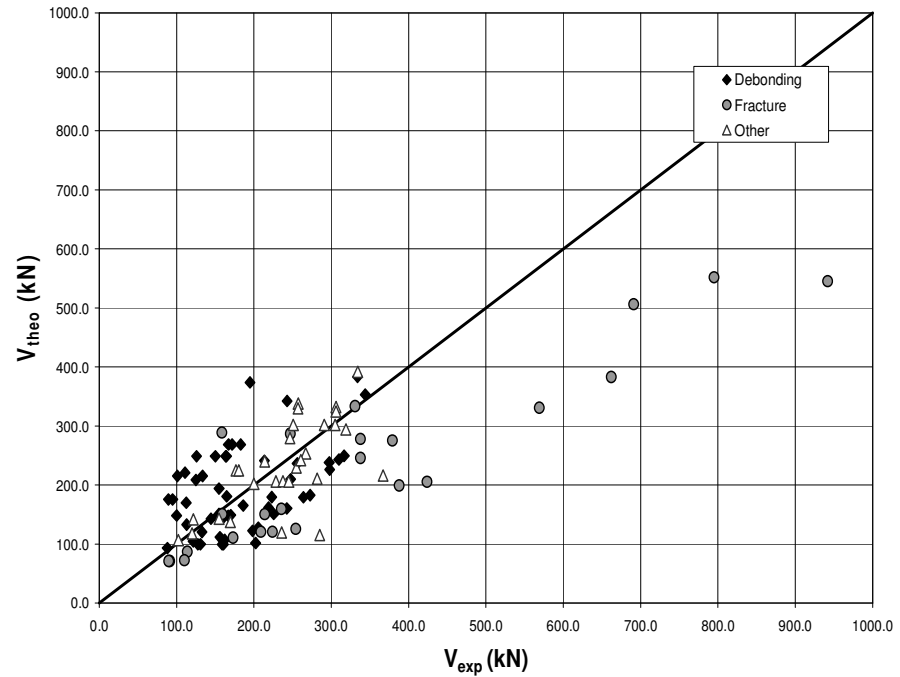
(d) AASHTO LRFD

Figure B.108. Comparison between Analytical Predictions of total shear capacity by Cao et al. (2005) and Experimental Results
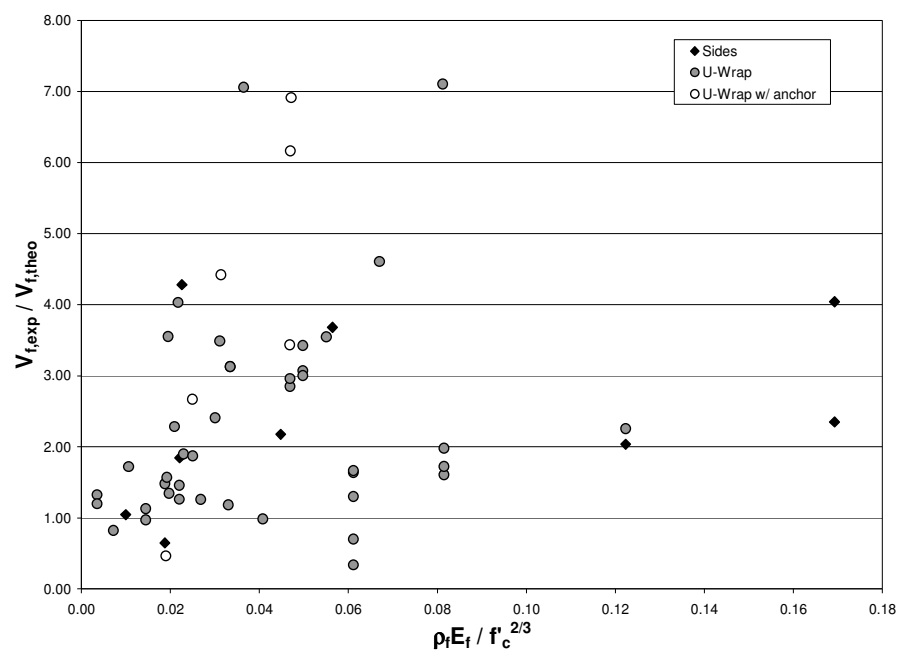
Figure B.109. $V_{f,\exp}/V_{f,theo}$ in terms of $E_f\rho_f/(f_c^{'})^{2/3}$ - FRP Debonding
Zhang and Hsu (2005)
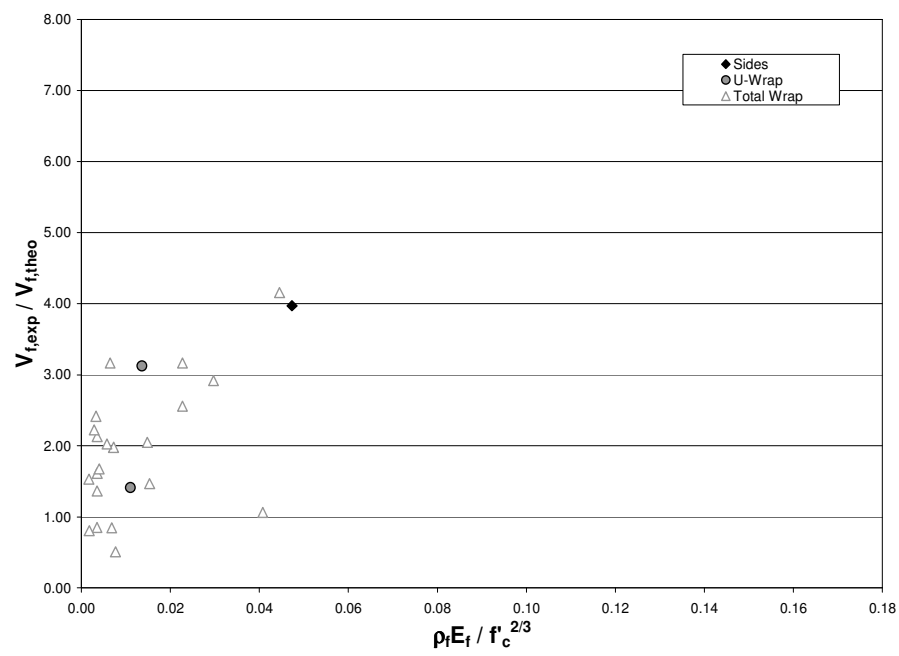
Figure B.110. $V_{f,\exp}/V_{f,theo}$ in terms of $E_f\rho_f/(f_c^{'})^{2/3}$ - FRP Fracture
Zhang and Hsu (2005)
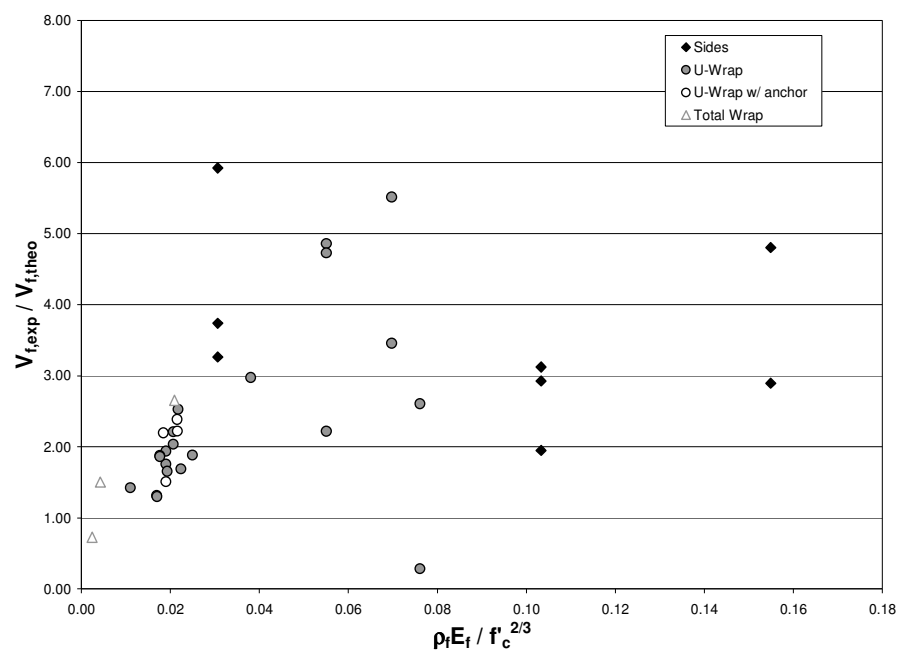
Figure B.111. $V_{f,\exp} / V_{f,theo}$ in terms of $E_f \rho_f / (f_c^{'})^{2/3}$ - Other Failure Modes
Zhang and Hsu (2005)
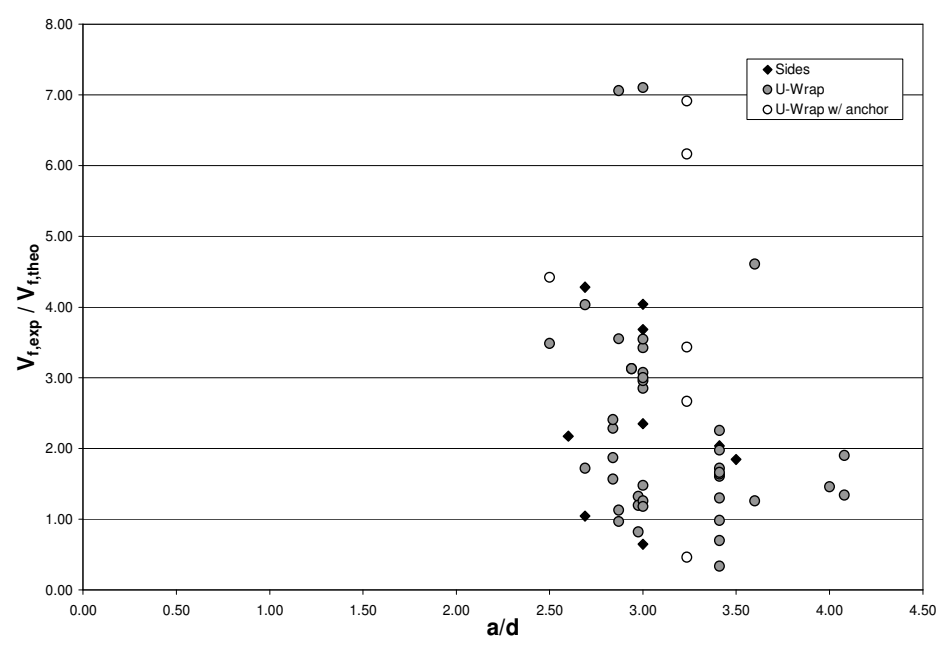
Figure B.112. $V_{f,\exp} / V_{f,theo}$ in terms of a/d – FRP Debonding
Zhang and Hsu (2005)
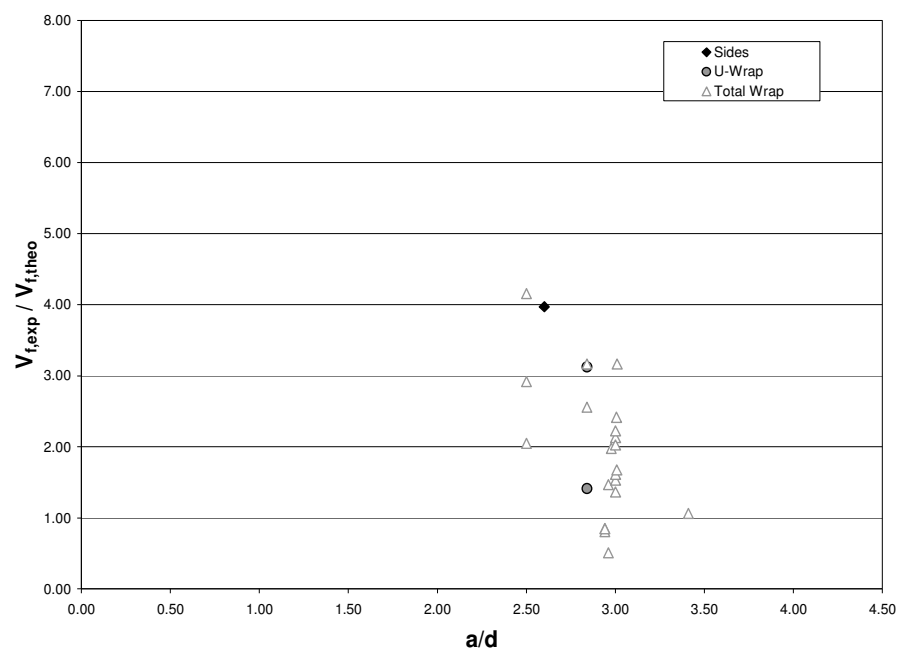
Figure B.113. $V_{f,\exp}/V_{f,theo}$ in terms of a/d – FRP Fracture
Zhang and Hsu (2005)
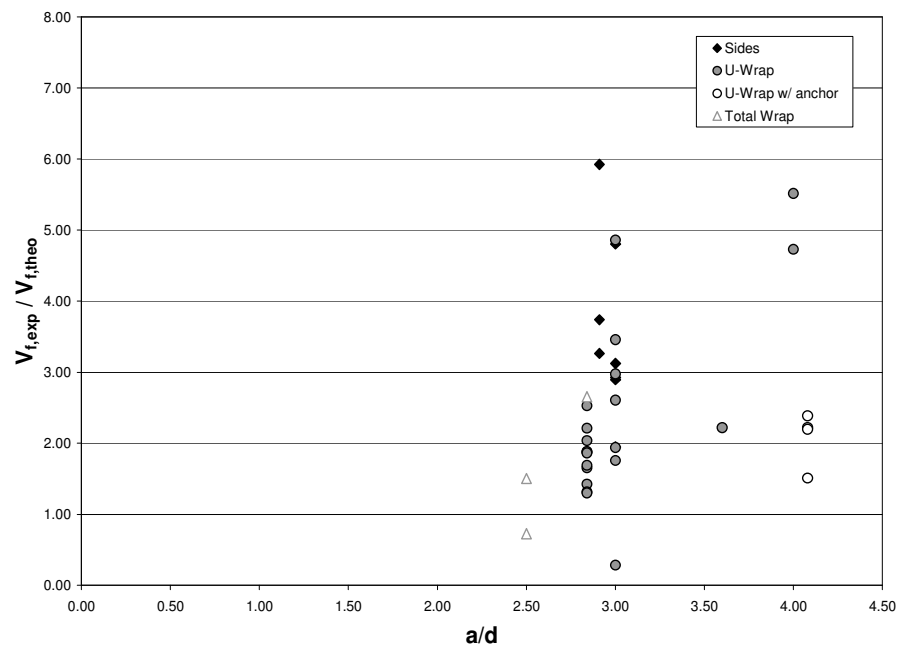
Figure B.114. $V_{f,\exp}/V_{f,theo}$ in terms of a/d – Other Failure Modes
Zhang and Hsu (2005)
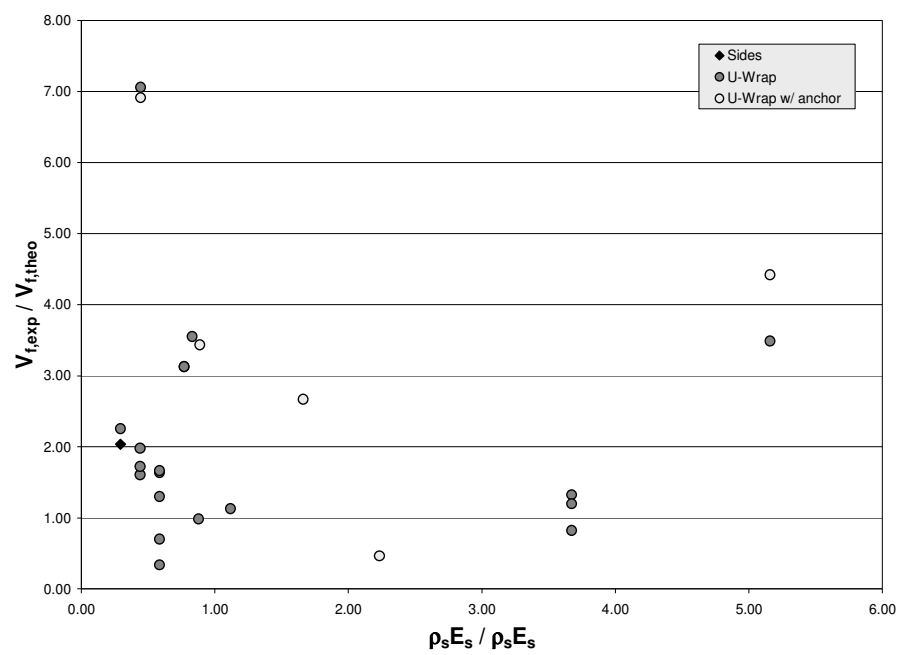
Figure B.115. $V_{f,\exp}/V_{f,theo}$ in terms of $\rho_s E_s / \rho_f E_f$ – FRP Debonding
Zhang and Hsu (2005)
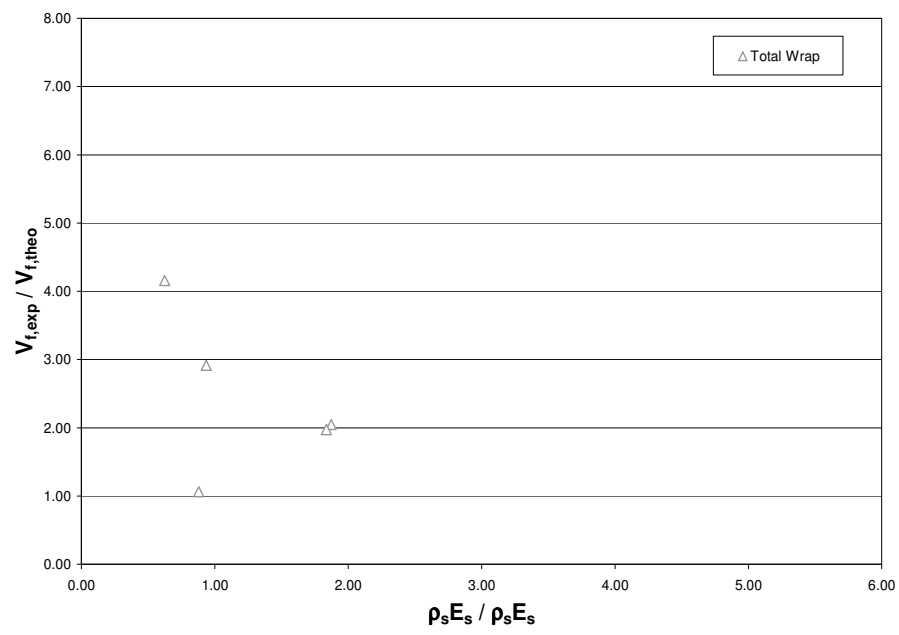
Figure B.116. $V_{f,\exp}/V_{f,theo}$ in terms of $\rho_s E_s / \rho_f E_f$ – FRP Fracture
Zhang and Hsu (2005)
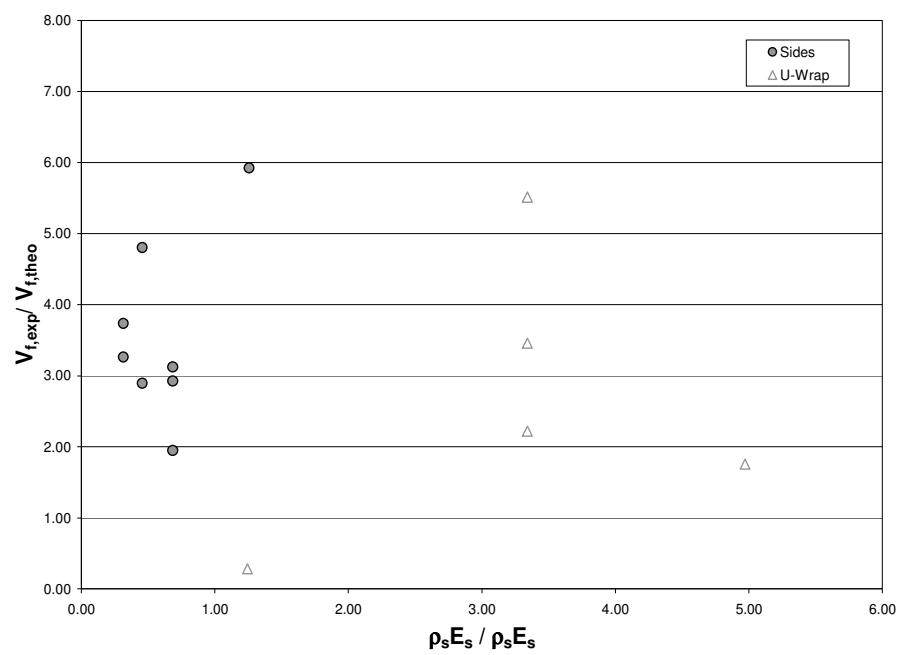
Figure B.117. $V_{f,\exp}/V_{f,theo}$ in terms of $\rho_s E_s / \rho_f E_f$ – Other Failure Modes
Zhang and Hsu (2005)

Figure B.118. Comparison between Predictions by Zhang and Hsu (2005) and
Experimental Results

(a) ACI 318-05
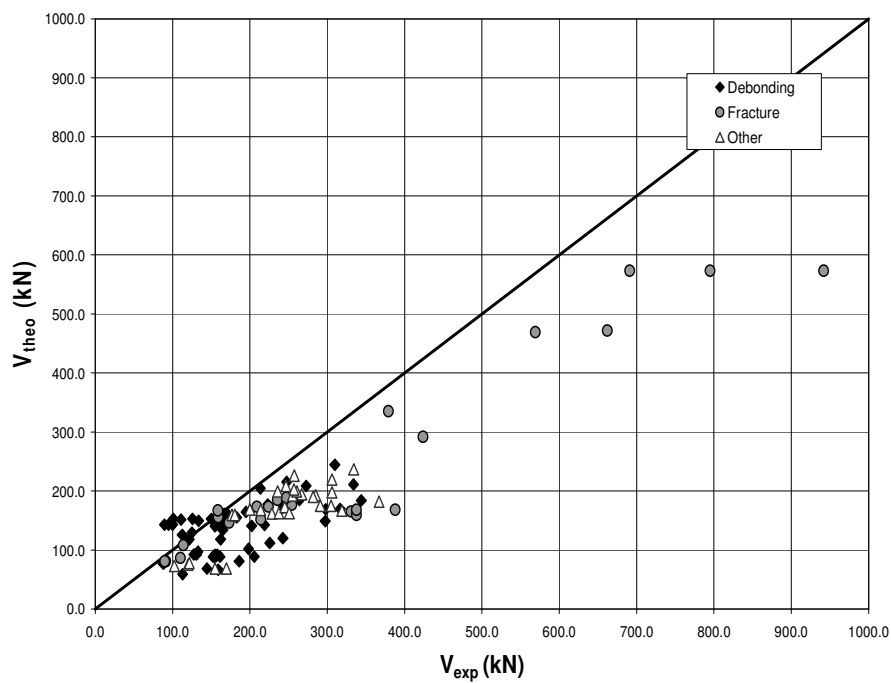
(b) Eurocode 2

Figure B.119. Comparison between Analytical Predictions of total shear capacity by
Zhang and Hsu (2005) and Experimental Results

(c) CSA A23.3-94

(d) AASHTO LRFD

Figure B.120. Comparison between Analytical Predictions of total shear capacity by
Zhang and Hsu (2005) and Experimental Results

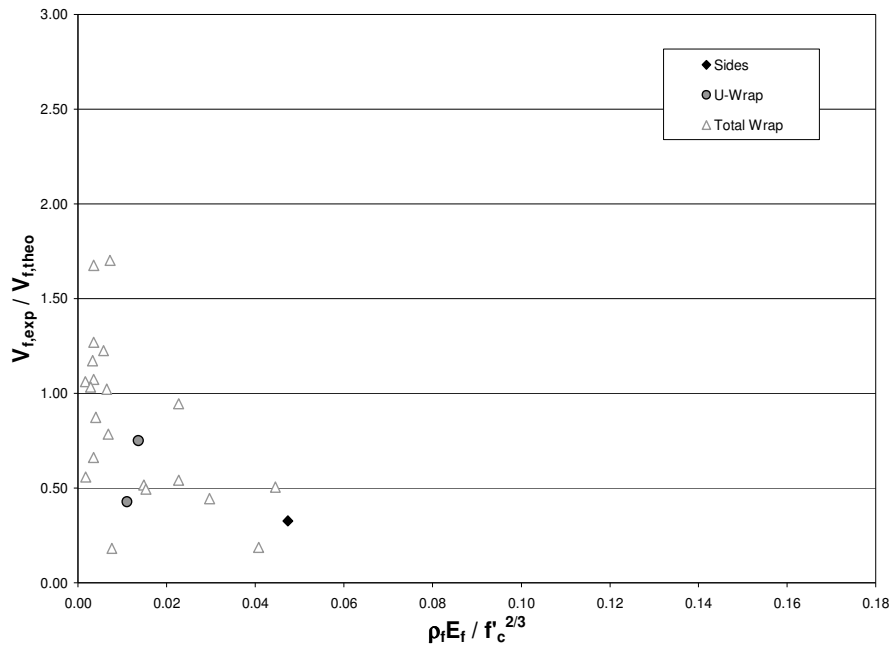Figure B.121. $V_{f,\exp}/V_{f,theo}$ in terms of $E_f\rho_f/(f_c^{'})^{2/3}$ - FRP Debonding
Carolin and Taljsten (2005)

Figure B.122. $V_{f,\exp}/V_{f,theo}$ in terms of $E_f\rho_f/(f_c^{'})^{2/3}$ - FRP Fracture
Carolin and Taljsten (2005)

Figure B.123 $V_{f,\exp}/V_{f,theo}$ in terms of $E_f \rho_f /(f_c^{'})^{2/3}$ - Other Failure Modes
Carolin and Taljsten (2005)
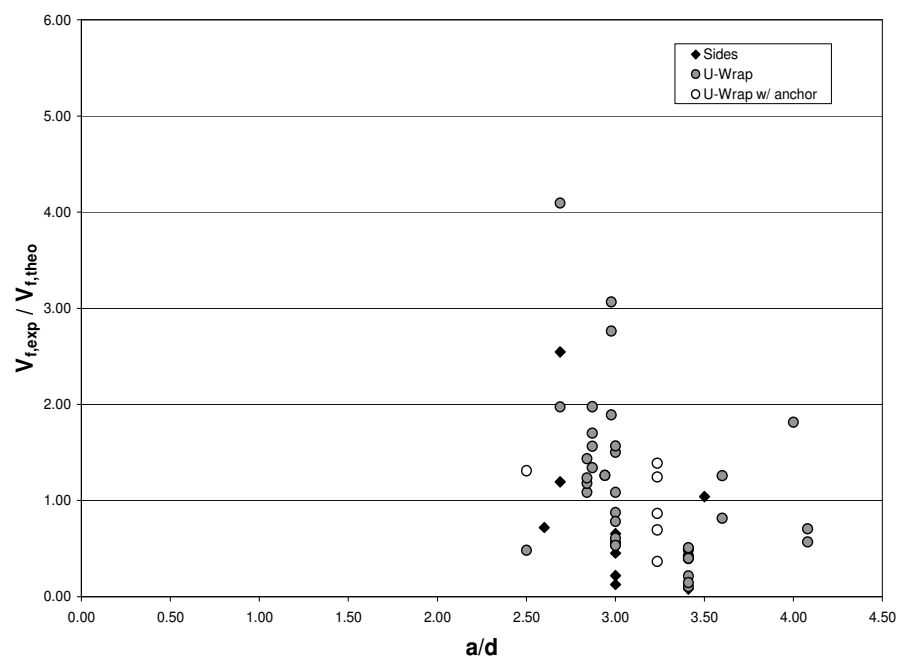
Figure B.124. $V_{f,\exp}/V_{f,theo}$ in terms of a/d – FRP Debonding
Carolin and Taljsten (2005)
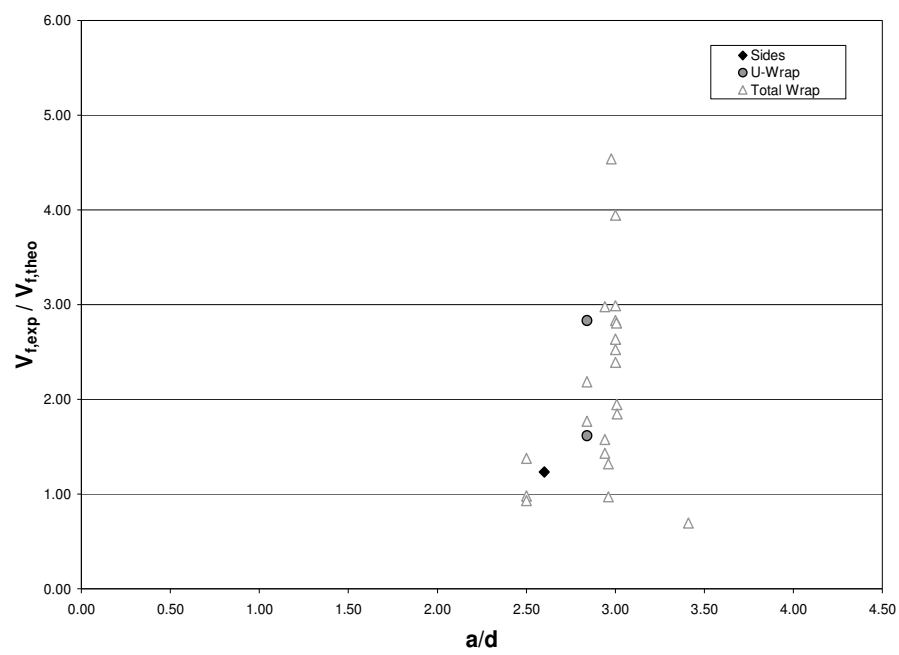
Figure B.125. $V_{f,\exp}/V_{f,theo}$ in terms of a/d – FRP Fracture
Carolin and Taljsten (2005)

Figure B.126. $V_{f,\exp}/V_{f,theo}$ in terms of a/d – Other Failure Modes
Carolin and Taljsten (2005)

Figure B.127. $V_{f,\exp}/V_{f,theo}$ in terms of $\rho_s E_s / \rho_f E_f$ – FRP Debonding
Carolin and Taljsten (2005)

Figure B.128. $V_{f,\exp}/V_{f,theo}$ in terms of $\rho_s E_s / \rho_f E_f$ – FRP Fracture
Carolin and Taljsten (2005)
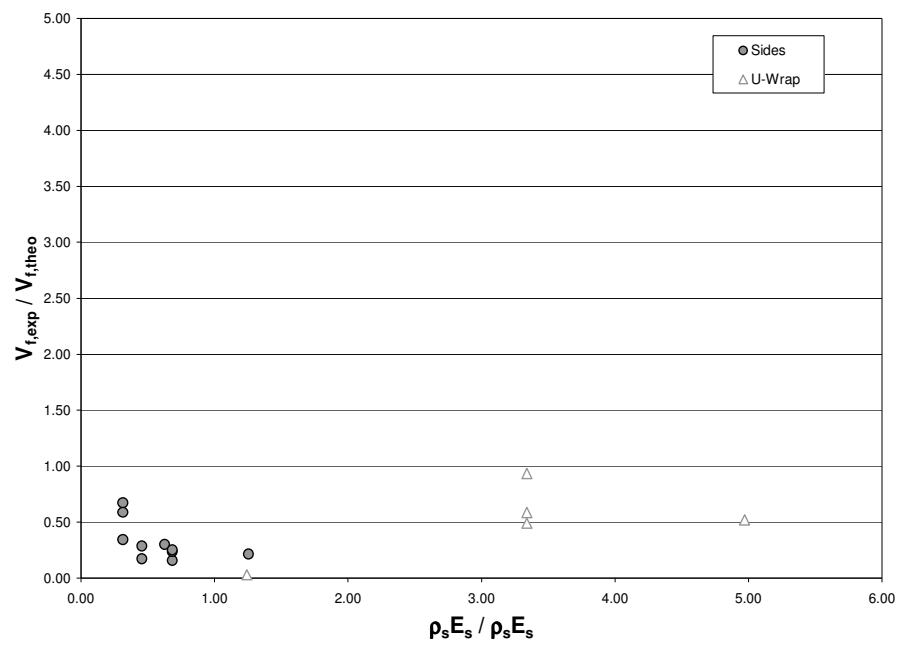
Figure B.129. $V_{f,\exp}/V_{f,theo}$ in terms of $\rho_s E_s / \rho_f E_f$ – Other Failure Modes
Carolin and Taljsten (2005)

Figure B.130. Comparison between Predictions by Carolin and Taljsten (2005) and
Experimental Results

(a) ACI 318-05
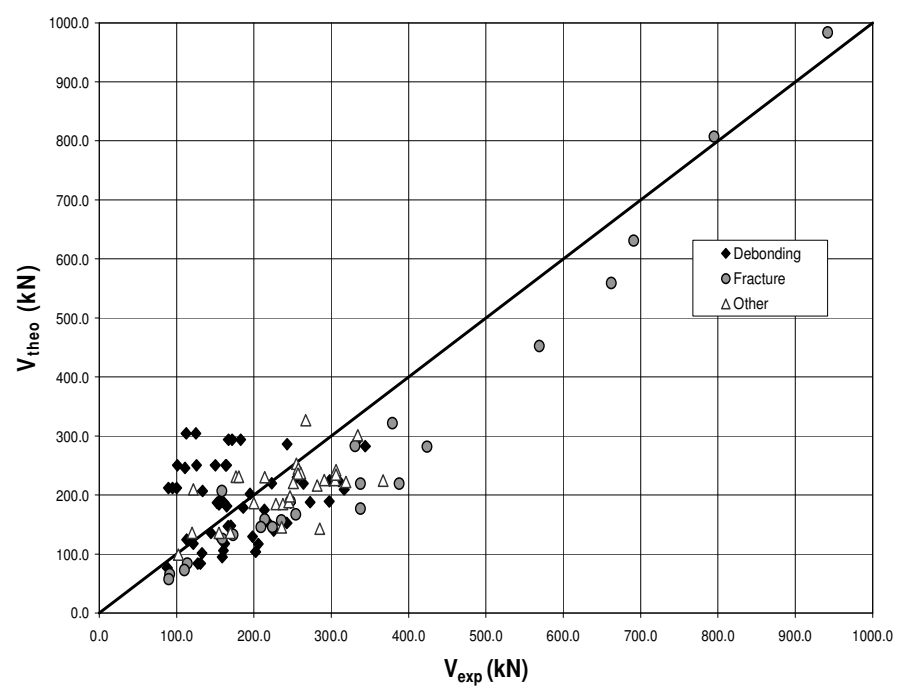
(b) Eurocode 2

Figure B.131. Comparison between Analytical Predictions of total shear capacity by
Carolin and Taljsten (2005) and Experimental Results
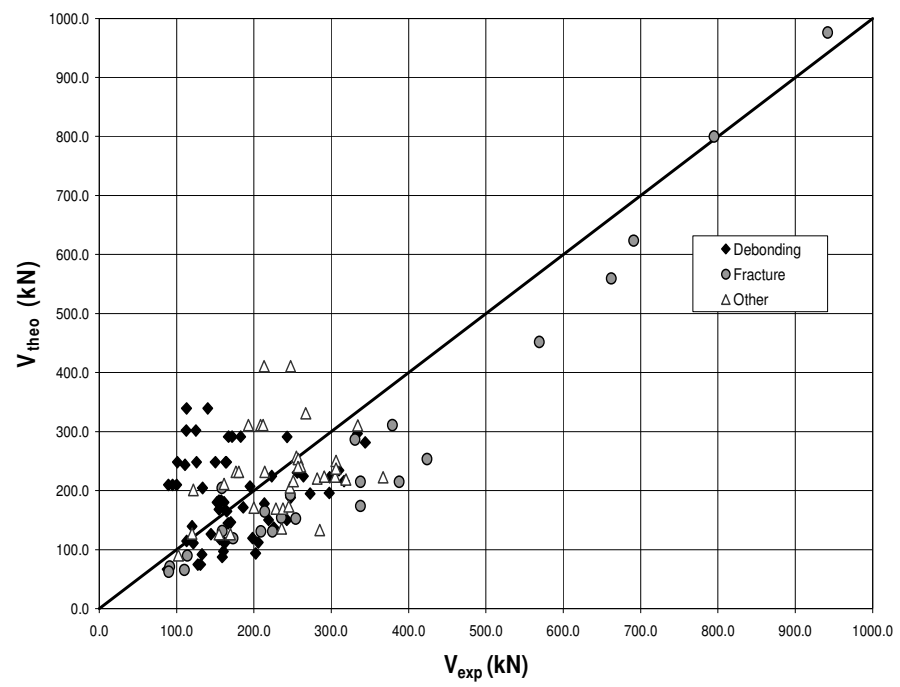
(c) CSA A23.3-94

(d) AASHTO LRFD

Figure B.132. Comparison between Analytical Predictions of total shear capacity by
Carolin and Taljsten (2005) and Experimental Results

APPENDIX C

COMPARISON BETWEEN EXPERIMENTAL OBSERVATIONS
AND ANALYTICAL PREDICTIONS
BY DESIGN GUIDELINES
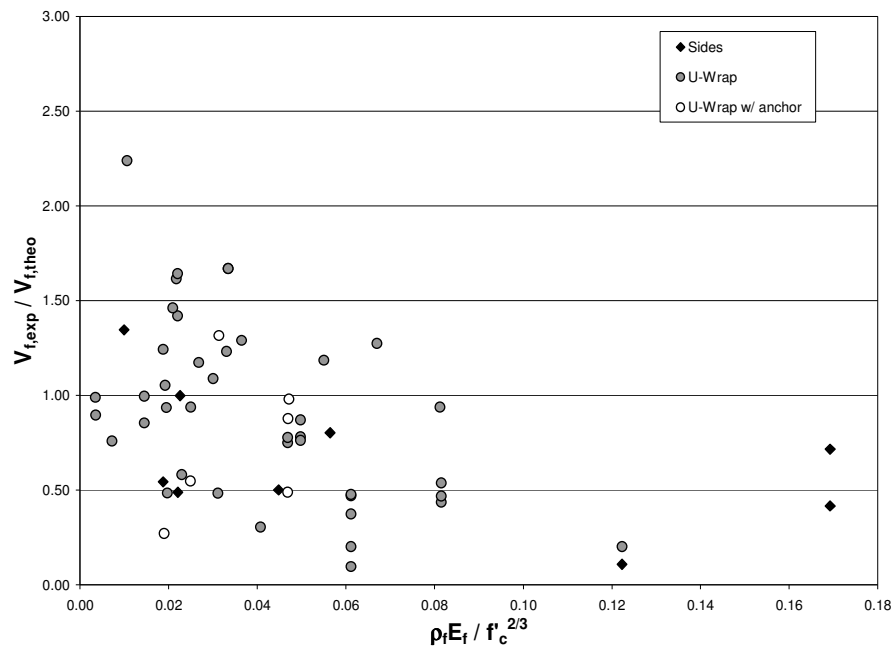
Figure C.1. $V_{f,\exp}/V_{f,theo}$ in terms of $E_f\rho_f/(f_c^{'})^{2/3}$ - FRP Debonding
fib TG 9.3
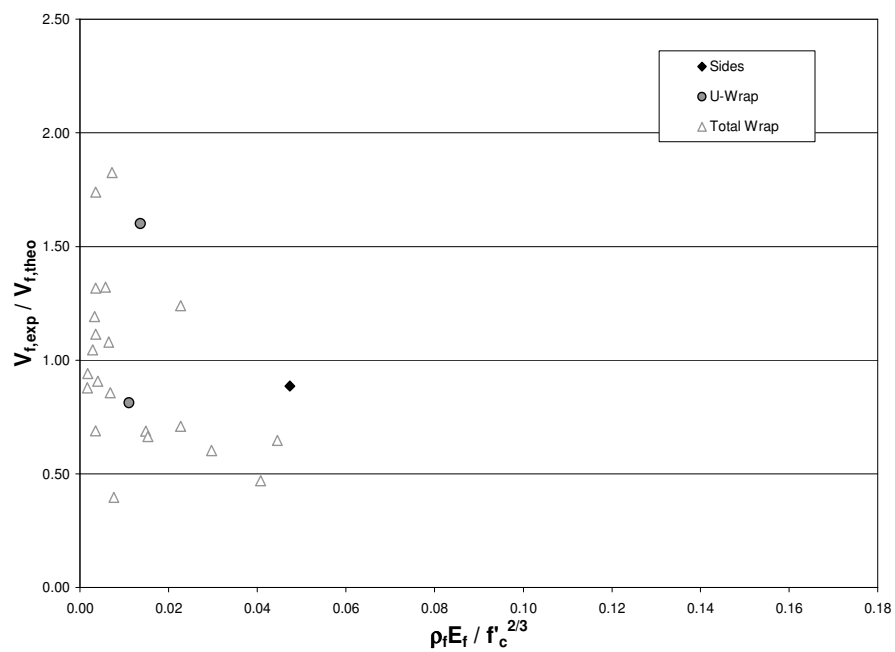
Figure C.2. $V_{f,\exp}/V_{f,theo}$ in terms of $E_f\rho_f/(f_c^{'})^{2/3}$ - FRP Fracture
fib TG 9.3
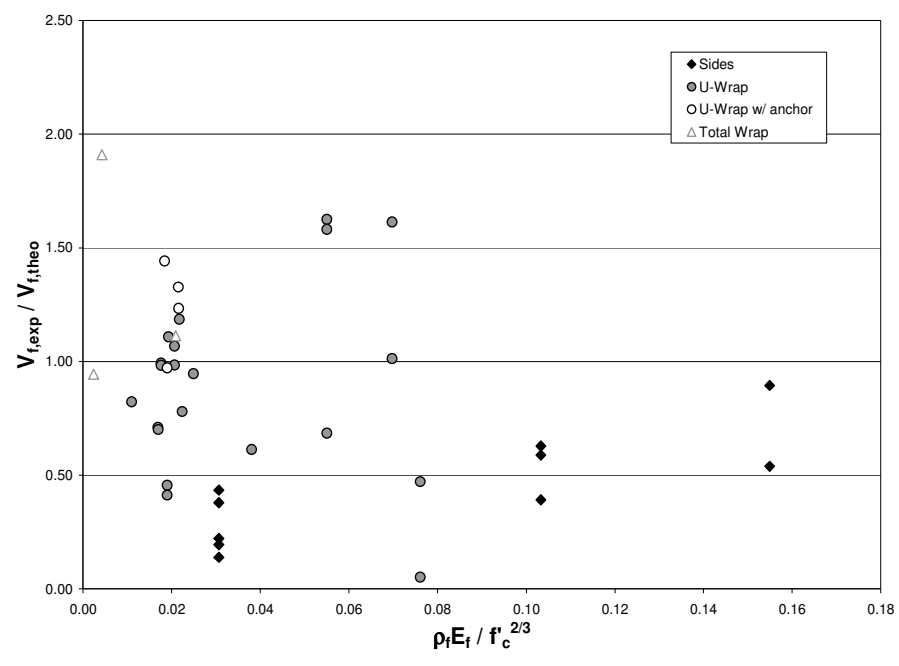
Figure C.3. $V_{f,\exp}/V_{f,theo}$ in terms of $E_f \rho_f/(f_c')^{2/3}$ - Other Failure Modes
fib TG 9.3
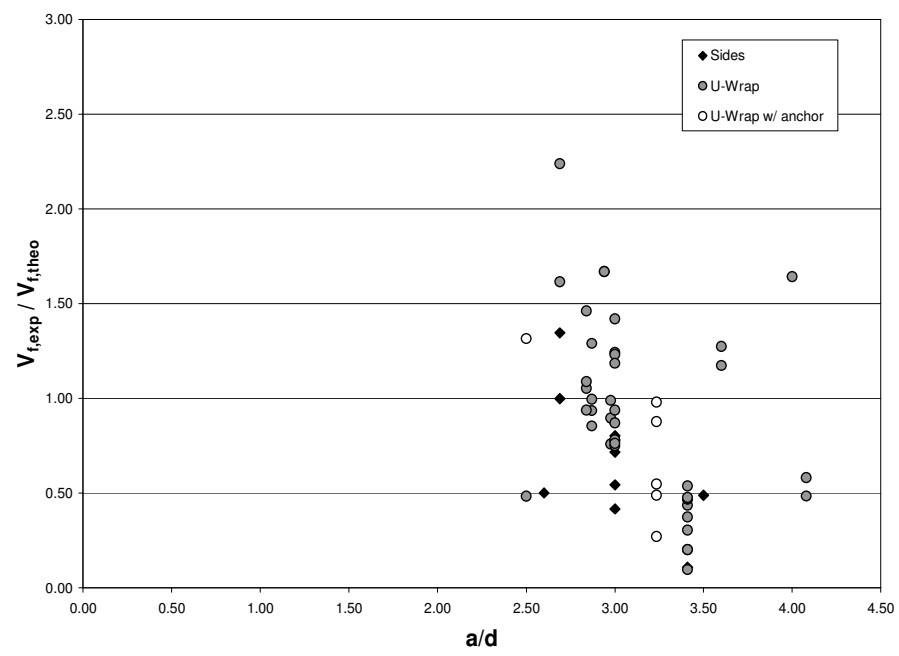
Figure C.4. $V_{f,\exp}/V_{f,theo}$ in terms of a/d - FRP Debonding
fib TG 9.3
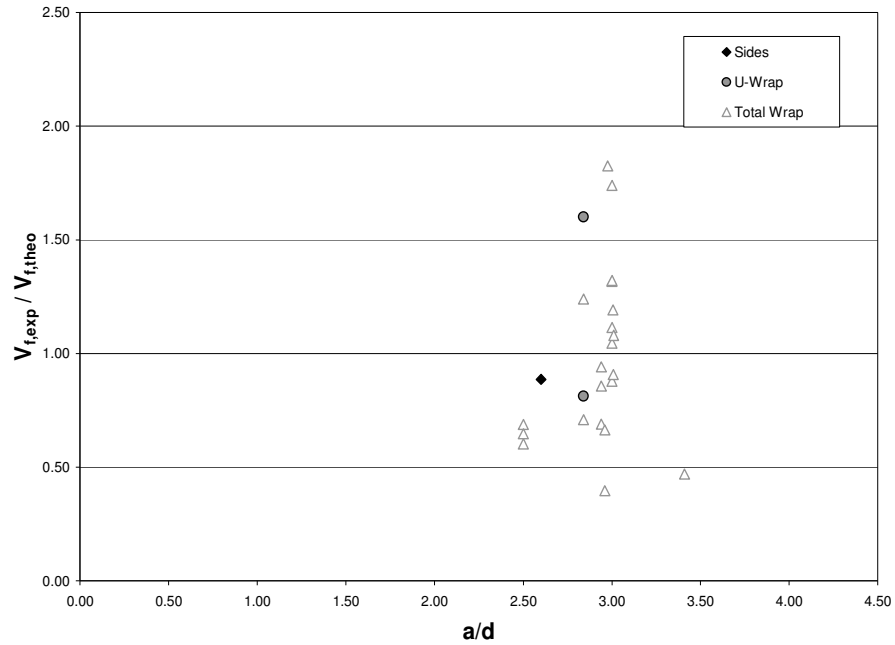
Figure C.5. $V_{f,\exp}/V_{f,theo}$ in terms of a/d - FRP Fracture
fib TG 9.3
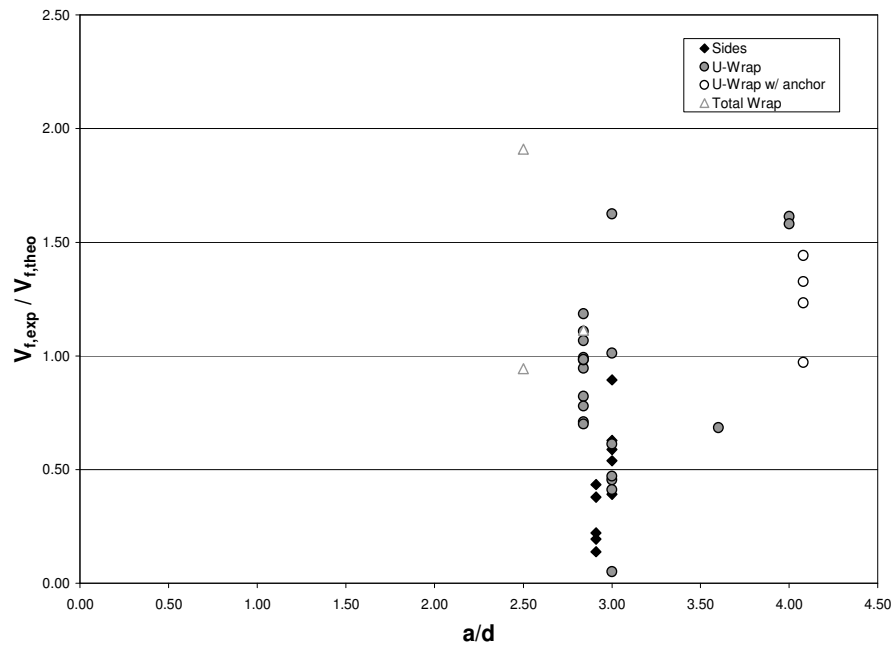
Figure C.6. $V_{f,\exp}/V_{f,theo}$ in terms of a/d - Other Failure Modes
fib TG 9.3
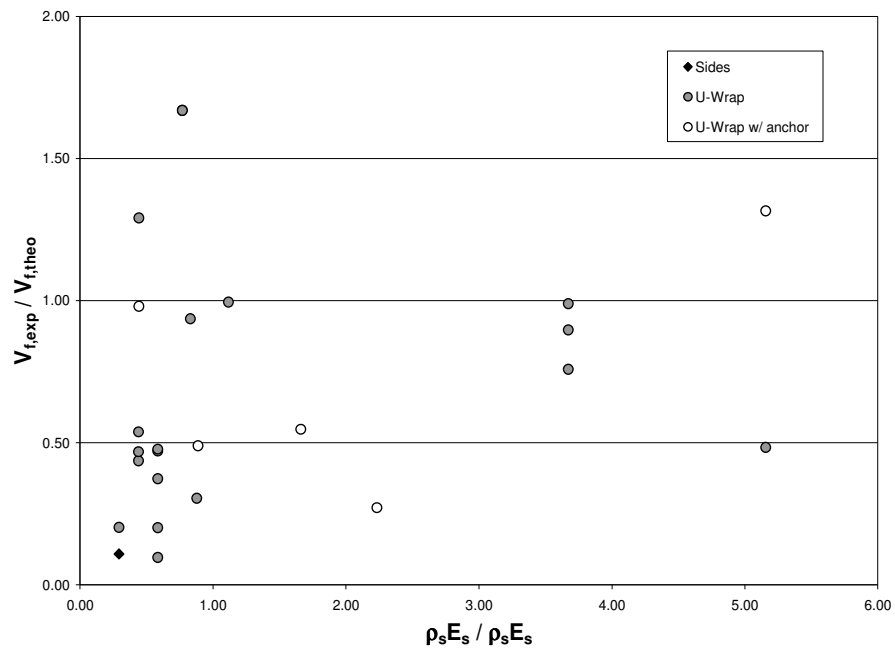
Figure C.7. $V_{f,\exp}/V_{f,theo}$ in terms of $\rho_s E_s / \rho_f E_f$ - FRP Debonding
fib TG 9.3
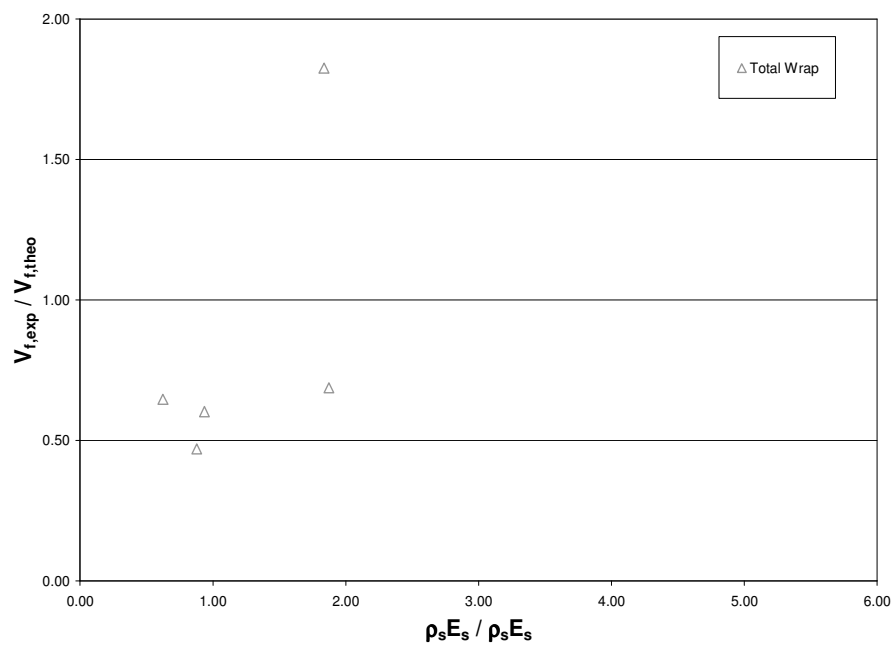
Figure C.8. $V_{f,\exp}/V_{f,theo}$ in terms of $\rho_s E_s / \rho_f E_f$ - FRP Fracture
fib TG 9.3
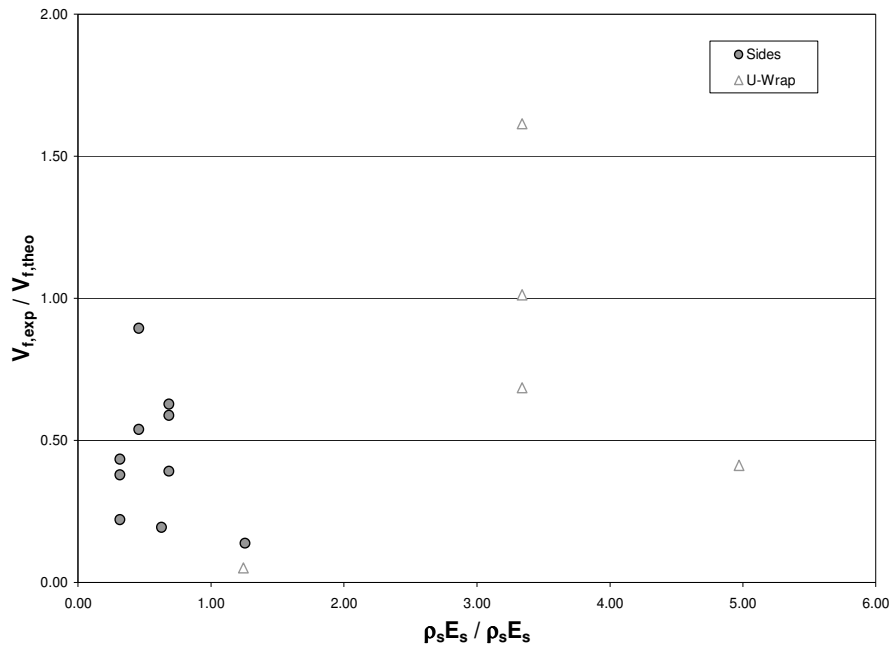
Figure C.9. $V_{f,\exp}/V_{f,theo}$ in terms of $\rho_s E_s / \rho_f E_f$ - Other Failure Modes
fib TG 9.3
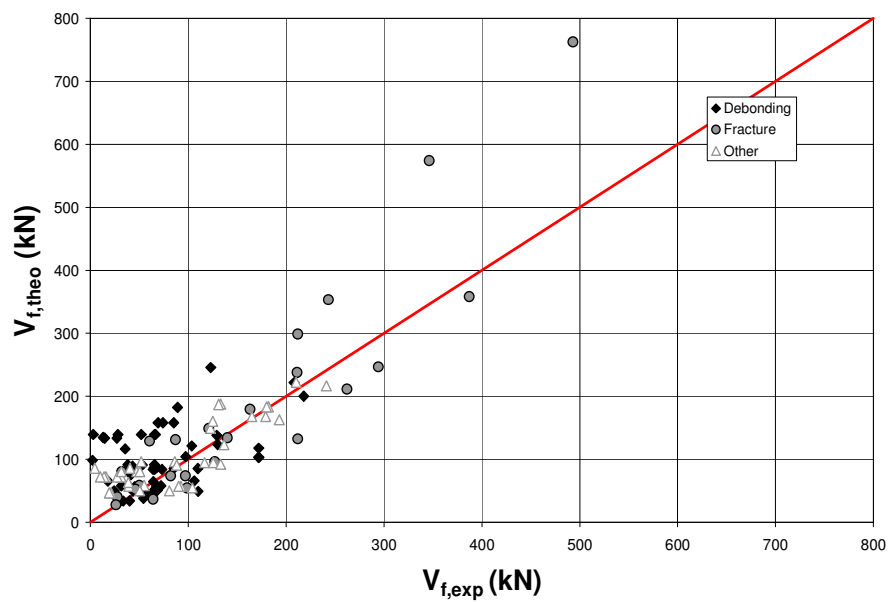
Figure C.10. Comparison between Analytical Predictions of FRP shear contribution by
fib-TG 9.3 and Experimental Results
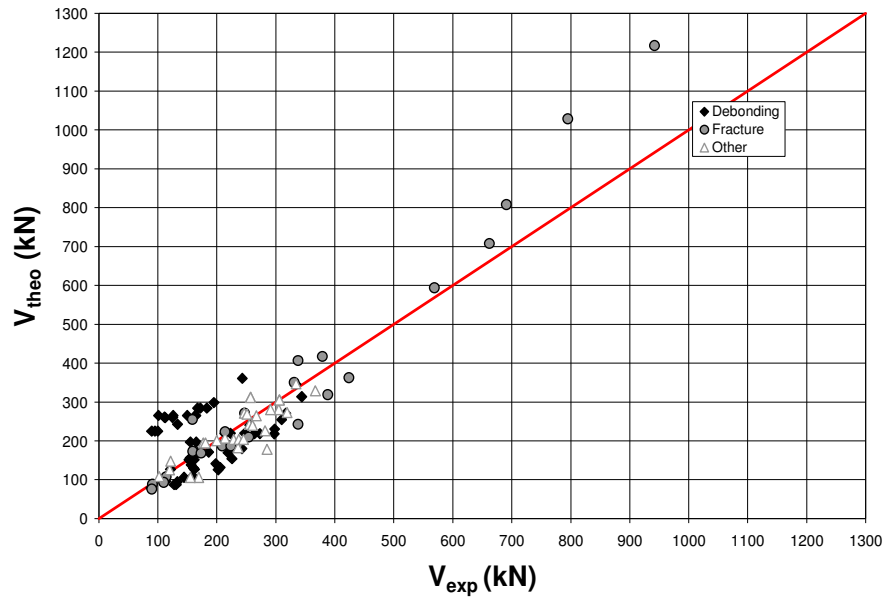
Figure C.11. Comparison between Analytical Predictions of total shear capacity by fib-TG 9.3 and Experimental Results
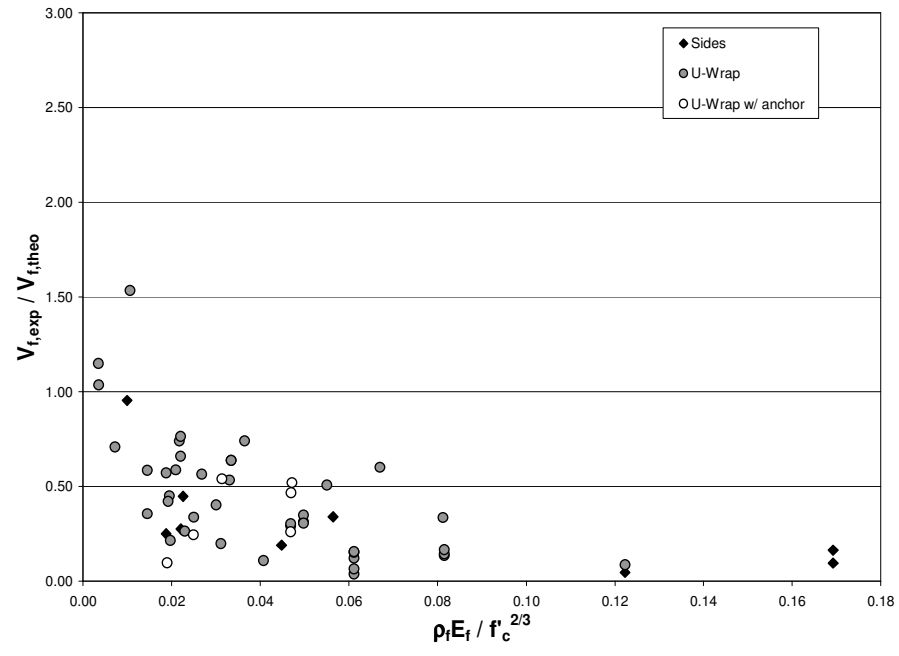
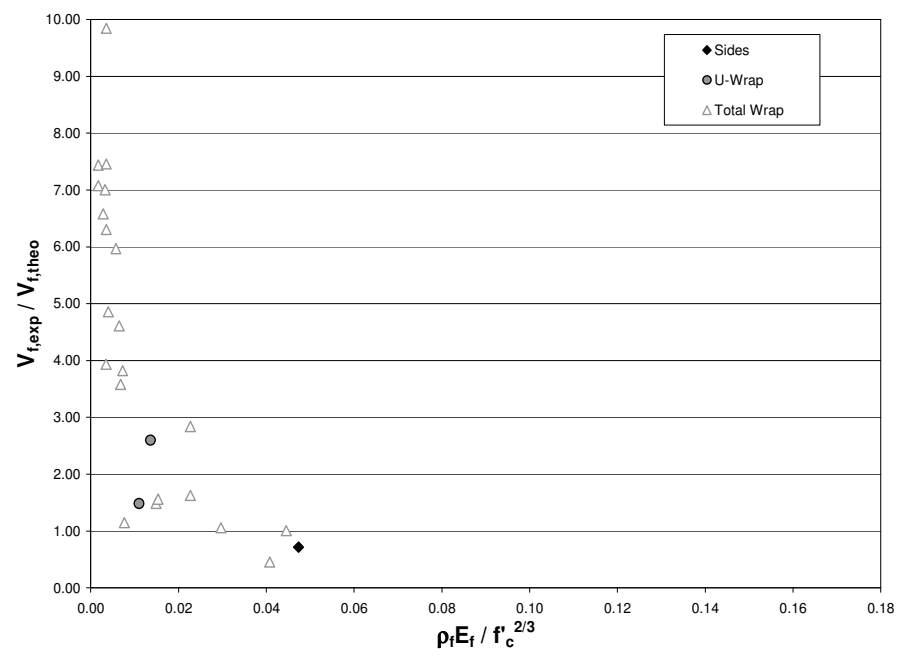Figure C.32. $V_{f,\exp}/V_{f,theo}$ in terms of $E_f \rho_f /(f_c^{'})^{2/3}$ - FRP Debonding JSCE Recommendations

Figure C.43. $V_{f,exp}/V_{f,theo}$ in terms of $E_f\rho_f/(f_c')^{2/3}$ - FRP Fracture
JSCE Recommendations
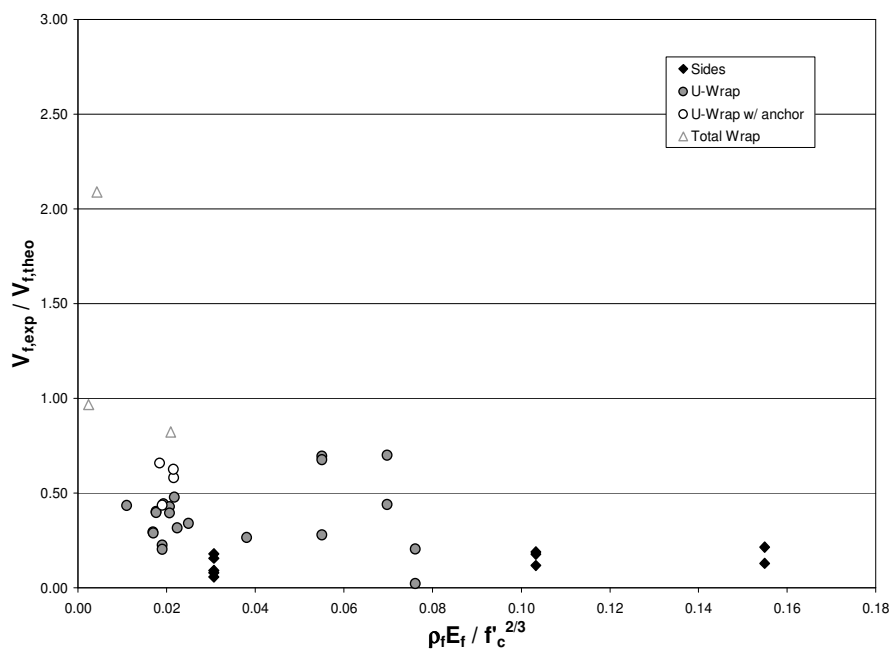
Figure C.54. $V_{f,exp}/V_{f,theo}$ in terms of $E_f\rho_f/(f_c')^{2/3}$ - Other Failure Modes
JSCE Recommendations
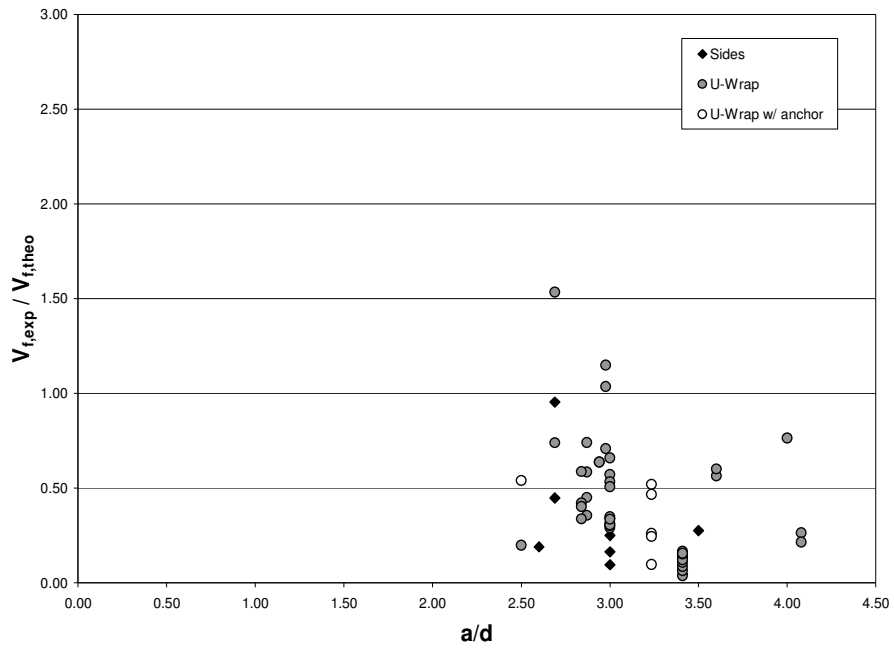
Figure C.65. $V_{f,\exp}/V_{f,theo}$ in terms of a/d - FRP Debonding
JSCE Recommendations
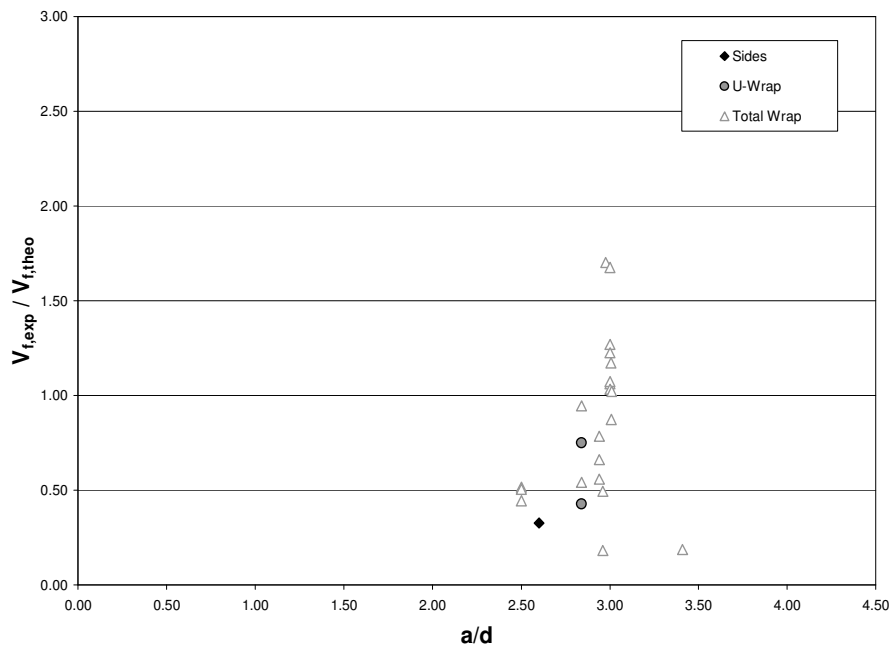
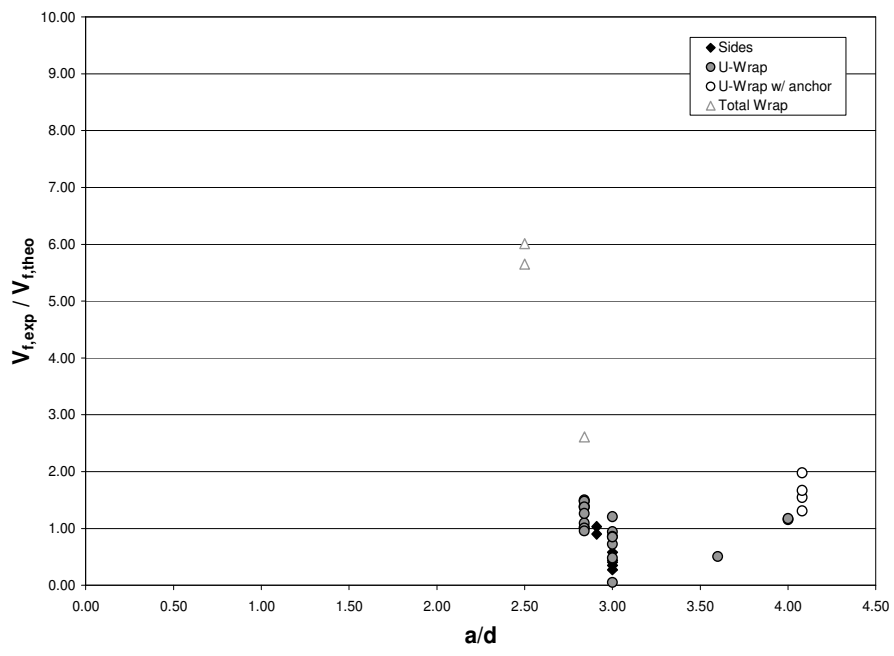Figure C.76. $V_{f,\exp}/V_{f,theo}$ in terms of a/d - FRP Fracture
JSCE Recommendations
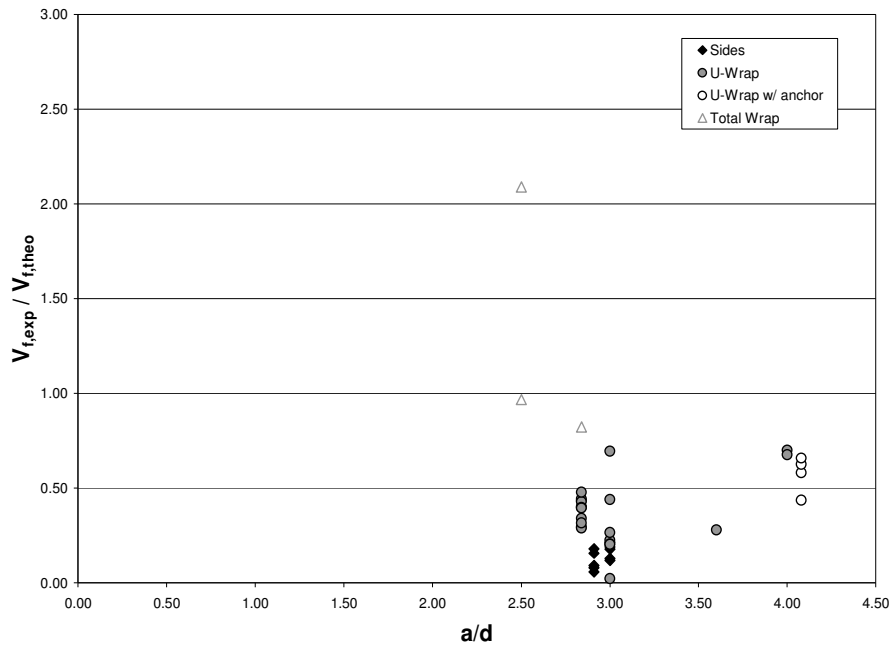
Figure C.87. $V_{f,\exp}/V_{f,theo}$ in terms of a/d - Other Failure Modes
JSCE Recommendations
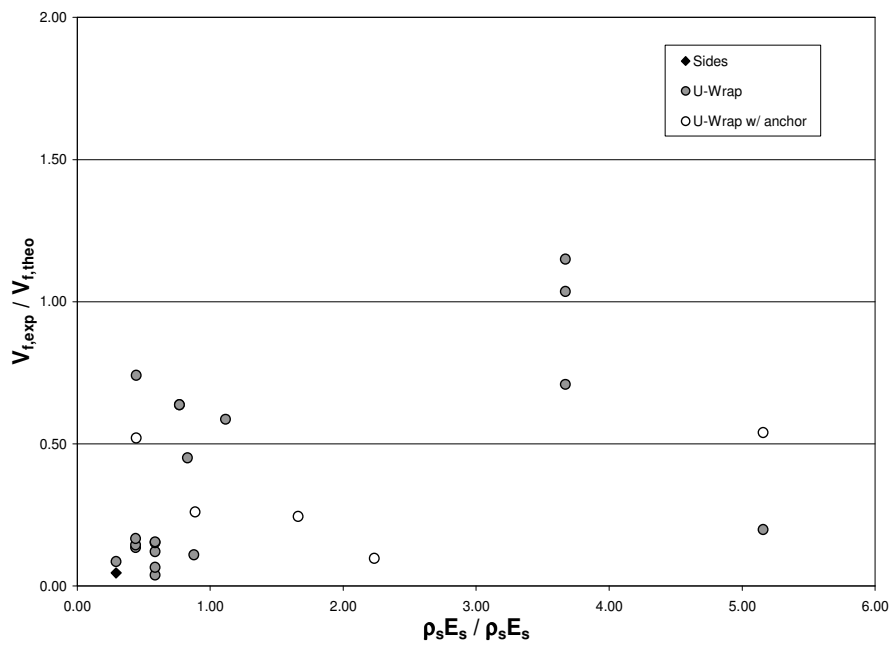
Figure C.98. $V_{f,\exp}/V_{f,theo}$ in terms of $\rho_s E_s / \rho_f E_f$ - FRP Debonding
JSCE Recommendations
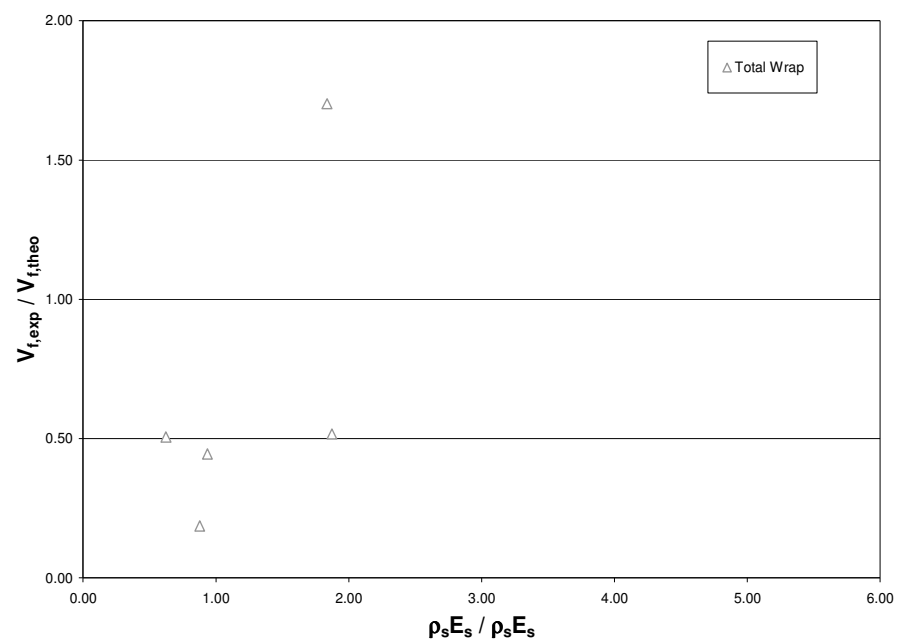
Figure C.109. $V_{f,\exp}/V_{f,theo}$ in terms of $\rho_s E_s/\rho_f E_f$ - FRP Fracture
JSCE Recommendations
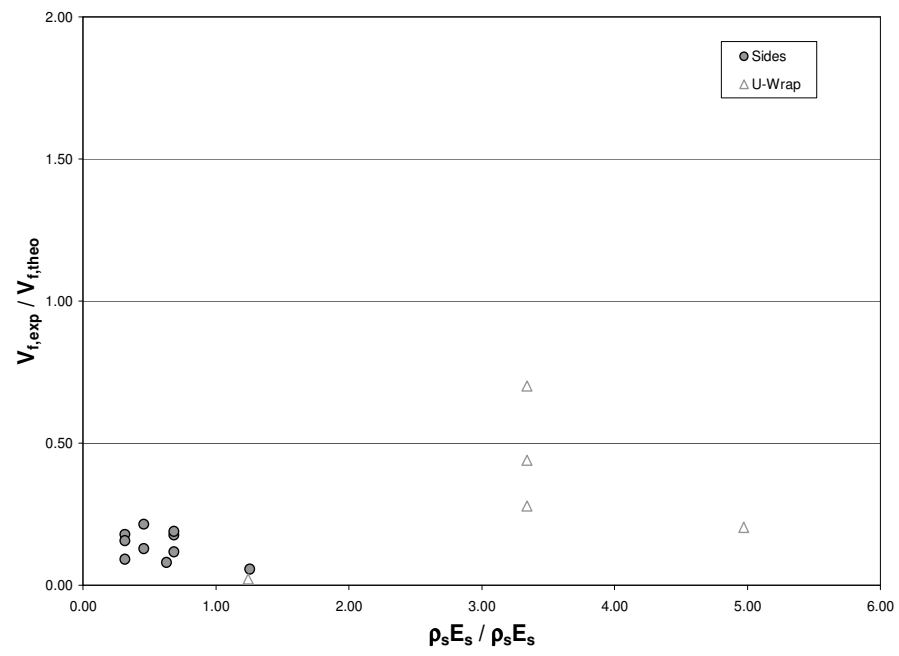
Figure C.20. $V_{f,\exp}/V_{f,theo}$ in terms of $\rho_s E_s/\rho_f E_f$ - Other Failure Modes
JSCE Recommendations
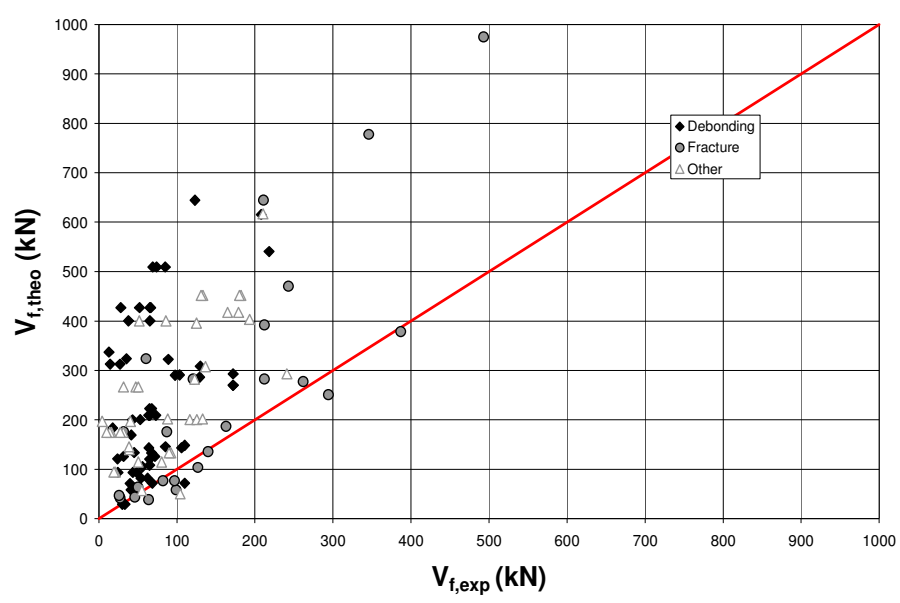
Figure C.21. Comparison between Analytical Predictions of FRP shear contribution by JSCE and Experimental Results
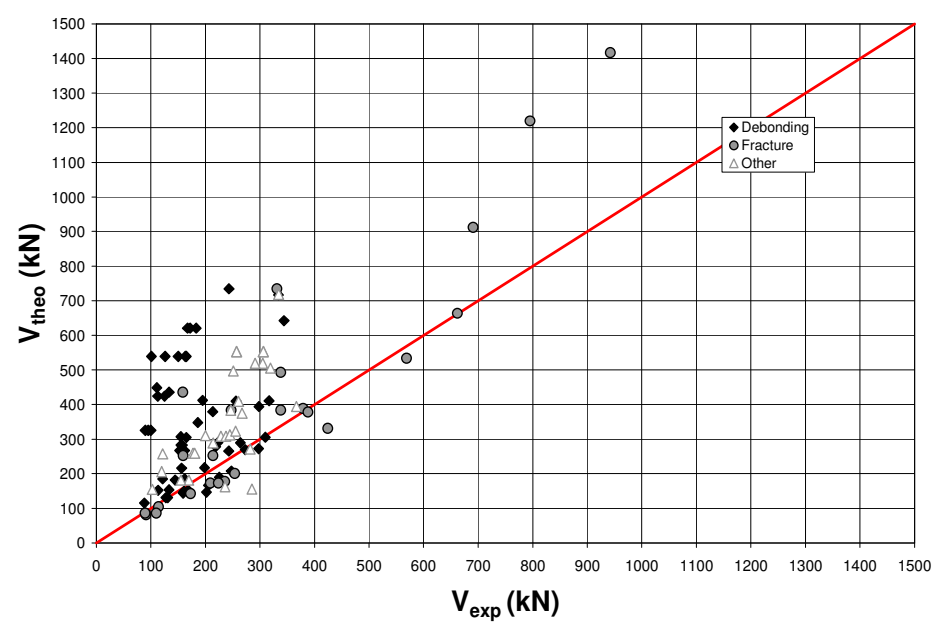
Figure C.22. Comparison between Analytical Predictions of total shear capacity by JSCE and Experimental Results
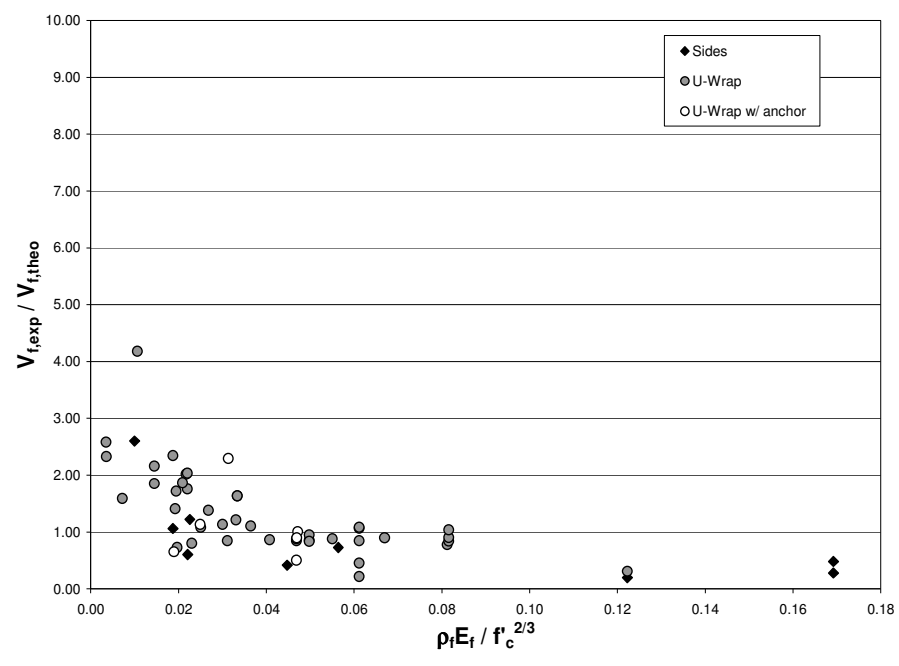
Figure C.23. $V_{f,\exp}/V_{f,theo}$ in terms of $E_f\rho_f/(f_c^{'})^{2/3}$ - FRP Debonding
ISIS Design Manual 4

Figure C.24. $V_{f,\exp}/V_{f,theo}$ in terms of $E_f\rho_f/(f_c^{'})^{2/3}$ - FRP Fracture
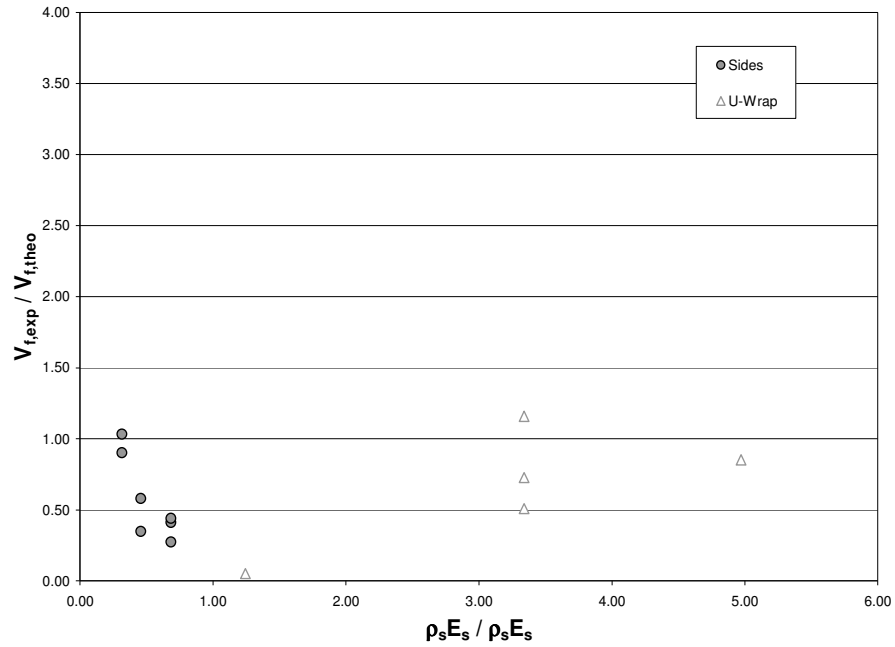ISIS Design Manual 4
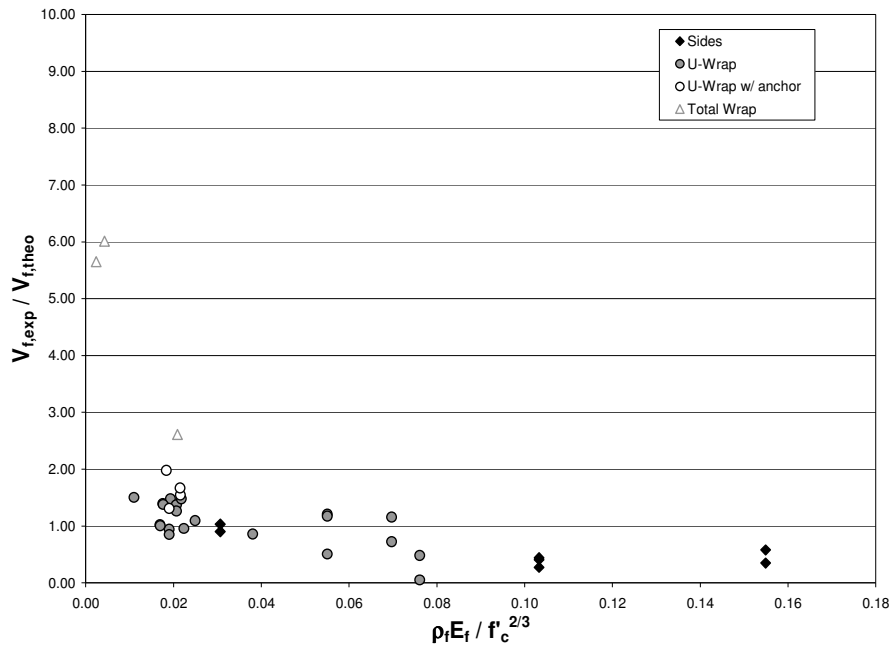
Figure C.25. $V_{f,\exp}/V_{f,theo}$ in terms of $E_f \rho_f /(f_c^{'})^{2/3}$ - Other Failure Modes
ISIS Design Manual 4
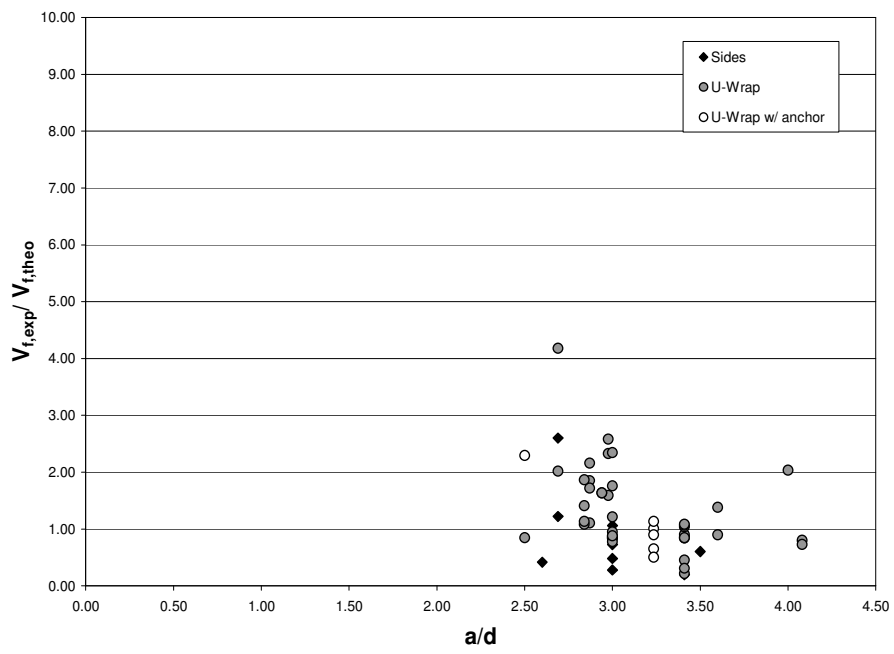
Figure C.26. $V_{f,\exp}/V_{f,theo}$ in terms of a/d - FRP Debonding
ISIS Design Manual 4
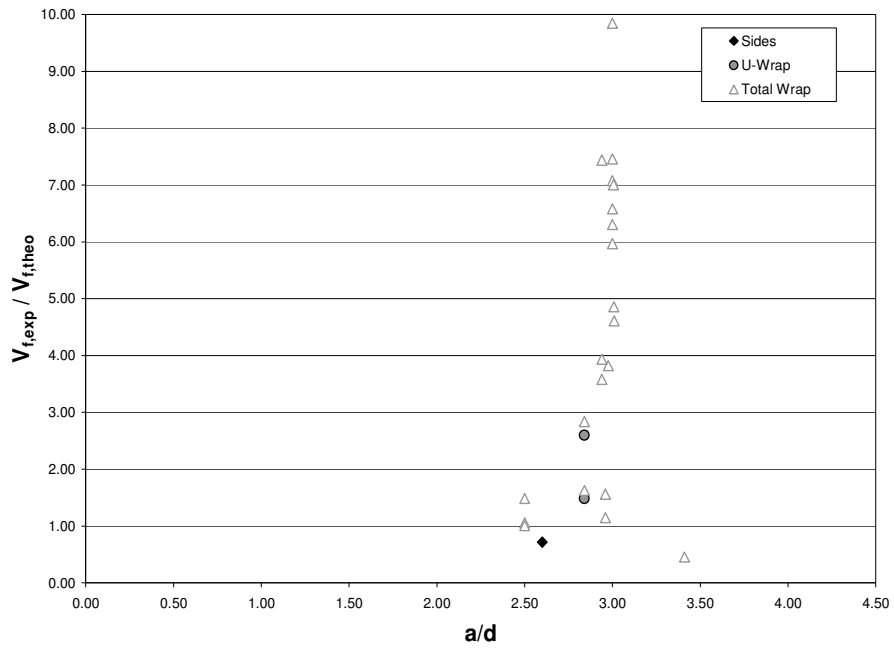
Figure C.27. $V_{f,\exp}/V_{f,theo}$ in terms of a/d - FRP Fracture
ISIS Design Manual 4

Figure C.28. $V_{f,\exp}/V_{f,theo}$ in terms of a/d - FRP Other Failure Modes
ISIS Design Manual 4
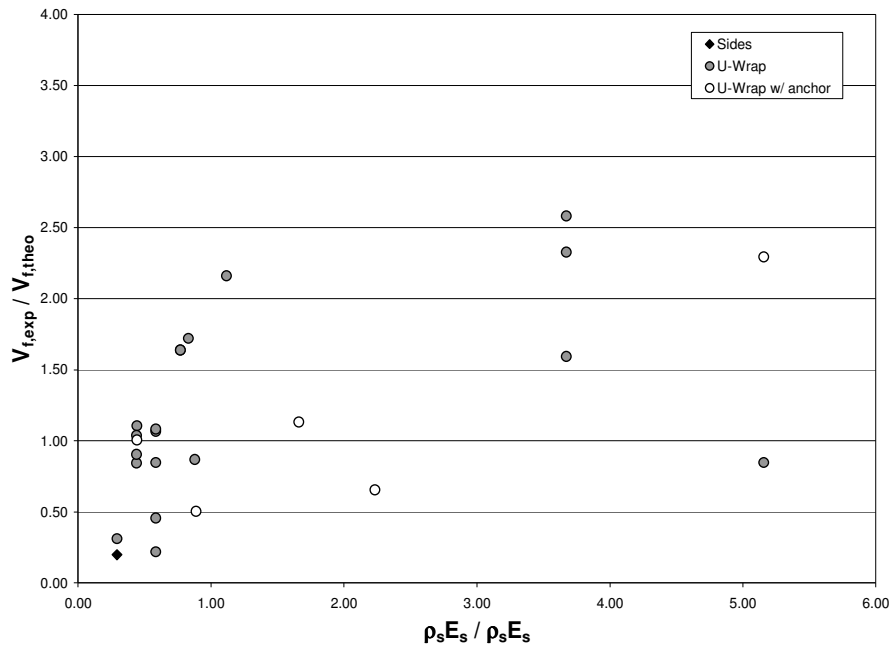
Figure C.29. $V_{f,\exp}/V_{f,theo}$ in terms of $\rho_s E_s/\rho_f E_f$ - FRP Debonding
ISIS Design Manual 4
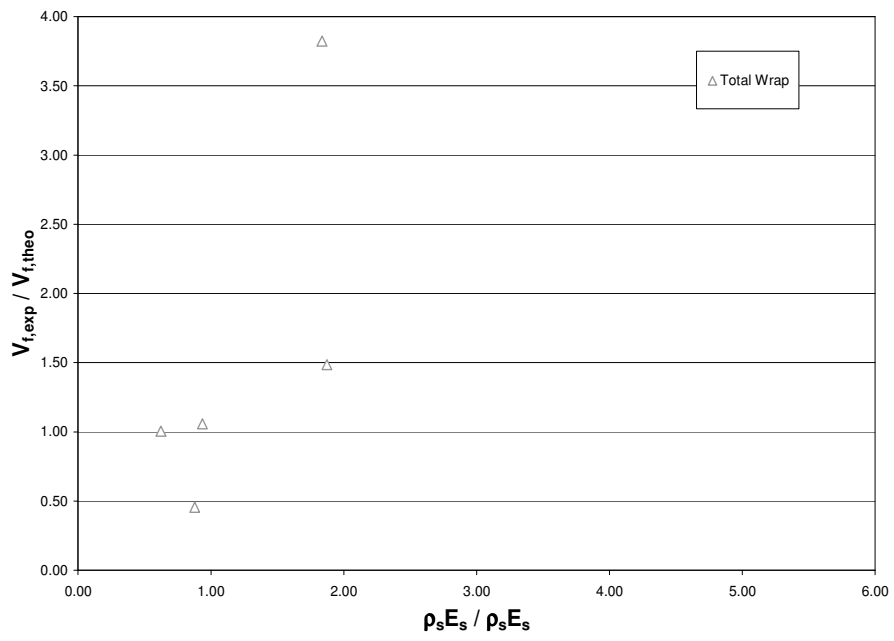
Figure C.30. $V_{f,\exp}/V_{f,theo}$ in terms of $\rho_s E_s/\rho_f E_f$ - FRP Fracture
ISIS Design Manual 4

Figure C.31. $V_{f,\exp}/V_{f,theo}$ in terms of $\rho_s E_s / \rho_f E_f$ - Other Failure Modes
ISIS Design Manual 4
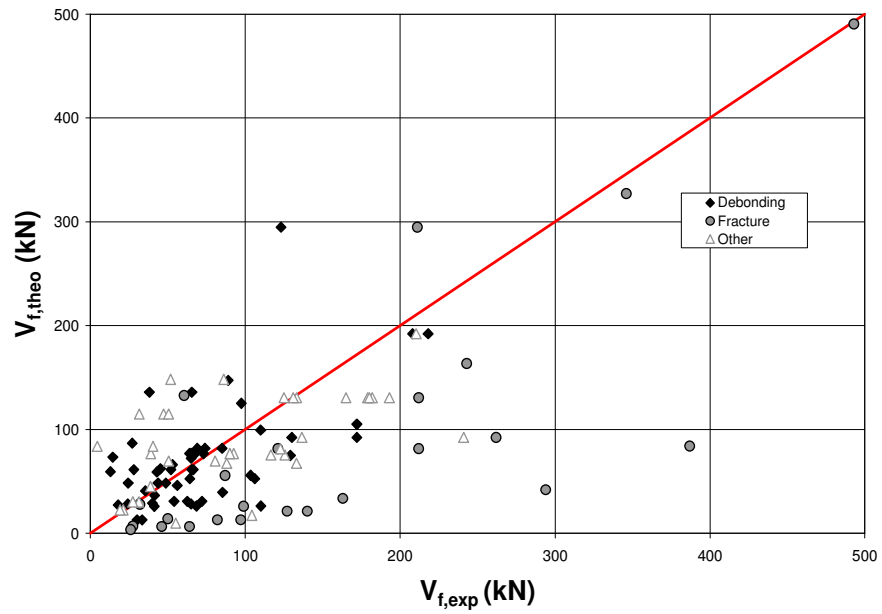
Figure C.32. Comparison between Analytical Predictions of FRP shear contribution by
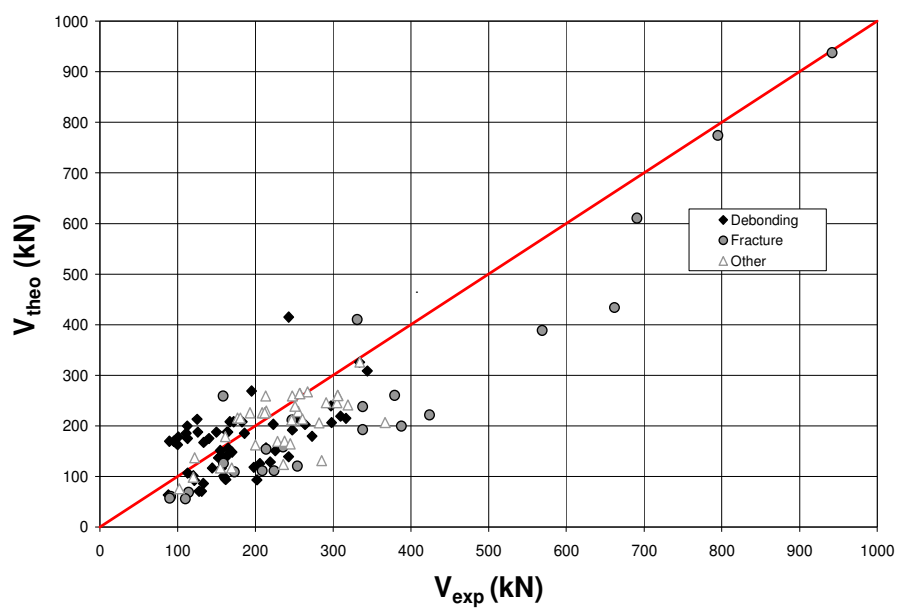ISIS and Experimental Results

Figure C.33. Comparison between Analytical Predictions of total shear capacity by ISIS and Experimental Results
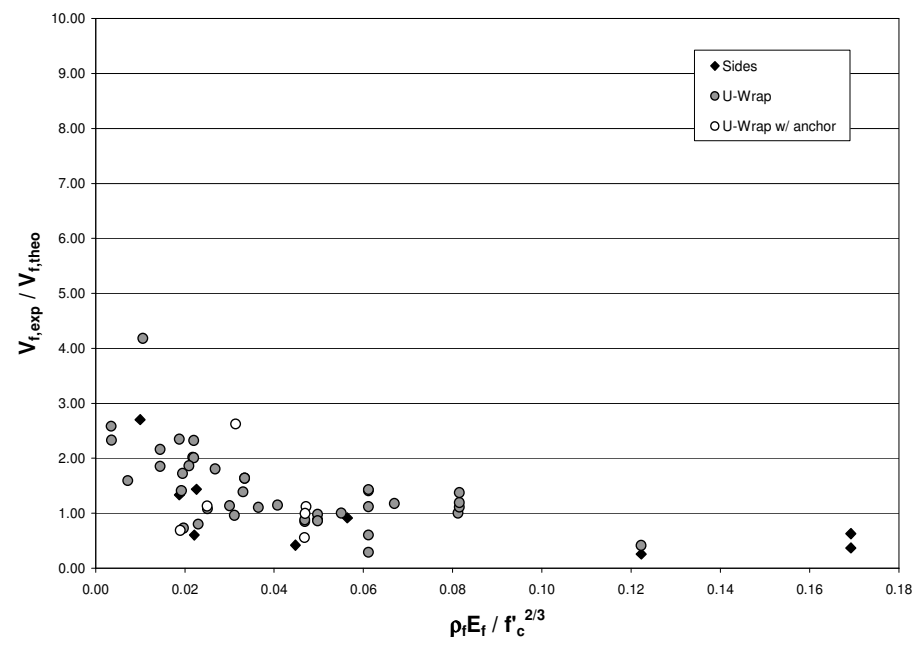

Figure C.34. $V_{f,\exp}/V_{f,theo}$ in terms of $E_f\rho_f/(f_c^{'})^{2/3}$ - FRP Debonding
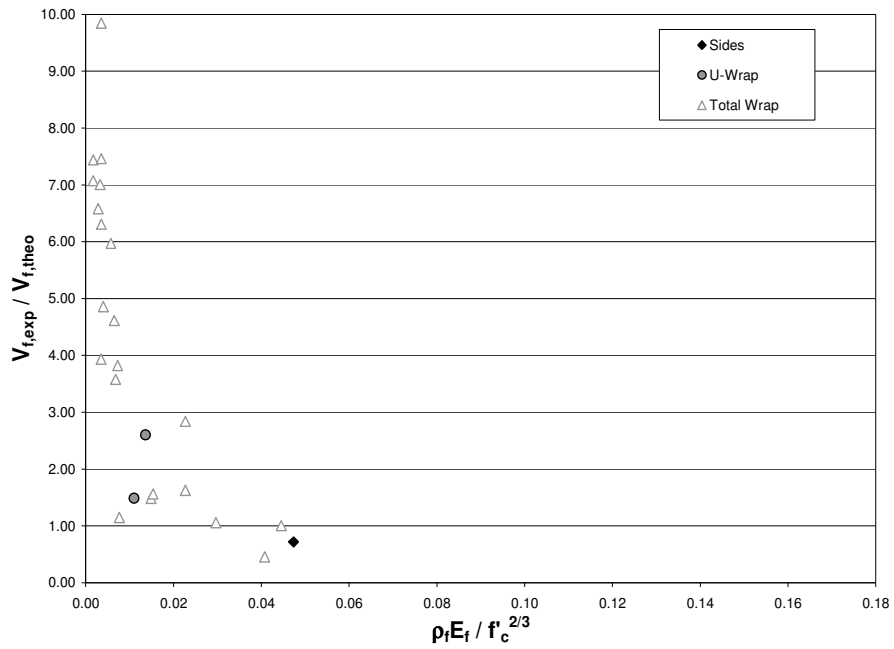ACI 440.2R-02

Figure C.35. $V_{f,\exp}/V_{f,theo}$ in terms of $E_f \rho_f /(f_c^{'})^{2/3}$ - FRP Fracture
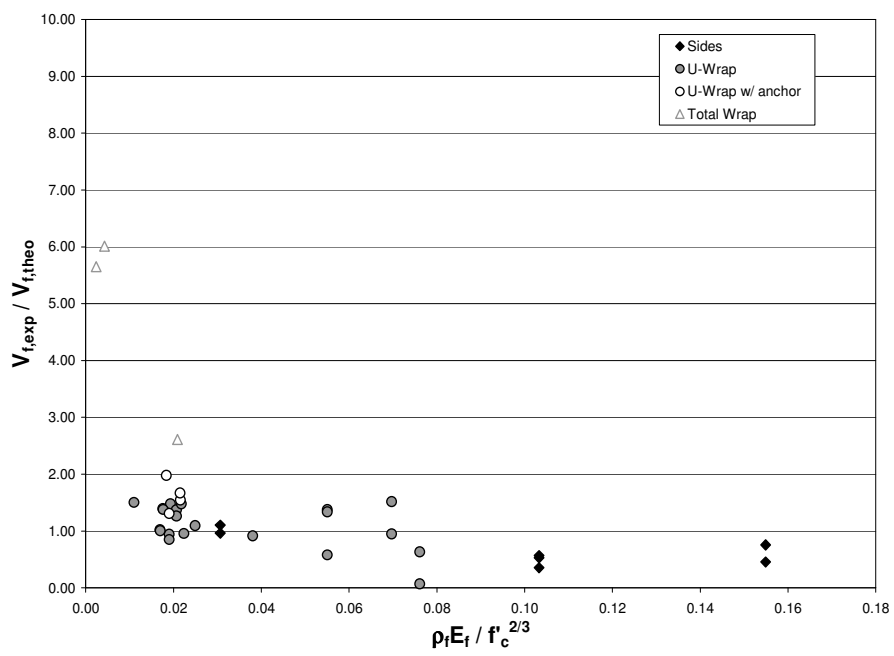ACI 440.2R-02

Figure C.36. $V_{f,\exp}/V_{f,theo}$ in terms of $E_f \rho_f /(f_c^{'})^{2/3}$ - Other Failure Modes
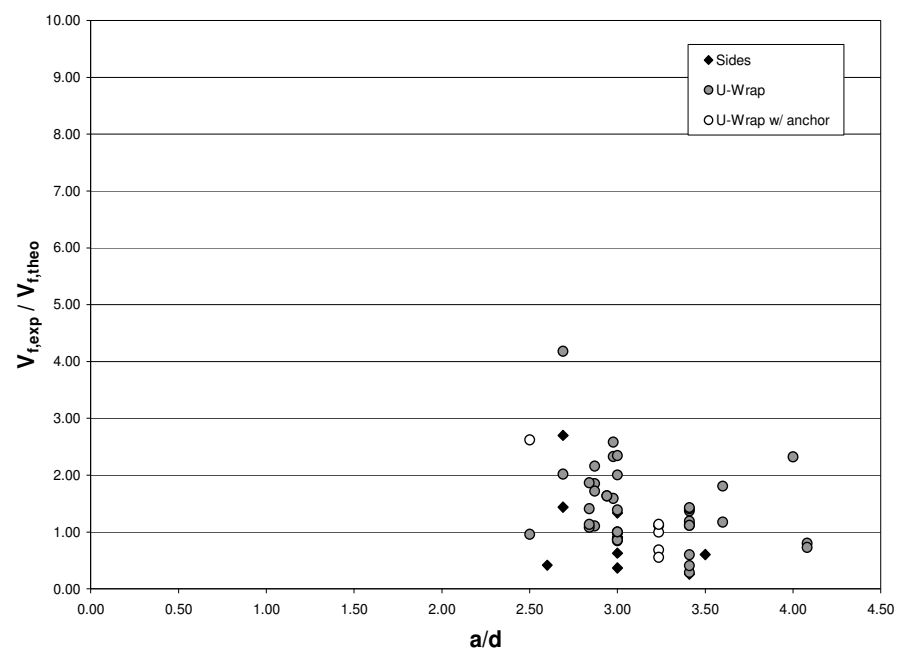ACI 440.2R-02

Figure C.37. $V_{f,\exp}/V_{f,theo}$ in terms of a/d - FRP Debonding
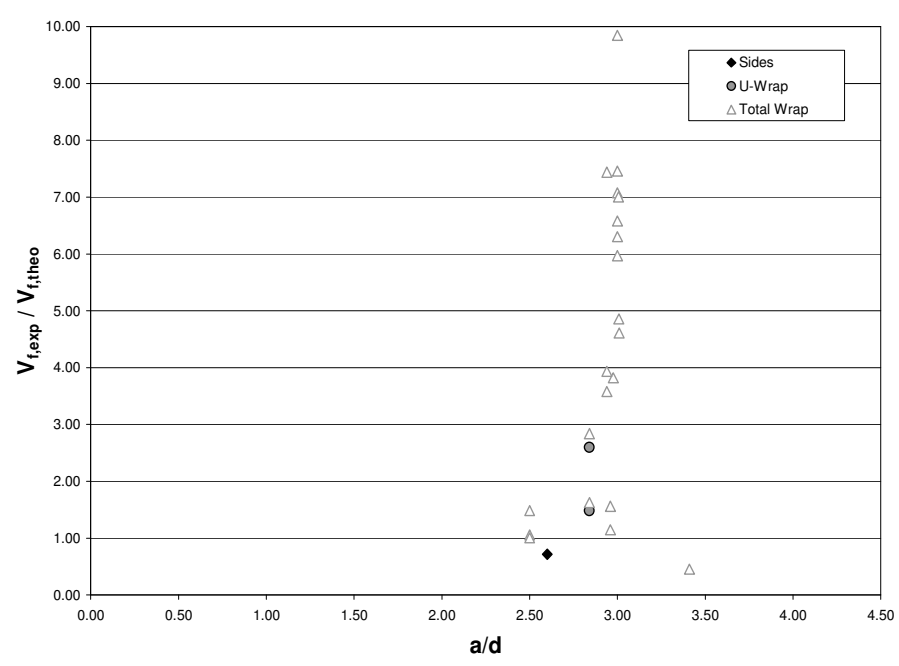ACI 440.2R-02

Figure C.38. $V_{f,\exp}/V_{f,theo}$ in terms of a/d - FRP Fracture
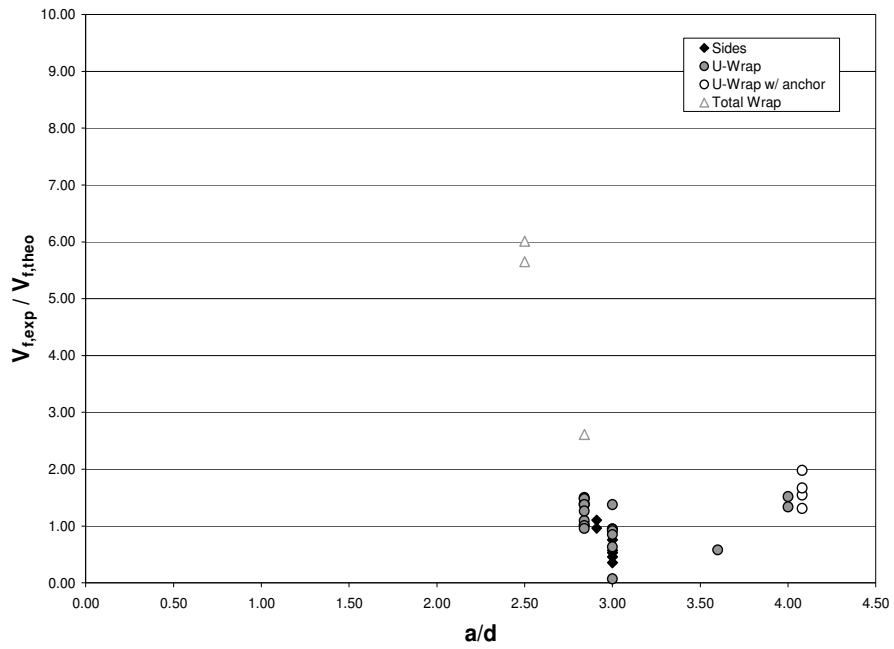ACI 440.2R-02

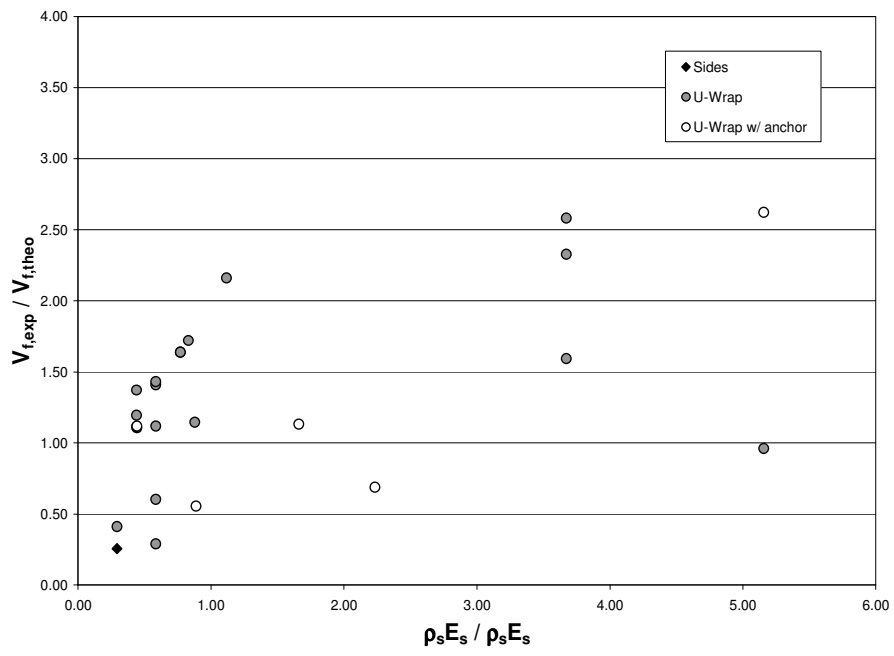Figure C.39. $V_{f,\exp}/V_{f,theo}$ in terms of a/d - Other Failure Modes
ACI 440.2R-02

Figure C.40. $V_{f,\exp}/V_{f,theo}$ in terms of $\rho_s E_s / \rho_f E_f$ - FRP Debonding
ACI 440.2R-02
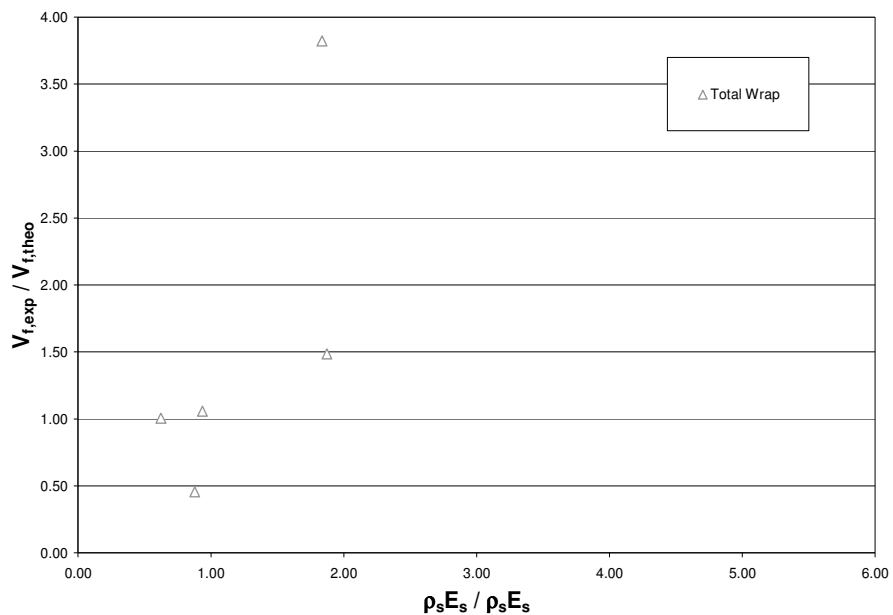
Figure C.41. $V_{f,\exp}/V_{f,theo}$ in terms of $\rho_s E_s / \rho_f E_f$ - FRP Fracture
ACI 440.2R-02

Figure C.42. $V_{f,\exp}/V_{f,theo}$ in terms of $\rho_s E_s / \rho_f E_f$ - Other Failure Modes
ACI 440.2R-02

Figure C.43. Comparison between Analytical Predictions of FRP shear contribution by ACI 440.2R-02 and Experimental Results

Figure C.44. Comparison between Analytical Predictions of total shear capacity by ACI 440.2R-02 and Experimental Results
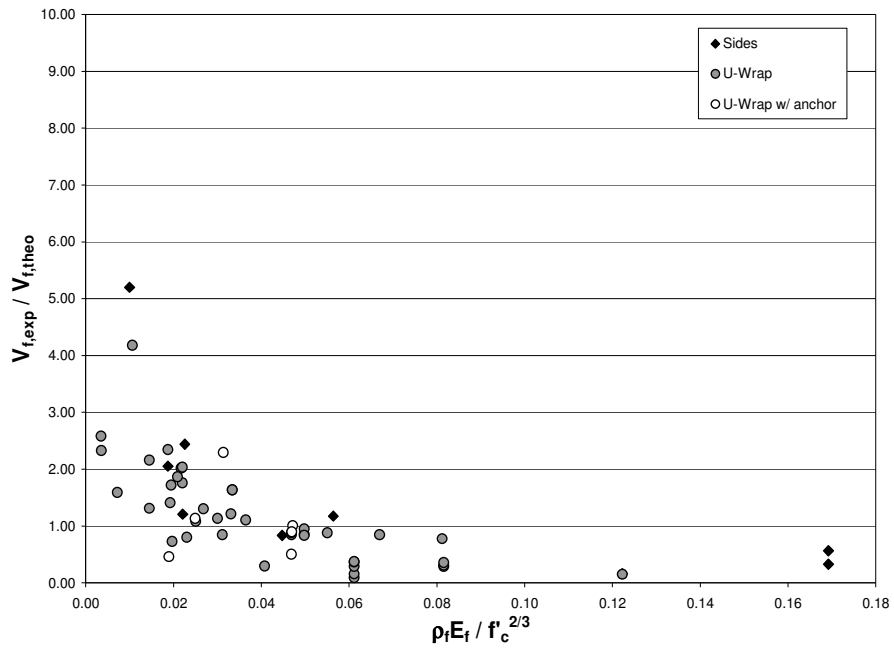
Figure C.45. $V_{f,\exp}/V_{f,theo}$ in terms of $E_f \rho_f /(f_c^{'})^{2/3}$ - FRP Debonding CSA-S806-02
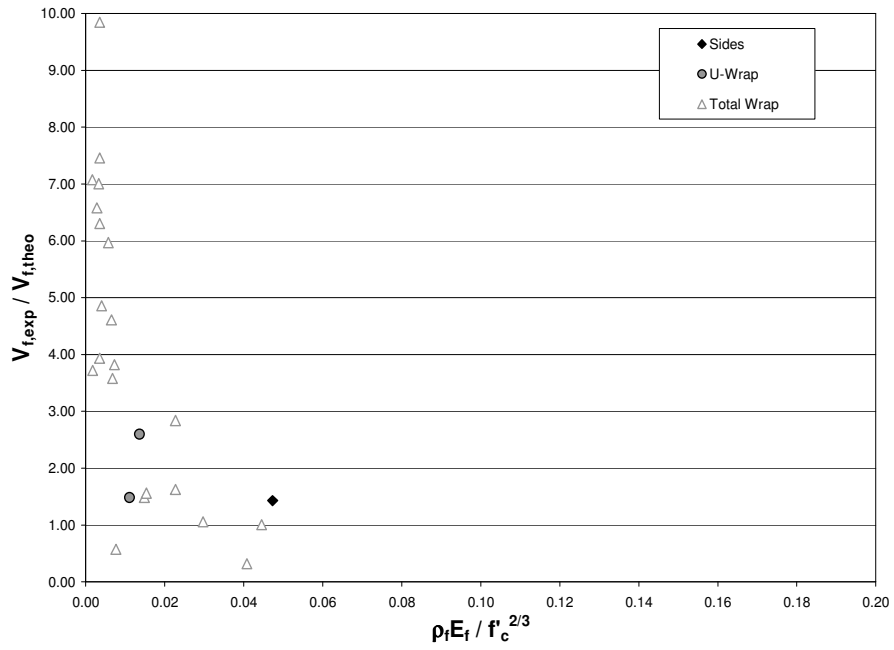
Figure C.46. $V_{f,\exp}/V_{f,theo}$ in terms of $E_f \rho_f /(f_c^{'})^{2/3}$ - FRP Fracture CSA-S806-02
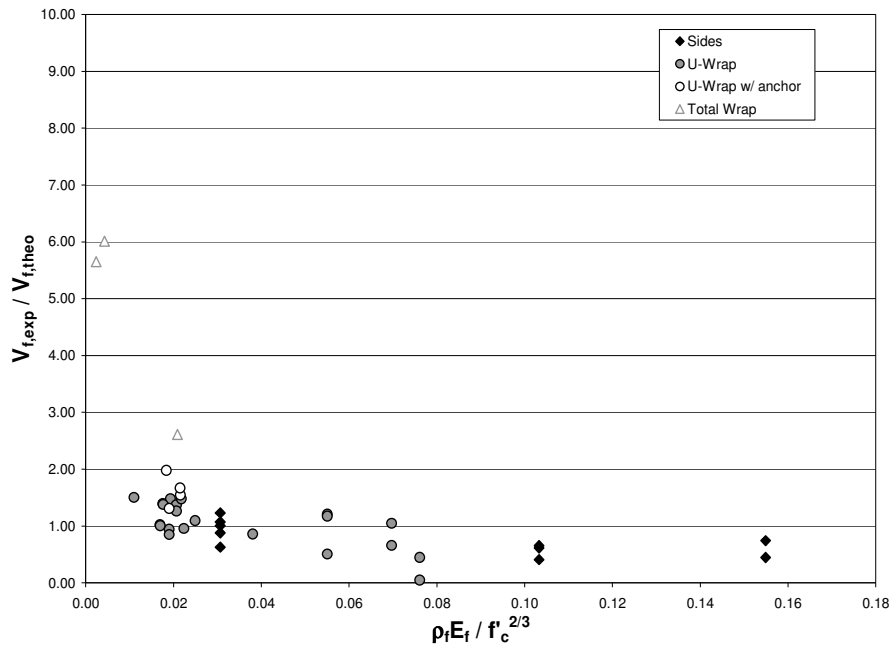
Figure C.47. $V_{f,\exp}/V_{f,theo}$ in terms of $E_f\rho_f/(f_c^{'})^{2/3}$ - Other Failure Modes
CSA-S806-02
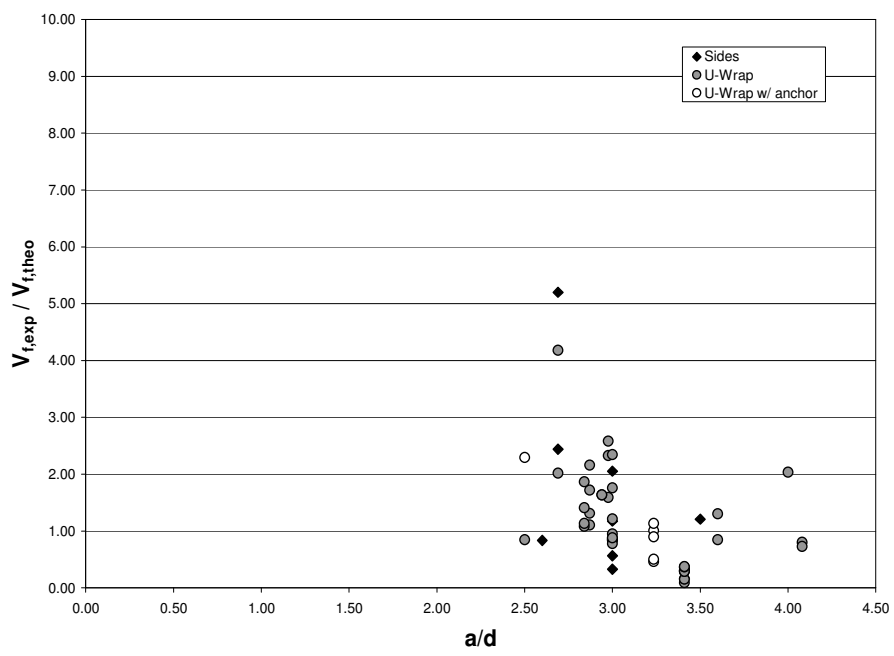
Figure C.48. $V_{f,\exp}/V_{f,theo}$ in terms of a/d - FRP Debonding
CSA-S806-02
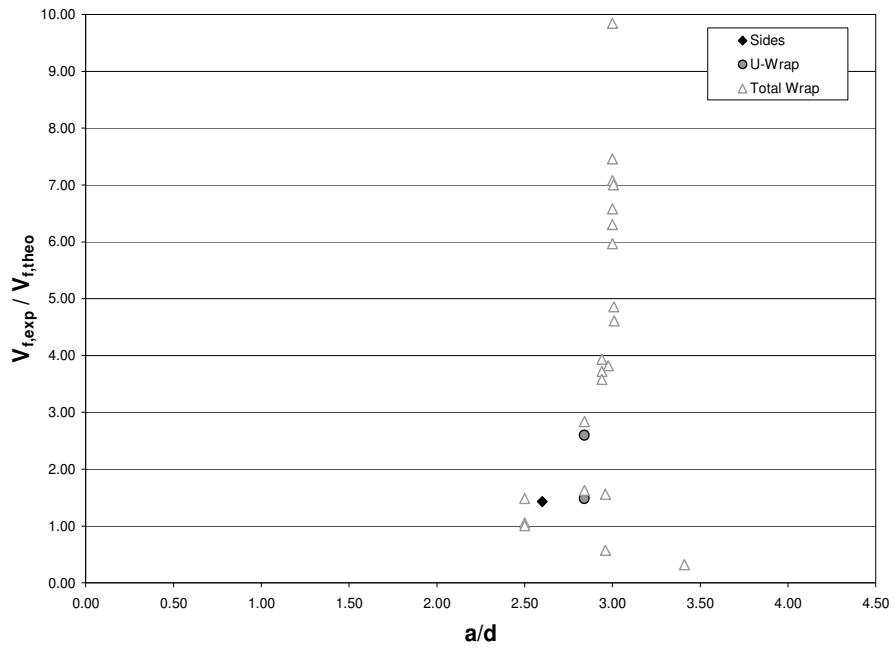
Figure C.49. $V_{f,\exp}/V_{f,theo}$ in terms of a/d - FRP Fracture
CSA-S806-02
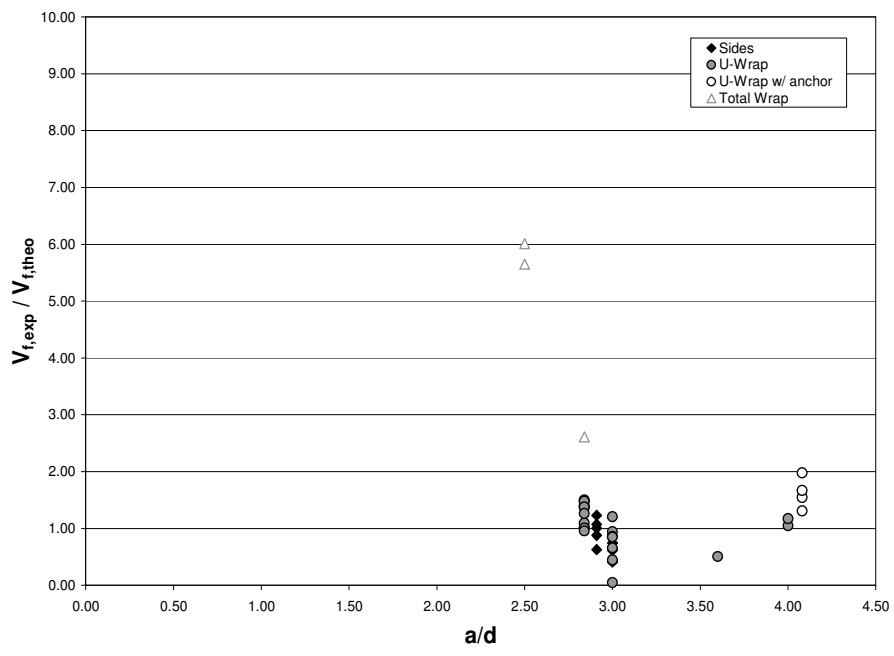
Figure C.50. $V_{f,\exp}/V_{f,theo}$ in terms of a/d - Other Failure Modes
CSA-S806-02
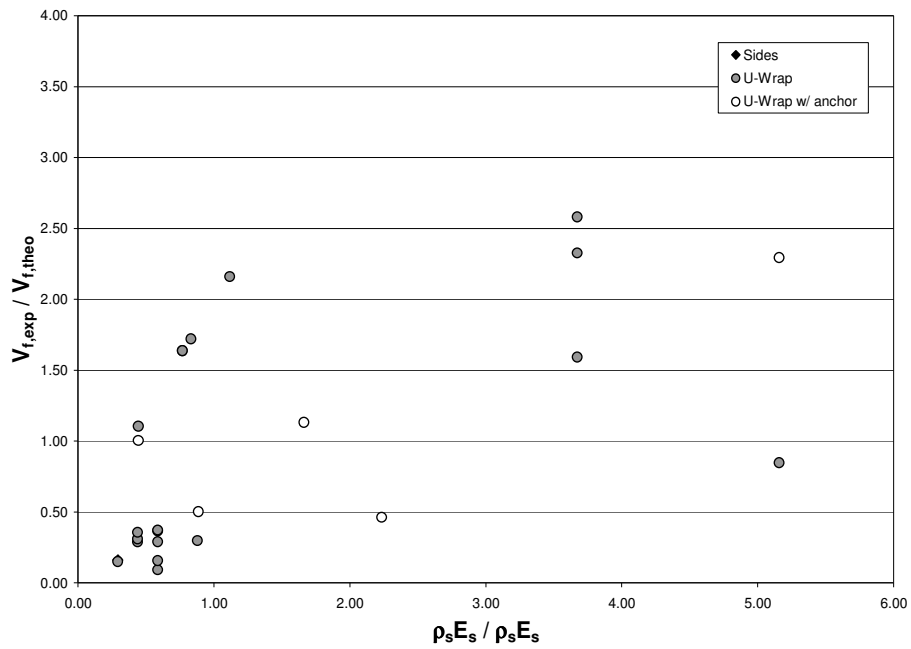
Figure C.51. $V_{f,\exp}/V_{f,theo}$ in terms of $\rho_s E_s / \rho_f E_f$ - FRP Debonding CSA-S806-02
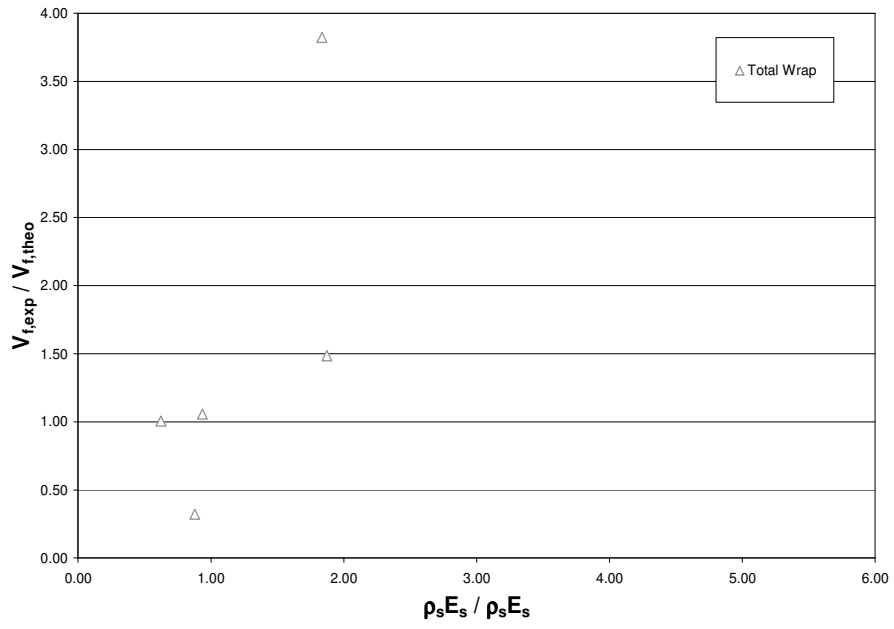
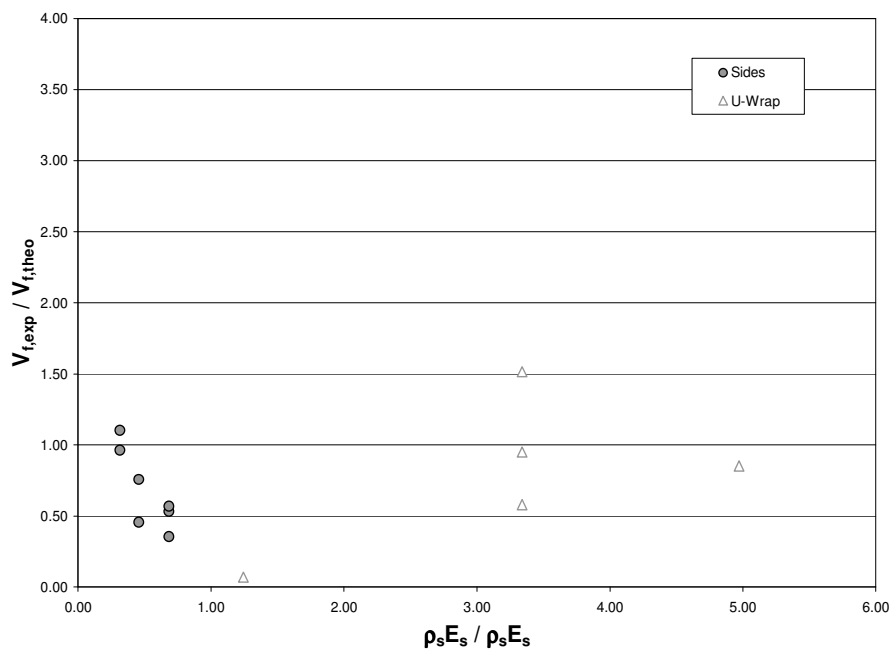Figure C.52. $V_{f,\exp}/V_{f,theo}$ in terms of $\rho_s E_s / \rho_f E_f$ - FRP Fracture CSA-S806-02

Figure C.53. $V_{f,\exp}/V_{f,theo}$ in terms of $\rho_s E_s / \rho_f E_f$ - Other Failure Modes
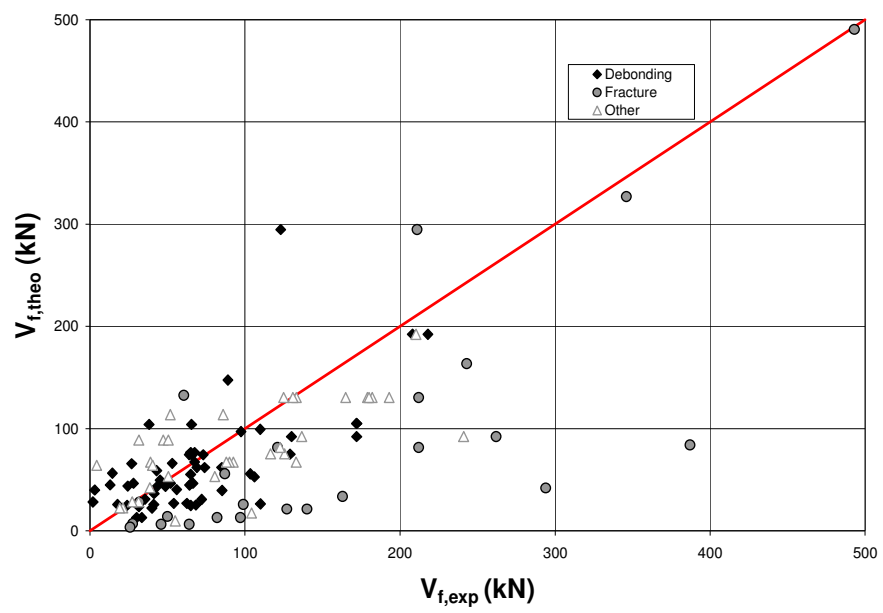CSA-S806-02

Figure C.54. Comparison between Analytical Predictions of FRP shear contribution by
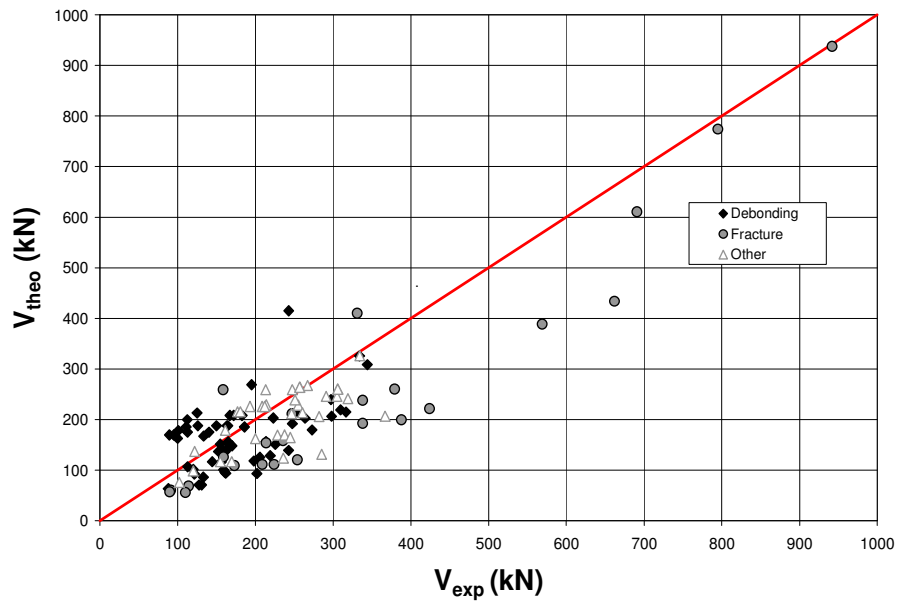CSA-S806-02 and Experimental Results

Figure C.55. Comparison between Analytical Predictions of total shear capacity by CSA-S806-02 and Experimental Results

BIBLIOGRAPHY

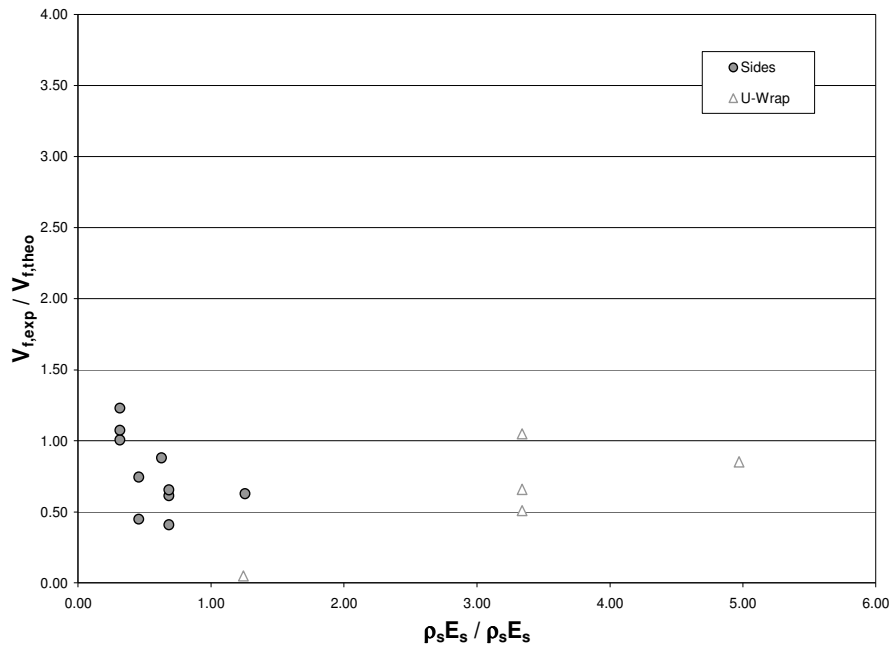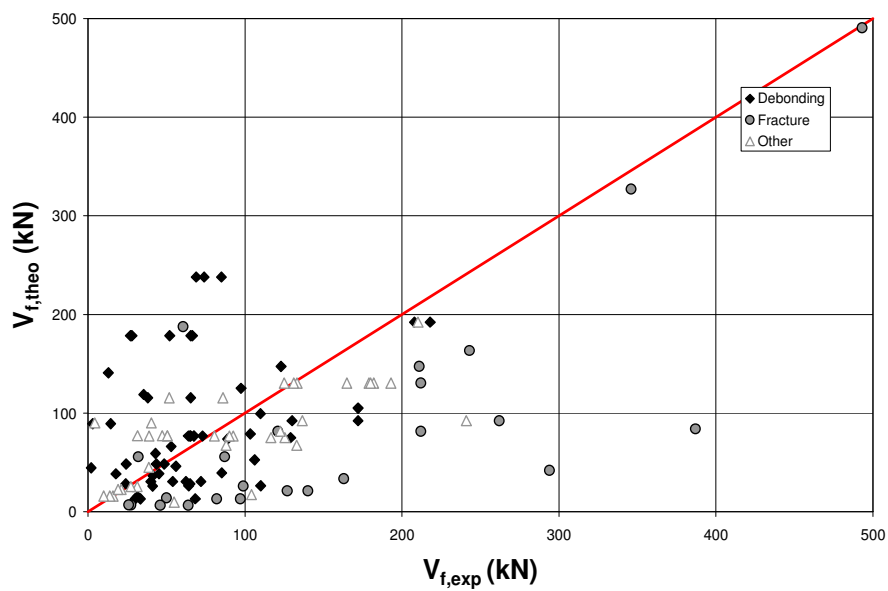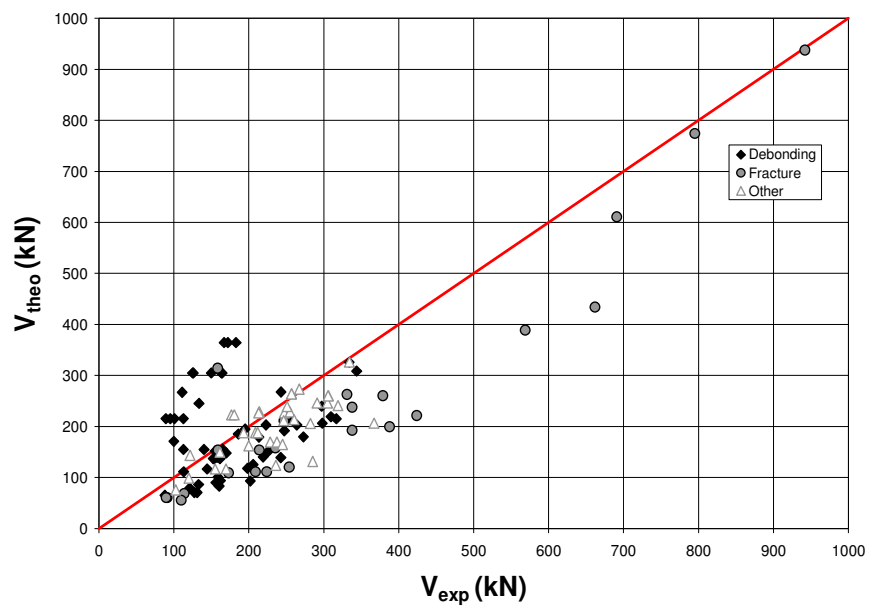AASHTO. (1998). *AASHTO LRFD Bridge Design Specifications*. American Association of State Highway and Transportation Official, Second edition, Washington DC. Including interim revisions for 1999 through 2003.

ACI Committee 318 (2005). *Building Code Requirements for Structural Concrete and Commentary (ACI 318-05 / ACI 318R-05)*. American Concrete Institute Farmington Hills, Michigan.

ACI Committee 318 (1999). *Building Code Requirements for Structural Concrete and Commentary (ACI 318-99 / ACI 318R-99)*. American Concrete Institute Farmington Hills, Michigan.

ACI Committee 440 (2002). *Guide for the Design and Construction of Externally Bonded FRP Systems for Strengthening Concrete Structures*. American Concrete Institute, Farmington Hills, Michigan.

Adhikary, B. B., Mutsuyoshi, H., and Ashraf, M. (2004). "Shear Strengthening of Reinforced Concrete Beams Using Fiber-Reinforced Polymer Sheets with Bonded Anchorage," *ACI Structural Journal*, Vol. 101, No. 5, pp. 660-668.

Al-Sulaimani, G. J., Sharif, A. M., Basunbul, I. A., Baluch, M. H., and Ghaleb, B. N., (1994). "Shear Repair for Reinforced Concrete by Fiberglass Plate Bonding," *ACI Structural Journal*, Vol. 91, No. 3, pp. 458-464.

Alexander, J., and Cheng, J. J. R. (1997). "Shear Rehabilitation of G-Girder bridges using CFRP sheets," *Structural Engineering Report No. 218,* Department of Civil and Environmental Engineering, University of Alberta, Edmonton, Canada.

Araki, N., Matsuzaki, Y., Nakano, K., Kataka, T., and Fukuyama, H. (1997). "Shear Capacity of Retrofitted RC Members with Continuous Fiber Sheets," *Non Metallic (FRP) Reinforcement for Concrete Structures*, Vol. 1, pp. 515-522.

Bank, L. C., Barkatt, A., and Gentry, T. R. (1995). "Accelerated test methods to determine the long-term behavior of FRP composite structures: environmental effects," *Journal of Reinforced Plastics and Composites*, Vol. 15, No. 6, pp. 559-587.

Berset, J. D. (1992). *Strengthening of Reinforced Concrete Beams for Shear Using FRP Composites.* M.S Thesis, Department of Civil and Environmental Engineering, Massachusetts Institute of Technology, MIT, Boston, MA.

Bousselham, A., and Chaallal, O. (2006a). "Behavior of Reinforced Concrete T-Beams Strengthened in Shear with Carbon Fiber-Reinforced Polymer- An Experimental Study," *ACI Structural Journal*, Vol. 103, No.3, pp. 339-347.

Bousselham, A., and Chaallal, O. (2006b). "Effect of transverse steel and shear span on the performance of RC beams strengthened in shear with CFRP," *Composites Part B: Engineering*, Vol. 37, No.1, pp. 37-46.

Bousselham, A., and Chaallal, O. (2004). "Shear Strengthening Reinforced Concrete Beams with Fiber-Reinforced Polymer: Assessment of Influencing Parameters and Required Research," *ACI Structural Journal*, Vol. 101, No. 2, pp. 219-227.

BS 8110. (1997). "Structural Use of Concrete, Part 1. Code of Practice for Design and Construction," *British Standards Institution,* London, UK.

Cao, S. Y., Chen, J. F., Teng, J. G., Hao, Z., and Chen, J. (2005). "Debonding in RC Beams Shear Strengthened with Complete FRP Wraps," *Journal of Composites for Construction,* Vol. 9, No. 5, pp. 417-428.

Carolin, A., and Taljsten, B. (2005a). "Experimental Study of Strengthening for Increased Shear Bearing Capacity," *Journal of Composites for Construction.* Vol. 9, No. 6, pp. 488-496.

Carolin, A., and Taljsten, B. (2005b). "Theoretical Study of Strengthening for Increased Shear Capacity," *Journal of Composites for Construction.* Vol. 9, No. 6, pp. 497-506.

Chaallal, O., Shahawy, M., and Hassan, M. (2002). "Performance of Reinforced Concrete T-Girders Strengthened in Shear with Carbon Fiber-Reinforced Polymer Fabric," *ACI Structural Journal*, Vol. 99, No. 3, pp.335-343.

Chaallal, O., Nollet, M. J., and Perraton, D. (1998). "Shear Strengthening of RC Beams by Externally Bonded Side CFRP Strips," *Journal of Composites for Construction*, Vol. 2, No. 2, pp. 111-114.

Chajes, M. J., Januszka, T. F., Mertz, D. R., Thomson, T. A. J., and Finch, W. W. J. (1995). "Shear Strengthening of Reinforced Concrete Beams Using Externally Applied Composite Fabrics," *ACI Structural Journal*, Vol. 92, No. 3, pp. 295-303.

Chen, J. F., and Teng, J. G. (2003a). "Shear capacity of FRP strengthened RC beams: FRP debonding," *Construction Building Materials,* Vol. 17, No. 1, pp. 27-41.

Chen, J. F. and Teng, J. G. (2003b). "Shear Capacity of FRP-Strengthened RC Beams: FRP Rupture," *Journal of Structural Engineering*, Vol. 129, No. 5, pp. 615-625.

Chen, J. F. and Teng, J. G. (2001). "Anchorage Strength Models for FRP and Steel Plates Bonded to Concrete," *Journal of Structural Engineering*, Vol. 127, No. 7, pp. 784-791.

CSA. (2004). *A23.3-04 Design of Concrete Structures for Buildings,* Canadian Standards Association Rexdale, Ontario, Canada.

CSA. (2002). *CAN/CSA S806-02 Design and Construction of Building Components with Fibre-Reinforced Polymers*, Canadian Standards Association, Rexdale Ontario,

Commission of the European Communities (2003). *Eurocode No. 2: Design of Concrete Structures-Part 1: General Rules and Rules for Buildings.* prEN 1992-1-1. draft.

Czaderski, C. (2002). "Shear Strengthening with Prefabricated CFRP L-Shaped plates. Test Beams S1 to S6," *EMPA. Report No. 116/7*, Switzerland, 78 p.

De Lorenzis, L., and Nanni, A. (2001). "Shear Strengthening of Reinforced Concrete Beams with Near-Surface Mounted Fiber-Reinforced Polymer Rods," *ACI Structural Journal,* Vol. 98, No. 1, pp. 60-68.

Deniaud, C., and Cheng, J. J. R. (2004). "Simplified Shear Design Method for Concrete Beams Strengthened with Fiber Reinforced Polymer Sheets," *Journal of Composites for Construction*, Vol. 8, No. 5, pp. 425-433.

Deniaud, C., and Cheng, J. J. R. (2003). "Reinforced Concrete T-Beams Strengthened in Shear with Fiber Reinforced Polymer Sheets," *Journal of Composites for Construction*, Vol. 7, No. 4, pp. 302-310.

Deniaud, C., and Cheng, J. J. R. (2001). "Shear Behavior of Reinforced Concrete T Beams with Externally Bonded Fiber-Reinforced Polymer," *ACI Structural Journal*, Vol. 98, No. 3, pp. 386-394.

Diagana, C., Li, A., Gedalia, B., Delmas, Y. (2003). "Shear Strengthening Effectiveness with CFF Strips," *Engineering Structures,* Vol. 25, No. 4, pp. 507-516.

fib-TG9.3. (2001). *Design and Use of Externally Bonded Fiber Polymer Reinforcement (FRP EBR) for Reinforced Concrete Structures*. Technical Report Prepared by EBR Task Group 9.3, Bulletin 14.

Funakawa, I., Shimono, K., Watanabe, T., Asada, S., and Ushijima, S. (1997). "Experimental Study on Shear Strengthening with Continuous Fiber Reinforcement Sheet and Methyl Methacrylate Resin," *Non-Metallic (FRP) Reinforcement for Concrete Structures*, Vol.1, pp. 491-498.

Horiguchi, T., and Saeki, N. (1997). "Effect of test methods and quality of concrete on bond strength of CFRP sheet," *Non-Metallic (FRP) Reinforcement for Concrete Structures,* Vol.1, pp. 475-482.

Hsu, C. T. T., Punurai, W., and Zhang, Z. (2003). "Flexural and Shear Strengthening of RC Beams Using Carbon Fiber Reinforced Polymer Laminates," *SP-211-05, Large Scale Structural Testing*, pp. 89-114.

ISIS Canada. (2001). *Design Manual 4 – Strengthening Reinforced Concrete Structures with Externally-Bonded Fiber Reinforced Polymers*, The Canadian Network of Centers of Excellence on Intelligent Sensing for Innovative Structures, University of Manitoba, Manitoba, Canada.

JBDPA. (1999). *Seismic Retrofitting Design and Construction Guidelines for Existing Reinforced Concrete (RC) Buildings with FRP Materials,* Japan Building Disaster Prevention Association, Japan.

JSCE. (2001). *Recommendations for the Upgrading of Concrete Structures with use of Continuous Fiber Sheets*. Concrete Engineering Series 41, Japanese Society of Civil Engineers, Tokyo.

Kachlakev, D. I., and Barnes, W. A. (1999). "Flexural and Shear Performance of Concrete Beams Strengthened with Fibre Reinforced Polymer Laminates," *SP-188-81, ACI Proceedings of the 4th International Symposium on FRP for Reinforcement of Concrete Structures (FRPRCS-4)*, pp. 959-971.

Kamiharako, A., Maruyama, K., Takada, K., and Shimomura, T. (1997). "Evaluation of Shear Contribution of FRP Sheets attached to Concrete Beams," *Non-Metallic (FRP) Reinforcement for Concrete Structures*, Vol.1, pp. 467-474.

Khalifa, A. and Nanni, A. (2002). "Rehabilitation of Rectangular Simply Supported RC Beams with Shear Deficiencies Using CFRP Composites," *Construction and Building Materials*, Vol. 16, No.3, pp. 135-146.

Khalifa, A. and Nanni, A. (2000a). "Improving Shear Capacity of Existing RC T-Section Beams Using CFRP Composites," *Cement and Concrete Composites*, Vol. 22, No.2, pp. 165-174.

Khalifa, A., Nanni, A., and De Lorenzis L. (2000b). "FRP Composites for Shear Strengthening of RC Beams," *Proceedings of the.3rd International Conference on Advanced Composite Materials in Bridges and Structures*, pp. 137-144.

Khalifa, A., Tumialan, G., Nanni, A., and Belarbi, A. (1999a). "Shear Strengthening of Continuous Reinforced Concrete Beams Using Externally Bonded Carbon Fiber Reinforced Polymer Sheets," *SP-188-84, ACI Proceedings of the 4th International Symposium on FRP for Reinforcement of Concrete Structures (FRPRCS-4)*, pp. 995-1008.

Khalifa, A. (1999b). *Shear Performance of Reinforced Concrete Beams Strengthened with Advanced Composites.* Ph.D. Thesis, Department of Structural Engineering, University of Alexandria, Egypt.

Khalifa, A., Gold, W.J., Nanni, A., and Aziz, A.M.I. (1998). "Contribution of Externally Bonded FRP to Shear Capacity of RC Flexural Members," *Journal of Composites for Construction*, Vol. 2, No. 4, pp. 195-202.

Lees, J. M., Winistöfer, A. U., and Meier, U. (2002). "External Prestressed Carbon Fiber-Reinforced Polymer Straps for Shear Enhancement of Concrete," *Journal of Composites for Construction*, Vol. 6, No. 4, pp. 249-256.

Li, A., Diagana, C., and Delmas Y. (2002). "Shear Strengthening Effect by Bonded Composite Fabrics on RC Beams," *Composites Part B: Engineering,* Vol. 33, No.3, pp. 225-239.

Loov, R. (1998). "Review of A23.3-94 simplified method of shear design and comparison with results using shear friction," *Canadian Journal of Civil Engineering,* Vol. 25, pp. 437-450.

MacGregor, J. G., and Wight, J. K. (2005). *Reinforced Concrete Mechanics and Design.* Fourth edition, Prentice Hall International Series in Civil Engineering Mechanics.

Maeda, T., Asano, Y., Sato, Y., Ueda, T., and Kakuta, Y. (1997). "A Study on Bond Mechanism of Carbon Fiber Sheet," *Non-Metallic (FRP) Reinforcement for Concrete Structures*, Vol. 1, pp. 279-286.

Matthys, S. (2000). *Structural Behavior and Design of Concrete Members Strengthened with Externally Bonded FRP Reinforcement.* Ph.D. Thesis, Department of Structural Engineering, University of Ghent, Belgium.

Meier, U. (1995). "Strengthening of concrete structures using carbon fibre/epoxy composites," *Construction and Building Materials*, Vol. 9, pp. 341-351.

Micelli, F., Annaiah, R. H., and Nanni, A. (2002). "Strengthening of Short Shear Span Reinforced Concrete T Joists with Fiber-Reinforced Plastic Composites," *Journal of Composites for Construction,* Vol. 6, No. 4, pp. 264-271.

Miller, B. (1999). *Bond between Carbon Fiber Reinforced Polymer Sheets and Concrete.* M.S. Thesis, Department of Civil Engineering, University of Missouri, Rolla, MO.

Mitsui, Y., Murakami, K., Takeda, K., and Sakai, H. (1998). "A Study on Shear Reinforcement of Reinforced Concrete Beams Externally Bonded with Carbon Fibre Sheets," *Composites Interfaces,* Vol. 5. No. 4, pp. 285-295.

Miyauchi, K., Inoue, S., Nishibayashi, S., and Tanaka, Y. (1997). "Shear behavior of Reinforced Concrete Beams Strengthened with CFRP Sheets," *Transactions of the Japan Concrete Institute,* Vol.19, pp. 97-104.

Monti, G., and Liotta, M. A. (2005). "FRP-Strengthening in Shear: Tests and Design Equation," *SP-230-32, ACI Proceedings of the 7th International Symposium on FRP for Reinforcement of Concrete Structures (FRPRCS-7).* pp. 543-562.

Nanni, A. (1999). "Composites: Coming on Strong," *Concrete Construction*, Vol. 44, No. 1, pp. 120-124.

Nanni, A. (1993). "Fiber-Reinforced Plastic (FRP) for Concrete Structures: Properties and Applications," *Elsevier Science*, New York.

Neubauer, U., and Rostasy, F. S. (1997). "Design aspects of concrete structures strengthened with externally bonded CFRP plates," *Proceedings of the Seventh International Conference on Structural Faults and Repairs,* pp. 109-118.

Ohuchi, H., Ohno, S., Katsumata, H., Kobatake, Y., Meta. T., Yamagata, K., Inokuma, Y., and Ogata, N. (1994). "Seismic Strengthening Design Technique for Existing Bridge Columns with CFRP," *Seismic Design and Retrofitting of Reinforced Concrete Bridges*, pp. 495-514.

Pellegrino, C., and Modena, C. (2002). "Fiber Reinforced Polymer Shear Strengthening of Reinforced Concrete Beams with Transverse Steel Reinforcement," *Journal of Composites for Construction*, Vol. 6, No. 2, pp. 104-111.

Priestley, M. J. N., Seible, F., and Fyfe, E. R. (1992). "Column seismic retrofit using fiberglass/epoxy jackets," *Advanced Composite Materials in Bridge and Structures (ACMBS)*, Canadian Society of Civil Engineering, Quebec, Canada, pp. 287-298.

Saadatmanesh, H. (1994). "Fiber Composites for new and existing structures," *ACI Structural Journal*, Vol. 91, No. 3, pp. 346-354.

Sato, Y., Ueda, T., Kakuta, Y., and Ono, S. (1997). "Ultimate Shear Capacity of Reinforced Concrete Beams with Carbon Fiber Sheet," *Non-Metallic (FRP) Reinforcement for Concrete Structures*, Vol. 1, pp. 499-506.

Sato, Y., Ueda, T., Kakuta, Y., and Tanaka, T. (1996). "Shear Reinforcing Effect of Carbon Fiber Sheet Attached to Side of Reinforced Concrete Beams," *Advanced Composite Materials in Bridges and Structures*, pp. 621-627.

Schuman, P. M. (2002). *Investigation on Mechanical Anchorage for Shear Rehabilitation of Continuous Reinforced Concrete T-Beams with CFRP Externally Bonded Stirrups.* M.S. Thesis, Department of Structural Engineering, University of California, San Diego, UCSD, San Diego, CA.

Taerwe, L., Khalil, H., and Matthys, S. (1997). "Behavior of RC Beams Strengthened in Shear by External CFRP Sheets," *Non-Metallic (FRP) Reinforcement for Concrete Structures*, Vol. 1, pp. 483-490.

Taljsten, B. (2003). "Strengthening Concrete Beams for Shear with CFRP Sheets," *Construction and Building Materials*, Vol.17, No. 1, pp. 15-26.

Taljsten, B. (1997). "Strengthening of Concrete Structures for Shear with Bonded CFRP Fabrics. Recent Advances in Bridge Engineering," *Proceedings of the US Canada-Europe Workshop on Bridge Engineering*, pp. 67-74.

Technical Report 55. (2000). *Design Guidance on Strengthening Concrete Structures Using Fibre Composite Materials,* Concrete Society, Great Britain.

Triantafillou, T. C., and Antonopoulos, C. P. (2000). "Design of Concrete Flexural Members Strengthened in Shear with FRP," *Journal of Composites for Construction*, Vol. 4, No. 4, pp. 198-205.

Triantafillou, T. C. (1998). "Shear Strengthening of Reinforced Concrete Beams Using Epoxy-Bonded FRP Composites," *ACI Structural Journal*, Vol. 95, No. 2, pp. 107-115.

Uji, K. (1992). "Improving Shear Capacity of Existing Reinforced Concrete Members by Applying Carbon Fiber Sheets," *Transactions of the Japan Concrete Institute*, Vol. 14, pp.253-266.

Umezu, K., Fujita, M., Nakai, H., and Tamaki, K. (1997). "Shear Behavior of RC Beams with Aramid Fiber Sheet," *Non-Metallic (FRP) Reinforcement for Concrete Structures*, Vol. 1, pp. 491-498.

Zhang, Z., and Hsu, C. T. T. (2005). "Shear Strengthening of Reinforced Concrete Beams Using Carbon-Fiber-Reinforced Polymer Laminates," *Journal of Composites for Construction*, Vol. 9, No. 2, pp. 158-169.

Zhang, Z., Hsu, C. T. T., and Moren, J. (2004). "Shear Strengthening of Reinforced Concrete Deep Beams Using Carbon Fiber Reinforced Polymer Laminates," *Journal of Composites for Construction*, Vol. 8, No. 5, pp. 403-414.

VITA

Rocio Patricia Tumialan was born in Lima, Peru, on April 20, 1980, and was raised in Lima, Peru. Rocio received her secondary education at Regina Pacis private school in Lima and graduated in December 1996. She then attended the Universidad de Lima in Peru. Following the steps of her father, who graduated from the University of Missouri-Rolla in 1969 with a Master Degree in Mining Engineering, and her brother, who graduated from the University of Missouri-Rolla in 1998 with a Master Degree in Civil Engineering and a Doctor or Philosophy Degree in 2001, Rocio then proceeded to transfer and continue pursuing her Bachelors Degree in Civil Engineering at the University of Missouri-Rolla. She graduated from the University of Missouri-Rolla in 2005. During the course of her studies, Rocio worked for the university as a student assistant in the Center for Infrastructure Engineering Studies (CIES). She also spent a summer working as a summer intern for Shively Geotechnical Inc., where she worked on construction field inspection at the St. Louis Lambert International Airport Expansion project. Rocio also worked as a summer intern in Golder Associates in Lima, Peru. She participates in projects performed at Antamina, one of the most important mining centers in the central mountains in Peru.

After receiving her Bachelors Degree, Rocio enrolled in the Civil Engineering Graduate Degree Program at the University of Missouri-Rolla in 2005. She received the Masters of Science Degree in Civil Engineering in December 2007.

Rocio is a member of both the American Society of Civil Engineers and the American Concrete Institute. She is also a member of the Society of Hispanic Engineers (SHPE).